

Predicting Stochastic Harmonics of Multiple Converters in a Power System (Microgrid)

by

Preye Milton Ivry, B.Eng, M.Sc.

Thesis submitted to the University of Nottingham
for the degree of Doctor of Philosophy

July 2016

Abstract

The microgrid concept integrates Renewable Energy Systems (RES) to the Electrical Power System (EPS) as a means to produce clean energy, meet consumer energy demands and preserve the depleting fossil fuels reserves. These RES are usually interfaced to the grid using power electronic converters (such as Voltage Source Converters) to achieve the required control and conversion of power. Nevertheless, Voltage Source Converters (VSCs) produce both current and voltage harmonics which negatively impact on the Power Quality (PQ) of a microgrid and may cause damage or malfunctions of equipment.

This thesis focuses on the impact of VSC harmonics on the power quality of a microgrid. It also investigates various factors that affect the harmonics generated by VSCs with the aim of predicting their impact on the PQ of the microgrid. The PQ of the microgrid is represented as a measure of the level of harmonic distortion of the voltage and current at the Point of Common Coupling (PCC) to the grid. The harmonic mean was used as a measure to determine if the VSCs harmonic level meets the IEEE Standard 519 harmonic limits.

The level of harmonic distortion of many VSCs can be significantly affected and difficult to predict in the presence of uncertainties, which may arise due to design parameter choice or system parameter changes. This necessitates the use of statistical techniques to quantify VSC harmonic distortion level in the presence of uncertainties.

A common statistical approach is to employ Monte Carlo Simulation (MCS), although accurate it is time consuming and burdensome for systems containing a large number of variables. This thesis utilizes the Univariate Dimension Reduction (UDR) technique formulated from an enhanced Unscented Transform (UT) equation in predicting the harmonic distortion level of large numbers of VSCs in a microgrid, when some system or design parameters are only known within certain constraints. The UDR technique drastically reduce the computation time and burden associated with the MCS approach and avoids assumptions that leads to system simplification required to implement other analytical methods. Various microgrid configuration and statistical distributions similar to practical system variations of RES are considered in order to achieve a good evaluation of the UDR performance in predicting the VSC harmonics. The UDR performance was also evaluated experimentally using a practical microgrid lab containing 3 VSCs. The MCS approach was used as a benchmark for the predicted UDR results. In all cases the UDR predicted results were obtained with significant time saved as compared to the MCS approach and the UDR results showed a good match with the MCS approach.

Acknowledgement

Firstly, I would like to express my gratitude to God for his faithfulness, blessings and grace in my life and during my studies.

My sincere gratitude goes to my supervisors, Prof David Thomas and Prof. Mark Sumner, for their invaluable assistance, patience and guidance throughout my PhD work. I would also like to appreciate Dr Oluwabukola Oke for her encouragement and technical support during my research and to Dr Richard Davies for helping conduct experiments necessary for this research work.

I would like to thank the Petroleum Technology Development Fund (PTDF), Nigeria for sponsoring this research work.

I appreciate Engr. Ebipuado Sapre-obi for his encouragement and continuous interest in my academic growth. A big thank you to my friend and brother Dr. Omonzejele Aigbomian and other friends in Nottingham and Nigeria. Thanks also goes to my pastor and friend Engr. Samuel Adeleke, his family and the entire members of RCCG, Beeston, Nottingham.

Words cannot express my gratitude to my parents Mr and Mrs M.E. Engbele-Ivry for their great sacrifice, love, support, care and prayers all through my life. I am grateful of my siblings Ofure, Matthew, Yvonne, Ebiware, Peter and Oyinlayefa for their love, support and belief in me to succeed.

Finally, my deepest gratitude goes to my wife and soulmate Oyinmi Gloria Ivry, thanks for bringing your glorious smiles and love into my life. Not forgetting my lovely children, Bekere Ariela Ivry and Perere Hepzibah Ivry for the days and nights you guys had to put up with my PhD research demands.

Contents

Abstract	i
Acknowledgement.....	ii
Contents	iii
List of Figures	ix
List of Tables	xviii
List of Abbreviations	xxi
Chapter 1 Introduction	1
1.1 Background and Motivation of Study	1
1.2 Microgrid Concept and Rationale for Power Quality Investigation	3
1.3 Research Aim	4
1.4 Research Objectives	5
1.5 Thesis Outline	5
1.6 Research Contributions	7
1.7 Research Publications	8
Chapter 2 Power Quality of a Microgrid.....	9
2.1 Power Quality	9
2.1.1 Classification of Power Quality Issues	10
2.2 Harmonic Generation in an Electric Power System	12
2.2.1 Harmonics	12
2.2.2 Common Terms used in Analysing Harmonics.....	15
2.2.3 Types and Sources of Harmonic in an Electric Power System ..	17
2.2.4 IEEE Standard for Harmonics on an Electric Power System	18
2.3 The Microgrid Concept	19
2.4 Rationale for Investigating Microgrid Power Quality Issues.....	21

2.5	Summary	25
Chapter 3	Power Electronic Converters.....	27
3.1	DER Interfacing Converter in a Microgrid	27
3.2	Current Source Converters (CSCs).....	28
3.3	Voltage Source Converters (VSCs)	28
3.3.1	Two (2) Level VSC Topology	30
3.3.2	Multilevel VSC (ML-VSC) Topology	33
3.4	Control Scheme.....	38
3.5	Summary	40
Chapter 4	Factors Affecting Harmonics Generated by a Voltage Source Converter.....	41
4.1	SPWM PI Controlled VSC	41
4.2	Harmonics Generated by a VSC Based on Design Specification.....	43
4.2.1	Amplitude Modulation Index (m_a) I.....	43
4.2.2	Switching Frequency/Frequency Modulation Index I.....	45
4.2.3	Converter Topology I	47
4.3	Harmonics Generated by a VSC Based on System/Operation Characteristics.....	50
4.3.1	Grid Voltage Waveform I.....	50
4.3.2	Grid System Impedance I	53
4.3.3	Inverter Operating Power I.....	55
4.4	Attenuation of VSC Harmonics Using Filters	58
4.4.1	L Filter	58
4.4.2	LC Filter.....	59
4.4.3	LCL Filter	59
4.5	Filter Design.....	60
4.5.1	Resonant Frequency and Damping of LC and LCL Filter	61

4.6	Harmonics Generated by an LCL Filtered VSC Based on Design Specification	64
4.6.1	Amplitude Modulation Index (m_a) II.....	64
4.6.2	Switching Frequency/Frequency Modulation Index II.....	66
4.6.3	Converter Topology II.....	68
4.7	Harmonics Generated by an LCL Filtered VSC Based on System/Operation Characteristics	70
4.7.1	Grid Voltage Waveform II.....	70
4.7.2	Grid System Impedance II.....	73
4.7.3	Inverter Operating Power II.....	76
4.8	Summary	78
Chapter 5 Quantifying/Predicting Harmonics of Multiple Voltage Source Converters.....		80
5.1	Harmonic Summation for Multiple Sources	80
5.2	Uncertainty Representation.....	82
5.3	Mathematical Terminology for Probabilistic Harmonic Studies	85
5.3.1	Definition.....	85
5.4	Moments of Random Variables	86
5.4.1	Relationship Between Moments and Cumulants.....	87
5.4.2	Quantiles	88
5.4.3	Cornish Fisher Expansion Method for Distribution Function Reconstruction.....	89
5.5	Schematics of N Number of Harmonic Sources	89
5.6	Probabilistic Harmonic Studies.....	90
5.7	Probabilistic Harmonic Summation.....	91
5.7.1	Random Harmonic Phasors	92
5.7.2	Important Statistical Functions of X_h and Y_h	93

5.7.3	Summation of N Random Harmonic Vectors.....	93
5.8	Probabilistic Harmonic Methods	98
5.8.1	Monte Carlo Simulation Approach.....	99
5.8.2	Results	103
5.8.3	Unscented Transform Method	109
5.9	Summary	112
Chapter 6 Unscented Transform and Dimension Reduction Technique.....		113
6.1	Unscented Transform based on Gaussian Quadrature	113
6.1.1	Gaussian Quadrature: Basics	115
6.1.2	Sigma Points and Weights Generation in Multivariate Problems.....	116
6.2	Dimension Reduction.....	118
6.2.1	Basics of Dimension Reduction.....	118
6.2.2	Univariate Dimension Reduction (UDR)	118
6.2.3	Bivariate Dimension Reduction (BDR).....	121
6.2.4	Output Moment Estimation	123
6.3	Dimension Reduction and Unscented Transform	124
6.4	The Use of Dimension Reduction in Predicting Harmonics.....	126
6.4.1	Predicting Harmonics of N VSCs Using the UDR.....	127
6.4.2	Predicting Harmonics of N VSCs Using the BDR.....	139
6.5	Summary	156
Chapter 7 Predicting Harmonics of Multiple VSCs Using the UDR Technique.....		158
7.1	Application of the UDR Technique	158
7.1.1	Step-by-Step Procedure of the UDR Technique.....	158
7.2	Case Study 1: Microgrid System with Filter Parameter Variation ..	159

7.2.1	Predicted Result and Discussion.....	160
7.3	Case Study 2: Microgrid System with Practical Power Variation ...	168
7.3.1	Predicted Result and Discussion.....	170
7.4	Case Study 3: Microgrid System with Grid Impedance Variation ..	174
7.4.1	Predicted Result and Discussion.....	175
7.5	Case Study 4: Microgrid System containing 20 VSCs with Power Variation	183
7.5.1	Predicted Result and Discussion.....	183
7.6	Case Study 5: Microgrid System with Other Non-Linear Loads.....	186
7.6.1	Predicted Result and Discussion.....	187
7.7	Summary	191
Chapter 8 Experimental Validation of the UDR Technique for Harmonic Prediction.....		194
8.1	Objective and Procedure	194
8.2	Structure of Microgrid Lab	195
8.3	Case Study 1 – Prediction of VSCs Harmonics under Uniform Power Variation	198
8.4	Case Study 2 - Prediction of VSCs Harmonics under Gaussian (Normal) Power Variation	201
8.5	Summary	203
Chapter 9 Conclusion		204
9.1	Power Quality in a Microgrid	204
9.2	Factors that Affect Harmonic Distortion Levels of VSCs in a Microgrid.	206
9.3	Dimension Reduction Techniques for Predicting Harmonic Distortion Levels of VSCs in a Microgrid	207
9.4	Research Contributions	209

9.5	Possible Areas for Further Research Work.....	209
9.5.1	Effect of Different Control Strategy and VSC Switching Pattern on VSCs Harmonic.....	209
9.5.2	Modelling of Microgrid System	210
9.5.3	Predicting other Power Quality Issues using Dimension Reduction Technique	210
9.5.4	Experimental Validation.....	210
	References.....	211
	Appendix.....	224
	Appendix A	225
	A.1: Park and Clarke’s Transformation Used in Modelling the VSC PI Controller and Transformations	225
	Appendix B	227
	B.1: Generation of Orthogonal Polynomial	227
	B.2: Stieltjes Procedure.....	228
	B.3: Generation of Sigma Points and Weights for Univariate Problems	230
	Appendix C	232
	C.1: Standard Deviation of Current and Voltage THD and IHD_n under Filter Inductance Variation	232
	C.2: Standard deviation for Harmonic Distortion Level Using MCS, 3pts and 5pts UDR under Grid Impedance Variation.....	234
	C.3: Modelled Plecs Circuit of Microgrid Structure with Linear and Non- Linear Load	236
	C.4: Percentage Error in Current and Voltage THD and IHD_n for Microgrid with Non-Linear Loads	237
	Appendix D.....	239
	D.1: Modelled Plecs Microgrid Structure Containing 10 VSCs	239
	D.2: Control and Transformation Blocks	240

List of Figures

Fig. 1.1: Concept of a Microgrid	3
Fig. 2.1: Sinusoidal Voltage and Current Waveform	14
Fig. 2.2: Non-Sinusoidal Voltage Waveform	14
Fig. 3.1: Basic Configuration of a Three Phase 2-Level CSC.....	28
Fig. 3.2: Basic Configuration of a Three Phase 2-Level VSC.....	30
Fig. 3.3: Simulated Plecs Model of Three Phase 2-Level VSC.....	30
Fig. 3.4: 2-Level VSC Voltage Output	31
Fig. 3.5: Sinusoidal Pulse Width Modulation (SPWM) Technique	31
Fig. 3.6: Gating Signal as obtained from Fig. 3.5.....	32
Fig. 3.7: Simulated Plecs Model of a Three Phase 3-Level NPC VSC	34
Fig. 3.8: 3-Level NPC VSC Voltage Output	34
Fig. 3.9: Multiple Carrier SPWM Technique for a 3-Level VSC	35
Fig. 3.10: Switching Signal for G1 and G4 Obtained from Fig. 3.9	35
Fig. 3.11: Simulated Plecs Model of a Three Phase 5-Level NPC VSC	36
Fig. 3.12: 5-Level NPC VSC Voltage Output	36
Fig. 3.13: Multiple Carrier SPWM Technique for 5-level VSC.....	37
Fig. 3.14: Switching Signal for G1,G2 and G7,G8 Obtained from Fig. 3.5.....	37
Fig. 3.15: Active and Reactive Power Control Scheme of the Grid interfacing VSC	40
Fig. 4.1: Modelled L -filtered VSC Connected to the Grid	42
Fig. 4.2: VSC Phase Current Waveform (a) and Harmonic Spectrum (b)	42
Fig. 4.3: VSC Phase Voltage Waveform (a) and Harmonic Spectrum (b).....	42
Fig. 4.4: The effect of VSC m_a on I_{THD} and V_{THD} at PCC	43
Fig. 4.5: VSC Current Waveform (a) and Harmonic Spectrum (b) at $m_a = 0.55$	44
Fig. 4.6: VSC Voltage Waveform (a) and Harmonic Spectrum (b) at $m_a = 0.55$	44
Fig. 4.7: VSC Current Waveform (a) and Harmonic Spectrum (b) at $m_a = 0.95$	45
Fig. 4.8: VSC Voltage Waveform (a) and Harmonic Spectrum (b) at $m_a = 0.95$	45

Fig. 4.9: The effect of VSC f_{sw}/m_f on I_{THD} and V_{THD} at PCC	46
Fig. 4.10: VSC Current Waveform (a) and Harmonic Spectrum (b) at $f_{sw} = 4\text{kHz}$	46
Fig. 4.11: VSC Voltage Waveform (a) and Harmonic Spectrum (b) at $f_{sw} = 4\text{kHz}$	47
Fig. 4.12: VSC Current Waveform (a) and Harmonic Spectrum (b) at $f_{sw} = 6\text{kHz}$	47
Fig. 4.13: VSC Voltage Waveform (a) and Harmonic Spectrum (b) at $f_{sw} = 6\text{kHz}$	47
Fig. 4.14: The effect of VSC Topology on I_{THD} and V_{THD} at PCC.....	48
Fig. 4.15: 3-L NPC VSC Current Waveform (a) and Harmonic Spectrum (b)	48
Fig. 4.16: 3-L NPC VSC Voltage Waveform (a) and Harmonic Spectrum (b)	49
Fig. 4.17: 5-L NPC VSC Current Waveform (a) and Harmonic Spectrum (b)	49
Fig. 4.18: 5-L NPC VSC Voltage Waveform (a) and Harmonic Spectrum (b)	49
Fig. 4.19: The effect of Grid Voltage Distortion on I_{THD} and V_{THD} at PCC.....	50
Fig. 4.20: VSC Current Waveform (a) and Harmonic Spectrum (b) at 1% V_{THD}	51
Fig. 4.21: VSC Voltage Waveform (a) and Harmonic Spectrum (b) at 1% V_{THD}	51
Fig. 4.22: VSC Current Waveform (a) and Harmonic Spectrum (b) at 3% V_{THD}	51
Fig. 4.23: VSC Voltage Waveform (a) and Harmonic Spectrum (b) at 3% V_{THD}	52
Fig. 4.24: VSC Current Waveform (a) and Harmonic Spectrum (b) at 5% V_{THD}	52
Fig. 4.25: VSC Voltage Waveform (a) and Harmonic Spectrum (b) at 5% V_{THD}	52
Fig. 4.26: The effect of Grid Impedance Variation on I_{THD} and V_{THD} at PCC .	53
Fig. 4.27: VSC Current Waveform (a) and Harmonic Spectrum (b) at 0Z	54
Fig. 4.28: VSC Voltage Waveform (a) and Harmonic Spectrum (b) at 0Z.....	54
Fig. 4.29: VSC Current Waveform (a) and Harmonic Spectrum (b) at 0.5Z ...	54
Fig. 4.30: VSC Voltage Waveform (a) and Harmonic Spectrum (b) at 0.5Z...	55
Fig. 4.31: VSC Current Waveform (a) and Harmonic Spectrum (b) at 2Z	55

Fig. 4.32: VSC Voltage Waveform (a) and Harmonic Spectrum (b) at 2Z.....	55
Fig. 4.33: The effect of VSC Operating Power on I_{THD} and V_{THD} at PCC.....	56
Fig. 4.34: VSC Current Waveform (a) and Harmonic Spectrum (b) at 0.25P .	56
Fig. 4.35: VSC Voltage Waveform (a) and Harmonic Spectrum (b) at 0.25P.	57
Fig. 4.36: VSC Current Waveform (a) and Harmonic Spectrum (b) at 0.5P ...	57
Fig. 4.37: VSC Voltage Waveform (a) and Harmonic Spectrum (b) at 0.5P ...	57
Fig. 4.38: VSC Current Waveform (a) and Harmonic Spectrum (b) at 2P	58
Fig. 4.39: VSC Voltage Waveform (a) and Harmonic Spectrum (b) at 2P	58
Fig. 4.40: L-filtered VSC Current Waveform (a) and Harmonic Spectrum (b)	62
Fig. 4.41: L-filtered VSC Voltage Waveform (a) and Harmonic Spectrum (b)	63
Fig. 4.42: LCL-filtered VSC Current Waveform (a) and Harmonic Spectrum (b)	63
Fig. 4.43: LCL-filtered VSC Voltage Waveform (a) and Harmonic Spectrum (b)	63
Fig. 4.44: Modelled LCL-filtered VSC Connected to the Grid	64
Fig. 4.45: The effect of VSC with LCL Filter m_a on I_{THD} and V_{THD} at PCC....	65
Fig. 4.46: VSC with LCL Filter Current Waveform (a) and Harmonic Spectrum (b) at $m_a = 0.55$	65
Fig. 4.47: VSC with LCL Filter Voltage Waveform (a) and Harmonic Spectrum (b) at $m_a = 0.55$	65
Fig. 4.48: VSC with LCL Filter Current Waveform (a) and Harmonic Spectrum (b) at $m_a = 0.95$	66
Fig. 4.49: VSC with LCL Filter Voltage Waveform (a) and Harmonic Spectrum (b) at $m_a = 0.95$	66
Fig. 4.50: The effect of VSC with LCL Filter f_{sw}/m_f on I_{THD} and V_{THD} at PCC	67
Fig. 4.51: VSC with LCL Filter Current Waveform (a) and Harmonic Spectrum (b) at $f_{sw} = 4\text{kHz}$	67
Fig. 4.52: VSC with LCL Filter Voltage Waveform (a) and Harmonic Spectrum (b) at $f_{sw} = 4\text{kHz}$	67
Fig. 4.53: VSC with LCL Filter Current Waveform (a) and Harmonic Spectrum (b) at $f_{sw} = 6\text{kHz}$	68
Fig. 4.54: VSC with LCL Filter Voltage Waveform (a) and Harmonic Spectrum (b) at $f_{sw} = 6\text{kHz}$	68

Fig. 4.55: The effect of VSC with LCL Filter Topology on I_{THD} and V_{THD} at PCC	69
Fig. 4.56: 3-L NPC VSC with LCL Filter Current Waveform (a) and Harmonic Spectrum (b)	69
Fig. 4.57: 3-L NPC VSC with LCL Filter Voltage Waveform (a) and Harmonic Spectrum (b)	69
Fig. 4.58: 5-L NPC with LCL Filter VSC Current Waveform (a) and Harmonic Spectrum (b)	70
Fig. 4.59: 5-L NPC VSC with LCL Filter Voltage Waveform (a) and Harmonic Spectrum (b)	70
Fig. 4.60: The effect of Grid Voltage Distortion on I_{THD} and V_{THD} at the PCC for an LCL Filtered VSC.....	71
Fig. 4.61: VSC with LCL Filter Current Waveform (a) and Harmonic Spectrum (b) at 1% V_{THD}	71
Fig. 4.62: VSC with LCL Filter Voltage Waveform (a) and Harmonic Spectrum (b) at 1% V_{THD}	72
Fig. 4.63: VSC with LCL Filter Current Waveform (a) and Harmonic Spectrum (b) at 3% V_{THD}	72
Fig. 4.64: VSC with LCL Filter Voltage Waveform (a) and Harmonic Spectrum (b) at 3% V_{THD}	72
Fig. 4.65: VSC with LCL Filter Current Waveform (a) and Harmonic Spectrum (b) at 5% V_{THD}	73
Fig. 4.66: VSC with LCL Filter Voltage Waveform (a) and Harmonic Spectrum (b) at 5% V_{THD}	73
Fig. 4.67: The effect of Grid Impedance Variation on I_{THD} and V_{THD} at PCC for an LCL Filtered VSC.....	73
Fig. 4.68: VSC with LCL Filter Current Waveform (a) and Harmonic Spectrum (b) at 0Z	74
Fig. 4.69: VSC with LCL Filter Voltage Waveform (a) and Harmonic Spectrum (b) at 0Z	74
Fig. 4.70: VSC with LCL Filter Current Waveform (a) and Harmonic Spectrum (b) at 0.5Z	74

Fig. 4.71: VSC with LCL Filter Voltage Waveform (a) and Harmonic Spectrum (b) at 0.5Z	75
Fig. 4.72: VSC with LCL Filter Current Waveform (a) and Harmonic Spectrum (b) at 2Z	75
Fig. 4.73: VSC with LCL Filter Voltage Waveform (a) and Harmonic Spectrum (b) at 2Z	75
Fig. 4.74: The effect of VSC Operating Power on I_{THD} and V_{THD} at PCC	76
Fig. 4.75: VSC with LCL Filter Current Waveform (a) and Harmonic Spectrum (b) at 0.25P.....	76
Fig. 4.76: VSC with LCL Filter Voltage Waveform (a) and Harmonic Spectrum (b) at 0.25P.....	77
Fig. 4.77: VSC with LCL Filter Current Waveform (a) and Harmonic Spectrum (b) at 0.5P.....	77
Fig. 4.78: VSC with LCL Filter Voltage Waveform (a) and Harmonic Spectrum (b) at 0.5P.....	77
Fig. 4.79: VSC with LCL Filter Current Waveform (a) and Harmonic Spectrum (b) at 2P.....	78
Fig. 4.80: VSC with LCL Filter Voltage Waveform (a) and Harmonic Spectrum (b) at 2P.....	78
Fig. 5.1: Schematic of Power Flow at Fundamental frequency [74]	81
Fig. 5.2: Schematic of Harmonic Power Flow [74].....	81
Fig. 5.3: Current flow from 3 phase Harmonic Source	82
Fig. 5.4: Multiple VSCs connected in Parallel to the PCC.....	90
Fig. 5.5: Result of I_{THD} and V_{THD} for 2 VSCs Connected in Parallel for Various Numbers of Simulations	101
Fig. 5.6 CDF of I_{THD} and V_{THD} of a VSC with Variable Filter Inductance....	104
Fig. 5.7: CDF of I_{THD} and V_{THD} of 5 VSCs with Variable Filter Inductance .	105
Fig. 5.8: CDF of I_{THD} and V_{THD} of 10 VSCs with Variable Filter Inductance	105
Fig. 5.9: CDF of I_{THD} and V_{THD} of a Single VSC with Variable Power.....	106
Fig. 5.10: CDF of I_{THD} and V_{THD} of 5 VSCs with Variable Power	106
Fig. 5.11: CDF of I_{THD} and V_{THD} of 10 VSCs with Variable Power	107
Fig. 5.12: CDF of I_{THD} and V_{THD} of a VSC with Inductor and Power Variation	108

Fig. 5.13: CDF of I_{THD} and V_{THD} of 5 VSCs with Inductor and Power Variation	108
Fig. 5.14: CDF of I_{THD} and V_{THD} of 10 VSCs with Inductor and Power Variation	108
Fig. 5.15: Mean I_{IHD_78} (Power Variation).....	110
Fig. 5.16: Mean I_{IHD_82} (Power Variation).....	111
Fig. 5.17: Mean I_{IHD_78} (Grid Impedance Variation).....	111
Fig. 5.18: Mean I_{IHD_82} (Grid Impedance Variation).....	112
Fig. 6.1: Continuous and Discrete Representation of a function [88]	114
Fig. 6.2: Number of Evaluations Required for the Harmonic Prediction Methods	135
Fig. 6.3: Computation Time Required for the Harmonic Prediction Methods.....	135
Fig. 6.4: Computation Time Saved Using UDR as compared to the MCS Technique for Harmonic Prediction	136
Fig. 6.5: UDR Predicted I_{THD} for 10 VSCs	137
Fig. 6.6: UDR Predicted I_{IHD} at the 38 th Harmonic Order for 10 VSCs.....	137
Fig. 6.7: UDR Predicted I_{IHD} at the 42 nd Harmonic Order for 10 VSCs	138
Fig. 6.8: UDR Predicted V_{THD} for 10 VSCs.....	138
Fig. 6.9: UDR Predicted V_{IHD} at the 38 th Harmonic Order for 10 VSCs	138
Fig. 6.10: UDR Predicted V_{IHD} at the 42 nd Harmonic Order for 10 VSCs.....	139
Fig. 6.11: Number of Evaluation Points Required for the Harmonic Prediction Methods	144
Fig. 6.12: Computation Time Required for the Harmonic Prediction Methods	144
Fig. 6.13: Computation Time Saved Using DR as compared to the MCS Technique for Harmonic Prediction	145
Fig. 6.14: UDR/BDR Predicted I_{THD} for 6 VSCs	146
Fig. 6.15: UDR/BDR Predicted I_{IHD_38} for 6 VSCs.....	146
Fig. 6.16: UDR/BDR Predicted I_{IHD_42} for 6 VSCs.....	147
Fig. 6.17: UDR/BDR Predicted V_{THD} for 6 VSCs.....	147
Fig. 6.18: UDR/BDR Predicted V_{IHD_38} for 6 VSCs	147
Fig. 6.19: UDR/BDR Predicted V_{IHD_42} for 6 VSCs	148
Fig. 6.20 UDR/BDR Predicted Skewness of I_{THD} for 6 VSCs	149

Fig. 6.21 UDR/BDR Predicted Skewness of I_{IHD_38} for 6 VSCs.....	149
Fig. 6.22 UDR/BDR Predicted Skewness of I_{IHD_42} for 6 VSCs.....	149
Fig. 6.23 UDR/BDR Predicted Skewness of V_{THD} for 6 VSCs.....	150
Fig. 6.24 UDR/BDR Predicted Skewness of V_{IHD_38} for 6 VSCs	150
Fig. 6.25 UDR/BDR Predicted Skewness of V_{IHD_42} for 6 VSCs	150
Fig. 6.26 UDR/BDR Predicted Kurtosis of I_{THD} for 6 VSCs	151
Fig. 6.27 UDR/BDR Predicted Kurtosis of I_{IHD_38} for 6 VSCs	151
Fig. 6.28 UDR/BDR Predicted Kurtosis of I_{IHD_42} for 6 VSCs	151
Fig. 6.29 UDR/BDR Predicted Kurtosis of V_{THD} for 6 VSCs.....	152
Fig. 6.30: UDR/BDR Predicted Kurtosis of V_{IHD_38} for 6 VSCs	152
Fig. 6.31: UDR/BDR Predicted Kurtosis of V_{IHD_42} for 6 VSCs	152
Fig. 6.32: Percentage error of the UDR/BDR Predicted I_{THD}	153
Fig. 6.33: Percentage error of the UDR/BDR Predicted I_{IHD_38}	153
Fig. 6.34: Percentage error of the UDR/BDR Predicted I_{IHD_42}	154
Fig. 6.35: Percentage error of the UDR/BDR Predicted V_{THD}	154
Fig. 6.36: Percentage error of the UDR/BDR Predicted V_{IHD_38}	155
Fig. 6.37: Percentage error of the UDR/BDR Predicted V_{IHD_42}	155
Fig. 7.1: Computation Time Saved by UDR Techniques wrt MCS	163
Fig. 7.2: Predicted I_{THD} using MCS, 3pts UDR and 5pts UDR.....	163
Fig. 7.3: Predicted I_{IHD_38} using MCS, 3pts UDR and 5pts UDR.....	163
Fig. 7.4: Predicted I_{IHD_42} using MCS, 3pts UDR and 5pts UDR.....	164
Fig. 7.5: Predicted V_{THD} using MCS, 3pts UDR and 5pts UDR.	164
Fig. 7.6: Predicted V_{IHD_38} using MCS, 3pts UDR and 5pts UDR.	164
Fig. 7.7: Predicted V_{IHD_42} using MCS, 3pts UDR and 5pts UDR.	165
Fig. 7.8: Percentage error in predicted I_{THD} using 3pts and 5pts UDR.	165
Fig. 7.9: Percentage error in predicted I_{IHD_38} using 3pts and 5pts UDR.	166
Fig. 7.10: Percentage error in predicted I_{IHD_42} using 3pts and 5pts UDR.	166
Fig. 7.11 Percentage error in predicted V_{THD} using 3pts and 5pts UDR.	166
Fig. 7.12 Percentage error in predicted V_{IHD_38} using 3pts and 5pts UDR.	167
Fig. 7.13: Percentage error in predicted V_{IHD_42} using 3pts and 5pts UDR....	167
Fig. 7.14: Schematic of 2 PV VSC commonly connected to the grid.	168
Fig. 7.15: Wind Speed Distribution and Power Curve [131].	169
Fig. 7.16: Condition 1 (PV) CDF plot of current THD.	171

Fig. 7.17: Condition 2 (PV) CDF plot of current THD.	171
Fig. 7.18: Condition 3 (PV) CDF plot of current THD.	172
Fig. 7.19: Condition 1 (WT) CDF plot of current THD.	173
Fig. 7.20: Condition 2 (WT) CDF plot of current THD.	173
Fig. 7.21: Condition 3 (WT) CDF plot of current THD.	174
Fig. 7.22: Computation Time Saved using UDR technique wrt MCS	176
Fig. 7.23: Predicted I_{THD} using MCS, 3pts UDR and 5pts UDR.....	176
Fig. 7.24: Predicted V_{THD} using MCS, 3pts UDR and 5pts UDR.	177
Fig. 7.25: Predicted $I_{IHD_{38}}$ using MCS, 3pts UDR and 5pts UDR.....	178
Fig. 7.26: Predicted $V_{IHD_{38}}$ using MCS, 3pts UDR and 5pts UDR.....	178
Fig. 7.27: Predicted $I_{IHD_{42}}$ using MCS, 3pts UDR and 5pts UDR.....	179
Fig. 7.28: Predicted $V_{IHD_{42}}$ using MCS, 3pts UDR and 5pts UDR.	180
Fig. 7.29: Percentage error in predicted I_{THD} using 3pts UDR and 5pts UDR.	180
Fig. 7.30: Percentage error in predicted $I_{IHD_{38}}$ using 3pts and 5pts UDR.	181
Fig. 7.31: Percentage error in predicted $I_{IHD_{42}}$ using 3pts and 5pts UDR.	181
Fig. 7.32: Percentage error in predicted V_{THD} using 3pts and 5pts UDR.	182
Fig. 7.33: Percentage error in predicted $V_{IHD_{38}}$ using 3pts and 5pts UDR....	182
Fig. 7.34: Percentage error in predicted $V_{IHD_{42}}$ using 3pts and 5pts UDR....	182
Fig. 7.35: Computation Time for the UDR Technique.....	184
Fig. 7.36: Predicted Mean Current Distortion Level using the 3pts, 5pts and 7pts UDR.....	184
Fig. 7.37: Predicted Mean Voltage Distortion Level using the 3pts, 5pts and 7pts UDR.....	185
Fig. 7.38: Predicted standard deviation Current distortion levels using the 3pts, 5pts and 7pts UDR.....	185
Fig. 7.39: Predicted standard deviation Voltage distortion levels using the 3pts, 5pts and 7pts UDR.....	185
Fig. 7.40: Diode Rectifier Non-Linear Load Model.....	186
Fig. 7.41: Predicted Mean I_{THD} and I_{IHD_n} using MCS, 3pts and 5pts UDR....	188
Fig. 7.42: Predicted Mean V_{THD} and V_{IHD_n} using MCS, 3pts and 5pts UDR.	189
Fig. 7.43: Predicted Std of I_{THD} and I_{IHD_n} using MCS, 3pts and 5pts UDR. ..	189
Fig. 7.44: Predicted Std of V_{THD} and V_{IHD_n} using MCS, 3pts 5pts UDR.	189

Fig. 7.45: Percentage error in Mean I_{THD} and I_{IHDn} using 3pts and 5pts UDR.	190
Fig. 7.46: Percentage error in Mean V_{THD} and V_{IHDn} using 3pts and 5pts UDR.	190
Fig. 7.47: Percentage error in Std of I_{THD} and I_{IHDn} using 3pts and 5pts UDR.	191
Fig. 7.48: Percentage error in Std of V_{THD} and V_{IHDn} using 3pts and 5pts UDR.	191
Fig. 8.1: Schematic of the Microgrid Laboratory Set-up.....	195
Fig. 8.2: Three VSCs and the Low Voltage Busbar	197
Fig. 8.3: Triphase Programmable Power/Voltage Supply (Microgrid Source)	197
Fig. 8.4: Current and Voltage Measuring Blocks	197
Fig. 8.5: Busbars and Transformer	198
Fig. 8.6: 1000V/415V Busbar and Three VSCs	198
Fig. 8.7: Laboratory Results of I_{THD} Predicted Statistical Moments (3pts UDR).	199
Fig. 8.8: Laboratory Results of V_{THD} Predicted Statistical Moments (3pts UDR).	200
Fig. 8.9: Laboratory Results of I_{THD} Predicted Statistical Moments (5pts UDR).	201
Fig. 8.10: Laboratory Results of V_{THD} Predicted Statistical Moments (5pts UDR).....	201
Fig. 8.11: Laboratory Results of I_{THD} Predicted Statistical Moments (5pts UDR Normal).....	202
Fig. 8.12: Laboratory Results of V_{THD} Predicted Statistical Moments (5pts UDR Normal).....	203

List of Tables

Table 2.1: Categories and Typical Characteristics of Power System Electromagnetic Phenomena as defined by IEEE Standard -1159 [26].	10
Table 2.2: Main Phenomena Causing Electromagnetic Disturbances as Classified by the IEC [27].	11
Table 2.3: Types of harmonics and their corresponding sources [21].	17
Table 2.4: Current Distortion Limit for Systems rated 120V through 69kV ...	18
Table 2.5: Voltage Distortion Limits.	19
Table 3.1: Gating Signal for a 3-level NPC VSC (Phase a)	35
Table 3.2: Gating Signal for a 5-level NPC VSC (Phase a)	37
Table 4.1: Studied Grid Integrated VSC System	41
Table 4.2: Filter Parameter and Achieved Harmonic Attenuation (THD)	62
Table 5.1: Result of Randomly Varying Filter Inductor Value with Multiple VSCs	104
Table 5.2: Result of Randomly Varying Operating Power of Multiple VSCs	106
Table 5.3: Result of Randomly Varying Filter Inductor Value and Operating Power of Multiple VSCs	107
Table 6.1: Distribution Functions and Associated Orthogonal Polynomials .	115
Table 6.2: Generation of Sigma Points (S_{in}) and Weight (W_{in}) for a Multivariate Problem Using 3 points Approximations	117
Table 6.3: Generation of Sigma Points and Weight for a Multivariate Problem Using 5 points Approximations	117
Table 6.4: Number of Evaluation Points Required for the Unscented Transform and Dimension Reduction Methods (Using $n = 3$)	126
Table 6.5: Predicted THD, IHD_{38} and IHD_{42} for 1 VSC Using UDR	127
Table 6.6: Predicted THD, IHD_{38} and IHD_{42} for 2 VSCs Using UDR	128
Table 6.7: Predicted THD, IHD_{38} and IHD_{42} for 3 VSCs Using UDR	129
Table 6.8: Predicted THD, IHD_{38} and IHD_{42} for 4 VSCs Using UDR	130
Table 6.9: Predicted THD, IHD_{38} and IHD_{42} for 5 VSCs Using UDR	130
Table 6.10: Predicted THD, IHD_{38} and IHD_{42} for 6 VSCs Using UDR	132
Table 6.11: Predicted THD, IHD_{38} and IHD_{42} for 7 VSCs Using UDR	132
Table 6.12: Predicted THD, IHD_{38} and IHD_{42} for 8 VSCs Using UDR	133

Table 6. 13: Predicted THD, IHD ₃₈ and IHD ₄₂ for 9 VSCs Using UDR	133
Table 6.14: Predicted THD, IHD ₃₈ and IHD ₄₂ for 10 VSCs Using UDR	134
Table 6.15: Significant Computation Time Saved Using UDR as compared to the MCS Technique for Harmonic Prediction	135
Table 6.16: Predicted THD, IHD ₃₈ and IHD ₄₂ for 2VSCs Using BDR.....	140
Table 6.17: Predicted THD, IHD ₃₈ and IHD ₄₂ for 3 VSCs Using BDR.....	140
Table 6.18: Predicted THD, IHD ₃₈ and IHD ₄₂ for 4 VSCs Using BDR.....	141
Table 6.19: Predicted THD, IHD ₃₈ and IHD ₄₂ for 5 VSCs Using BDR.....	142
Table 6.20: Predicted THD, IHD ₃₈ and IHD ₄₂ for 6 VSCs Using BDR.....	143
Table 6.21: Computation Time Saved Using UDR as compared to the MCS Technique for Harmonic Prediction	145
Table 7.1: Predicted Current Harmonic Distortion Level Using MCS, 3pts and 5pts UDR under Filter Inductance Variation.....	160
Table 7.2: Predicted Voltage Harmonic Distortion Level Using MCS, 3pts and 5pts UDR under Filter Inductance Variation.....	161
Table 7.3 Predicted Current and Voltage THD of the PV VSCs.....	170
Table 7.4: Predicted Current and Voltage THD of the WT VSCs	172
Table 7.5: Predicted Total Harmonic Distortion Level Using MCS, 3pts and 5pts UDR under Grid Impedance Variation.....	175
Table 7.6: Predicted 38 th order Individual Harmonic Distortion Level Using MCS, 3pts and 5pts UDR under Grid Impedance Variation	177
Table 7.7: Predicted 42 nd order Individual Harmonic Distortion Level Using MCS, 3pts and 5pts UDR under Grid Impedance Variation	179
Table 7.8: Predicted Current and Voltage Harmonic Distortion Level Using 3pts, 5pts and 7pts UDR for 20 VSCs Variable Power Output.....	183
Table 7.9: Predicted Harmonic Distortion Level Using MCS, 3pts and 5pts UDR for a Microgrid with Non-linear Loads	187
Table 7.10: Computation Time.....	188
Table 8.1: Microgrid and VSC Laboratory Parameters.....	196
Table 8.2: Approximate Time Utilized by Microgrid to Conduct Practical...	196
Table 8.3: Laboratory Results Showing Predicted Moments of I _{THD} and V _{THD} using MCS and 3pts UDR	199

Table 8.4: Laboratory Results Showing Predicted Moments of I_{THD} and V_{THD} using MCS and 5pts UDR	200
Table 8.5: Laboratory Results Showing Predicted Moments of I_{THD} and V_{THD} using MCS and 5pts UDR Normal Variation	202
Table C.1: Predicted Standard Deviation of Current and Voltage THD and IHD_n Using MCS, 3pts and 5pts UDR under Filter Inductance Variation	232
Table C.2: Predicted Standard deviation for Harmonic Distortion Level Using MCS, 3pts and 5pts UDR under Grid Impedance Variation	234
Table C.3: Predicted Current and Voltage Harmonic Distortion Level Percentage Error Using 3pts and 5pts UDR for Microgrid with Non-Linear Loads	237

List of Abbreviations

BDR	Bivariate Dimension Reduction
CDF	Cumulative Distribution Function
CF	Cornish Fisher
DER	Distributed Energy Resource
DR	Dimension Reduction
EMC	Electromagnetic Compatibility
EPS	Electrical Power System
FFT	Fast Fourier Transform
HVDC	High Voltage Direct Current
IEC	International Electrotechnical Commission
IEEE	Institute of Electrical and Electronics Engineering
IGBT	Insulated Gate Bipolar Transistor
IHD	Individual Harmonic Distortion
LCL	Inductance Capacitance Inductance
MCS	Monte Carlo Simulation
MLVSC	Multi-level Voltage Source Converter
NPC	Neutral Point Clamped
PCC	Point of Common Coupling
PDF	Probability Density Function
PI	Proportional Integral
PQ	Power Quality

PV	Photovoltaic
PWM	Pulse Width Modulation
RES	Renewable Energy System
SPWM	Sinusoidal Pulse Width Modulation
Std	Standard Deviation
THD	Total Harmonic Distortion
UDR	Univariate Dimension Reduction
UT	Unscented Transform
VSC	Voltage Source Converter
WTS	Wind Turbine System

Chapter 1

Introduction

This chapter gives a brief introduction by discussing the background and motivation for this work. It also states the main objectives of the research work and outlines the thesis chapters.

1.1 Background and Motivation of Study

The advancement of innovative technology and the increased penetration of renewable/sustainable energy generation systems upon the electrical network have led to new concepts like the smart grids and microgrids [1]. These concepts integrate Renewable Energy Systems (RES) such as wind turbines and photovoltaics to the Electrical Power System (EPS) as a means to produce clean energy, meet energy demands and preserve the depleting fossil fuel's reserves [2].

The RES are usually interfaced to the grid using power electronic converters [3] which are also utilized to achieve the required control and conversion of power [4] in the RES. Recently, power converters such as the Voltage Source Converters (VSCs) have enjoyed more attention and use due to their better controllability and fast switching responses. Nevertheless, the converters produce both current and voltage harmonics at their terminals and these disturbances are transmitted to the rest of the grid [4], [5]. These harmonics can cause malfunction, damage or interference with many other electrical/electronic devices [6-8]. Some examples include; causing fuses and circuit breakers to trip, damaging or blowing up EPS components based on false signals. Harmonics also cause transformer copper and iron losses due to stray flux losses and overheating of transformer windings [7]. While, harmonics at high frequency affect telecommunication lines and smart meters through electromagnetic interference leading to incorrect readings and measurements [9].

Harmonics can significantly increase on an EPS and become difficult to predict where variations are present in certain factors like the operating conditions (output power) or system parameters (grid voltage background distortion). Furthermore, in a case where many VSCs are connected to the EPS, the net effect of the harmonics on the EPS Power Quality (PQ) becomes difficult to predict as harmonics do not add up arithmetically. This and the inherent stochastic nature of harmonics, necessitates the use of statistical techniques in predicting the cumulative harmonic distortion level of power converters in an EPS.

Statistical technique such as the Monte Carlo Simulation (MCS) [10], has been extensively used as a common approach in predicting the harmonic distortion level of power converters [11, 12]. However, it requires tens of thousands of simulations to obtain an accurate prediction and this affects the feasibility of using such approach for systems containing large number of VSCs.

This research work focuses on the impact of VSCs of RES on the power quality of a microgrid. It investigates various factors that can significantly increase or reduce the level of harmonic distortion generated by VSCs with the aim of quantifying and predicting their impact on the PQ of the microgrid. Considering the drawback of the MCS, this research work also seeks to develop an efficient and time saving method that can be employed to predict the PQ in the design, operation and/or management of the microgrid when certain parameters are only known within a given constraint. This technique will give a measure of the VSCs harmonic distortion levels by evaluating if they are within the required harmonic limits as stated by regulatory harmonic standards.

The research work further investigates the statistical nature of these harmonics and proposes some design techniques to minimise these impacts and ensure good PQ on the microgrid. In order to achieve this, typical VSC converters utilized in integrating RES to the grid are simulated with suitable control and protection techniques incorporated into the VSCs and the microgrid to enable continuity of power supply. Multiple RES VSC are connected together to form a microgrid and modelled using MatlabTM Simulink [13] and PlecsTM [14] simulation tools.

1.2 Microgrid Concept and Rationale for Power Quality Investigation

Microgrids, one of the new concepts used in some modern day EPS can be defined as a controllable close assemblage of small generators, storage devices and loads for optimizing the use of renewable and/or alternative generation [3, 15]. Fig. 1.1 illustrates this concept, as it shows renewable energy generators such as wind turbines and photovoltaics, the Combined Heat and Power (CHP) for alternative energy generation, the loads and battery for energy storage.

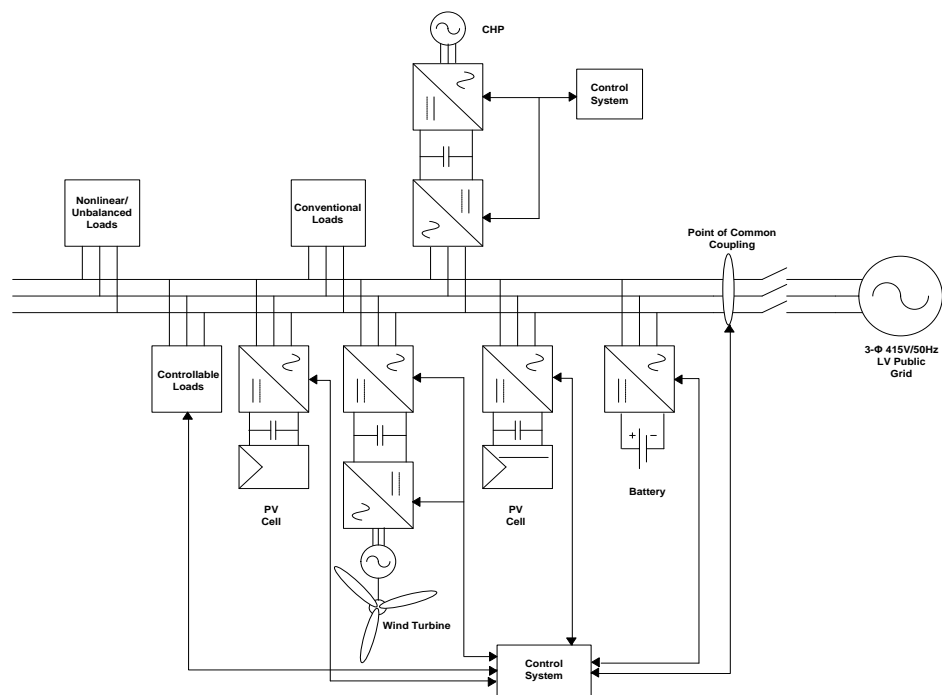


Fig. 1.1: Concept of a Microgrid

An advantage of the microgrid is that it can supply its locality, which may be a small community or an industrial area, by its own small distributed generation plants and can also be used to support the grid's load demand. They are also expected to separate from the grid during faults and other network discrepancies [3, 15].

Suitable operational strategies, control techniques and protection schemes sustain a balance between supply and demand and ensures continuity of supply to its local areas even after being disconnected from the public grid so as to operate in a stand-alone mode also referred to as islanding mode [16].

There have been a large amount of research and studies carried out on various microgrid concepts, the studies have focused on the dynamics of the microgrid, the controllability of the microgrid and its generating units and power quality issues. In terms of the power quality issues, most have focused on the impacts of converters, non-linear loads and unbalanced loads on a microgrid and have hoped to improve the power quality of the microgrid by proposing various control schemes for the converters and the microgrid and various switching techniques for the converters in the microgrid [17-20].

The conventional grid has enjoyed years of growth based on established techniques and for the microgrid to advance rapidly within the future, researchers have to also consolidate on established research utilized in control and operation of real world microgrids to optimise them.

For these reasons this research will look at a realistic microgrid based on tried and proven technology in the interfacing VSC topology, its switching strategy and control techniques, focusing on a model that guarantees good PQ in the microgrid. Investigation and analysis of the power quality of the microgrid will be carried out based on predicting the harmonic distortion level of the converters utilized in a microgrid and the impact of various factors that affect the generated harmonics. This will avail researchers/ design engineers a tool to assess the PQ of a microgrid and design/operate an EPS within certain constraints to ensure good PQ.

1.3 Research Aim

The aim of this research is to develop a fast and accurate technique for predicting and quantifying the harmonic distortion level of many connected VSCs and their impact on the PQ of a microgrid operating under various conditions and design or having different system parameters varying within certain constraints. This technique will give a measure of the power quality in the microgrid in terms of harmonic distortion levels.

1.4 Research Objectives

The main objective of this research work is to develop a method that is fast and accurate for performing probabilistic harmonic studies, such as in predicting and quantifying harmonic distortion levels of many connected VSCs of RES in a microgrid with varying sources and/or systems parameter/load. To achieve this, a technique that avoids the complexities of other analytical probabilistic harmonic methods and that significantly reduces the computation time and burden associated with the Monte Carlo Simulation (MCS) approach while producing comparable level of accuracy to the MCS approach is important.

Other research objectives are as follows:

- i. To develop models of typical VSCs that are utilized in various RES and microgrids using MatlabTM Simulink [13] and PlecsTM simulation tool [14].
- ii. To simulate and study the effects of VSC harmonics on the PQ of a microgrid.
- iii. To investigate the effects of factors such as switching frequency, converter topology, system impedance and other statistical variations on VSC harmonics in relation to the PQ of the microgrid.
- iv. To apply the proposed harmonic prediction technique to a practical microgrid system containing VSCs.
- v. Propose design rules and techniques to minimise the impact of VSC harmonic distortion on the PQ of the microgrid, by evaluating if the VSC harmonic distortions are within the required harmonic limits as stated by regulatory harmonic standards.

1.5 Thesis Outline

This chapter gives an introduction to the research work by discussing the background and motivation for the study. It also presents the thesis aim, objectives and outline.

Chapter 2 gives an overview of power quality and classifications based on the IEEE and IEC standards. It also defines harmonics and discusses how it affects power quality of an electrical power system. This Chapter also gives a

description of the microgrid concept and discusses the rationale for investigating microgrid power quality issues.

Chapter 3 discusses power electronic converters utilized in microgrids and for interfacing RES to the grid. Different configurations of VSCs are presented and the switching patterns of the IGBTs illustrated. The control technique used for the VSCs are also presented.

In Chapter 4, various factors that affect harmonics generated by a VSC are discussed and evaluated. Firstly from the point of the VSC design specification and then from the electrical power systems characteristics and operation. A review of filters and the design adopted for this research work is also given.

Chapter 5 reviews probabilistic harmonic summation as a method employed in predicting/quantifying harmonics generated by many connected harmonic sources in an electrical power system. It also reviews various uncertainty that might arise in a modern EPS. Mathematical terminology and definition of terms used in probabilistic harmonic studies are also given. The concept of the summation of random harmonic vectors/phasors and its limitations is explained. Lastly, probabilistic harmonic methods such as the MCS and the Unscented Transform (UT) are discussed and their performance/limitations evaluated.

Chapter 6 presents the mathematical basis of the UT based on the Gaussian quadrature technique. The estimation of sigma points and weights of random variables are discussed using orthogonal polynomials. The limitation of the tensor product for estimating sigma points and weights for systems with more than one random variable (multivariate problems) is presented. Dimension reduction is employed as a technique to overcome the limitation of the UT tensor product approach in dealing with multivariate problems. Two variants of the dimension reduction technique are presented and the mathematical basis given. The accuracy and speed of the two methods (the univariate and bivariate dimension reduction) are evaluated for an EPS with a varying power source.

Chapter 7 focuses on evaluating the performance of the univariate dimension reduction technique in predicting harmonic distortion levels of the current and voltage of different electrical power system configurations where certain operating/system parameters are known to vary within certain constraints.

Chapter 8 presents the practical results of employing the univariate dimension technique in predicting the harmonic distortion of 3 practical VSCs connected in parallel and having varying operating output power.

Chapter 9 concludes the thesis by discussing and summarizing the results, challenges/limitations faced in conducting the research work. It also provides some potential areas for further studies.

1.6 Research Contributions

The summary of the main contributions of this research work are as follows;

- i. The identification of the characteristic responses of various factors that affects the harmonics generated by VSCs in a microgrid/EPS.
- ii. The application of the Unscented Transform method in predicting VSC harmonic distortion level.
- iii. The application of the univariate and bivariate dimensionally reduced Unscented Transform in predicting harmonic distortion levels of many connected VSCs in a microgrid/ EPS.
- iv. The application of a probabilistic harmonic summation method that can accommodate realistic microgrids/EPS without assumptions to simplify the microgrid/EPS. (The studied harmonic sources (VSCs) have full interactions with each other and the EPS, reflective of a realistic EPS.)
- v. The application of a probabilistic harmonic summation method that gives accurate and fast prediction of harmonic distortion levels of VSCs in a microgrid/EPS.

1.7 Research Publications

- 1) P. M. Ivry, O. A. Oke, D. W. P. Thomas, and M. Sumner, "Predicting Conducted Emissions of Multiple VSCs Using Dimension Reduction Technique," *presented at the IEEE EMC/EMC Europe International Symposium, Dresden, August 2015.*
- 2) P. M. Ivry, O. A. Oke, D. W. P. Thomas, and M. Sumner, "Method of Efficiently Predicting the Conducted Emissions of Multiple VSCs," *presented at the IEEE EMC Europe International Symposium, Gothenburg, pp. 65-68, September 2014.*
- 3) P. M. Ivry, O. A. Oke, D. W. P. Thomas, and M. Sumner, "Predicting Harmonic Distortion Level of a Voltage Source Converter at the PCC of a Grid," *2nd International Symposium on Energy Challenges and Mechanics, Aberdeen, August 2014.*
- 4) P. M. Ivry, M. J. Rawa, D. W. P. Thomas, and M. Sumner, "Power Quality of a Voltage Source Converter in a Smart Grid," *presented at the IEEE PowerTech Conference, Grenoble, pp. 1-6, June 2013.*
- 5) P. M. Ivry, M. J. Rawa, and D. W. P. Thomas, "Factors Affecting the Harmonics Generated by a Generic Voltage Source Converter within a Microgrid," *presented at the Saudi Arabia Smart Grid Conference, Jeddah, December 2012.*

Chapter 2

Power Quality of a Microgrid

This chapter highlights various standards used in classifying power quality and discusses the link between power quality and harmonics in an electric power system. It also presents the rationale for investigating power quality in a microgrid in terms of harmonic distortion level.

2.1 Power Quality

Power quality is a term that has different definitions depending on the authors frame of reference [8, 21, 22]. Various authors relate power quality to voltage quality, current quality, supply quality, service quality, quality of consumption [21] and some utility defines power quality as the reliability of its system [8].

The IEEE Standard -1100 [23] defines power quality as “the concept of powering and grounding electronic equipment in a manner that is suitable to the operation of that equipment and compatible with the premise wiring system and other connected equipment”. This description appears appropriate, however; it limits power quality to only electronic equipment. Power quality problems affects, and are detrimental to all electrical devices and systems [22, 24, 25]. This includes electric generators and motors, transformers, communication equipment or household devices.

In technical engineering terms, electrical power is defined as the rate of energy delivered and it is proportional to the product of the voltage and current [8]. Meaning power quality can be seen as the quality of the voltage and/or the quality of current in an electrical network. Therefore, given the different definitions in books, articles and papers in the area of electric power quality, the following power quality definition would be used in this thesis:

Power quality is the measurement, analysis, and improvement of an electrical network’s voltage, current and frequency to maintain a sinusoidal waveform at rated values and frequency that results in the proper operation of all electrical

devices on the electric network. This definition takes into account all steady state and momentary phenomena.

2.1.1 Classification of Power Quality Issues

Power quality issues have been classified in various forms using specific properties. This has been done to better understand and solve different power quality problems. Table 2.1 and Table 2.2 are defined by the IEEE and IEC respectively. They present various classifications of power quality problems using the duration of the event, the magnitude and frequency range of the signal waveform.

Table 2.1: Categories and Typical Characteristics of Power System Electromagnetic Phenomena as defined by IEEE Standard -1159 [26].

Categories	Typical spectral content	Typical duration	Typical voltage magnitude
1.0 Transients			
1.1 Impulsive			
1.1.1 Nanosecond	5 ns rise	<50 ns	
1.1.2 Microsecond	1 μ s rise	50 ns-1 ms	
1.1.3 Millisecond	0.1 ms rise	>1 ms	
1.2 Oscillatory			
1.2.1 Low frequency	<5 kHz	0.3-50 ms	0-4 pu
1.2.2 Medium frequency	5-500 kHz	20 μ s	0-8 pu
1.2.3 High frequency	0.5-5 MHz	5 μ s	0-4 pu
2.0 Short-duration root-mean-square (rms) variation			
2.1 Instantaneous			
2.1.1 Sag		0.5-30 cycles	0.1-0.9 pu
2.1.2 Swell		0.5-30 cycles	1.1-1.8 pu
2.2 Momentary			
2.2.1 Interruption		0.5 cycle-3 s	<0.1 pu
2.2.2 Sag		30 cycles-3 s	0.1-0.9 pu
2.2.3 Swell		30 cycles-3 s	1.1-1.4 pu
2.3 Temporary			
2.3.1 Interruption		>3 s-1 min	<0.1 pu
2.3.2 Sag		>3 s-1 min	0.1-0.9 pu
2.3.3 Swell		>3 s-1 min	1.1-1.2 pu

3.0 Long duration rms variation			
3.1 Interruptions, sustained		>1 min	<0.0 pu
3.2 Undervoltage		>1 min	0.1-0.9 pu
3.3 Overvoltage		>1 min	1.1-1.2 pu
3.4 Current overload		>1 min	
4.0 Imbalance			
4.1 Voltage		steady state	0.5-2%
4.2 Current		steady state	1.0-30%
5.0 Waveform Distortion			
5.1 DC offset		steady state	0-0.1%
5.2 Harmonics	0-9 kHz	steady state	0-20%
5.3 Interharmonics	0-9 kHz	steady state	0-2%
5.4 Notching		steady state	
5.5 Noise	broadband	steady state	0-1%
6.0 Voltage fluctuation	<25 kHz	intermittent	0.1-7% 0.2-2P _{st} *
7.0 Power frequency variation		<10 s	±0.10Hz

* P_{st} refers to Flicker severity index

Table 2.2: Main Phenomena Causing Electromagnetic Disturbances as Classified by the IEC [27].

Categories
1.0 Conducted low-frequency phenomena
1.1 Harmonics, interharmonics
1.2 Signalling systems
1.3 Voltage fluctuation
1.4 Voltage unbalance
1.5 Power frequency variations
1.6 Induced low-frequency voltages
1.7 DC in AC networks
2.0 Radiated low-frequency field phenomena
2.1 Magnetic fields
2.1.1 continuous
2.1.2 transient
2.2 Electric fields
3.0 Conducted high-frequency phenomena
3.1 Directly coupled or induced voltages or currents
3.1.1 continuous wave
3.1.2 modulated waves
3.2 Unidirectional transients*
3.3 Oscillatory transients*
* Single or repetitive (bursts)

4.0 Radiated high-frequency field phenomena
4.1 Magnetic fields
4.2 Electric fields
4.3 Electromagnetic fields
4.3.1 continuous wave
4.3.2 modulated waves
4.3.3 transients
5.0 Electrostatic discharge phenomena (ESD)
6.0 High-altitude nuclear electromagnetic pulse (HEMP)

2.2 Harmonic Generation in an Electric Power System

The modern Electric Power System (EPS) contains a significant number of non-linear devices and systems that generate harmonics when in operation. Some of these harmonic sources include, but are not limited to; power electronic converters of RES, non-linear loads, computers, fluorescent lighting, arcing devices and adjustable speed drives. Section 2.2.1 introduces harmonics and gives the fundamental indices used in quantifying harmonics on an electric power system.

2.2.1 Harmonics

In the early 1800s, the French mathematician Jean Baptiste Fourier formulated that a periodic non-sinusoidal function of a fundamental frequency may be expressed as the sum of sinusoidal functions of frequencies which are integer multiples of the fundamental frequency [22]. This can be expressed as in (2.1) [28, 29] where a generic periodic function $f(t)$ with a period $T = 2\pi$ is defined within the interval $0 \leq t \leq 2\pi$ [28-30];

$$\begin{aligned}
 f(t) &= \frac{a_0}{2} + a_1 \cos(\omega t) + b_1 \sin(\omega t) + \dots \\
 &+ a_2 \cos(2\omega t) + b_2 \sin(2\omega t) + \dots \\
 &+ a_n \cos(n\omega t) + b_n \sin(n\omega t) + \dots
 \end{aligned} \tag{2.1}$$

$$f(t) = \frac{a_0}{2} + \sum_{n=1}^{\infty} a_n \cos(n\omega t) + \sum_{n=1}^{\infty} b_n \sin(n\omega t) \tag{2.2}$$

$$f(t) = \frac{a_0}{2} + \sum_{n=1}^{\infty} c_n \sin(n\omega t + \phi_n) \quad (2.3)$$

alternatively [28, 30];

$$f(t) = \frac{a_0}{2} + \sum_{n=1}^{\infty} c_n \sin\left(\frac{2n\pi t}{T} + \phi_n\right) \quad (2.4)$$

where [28-30];

$$a_0 = \frac{\omega}{\pi} \int_0^{2\pi/\omega} f(t) dt = \frac{2}{T} \int_0^T f(t) dt \quad (2.5)$$

$$a_n = \frac{\omega}{\pi} \int_0^{2\pi/\omega} f(t) \cos n\omega t dt = \frac{2}{T} \int_0^T f(t) \cos \frac{2n\pi t}{T} dt \quad (2.6)$$

$$b_n = \frac{\omega}{\pi} \int_0^{2\pi/\omega} f(t) \sin n\omega t dt = \frac{2}{T} \int_0^T f(t) \sin \frac{2n\pi t}{T} dt \quad (2.7)$$

$$c_n = \sqrt{a_n^2 + b_n^2} \quad (2.8)$$

$$\phi_n = \arctg(a_n + jb_n) \quad (2.9)$$

a_0 is the dc component of the function, a_n and b_n are constants called the Fourier series coefficients, n is an integer number from 1 to infinity, c_n is the magnitude of a_n and b_n , ϕ_n is the angle between a_n and b_n [28-30].

The periodic function that is of concern to this research is that of voltages and currents and this is due to their importance in analysing power quality. When a periodic voltage/current waveform is deconstructed into a sinusoid at the fundamental frequency the other sinusoidal functions present at frequencies that are multiples of the fundamental frequency are referred to as harmonics. Based on the IEEE Standard -519 [31], a ‘‘Harmonic’’ is defined as a sinusoidal component of a periodic wave having a frequency that is an integer multiple of the fundamental frequency [31]. This definition by [31] was tailored specifically to the harmonics generated by static electronic power converters at utility system frequencies. An AC periodic voltage or current can be represented by a Fourier series of pure sinusoidal waves which contain the fundamental frequency and its multiples called harmonics [31, 32].

A sinusoidal voltage or current waveform as shown in Fig. 2.1, that is time dependent can be represented by (2.10) and (2.11) respectively [22]. In (2.11) the current waveform can either lead (+) or lag (-) the voltage waveform by a certain angle (ϕ), known as the difference in the phase angle between the waveforms. In Fig. 2.1 the current waveform lags the voltage waveform.

$$v(t) = V \sin(\omega t) \quad (2.10)$$

$$i(t) = I \sin(\omega t \pm \phi) \quad (2.11)$$

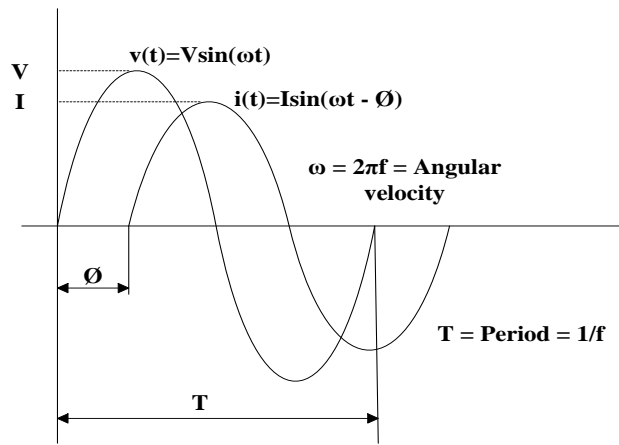


Fig. 2.1: Sinusoidal Voltage and Current Waveform

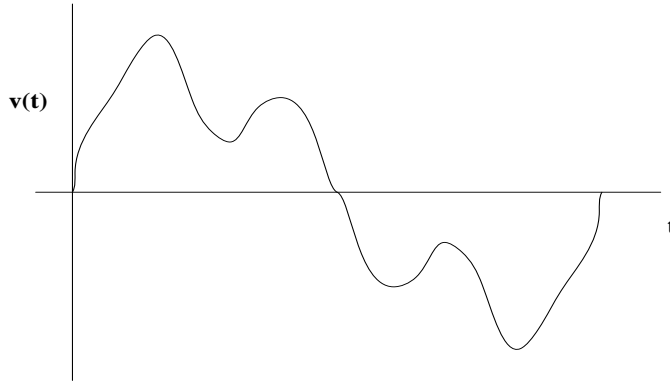


Fig. 2.2: Non-Sinusoidal Voltage Waveform

Using Fourier representation a periodic non-sinusoidal voltage waveform as shown in Fig. 2.2 can be represented in a simplified form as (2.12) [22]:

$$v(t) = V_0 + V_1 \sin(\omega t \pm \alpha_1) + V_2 \sin(2\omega t \pm \alpha_2) + V_3 \sin(3\omega t \pm \alpha_3) + \dots \\ + V_n \sin(n\omega t \pm \alpha_n) + V_{n+1} \sin((n+1)\omega t \pm \alpha_{n+1}) + \dots \quad (2.12)$$

In (2.12), V_0 represent the DC component of the waveform, while V_1, V_2, V_3 and V_n are the peak values of the successive terms of the expression having $\alpha_1, \alpha_2, \alpha_3$ and α_n as their corresponding harmonic angles. These terms are referred to as the harmonics of the periodic waveform $v(t)$ [22]. However, V_1 is the first harmonic (fundamental) amplitude at the first harmonic (fundamental) frequency f .

Voltage/current harmonics are sometimes caused by non-linear loads such as television, fluorescent lighting, computers, office equipment, transformer saturation, arc furnaces, motor control and non-linear systems such as RES interfacing converter, switch mode power supplies [22, 32]. As can be seen, some of these sources of harmonics are sometimes caused by the utility provider or by the consumer load.

The consequences that arise from harmonics include; Transformer overheating, which reduces its life span and rating, nuisance tripping of residual current circuit breakers, tripping of sensitive equipment like medical monitors, overstressing of power factor correction capacitors, increased losses in motors resulting in reduce power output, increased heating in motors which reduces its life span and interference in devices that uses power line carrier signals like telephone, synchronised clocks and control modules [8, 32, 33]. Going by the definition of power quality in section 2.1 and the consequences of harmonics mentioned in this section, it is clear that harmonics negatively impact the proper operation of devices on an EPS and hence the power quality of the EPS.

2.2.2 Common Terms used in Analysing Harmonics

Harmonic Distortion refers to the distortion factor of a voltage or current waveform with respect to a pure sine wave [32].

Interharmonics refers to a frequency component of a periodic quantity that is not an integer multiple of the frequency at which the supply system is operating [32].

Individual Harmonic Distortion (IHD_n) is the ratio between the Root Mean Square (RMS) of the individual harmonic current/voltage and the RMS value of the fundamental component of the current/voltage (2.13) [22, 31, 32].

$$IHD_n = \frac{V_n}{V_1} \quad (2.13)$$

where, V_n is the RMS individual harmonic voltage component and V_1 is the RMS fundamental component of the voltage.

Distortion Factor (Harmonic factor) is defined as the ratio of the sum of the root mean square of the harmonic component of the current/voltage to the root mean square of the fundamental component of the current/voltage, expressed as a percentage [22, 31, 32]. It is also referred to as the **Total Harmonic Distortion (THD)** as in the case of this thesis. It can be described as the degree by which an input quantity is distorted, and is the ratio of all the harmonics combined, as a percentage of the fundamental component of the input quantity (2.16) [33].

$$THD = \frac{V_H}{V_1} \quad (2.14)$$

where V_H is

$$V_H = \sqrt{(V_2^2 + V_3^2 + V_4^2 + V_5^2 \dots)} = \sqrt{\sum_{h>1}^{h_{\max}} V_h^2} \quad (2.15)$$

THD can be written in percentage as

$$THD = \frac{\sqrt{\sum_{h>1}^{h_{\max}} V_h^2}}{V_1} \times 100\% \quad (2.16)$$

In [34], THD is defined as “the ratio of the root mean square of the harmonic content, considering harmonic components up to the 50th order and specifically excluding interharmonics, expressed as a percent of the fundamental”. It was further stated in [34] that “harmonic components of order greater than 50 may be included when necessary”. Based on the definition by [34] THD can be expressed as in (2.17).

$$THD = \frac{\sqrt{\sum_{h>1}^{h_{50}} V_h^2}}{V_1} \times 100\% \quad (2.17)$$

Another indices commonly used in [31] and [34] to specifically quantify current harmonics is the **Total Demand Distortion (TDD)**. It is defined in [34] as “the ratio of the root mean square of the harmonic content, considering harmonic components up to the 50th order and specifically excluding interharmonics,

expressed as a percent of the maximum demand current. Harmonic components of order greater than 50 may be included when necessary”.

$$TDD = \frac{\sqrt{\sum_{h>1}^{h_{50}} I_h^2}}{I_{D_max}} \times 100\% \quad (2.18)$$

where I_{D_max} , is the maximum demand current

2.2.3 Types and Sources of Harmonic in an Electric Power System

Harmonics are further classified as listed in Table 2.3.

Table 2.3: Types of harmonics and their corresponding sources [21].

Type of Harmonic	Sources of Harmonic
DC	Electronic switching devices, half-wave rectifiers, arc furnaces (with random arcs), geomagnetic induced currents (GICs)
Odd harmonics	Non-linear loads and devices
Even harmonics	Half wave rectifiers, geomagnetic induced currents (GICs)
Triplen harmonics	Unbalanced three-phase load, electronic switching devices
Positive sequence harmonics Negative sequence harmonics Zero sequence harmonics	Operation of power system with non-linear loads Operation of power system with non-linear loads Unbalanced operation of power system or a balanced 3-phase 4-wire system with a single phase non-linear load connected phase to neutral [35]
Time harmonics	Voltage and current source inverters, pulse-width modulated rectifiers, switch-mode rectifiers and inverters
Spatial harmonics	Induction machines
Interharmonics	Static frequency converters, cycloconverters, induction machines, arcing devices, computers
Subharmonics	Fast control of power supplies, subsynchronous resonances, large capacitor banks in highly inductive systems, induction machines

Characteristic harmonics	Rectifiers, inverters
Uncharacteristic harmonics	Weak and unsymmetrical AC systems

From the classification of harmonic sources given above in Table 2.3, it is clear that majority of the harmonics on the electric power system are caused by non-linear loads and devices. This includes rectifiers, inverters, converters and other electronic switching devices.

2.2.4 IEEE Standard for Harmonics on an Electric Power System

The most common harmonic standard used in the research community for power quality limits is the IEEE 519 harmonic standards. The IEEE 519 is the IEEE recommended practices and requirements for harmonic control in electric power systems. Table 2.4 and Table 2.5 show the revised IEEE-Standard 519 [34] harmonic limits on current and voltage harmonics distortion measured at the PCC of an EPS.

Table 2.4: Current Distortion Limit for Systems rated 120V through 69kV

Maximum harmonic current distortion in percent of I_L						
Individual harmonic order (Odd harmonics) ^{a, b}						
I_{SC}/I_L	$3 \leq h < 11$	$11 \leq h < 17$	$17 \leq h < 23$	$23 \leq h < 35$	$35 \leq h$	TDD
$< 20^c$	4.0	2.0	1.5	0.6	0.3	5.0
20<50	7.0	3.5	2.5	1.0	0.5	8.0
50<100	10.0	4.5	4.0	1.5	0.7	12.0
100<1000	12.0	5.5	5.0	2.0	1.0	15.0
>1000	15.0	7.0	6.0	2.5	1.4	20.0

^aEven harmonics are limited to 25% of the odd harmonic limits above

^bCurrent distortions that results in a dc offset, e.g., half-wave converters, are not allowed

^cAll power generation equipment is limited to these values of current distortion regardless of actual I_{SC}/I_L

where

I_{SC} = maximum short circuit current at PCC

I_L = maximum demand load current (fundamental frequency component) at the PCC under normal operating conditions

Table 2.5: Voltage Distortion Limits.

Bus voltage V at PCC	Individual harmonic (%)	Total harmonic distortion THD (%)
$V \leq 1.0$ kV	5.0	8.0
1 kV $< V \leq 69$ kV	3.0	5.0
69 kV $< V \leq 161$ kV	1.5	2.5
161 kV $< V$	1.0	1.5 ^a

^aHigh-voltage systems can have up to 2.0% THD where the cause is an HVDC terminal whose effects will have attenuated at points in the network where future users may be connected.

2.3 The Microgrid Concept

The microgrid concept was originally introduced to handle critical loads and improve reliability for specific customers. Presently, the microgrid can be installed to improve electrical power systems reliability, provide better load dispatch, regulate variable generation, and control energy costs [36]. The microgrid has been defined in various ways by most principal electrical regulatory organisations, boards and standards.

However, the most adopted definition was given by the United States Department of Energy (U.S. DOE) Microgrid Exchange Group. The US DOE defined the microgrid as a group of interconnected loads and Distributed Energy Resources (DER) within clearly defined electrical boundaries that acts as a single controllable entity with respect to the grid and that connects and disconnects from such grid to enable it to operate in both grid-connected or island mode [36-38].

The *CIGRÉ C 6.22 Working Group: Microgrids Evolution Roadmap*, defined (in draft) the microgrid as “electricity distribution systems containing loads and DERs, (such as distributed generators, storage devices, or controllable loads) that can be operated in a controlled, coordinated way either while connected to the main power network or while islanded” [37].

The IEEE refers to the microgrid as a Distributed Resource (DR) island system in IEEE Standard -1547.4 [39, 40]. It defined the DR island systems (microgrids)

in [39] as follows: “DR island systems are parts of Electric Power Systems (EPSs) that have DR and load, have the ability to disconnect from and parallel with the area EPS, include the local EPS and may include portions of the area EPS, and are intentional and planned” [39].

Certain recurring terms can be deduced from these definitions, they include;

- DR/DER which refers to small alternative or renewable power generation, loads and storage devices located close to the point of energy consumption [41].
- Coordinated control of the connection and disconnection from the grid, DER, loads, and storage devices.
- Ability to connect to the grid (grid-tie mode) and disconnect from the grid (Island mode)
- A separate part of the EPS with defined electrical boundaries that can enable it to operate as a single electrical entity.

From these points, the following definition is adopted for this thesis:

Microgrids can be defined as a coordinated controlled close assemblage of small DER generators, storage devices and loads for optimizing the use of renewable/alternative energy generation while connected or disconnected from the main electrical power network (grid).

This definition was chosen to highlight the importance of RES in achieving one major objectives of the microgrid concept which is; grid integration of RES. This is a key distinguishing feature of microgrids from other EPS [42].

One of the earliest research on the concept of a microgrid was carried out by R.H. Lasseter in [3] and it was later called the Consortium for Electric Reliability Technology Solutions (CERTS) Microgrid [43]. The CERTS microgrid was presented as an entirely new approach for integrating small scale DER into the electric distribution network. According to the white paper on the CERTS microgrid concept [43], “The CERTS microgrid concept assumes an aggregate of loads and microsources operating as a single system providing both power and heat. The majority of the microsources must be power electronic based to provide the required flexibility to ensure operation as a single aggregated system.

This control flexibility allows the CERTS Microgrid to present itself to the bulk power system as a single controlled unit that meets local needs for reliability and security”. The CERTS microgrid consisted of power electronic converter interfaced DER systems comprising of Combined Heat and Power (CHPs), storage devices, alternative power sources with the possibility of RES (such as photovoltaic and wind turbines) that utilizes power electronic converter. [44, 45]. Barnes et al. [46], within the frame of the European project “Microgrids” proposed a system containing DERs that are solely based on RES. The studied microgrid consisted of a small wind turbine system, two PV generators, battery energy storage, controllable loads and a controllable interconnection to the local low voltage grid [44, 46]. There are many other microgrid concepts that have been proposed and some are now operational [45]. Some studies carried out on various microgrid concepts, that have investigated the dynamics, controllability and power quality issues associated with the microgrid generating units and grid interfacing DER power converters will be briefly described so as to establish common grounds and rationale for further research.

2.4 Rationale for Investigating Microgrid Power Quality Issues

Over the years, the power quality of a microgrid as affected by power converters has been analysed in various forms and the analysis depends on the type of power converter topology involved, the converter switching technique, the type of control scheme utilized, and the condition of its operation [17].

In [3], R.H. Lasseter proposed a microgrid with converter interfaced DER systems comprising of both renewable and alternative power sources that the converters are controlled using PI controllers and P-f (real power-frequency droop) and V-Q (Voltage magnitude-reactive power) droop control line [3, 16, 45]. The control techniques were proposed so as to ensure the microgrid control, protection and energy management.

So as to mitigate the power quality issues introduced on a microgrid by non-linear loads and power converters of DERs, H. Jinwei et al. [18], proposed a

flexible harmonic control that does not require a harmonic current tracking loop and is based solely on the voltage control of the grid interfacing converters. It was stated by the authors that the harmonic control technique can be easily incorporated into a voltage controlled DER unit to provide direct voltage and frequency support in a microgrid. This was considered for possible autonomous islanding operations of the microgrid [18]. The load sharing in the voltage control method is achieved by V-f droop control (real power-frequency droop and reactive power-voltage magnitude droop). In order to overcome the limitation of not being able to use traditional filters as in the case of a current control scheme, the authors proposed a novel voltage control mode based harmonic control method. Although, it was observed that the voltage control method can only achieve a similar compensation performance and not more as compared to the traditional current control mode method in the mitigation of harmonics [18].

A. J. Roscoe et al. [17], studied the trade-off between the dc bus ripple and the power quality of a grid side converter within a microgrid under four different control schemes. The authors further studied the grid interfacing inverter at different microgrid scenario and grid impedance to establish the power quality of the microgrid. They discovered that voltage driven mode provides the best ac power quality, but at the expense of high dc bus ripple. Sinusoidal current generation and dual sequence controller provides relatively low dc bus ripple and relatively small effects on power quality. Four different control modes for a standard 6-switch 2 level IGBT bridge of 10kVA was investigated [17]. It was discovered that high bandwidth dc bus ripple minimization technique works well in environments of low grid impedance, but is highly unsuitable within higher impedance microgrid environments and/or at low switching frequencies [17]. The authors defined an improved power quality in the microgrid by reduced harmonic levels and unbalance voltage at the PCC. This reduction was achieved by the control technique utilized; high bandwidth dc bus ripple minimization [17].

T. Hornik and Q-C. Zhong [19], proposed a current control technique with the objective of injecting pure sinusoidal current into the grid. The controller is also

required to meet its objective under unbalanced/non-linear loads and/or grid voltage distortions. The main focus of the work was harmonic distortions and the tracking performance of the controller. By utilizing a frequency adaptive mechanism the controller maintained a very good tracking performance over a wider range of frequencies resulting in the improvement of the power quality and current THD [19]. The controller has an internal model and a compensator for stability, designed by utilizing the H^∞ repetitive control theory. The controller was further compared with the PI controller, PR controller and the Predictive Dead Beat controller (PDB). The performance of the controller was demonstrated under steady state and transients' states and it was discovered that in terms of the THD level it performs better than other traditional control techniques studied such as the PI, PR and PDB controller. It provides a very low THD for the current output but it has a slower dynamic response [19]. The authors were very clear that the work only looked at the grid connected VSC but assumed a constant DC voltage source hence; no controller was provided for the DC Voltage. In a real system, the DC voltage would have a controller, especially if it is a back-to-back VSC converter used in a wind farm or that of a VSC HVDC link as the voltage across the DC link capacitor would have to be regulated.

So far the literature review has been on the harmonics generated by VSC converters on a microgrid, how it affects the AC power quality of the microgrid and various control strategy to improve the power quality. The converters are not the only factor that affects the AC power quality of a microgrid; there are also lots of single phase loads on a microgrid as it is basically a distribution network with interconnected sources and loads. These loads have been known to cause voltage unbalance and impedance variation which also affects the AC power quality of the microgrid.

M. Griffiths and C. Coates [47], presented a microgrid system that comprises of the grid side of a converter; probably that of a photovoltaic cell, fuel cell or a DC wind farm. The control technique utilized was a P-f/Q-V droop type controller. Unbalanced loads were introduced upon a low voltage distribution network acting as the microgrid, and it was observed that this gives rise to significant unbalanced voltages in the system. The droop controller attempts to

eliminate the negative sequence components of the load voltage thereby reducing the imbalance. The imbalances can also lead to low frequency harmonics in non-linear loads, although the controller achieved a reduction in the imbalance, the deviation of the voltage frequency affects the droop controller performance [47].

S. Kusagawa et al. [20], investigated a microgrid consisting of a grid side converter of a distributed energy generator and a synchronous generator employing a coordinated control scheme between the grid side converter and the synchronous generator. The control was as to maintain stable power system operation and improve the power quality of the microgrid. A hybrid control based on automatic voltage regulation (AVR), active and reactive power control of the inverter was proposed and the synchronous generator (SG) was controlled with the AVR and the governor control [20]. During load fluctuations the grid side converter autonomously supplies the active and reactive power to regulate the grid. It was stated that when non-linear loads were connected, harmonics components and high frequency components are absorbed by the grid side converter and the low frequency components are absorbed by the SG [20]. Although the authors did not go further to tell exactly how their hybrid controller achieves this, they stated that harmonic components should be suppressed in the microgrid so as not to affect the public grid and other loads. The control scheme, however, proved that each DG can be autonomously regulated so as to provide more freedom to a microgrid and hence to support the public grid [20].

U. Borup et al. [48], proposed a control based on the concept of linear load sharing by droop controllers. The harmonic controllers are applied to provide harmonic load sharing which were caused by non-linear loads. The converters were connected in parallel and they didn't require any communication to achieve the sharing of the harmonic load current. This was for a diode bridge converter [48]. The authors also stated that small scale distribution systems contains a significant number of single phase loads, unbalanced loads and non-linear loads making up a high proportion of the total system load and the power quality assessment was mainly based on the total harmonic distortion (THD) in voltages and current [48].

It is clear that majority of the authors in the discussed literatures are aware of the challenges and problems of the microgrid. They have focused on the effects of converters, unbalanced loads and non-linear loads/systems on a microgrid with the aim to improve the microgrid power quality by proposing several control techniques for the converters and the microgrid.

As earlier stated in section 1.2, the conventional grid has enjoyed years of continuous progress based on tried and proven technology from established research. More so, the advancement of the microgrid in the nearest future requires research collaboration and consolidation on established research presently utilized in the control and operation of real world microgrids by optimizing them while others continue to propose control techniques which might be realized sometime in the future.

Hence, this study looks at a realistic microgrid based on tried and proven technology in the RES interfacing power electronic converter topology, the switching method, control schemes then focusing on the improvement of the microgrid power quality. Investigation and analysis of the power quality of the microgrid will be carried out based on the impact of various factors that affect the generated harmonics of power electronic converters and non-linear loads in a microgrid. It will further proffer a method that can be used to efficiently predict the level of current/voltage harmonic distortion of many DER converters in a microgrid. As an efficient prediction of harmonics will give a better understanding of the effects of power electronic converters in a microgrid, enabling design engineers to attenuate the harmonics and improve the overall power quality of the microgrid.

2.5 Summary

Power quality is clearly defined and the relationship between power quality and harmonics were stated in this chapter. Various sources of harmonics were given and power electronic converters was stated as a very common source of harmonics in modern day electric power systems (EPS). These harmonics affect power quality and are detrimental to the power system and other electrical equipment on the EPS.

As modern EPS including the microgrid rely mostly on power electronic converters for proper control of renewable energy generated by wind turbines and photovoltaics to the grid. It becomes necessary to investigate the power quality of the microgrid.

Various literatures including some applicable standards like the IEEE 519 standard on harmonic limits and the IEEE 1159 standard for categorizing power quality issues was reviewed in this chapter to give a foundation and justify the study on harmonics generated by power electronic converters in a microgrid and how this affects the power quality in the microgrid.

Chapter 3

Power Electronic Converters

This chapter investigates different classification of power electronic converters focusing mainly on Voltage Source Converters (VSCs). It presents different VSC topology and the corresponding switching pattern of the VSC gates. The chapter concludes by stating the control technique utilized for the proper operation of the VSC.

3.1 DER Interfacing Converter in a Microgrid

A power electronic converter can be said to be a power circuit which is realized by the configuration of various semiconductor power switches (like thyristors, IGBTs) and passive components (like resistors, capacitors) sometimes containing control and protection system [4].

Present day power electronic converter utilizes controllable switching devices in the conversion of electrical power from ac to dc and vice versa. Some of these switching devices are the Gate Turn-off Thyristors (GTOs), Integrated Gate Commutated Thyristors (IGCTs), Metal-Oxide Semiconductor Field Effect Transistors (MOSFETs) and Insulated Gate Bipolar Transistors (IGBTs) [4]. The IGBTs and MOSFETs are fully controllable reverse conducting switches utilized in Voltage Source Converters (VSC), they also have the ability to switch at very high frequencies (1-100 kHz) [4, 49]. The IGBT has enjoyed more use in VSC converters technology as against the MOSFETs because it has higher electrical capabilities [49]. The traditional Line Commutated Converters (LCC) which are usually current source converters, utilizes thyristors that are slow switching device with limited control [4, 49].

Power electronic converters have been utilized in various power system applications; including Flexible AC Transmission System (FACTS), Electrical Motors and Drives, High Voltage Direct Current (HVDC) links, Smart-Grids, Micro-Grids and Distributed Energy Resource (DER) systems [50]. The application of VSC converters in DER systems helps in the control of real and

reactive power to the grid [4], it also provides other ancillary services like power factor compensation, flicker mitigation, voltage support, harmonic compensation, and compensation of voltage imbalance [18].

The mode of operation and main differences between a current source converter and a voltage source converter will be discussed in the following sections.

3.2 Current Source Converters (CSCs)

A current source converter is defined in [4] as a converter that retains the same DC side current polarity, and the polarity of the DC side voltage determines the direction of the average power flow through the converter. The DC side input appears as a DC current to the converter [5]. A large inductor used to regulate current ripple is generally connected in series to the DC side of the CSC. This makes the CSC appear more as a current source [4].

CSCs are usually operated as a Line (naturally) Commutated Converter (LCC). For the LCC, the electrical system controls the process of commutation, whereby the reversal of the AC voltage polarity initiates the commutation process [4]. An example of a line commutated CSC is the traditional six-pulse thyristor bridge converter as seen in Fig. 3.1. CSCs are currently employed mostly for very high power ac motor drives and this is due mostly to the availability of controllable switches (such as IGBTs) in ever-increasing power ratings [5].

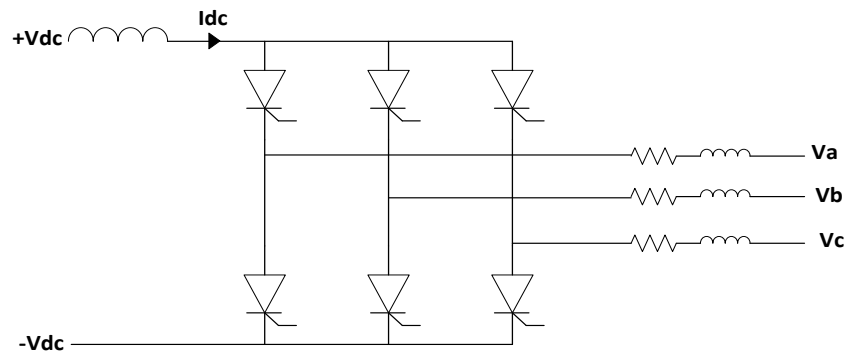


Fig. 3.1: Basic Configuration of a Three Phase 2-Level CSC

3.3 Voltage Source Converters (VSCs)

The VSC is a converter that retains the same polarity of the DC side voltage, and the polarity of the DC side current determines the direction of the average power

flow in the converter [4]. A relatively large capacitor is generally connected to the DC side terminal of the VSC so that it appears as a voltage source [4].

The VSC is usually a force commutated converter. This implies that the commutation process is triggered by the flow of current from one switch to another in a controllable manner [4]. The VSC forced commutation therefore requires fully controllable switching devices with gate turn-on and turn-off capability. In the unavailability of a switch with turn-off capability, the turn-off process can then be achieved using auxiliary capacitors or switches to serve as an auxiliary turn-off circuitry [4]. Forced commutated converters that exploit switches with gate turn-on and turn-off capability are referred to as self-commutated converters.

A CSC can also be made to achieve forced commutation if the characteristics of commercially available bipolar switches such as GTOs and IGCTs are exploited. However, they are limited in operating with a switching frequency below 1kHz making them useful for mainly very high power applications [4].

The VSC makes use of reverse conducting switches or switch cells like the IGBTs or reverse conducting IGCTs [4]. Some of the advantages of the VSC technology include; self-commutation which enables operation without an external voltage source, independent control of active and reactive power flow in the system [51]. These features make the VSC technology attractive for interconnecting RES systems such as wind turbines, as the systems AC voltage at either ends can be controlled and power can be transmitted to the wind farm at time of little or no wind [51]. In HVDC links, the VSC terminal does not require the control of reactive power by shunt/series compensators in form of capacitors or FACTS which are very bulky. These compensators are also required in a LCC (CSC) HVDC as switchable AC harmonic filters. This makes VSC based HVDC stations relatively compact [51].

There are various types of VSC converters configuration utilized in a microgrid but the 2-level topology and 3-level topology are the most commonly used in small and medium distribution systems [50, 52].

3.3.1 Two (2) Level VSC Topology

The 2-level topology is the basic circuit topology for a voltage source converter and Fig. 3.2 below shows a three-phase 2-level VSC [4, 5], it consists of 6 IGBT switches each having an anti-parallel diode. It is referred to as a 2-level VSC for it assumes either $-V_{dc}$ or $+V_{dc}$ at each of its AC voltage terminal (see Fig. 3.4). Fig. 3.4 shows the 2-level voltage of the VSC on phase 'a' ($+V_{dc}$ and $-V_{dc}$). Each of the voltage terminals are connected to a phase of the AC system through a reactor [4]. It also provides a bidirectional power flow between the DC and the AC side. The switching of the IGBTs is achieved by pulse width modulating signals [4, 5, 53]. Fig. 3.3 shows the simulated three phase 2-level VSC using Plects.

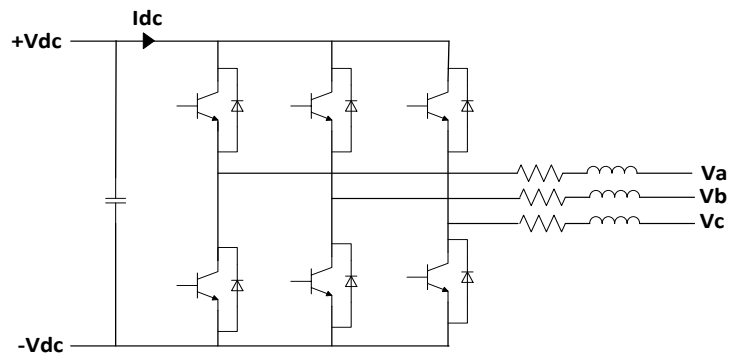


Fig. 3.2: Basic Configuration of a Three Phase 2-Level VSC

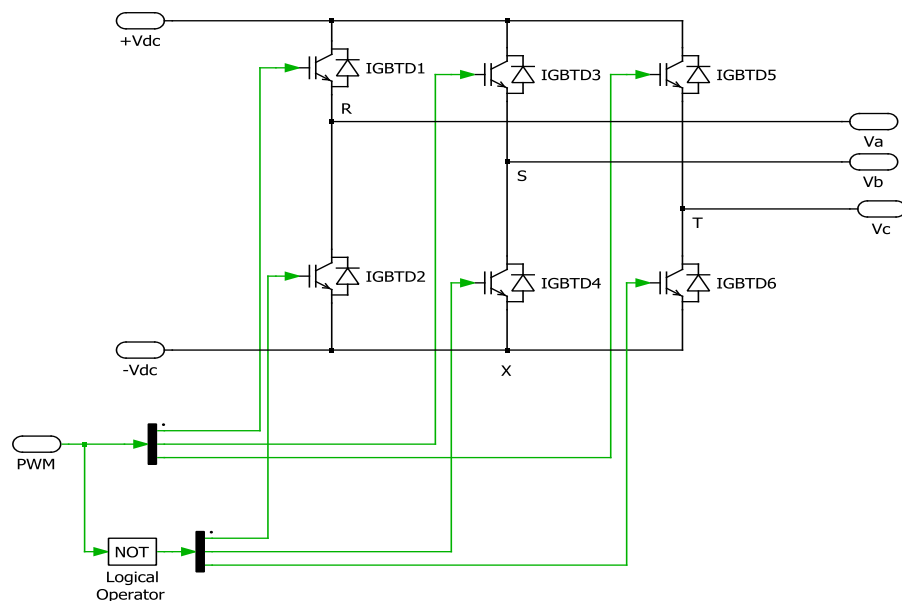


Fig. 3.3: Simulated Plects Model of Three Phase 2-Level VSC

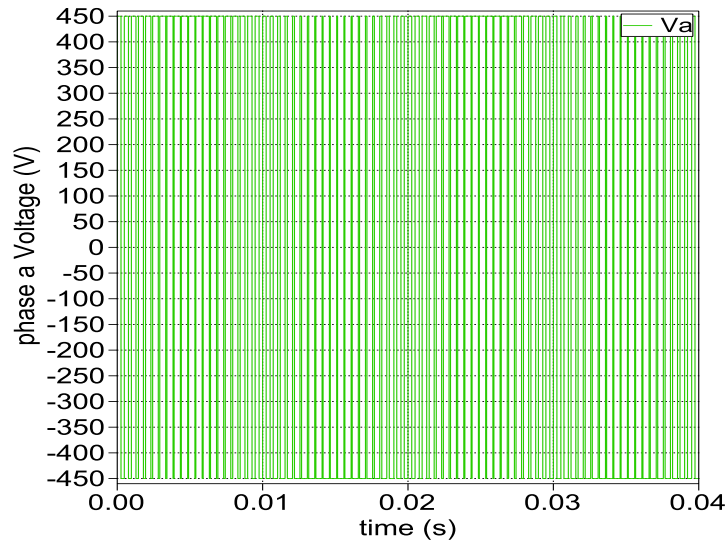


Fig. 3.4: 2-Level VSC Voltage Output

Sinusoidal Pulse Width Modulation

There are numerous Pulse Width Modulation (PWM) techniques like the Space Vector PWM (SVPWM), and the Selected Harmonic Elimination (SHE) PWM. However, this research work will consider converters controlled by the Sinusoidal Pulse Width Modulation (SPWM) technique as it is very simple to implement and most common in industrial applications [4, 53]. SPWM technique compares a high frequency triangular waveform which is also referred to as the carrier wave against a sinusoidal modulating waveform at the fundamental frequency to generate the gating signal for the IGBTs with respect to the voltage [4, 5, 53].

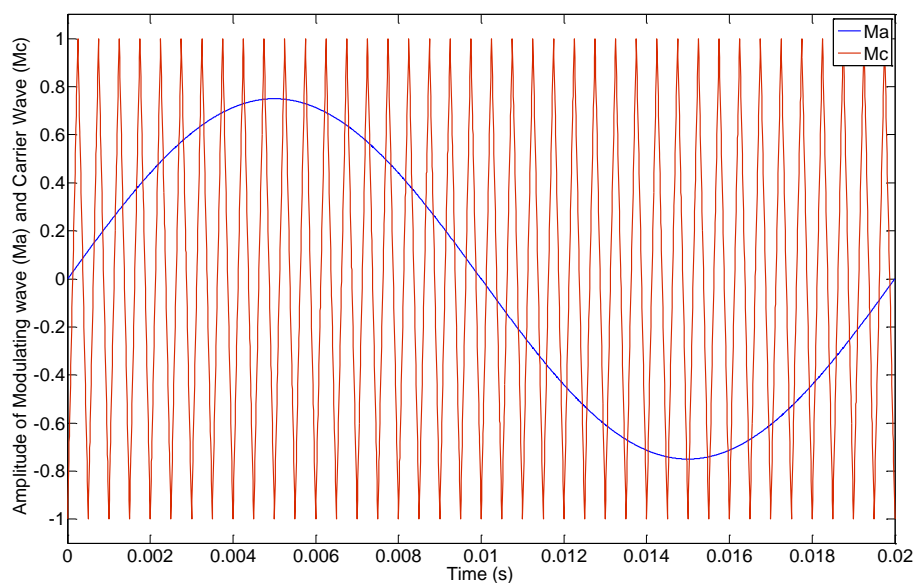


Fig. 3.5: Sinusoidal Pulse Width Modulation (SPWM) Technique

The points of intersection between the carrier wave and the modulating wave determine the switching points for the IGBTs switches [4, 5, 53]. Fig. 3.5 shows the SPWM technique; which is the triangular carrier signal and one cycle of the modulating signal and Fig. 3.6 shows the resulting pulse width as the gating signal.

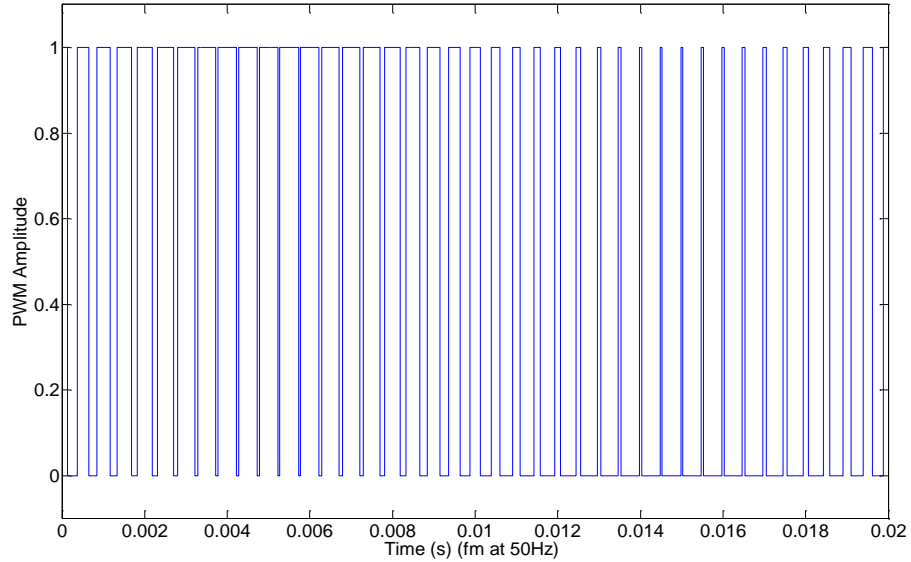


Fig. 3.6: Gating Signal as obtained from Fig. 3.5

In the case of the VSC, SPWM helps to control the AC output voltage V_{ac} waveform by performing multiple switching within the VSC with the constant DC voltage V_{dc} , this also helps to improve the harmonics performance [53].

The ratio of the peak amplitude of the modulating wave signal (\hat{V}_m) to the amplitude of the carrier/triangular wave (\hat{V}_{tri}) signal (3.1) is called the modulation index (m_a) [4, 5].

$$m_a = \frac{\hat{V}_m}{\hat{V}_{tri}} = \frac{2(\hat{V}_a)_1}{V_{dc}} \quad (3.1)$$

The second term in (3.1) shows the relationship between the DC link capacitor voltage (V_{dc}) and the peak amplitude of the phase voltage at fundamental frequency ($(\hat{V}_a)_1$) [4, 5].

The ratio of the frequency of the carrier/triangular wave signal f_{tri} to the frequency of the modulating wave signal f_m is called the frequency modulation index [5], this is shown in (3.2).

$$m_f = \frac{f_{tri}}{f_m} = \frac{f_{sw}}{f_m} \quad (3.2)$$

where f_{sw} is the switching frequency of the converter and f_m is the fundamental frequency of the AC system.

3.3.2 Multilevel VSC (ML-VSC) Topology

Multilevel (ML) VSCs have been introduced in recent years as an option for many medium and high power/voltage applications. The introduction of ML-VSC is partly due to the fact that the DC voltage level that a single switch cell is to withstand is greatly increased in medium and high voltage applications.

Multilevel VSCs are configured to form high voltage switch cells by connecting several lower voltage switches in series [4]. It however, requires some additional components like capacitors and diodes [4, 54]. The ML-VSC topology greatly reduces voltage stress on switch cells, lower dv/dt resulting in reduced voltage and current harmonics, lower electromagnetic interference [54, 55].

The 3 most common ML-VSCs include the cascade H-bridge, the flying capacitor ML-VSC, and the Neutral Point Clamped (NPC) ML-VSC [54, 55]. They have been extensively studied and applied in HVDC technology, induction machines, Flexible AC Transmission systems (FACTS), motor drives and in integrating renewable energy sources to the grid [54, 55].

The ML-VSC produces the desired output voltage from several levels of DC input voltage sources, if operated as an inverter. Multilevel VSCs presently utilized in industrial applications range from 3-level to 9-level VSCs [56]. High levels are sometimes desired as the output voltage waveform becomes more sinusoidal with increase of the ML-VSC number of levels [56].

a) **Three (3) Level VSC Topology**

The 3-level VSC is one of the multilevel VSC topology utilized in distributed power generation. The Neutral Point Clamped (NPC) ML-VSC topology as illustrated in Fig. 3.7, which is also called the Diode Clamped ML-VSC topology [54] will be considered in this research. In a 3-level NPC each switch cell has to withstand only half the DC side voltage as can be seen in Fig. 3.8, it also provides

voltage and current waveforms with lower harmonic distortion as compared to the two level VSC [5, 53, 57].

Based on its principle of operation the NPC 3-level VSC can be said to consist of two coordinated 2-level converters, one responsible for the positive AC phase voltage and the other responsible for the negative AC phase voltages which are the modulating signal [4]. The two half bridge generates either positive or negative voltage at their common AC side [4].

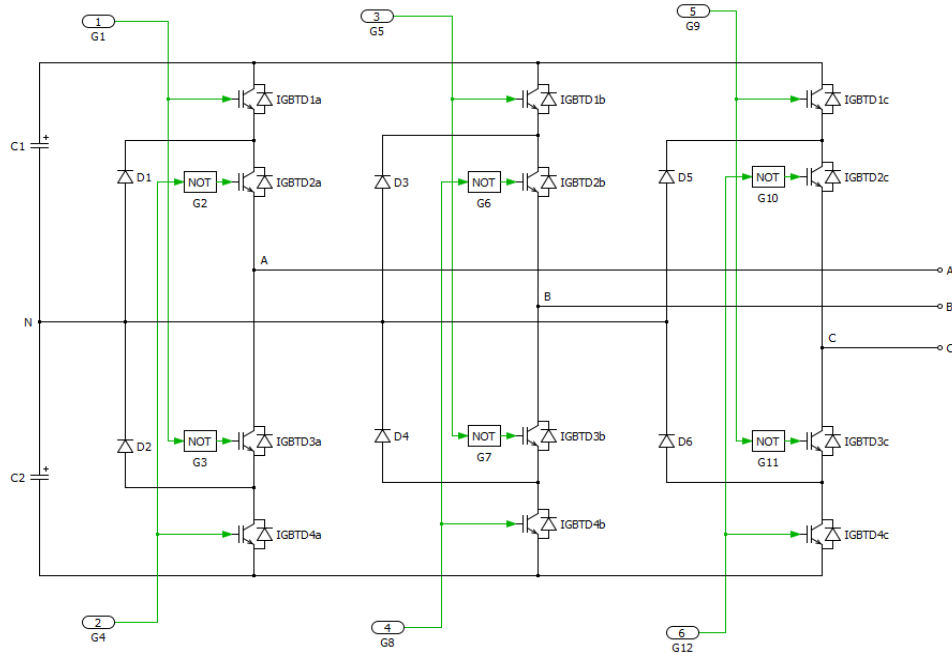


Fig. 3.7: Simulated Plescs Model of a Three Phase 3-Level NPC VSC

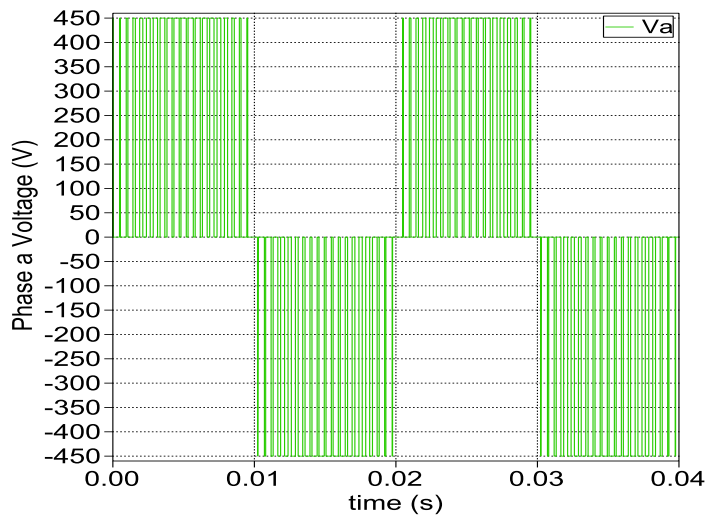


Fig. 3.8: 3-Level NPC VSC Voltage Output

A common method used to achieve the switching of the IGBTs is the Multiple-Carrier SPWM [54, 58]. For an n -level VSC, $n-1$ carrier wave is required [59].

Fig. 3.9 illustrates the multiple carrier SPWM technique for a 3-level NPC VSC and Fig. 3.10 shows the corresponding PWM signals that are used to control the gating of the IGBTs in the NPC VSC. The switching state for phase ‘a’ is shown in Table 3.1.

Table 3.1: Gating Signal for a 3-level NPC VSC (Phase a)

Output Voltage	Gating Signals				Switching State
v_{an}	GS1	GS2	GS3	GS4	SS
$V_{dc}/2$	1	1	0	0	+1
0	0	1	1	0	0
$-V_{dc}/2$	0	0	1	1	-1

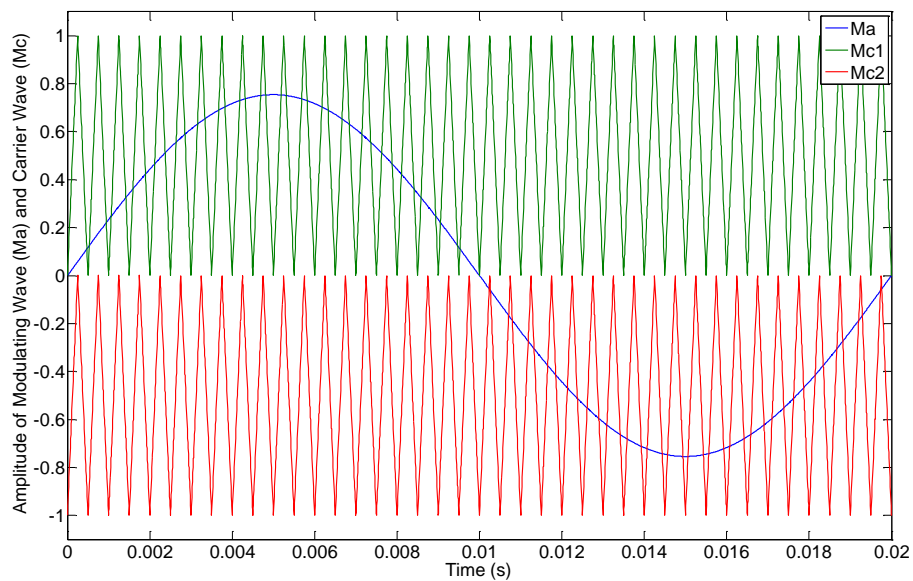


Fig. 3.9: Multiple Carrier SPWM Technique for a 3-Level VSC

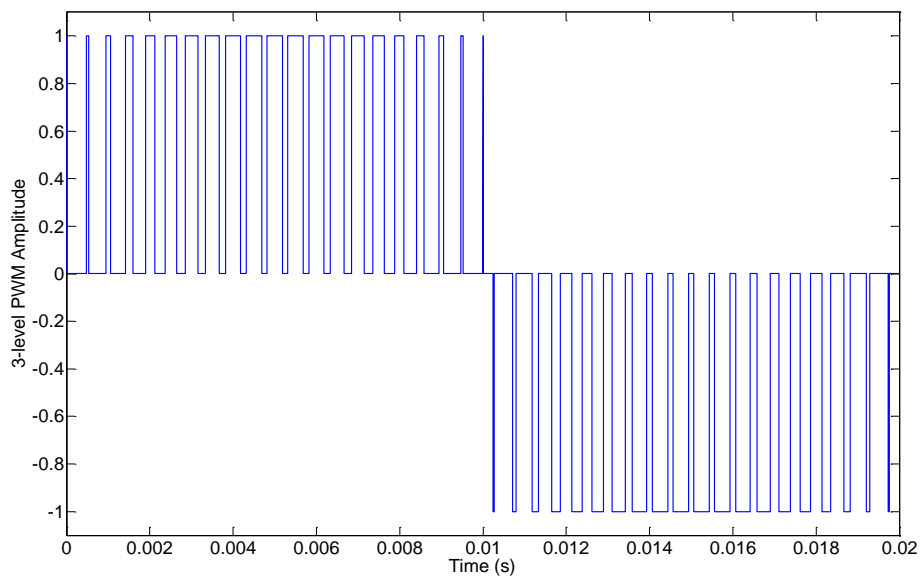


Fig. 3.10: Switching Signal for G1 and G4 Obtained from Fig. 3.9

b) Five (5) Level VSC Topology

A higher level than the 3-level VSC is the 5-level (5-L) VSC. In the 5-L VSC the DC voltage is divided into 5 levels using 4 capacitors [55]. The neutral point of the 5-L VSC is the midpoint between the four capacitors. The neutral point is assumed as the output phase voltage reference [55] (see Fig. 3.11).

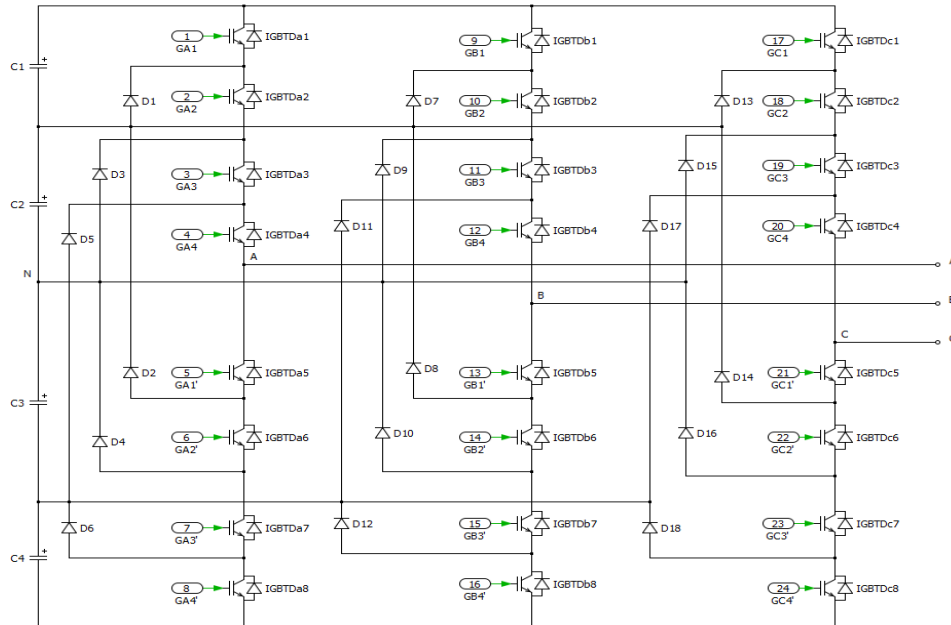


Fig. 3.11: Simulated PLECS Model of a Three Phase 5-Level NPC VSC

In a 5-L NPC VSC, a set of four switches is ON at any given period of time [55], as illustrated in Table 3.2 and each switch cell has to withstand only a quarter of the DC side voltage as seen in Fig. 3.12. The 5-L NPC VSC gives a more reduced voltage and current harmonic content, this is because the output voltage of the 5-L NPC VSC is more sinusoidal than that of the 3-L NPC VSC.

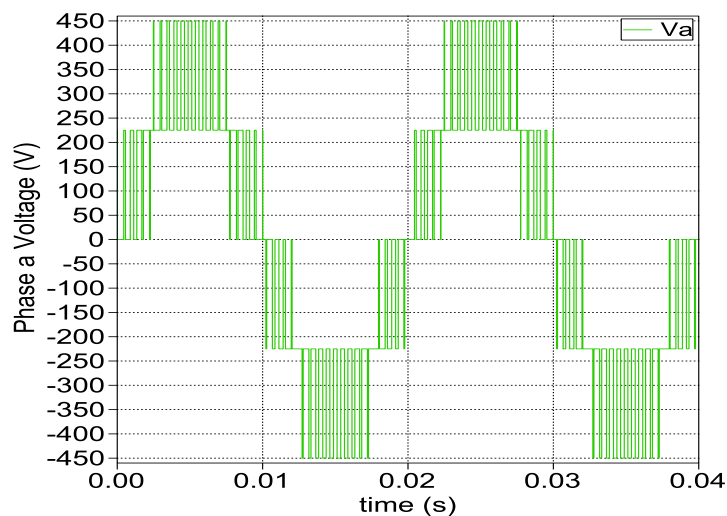


Fig. 3.12: 5-Level NPC VSC Voltage Output

Table 3.2: Gating Signal for a 5-level NPC VSC (Phase a)

Output Voltage	Gating Signals								Switching State
v_{an}	GS1	GS2	GS3	GS4	GS5	GS6	GS7	GS8	SS
$V_{dc}/2$	1	1	1	1	0	0	0	0	+2
$V_{dc}/4$	0	1	1	1	1	0	0	0	+1
0	0	0	1	1	1	1	0	0	0
$-V_{dc}/4$	0	0	0	1	1	1	1	0	-1
$-V_{dc}/2$	0	0	0	0	1	1	1	1	-2

The switching states of the 5-level NPC VSC phase ‘a’ are given in Table 3.2, while Fig. 3.13 and Fig. 3.14 show the SPWM scheme and corresponding pulse width used for controlling the gating of the IGBTs in the 5-level NPC VSC.

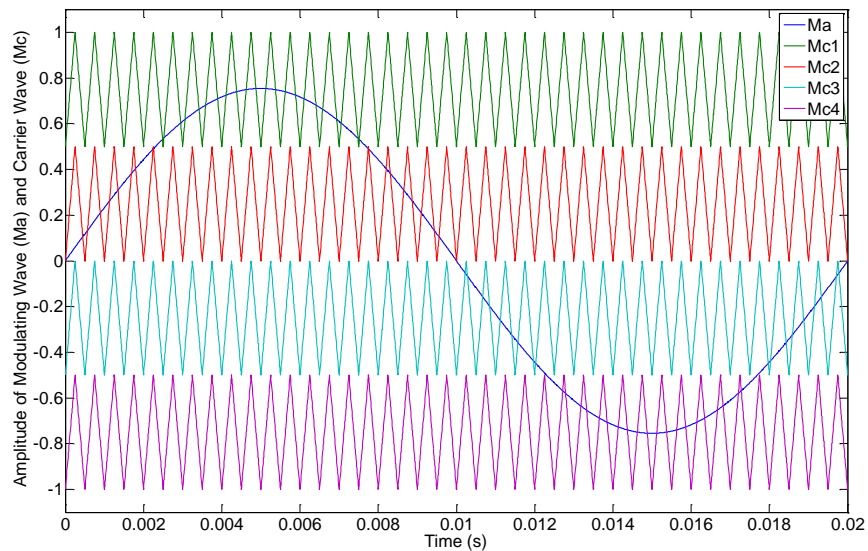


Fig. 3.13: Multiple Carrier SPWM Technique for 5-level VSC

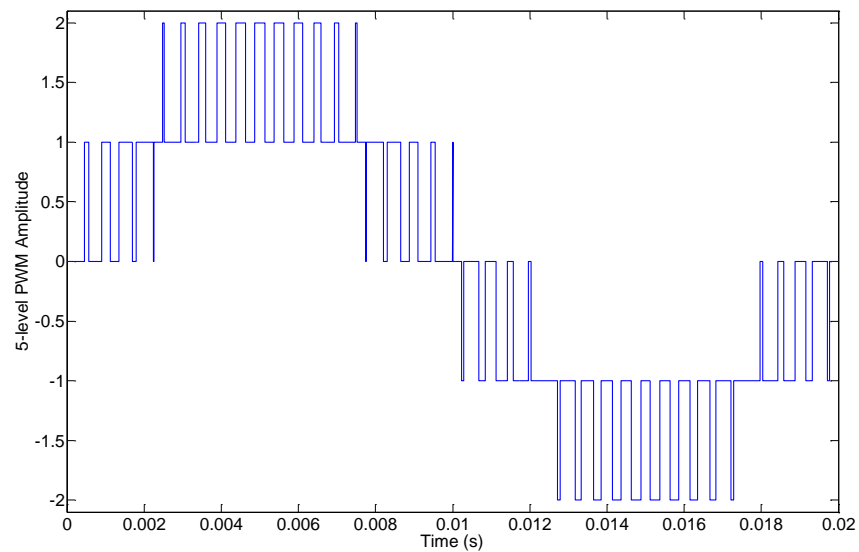


Fig. 3.14: Switching Signal for G1,G2 and G7,G8 Obtained from Fig. 3.5

3.4 Control Scheme

Most VSCs usually require some sort of control technique to maintain its power flow to and from the grid. In this research the active and reactive current control technique is employed to control the instantaneous active and reactive power of the VSC converter using a PI vector controller. This is chosen as it is simple to design, less complex to implement and has a robust control response in a balanced system [19], [60].

The active and reactive power flow on the system is regulated by controlling the active current component I_{gd} and the reactive current component I_{gq} . The PI controllers forces I_{gd} and I_{gq} to track certain reference commands I_{gdref} and I_{gqref} , respectively [60]. I_{gdref} is provided by the DC capacitor controller and I_{gqref} is provided by a reference signal generator block.

Utilizing the instantaneous power theory [4] and assuming the power lost between the DC and AC side of the converter is negligible:

$$P_{dc} = P_{ac} \quad (3.3)$$

$$P_g = \frac{3}{2}(V_{gd}I_{gd} - V_{gq}I_{gq}) \quad (3.4)$$

$$Q_g = \frac{3}{2}(V_{gq}I_{gd} - V_{gd}I_{gq}) \quad (3.5)$$

where, P_{dc} is the DC power source and P_{ac} is the active power on the grid (P_g), Q_g is the reactive power on the grid.

Since the phase voltage of the grid is aligned to the d-axis reference frame then $V_{gq} = 0$ [60], so the equation can be further reduced to:

$$P_g = \frac{3}{2}(V_{gd}I_{gd}) \quad (3.6)$$

$$Q_g = -\frac{3}{2}(V_{gd}I_{gq}) \quad (3.7)$$

If $I_{gd} = I_{gdref}$ and $I_{gq} = I_{gqref}$ then P_g and Q_g can be controlled by P_{gref} and Q_{gref} [4].

So that:

$$I_{gdref} = \frac{2}{3V_{gdref}} P_{gref} \quad (3.8)$$

$$I_{gqref} = -\frac{2}{3V_{gdref}} Q_{gref} \quad (3.9)$$

The DC capacitor voltage is regulated by a separate PI controller and the controller provides the required I_{gdref} for the control of the active power on the VSC. However, I_{gdref} is synthesized from P_{gref} if the VSC is operated as a rectifier.

The PI controller for the active and reactive current is designed based on the plant (G_{pc}) of the system which is [4]:

$$G_{pc}(s) = \frac{1}{R_c + sL_c} \quad (3.10)$$

where R_c is the resistance of the VSC line (Ω) and L_c is the line/filter inductance of the VSC line (mH).

The DC capacitor voltage is regulated to make sure the voltage across the capacitor is fixed as demanded by the control [4].

$$G_{pv}(s) = \frac{E_{dc}(s)}{I_{gd}(s)} = \frac{3m}{4C_s} \quad (3.11)$$

The DC capacitor PI controller is designed based on (3.11) where $\frac{3m}{4}$ is a constant, it can be further modified to

$$G_{pv}(s) = \frac{E_{dc}(s)}{I_{gd}(s)} = \frac{1}{C_s} \quad (3.12)$$

where E_{dc} is the DC capacitor voltage, C is the DC capacitance (μF) and G_{pv} is the DC side plant.

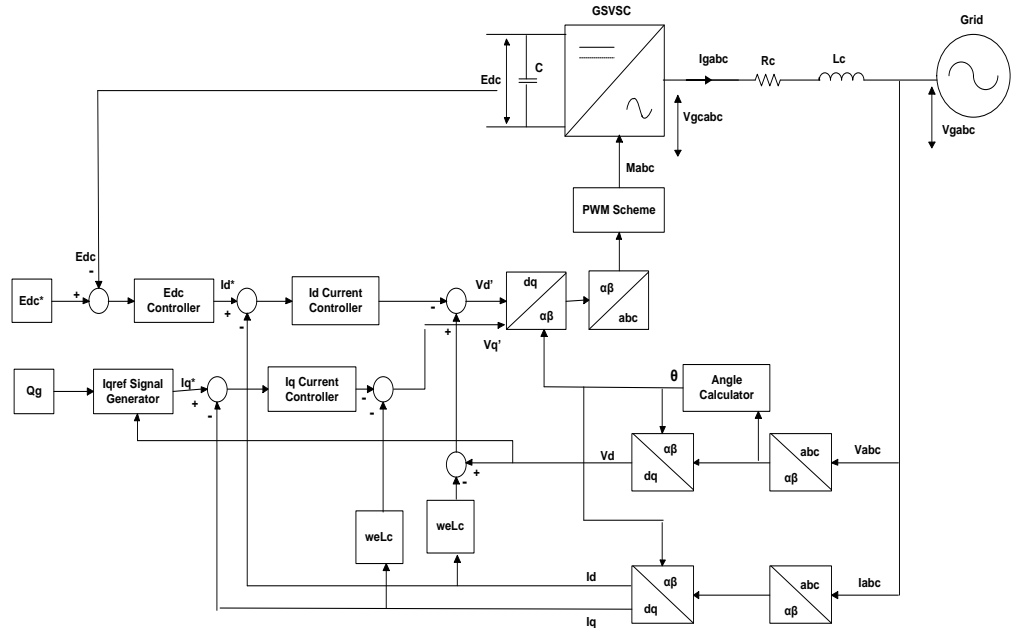


Fig. 3.15: Active and Reactive Power Control Scheme of the Grid interfacing VSC

Fig. 3.15 shows the control scheme utilized in the control of the active and reactive power that flows to and from the grid interfacing VSC. The inner loop is usually designed to be faster than the outer loop, and it directly controls the active and reactive current flow. The outer loop is slower and it is used to regulate the DC capacitor voltage and provides the reference active current

3.5 Summary

The two most commonly used VSC topology in small and medium distribution systems (the 2-level and 3-level VSC) was discussed in this chapter. The switching pattern of the IGBT gates was also presented including that of a 5-level NPC VSC. The chapter was concluded by giving the control technique and schematics that regulates the DC capacitor voltage of the VSC and controls the active and reactive power flow in the VSC.

Chapter 4

Factors Affecting Harmonics Generated by a Voltage Source Converter

Voltage Source Converters (VSCs) are known to generate current and voltage harmonics and when integrated to an Electrical Power System (EPS) these harmonics flow through the EPS. This chapter investigates various factors that may affect the harmonics generated by a VSC first due to the VSC design, then from the point of the EPS. It also presents some filter designs for harmonic attenuation.

4.1 SPWM PI Controlled VSC

For an SPWM PI controlled VSC, there are basically 2 categories of factors that might affect the level of harmonics generated as seen at the PCC of the DER to the grid, excluding the filter system utilized [1, 60]. They include:

- The converter design specification
- The system/operation characteristics

It is necessary to evaluate the VSC performance based on these factors before designing the filters. The parameters of the investigated 2-level VSC system are listed in Table 4.1 and they represent typical values of a small power system [61-63] simulated using PLECS™ and controlled as discussed in section 3.4.

Table 4.1: Studied Grid Integrated VSC System

Rated power, P	10 kW
Grid voltage phase a, V_a	240 V (rms)
Grid frequency, f_m	50 Hz
VSC DC capacitor voltage, V_{dc}	905 V
VSC switching frequency, f_{sw}	2 kHz
Converter interfacing inductance, L_{fl}	7.5 mH
Converter line resistance, R_{fabc}	0.1 Ω
Grid Impedance, Z_{gabc}	(0.4+j0.25) Ω /phase
Modulation index, m_a	0.75

The grid impedance was modelled as a series 3 phase inductance and resistance using the values in Table 4.1. The current-voltage waveform and harmonic performance of the VSC system simulated using PLECS™ is given in Fig. 4.2 and Fig. 4.3 and it will act as the standard for comparison.

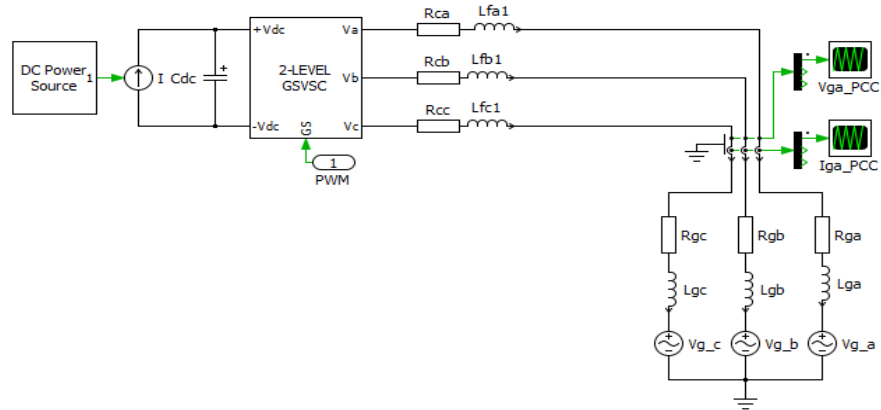


Fig. 4.1: Modelled L-filtered VSC Connected to the Grid

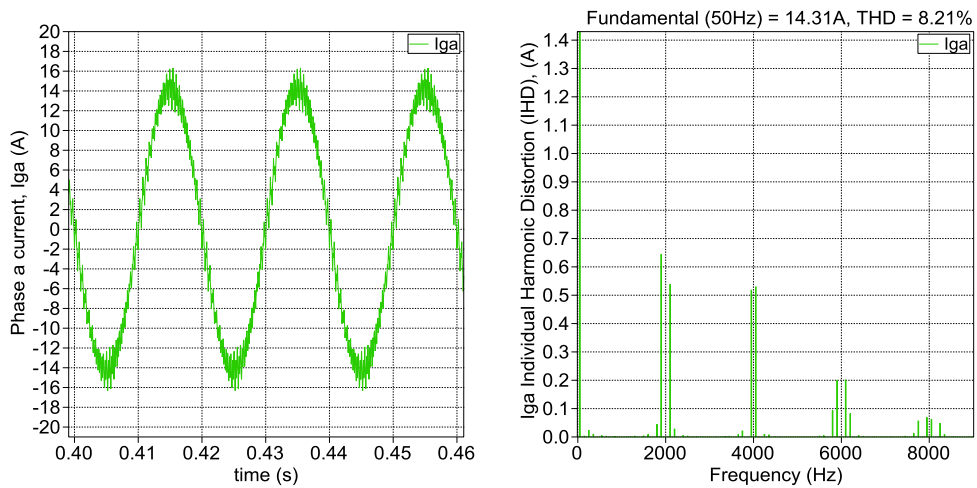


Fig. 4.2: VSC Phase Current Waveform (a) and Harmonic Spectrum (b)

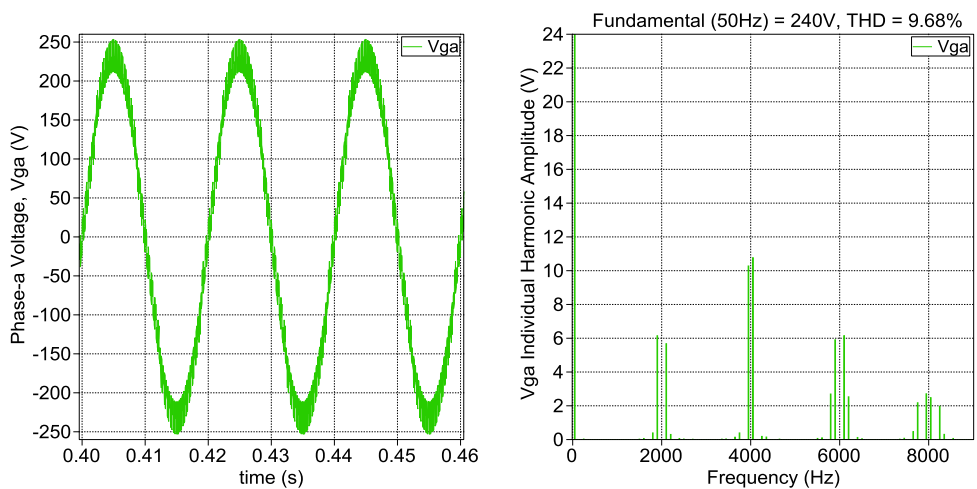


Fig. 4.3: VSC Phase Voltage Waveform (a) and Harmonic Spectrum (b)

From Fig. 4.2a and Fig. 4.3a it is clear that there are harmonic distortions in the current and voltage waveform. Fig. 4.2b and Fig. 4.3b gives the harmonic spectrum of the current and voltage waveform of the 2-level VSC measured at the PCC to the grid. The harmonic spectrum reveals the magnitude of harmonics in amperes and volts for the current and voltage waveform respectively. It also reveals the frequency at which these harmonics occur and the majority of the VSC harmonic components appear at the switching frequency (2 kHz) and its multiples (4 kHz, 6 kHz, 8 kHz). The Total Harmonic Distortion (THD) of the current and voltage waveforms was also given and it appears to be beyond the IEEE 519 harmonic standard presented in Chapter 2.

4.2 Harmonics Generated by a VSC Based on Design Specification

For the converter design, the factors that can affect the level of harmonic distortion and hence power quality of the VSC include [60];

- The Amplitude Modulation Index (m_a)
- The Switching Frequency (f_{sw})/Frequency Modulation Index (m_f)
- The Converter Topology

4.2.1 Amplitude Modulation Index (m_a) I

The effect of varying the amplitude modulation index from 0.55 - 0.95 in the simulation of the 2 level VSC is presented in Fig. 4.4 - Fig. 4.8. The m_a determines the amplitude of the generated current and voltage harmonics at the switching frequency and its multiples.

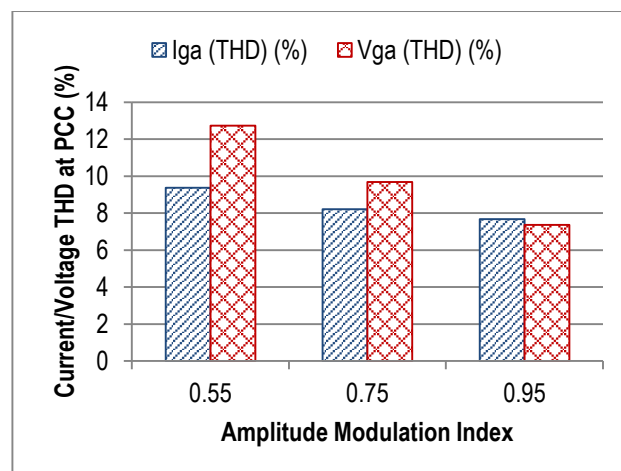


Fig. 4.4: The effect of VSC m_a on I_{THD} and V_{THD} at PCC

It can be seen from Fig. 4.4 that with the increase of m_a the V_{THD} and I_{THD} at the PCC also decreases. Fig. 4.5 - Fig. 4.8 shows the voltage-current waveform and their corresponding harmonic spectrum for each m_a used. Fig. 4.5 - Fig. 4.8 clearly shows that increasing m_a helps to reduce the amplitude of the individual harmonics thus reducing I_{THD} and V_{THD} at PCC [60]. More decrease is noticed in V_{THD} than in I_{THD} because m_a is a ratio between voltages and hence its effect is more pronounced in V_{THD} .

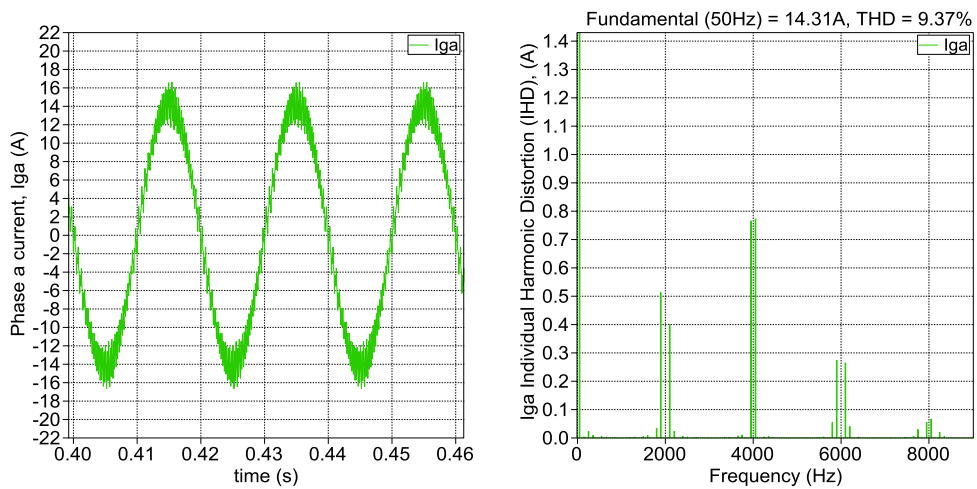


Fig. 4.5: VSC Current Waveform (a) and Harmonic Spectrum (b) at $m_a = 0.55$

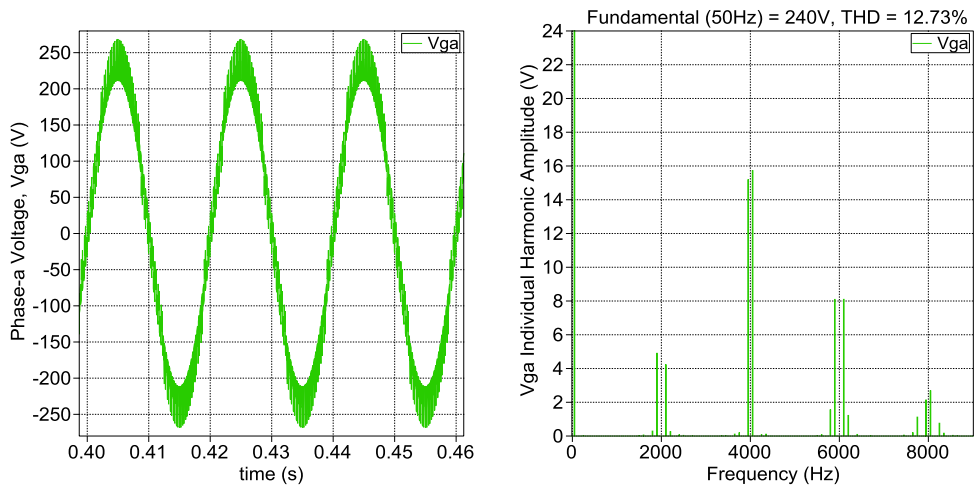


Fig. 4.6: VSC Voltage Waveform (a) and Harmonic Spectrum (b) at $m_a = 0.55$

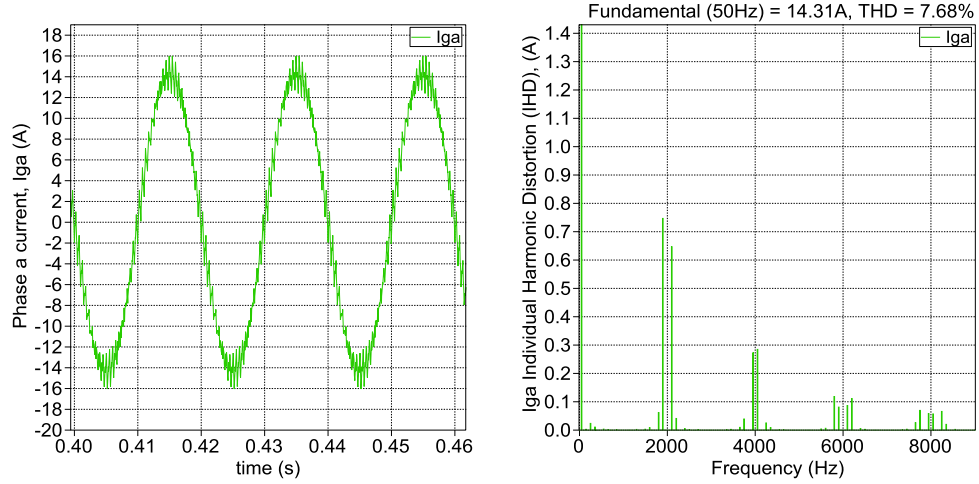


Fig. 4.7: VSC Current Waveform (a) and Harmonic Spectrum (b) at $m_a = 0.95$

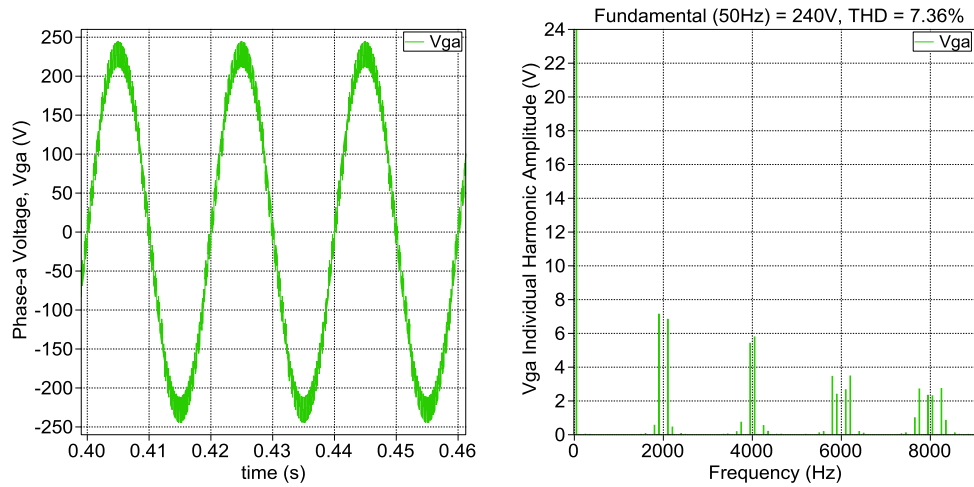


Fig. 4.8: VSC Voltage Waveform (a) and Harmonic Spectrum (b) at $m_a = 0.95$

4.2.2 Switching Frequency/Frequency Modulation Index I

For an SPWM VSC grid interfacing converter, the generated harmonics would appear at f_{sw} , and its multiples. There would also be positive and negative sidebands centred around the f_{sw} and its multiples [5, 53]. The frequency modulation index, m_f (as discussed in section 3.2.1) defines the frequency at which the harmonic voltage or current would occur. The frequency, f_h and the harmonic order, h at which the individual harmonic voltage or current would occur is given in [5, 53, 57, 60], as;

$$f_h = (jm_f \pm k) f_1 \quad (4.1)$$

and

$$h = jm_f \pm k \quad (4.2)$$

where f_1 is the fundamental frequency and the harmonic order at this frequency is, $h = 1$. j and k are integers and $j + k =$ an odd integer [53]. From [5], it was noticed that when j is odd, k is even, and when j is even, k is odd.

The amplitude of the individual harmonic depends on the modulation index m_a , and are independent of the frequency index m_f [5, 53, 57]. It also diminishes with a higher value of j and k [53].

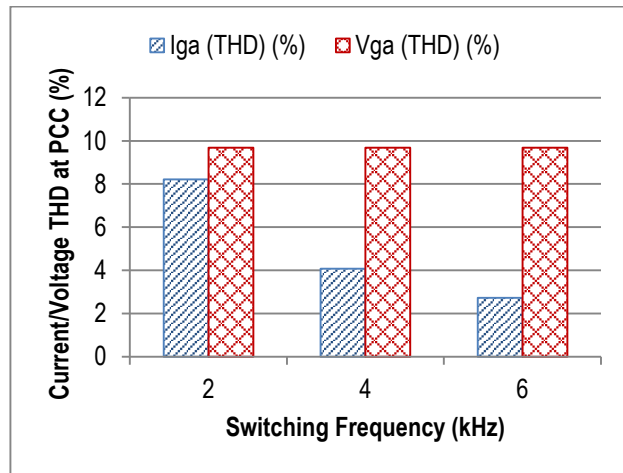


Fig. 4.9: The effect of VSC f_{sw}/m_f on I_{THD} and V_{THD} at PCC

Fig. 4.9 - Fig. 4.13 shows the observed effect of increasing the VSC switching frequency on the VSC current and voltage harmonics. It shows that the utilization of higher f_{sw}/m_f can help improve the I_{THD} of the VSC however; the V_{THD} remains the same for all cases. This is because the individual harmonics at the switching frequency are still present and appear after every 4 kHz as seen in Fig. 4.11 and after every 6 kHz in Fig. 4.13. Increasing the f_{sw} to improve current THD is done at the expense of increasing the switching losses within the VSC.

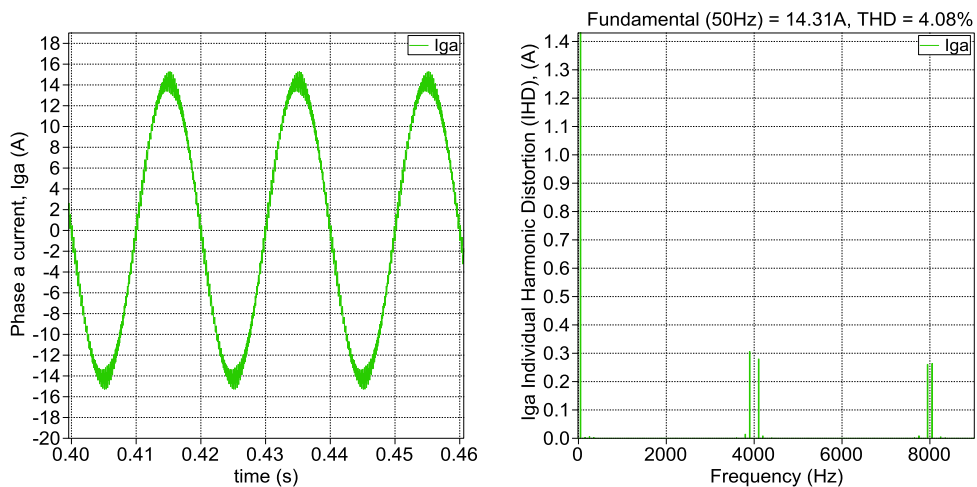


Fig. 4.10: VSC Current Waveform (a) and Harmonic Spectrum (b) at $f_{sw} = 4$ kHz

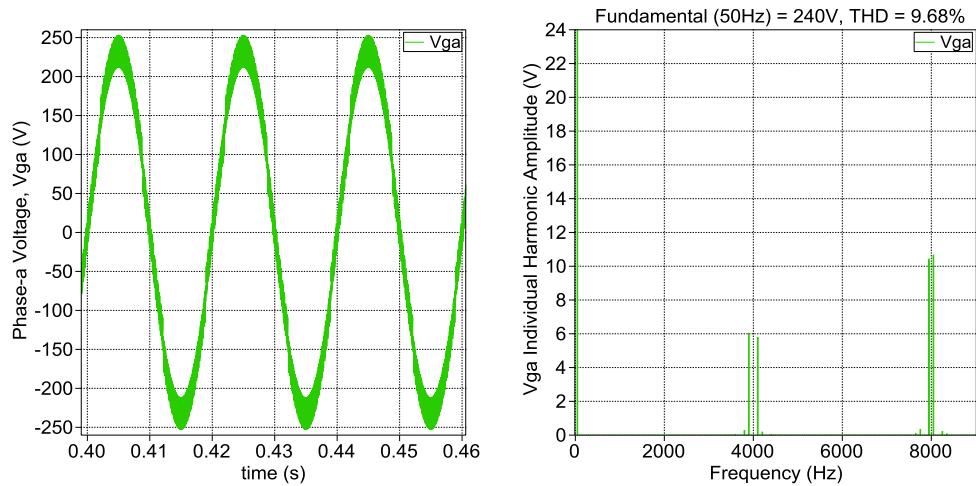


Fig. 4.11: VSC Voltage Waveform (a) and Harmonic Spectrum (b) at $f_{sw} = 4\text{kHz}$

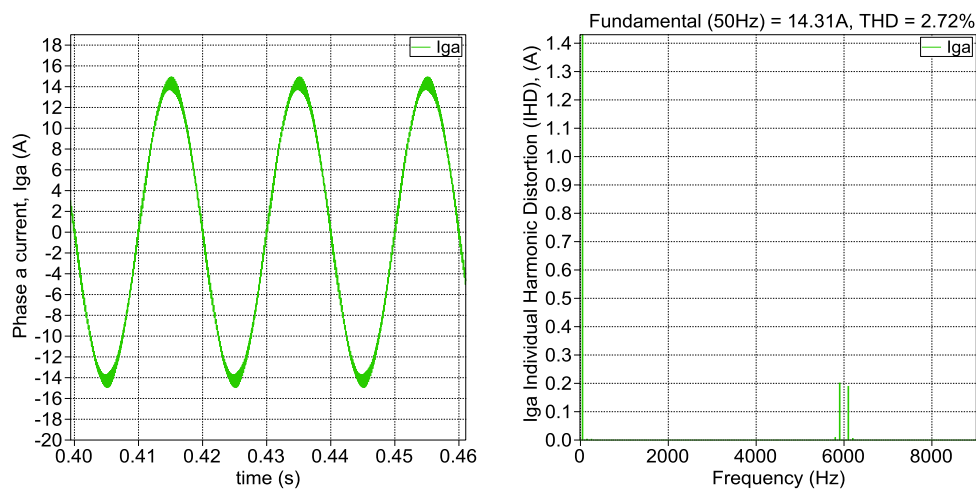


Fig. 4.12: VSC Current Waveform (a) and Harmonic Spectrum (b) at $f_{sw} = 6\text{kHz}$

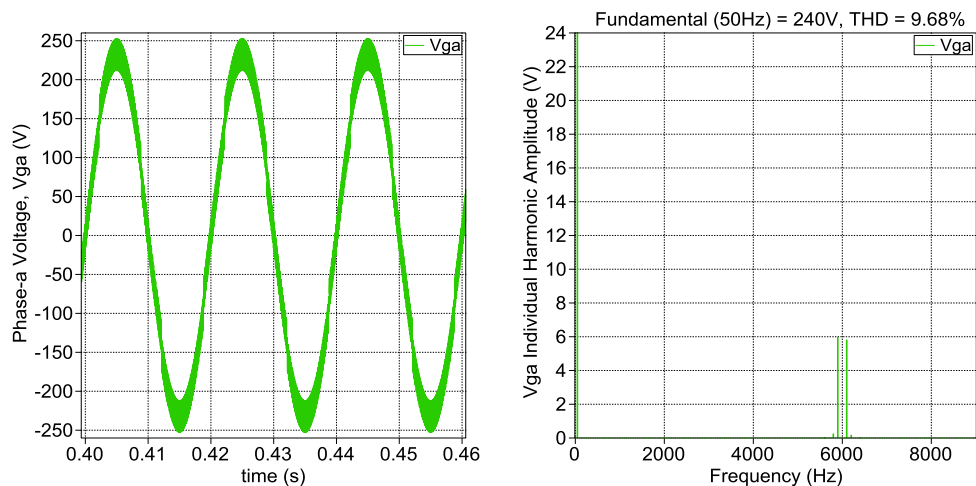


Fig. 4.13: VSC Voltage Waveform (a) and Harmonic Spectrum (b) at $f_{sw} = 6\text{kHz}$

4.2.3 Converter Topology I

The converter topology determines the maximum voltage a single IGBT would be required to switch through [57]. In the basic 2-level VSC topology, the IGBTs

are made to switch through the full DC voltage. In series connection of these devices the maximum voltage an IGBT is required to switch through reduces and this has led to the introduction and use of Multilevel (ML) VSCs in medium and high voltage level applications and in HVDC links [57]. The ML-VSC considered in this analysis is the Neutral Point Clamped (NPC) VSC as discussed in section 3.2.2. The simulation results for each topology are given in Fig. 4.13.

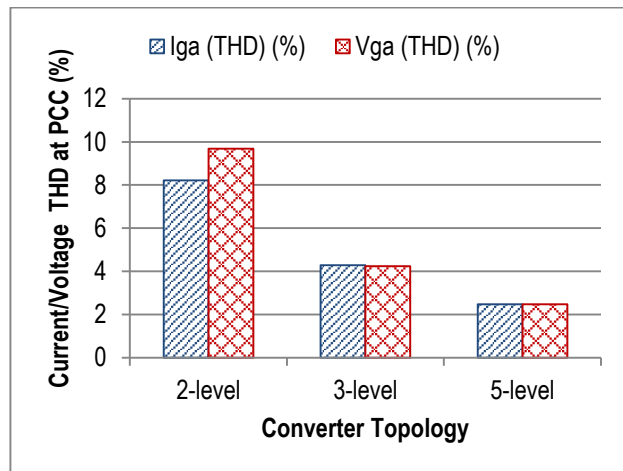


Fig. 4.14: The effect of VSC Topology on I_{THD} and V_{THD} at PCC

It is clear from Fig. 4.14 that the higher the VSC topology levels the better the current and voltage harmonic performance. It can then be deduced that increasing the VSC topology level helps to reduce the current and voltage harmonics generated by the VSC.

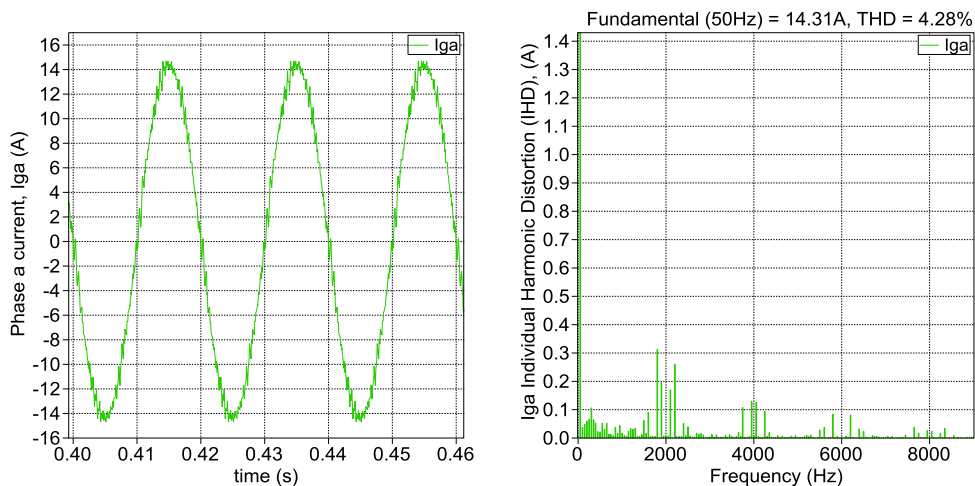


Fig. 4.15: 3-L NPC VSC Current Waveform (a) and Harmonic Spectrum (b)

Fig. 4.15 -Fig. 4.18 clearly show a reduction of the current and voltage IHD and THD of the VSC when the VSC topology level is increased. These results are far better compared to the 2-level VSC result in Fig. 4.2 and Fig. 4.3.

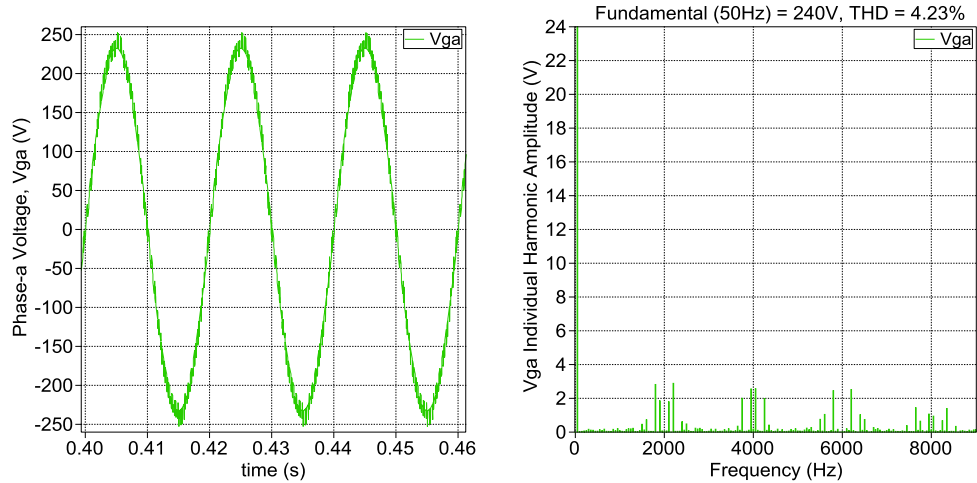


Fig. 4.16: 3-L NPC VSC Voltage Waveform (a) and Harmonic Spectrum (b)

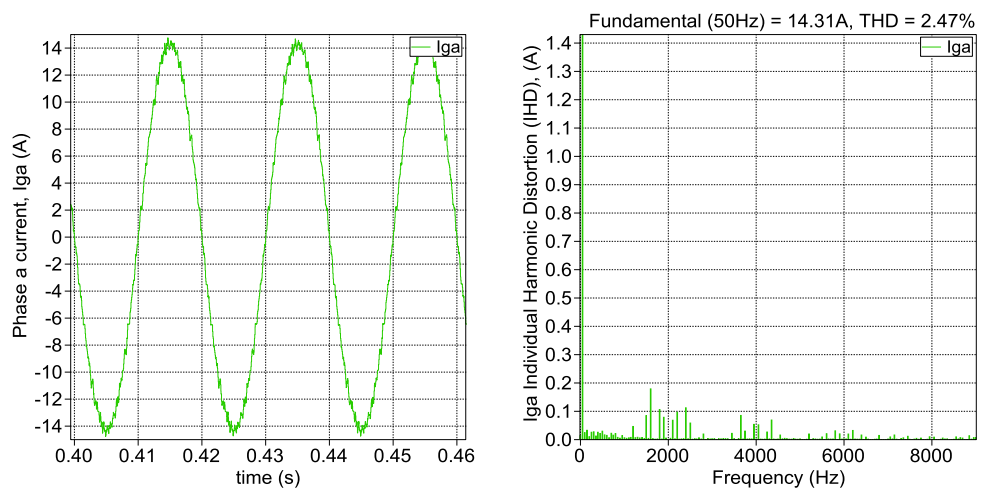


Fig. 4.17: 5-L NPC VSC Current Waveform (a) and Harmonic Spectrum (b)

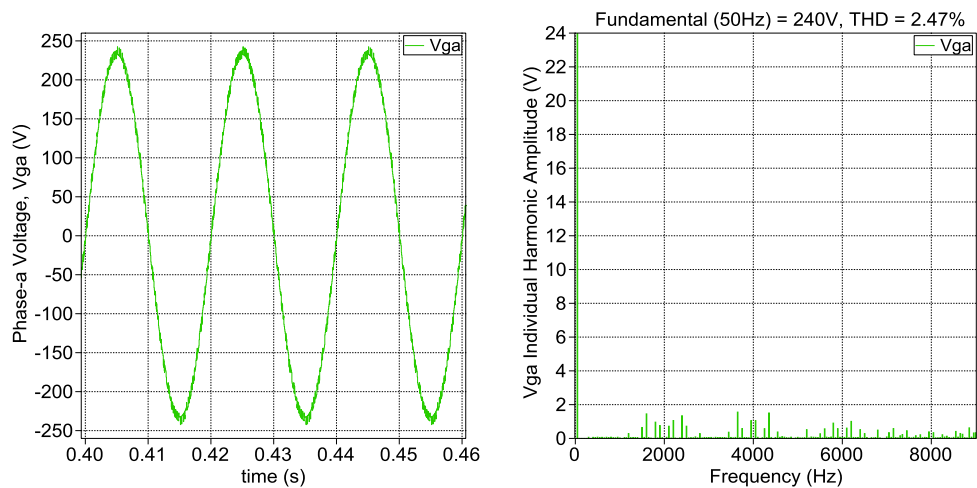


Fig. 4.18: 5-L NPC VSC Voltage Waveform (a) and Harmonic Spectrum (b)

4.3 Harmonics Generated by a VSC Based on System/Operation Characteristics

Most analysis of VSC integrated to the grid usually assumes the grid characteristics are perfect and attributes the power quality issues (such as harmonics) as a result of only the VSC [64]. In reality, the grid impedance usually varies with the addition of more load to the grid and the voltage waveform of the grid have been known to contain harmonics and other forms of disturbances that significantly affect the quality of the current and voltage injected by the VSC to the grid [64].

4.3.1 Grid Voltage Waveform I

The effect of the grid voltage distortion on the VSC harmonics is presented in Fig. 4.19. The voltage distortions (1-5% V_{THD}) were obtained using a programmable power/voltage source and then simulated into the grid voltage source. This was chosen as measurements on most distribution networks comes up with a voltage background distortion of about 2.4% [64]. The current THD (I_{THD}) was reduced when voltage harmonics was introduced into the system from 8.26% at 0% grid V_{THD} to 4.61% at 1% grid V_{THD} . Subsequent increase from 1-5% grid V_{THD} caused only a slight increase in the VSC current harmonics at the PCC. However, there was a large increase in the VSC voltage THD (V_{THD}) seen at the PCC to the grid.

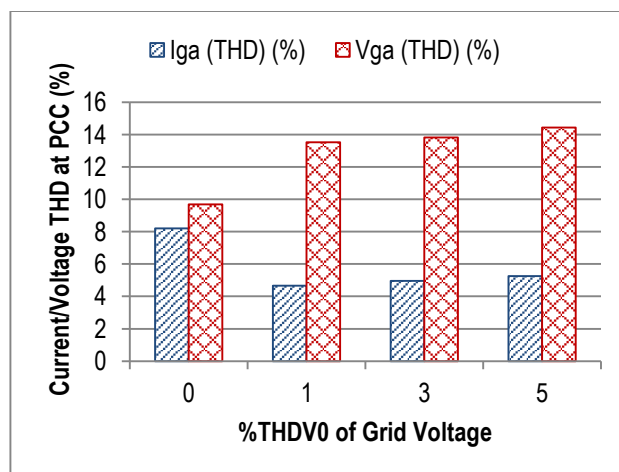


Fig. 4.19: The effect of Grid Voltage Distortion on I_{THD} and V_{THD} at PCC

Fig. 4.20 - Fig. 4.25 shows the VSC current and voltage waveform and harmonic performance at the PCC to the grid when different voltage distortion is introduced from the grid. It is clearly noticed that majority of the effect is on the V_{THD} as in the previous case and not the I_{THD} .

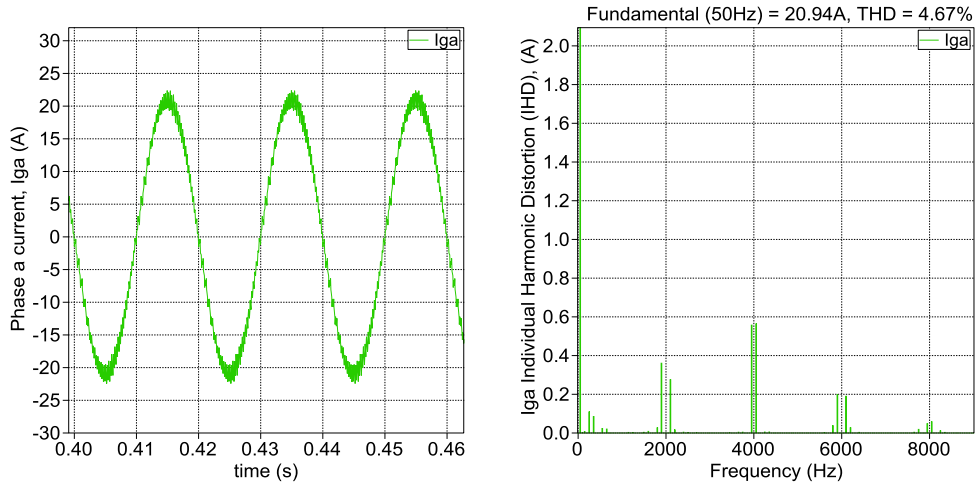


Fig. 4.20: VSC Current Waveform (a) and Harmonic Spectrum (b) at 1% V_{THD}

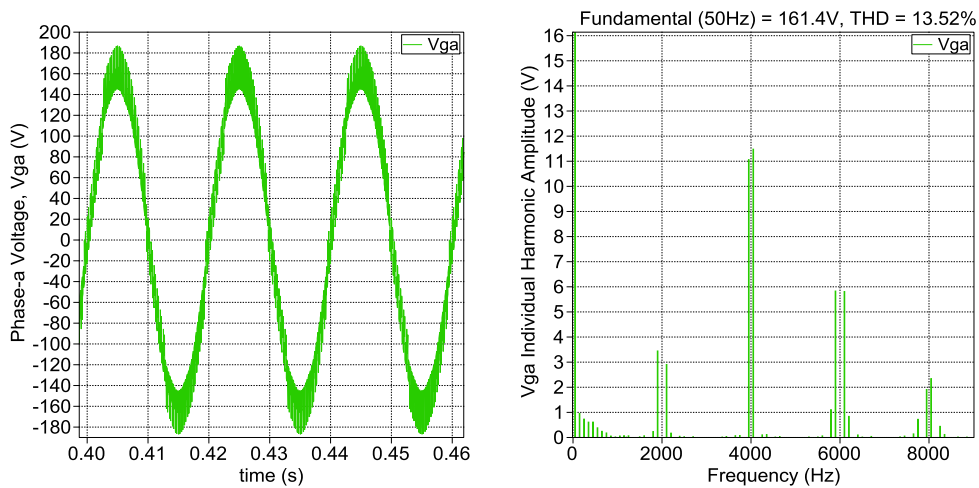


Fig. 4.21: VSC Voltage Waveform (a) and Harmonic Spectrum (b) at 1% V_{THD}

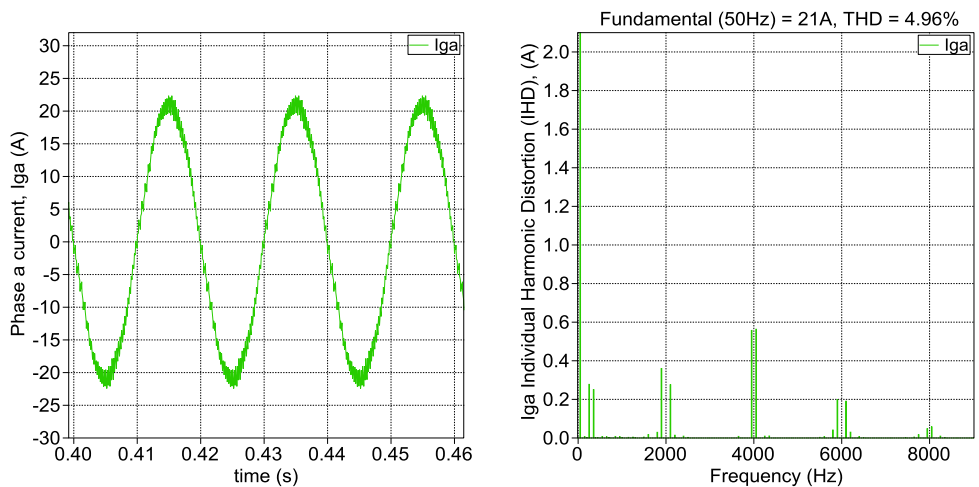


Fig. 4.22: VSC Current Waveform (a) and Harmonic Spectrum (b) at 3% V_{THD}

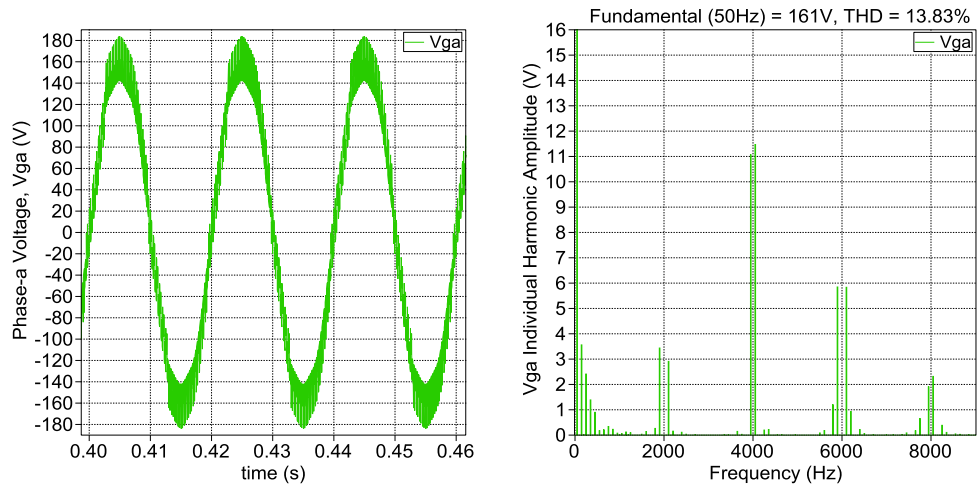


Fig. 4.23: VSC Voltage Waveform (a) and Harmonic Spectrum (b) at 3% V_{THD}

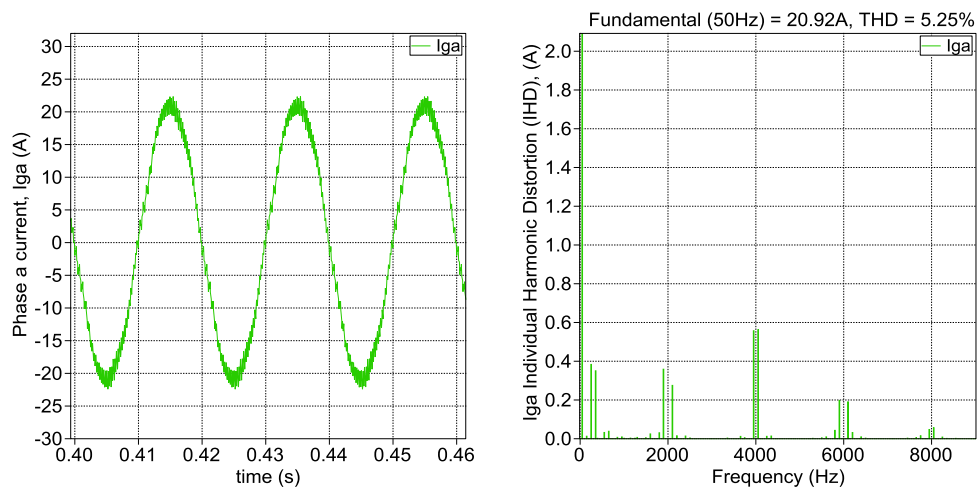


Fig. 4.24: VSC Current Waveform (a) and Harmonic Spectrum (b) at 5% V_{THD}

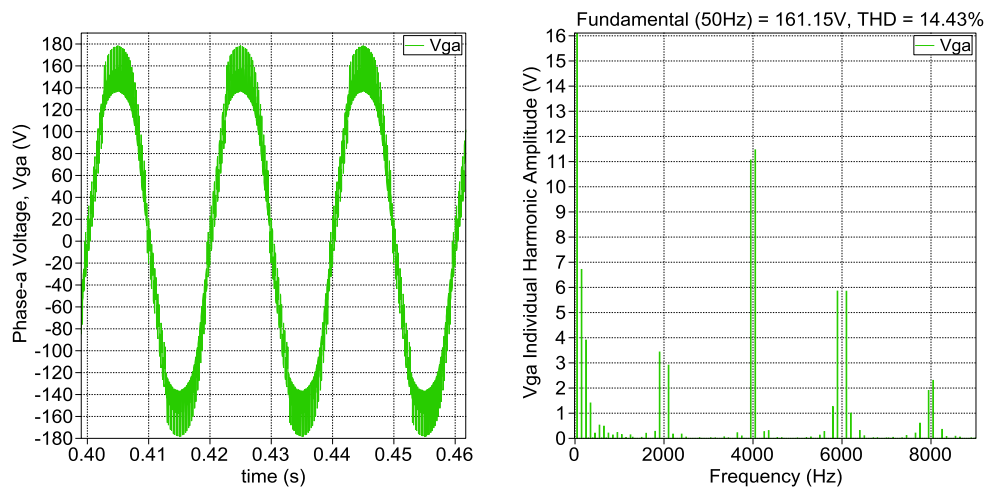


Fig. 4.25: VSC Voltage Waveform (a) and Harmonic Spectrum (b) at 5% V_{THD}

4.3.2 Grid System Impedance I

A typical grid impedance of $(0.4 + j0.25) \Omega/\text{phase}$ [62] was utilized as it represents a system impedance for a small electric distribution network just like the microgrid. This impedance represents the interconnecting cables and the transformer impedance to the PCC [64]. The grid impedance interacts with the filter impedance on the system to provide the overall attenuation observed at the PCC. Assuming there is no impedance between the grid and the PCC, the undistorted voltage waveform of the grid would appear at the PCC (see Fig. 4.28). As from Ohm's law [65] a zero impedance will give a zero voltage, hence zero voltage distortion is seen at PCC. However, this can only be achieved in simulation as in reality there is always an impedance between the VSC and the grid. Fig. 4.26 shows that, at zero impedance the I_{THD} is very high but there is no voltage harmonics at the PCC. It was also observed that the I_{THD} at the PCC reduces as the grid impedance increases, while the V_{THD} increases at almost the same rate of increase of impedance.

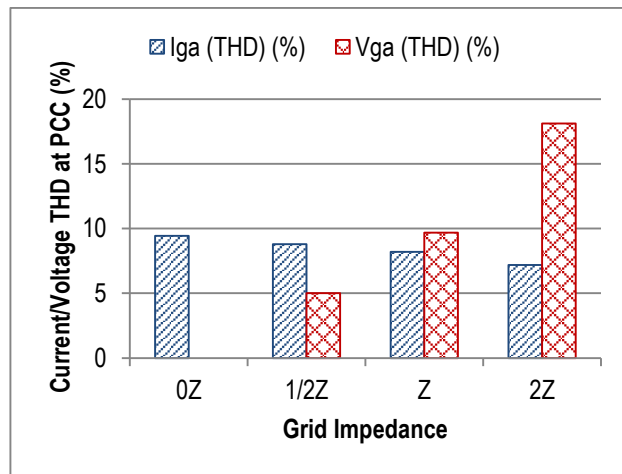


Fig. 4.26: The effect of Grid Impedance Variation on I_{THD} and V_{THD} at PCC

That is at low impedances there is better V_{THD} at the PCC and at high impedances there is better I_{THD} . Based on this, it is clear that the VSC harmonic performance is also affected by grid impedance variation.

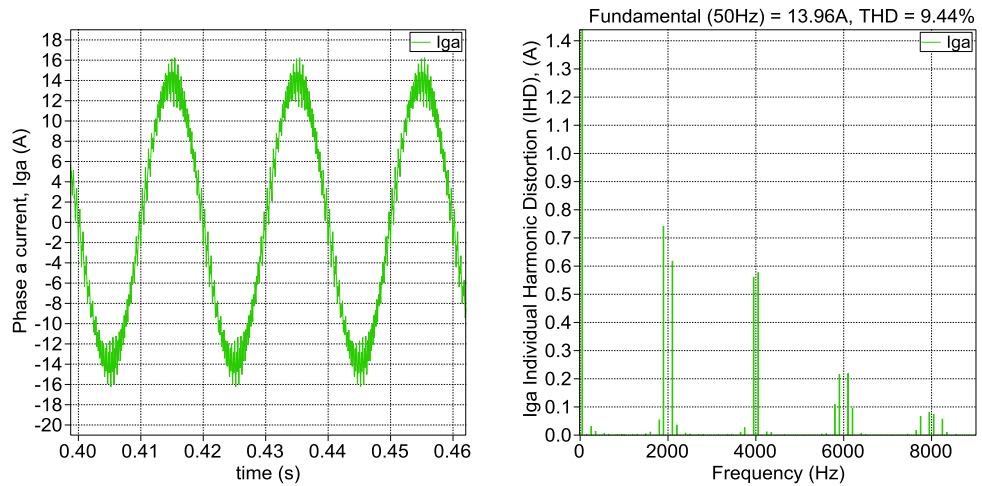


Fig. 4.27: VSC Current Waveform (a) and Harmonic Spectrum (b) at 0Z

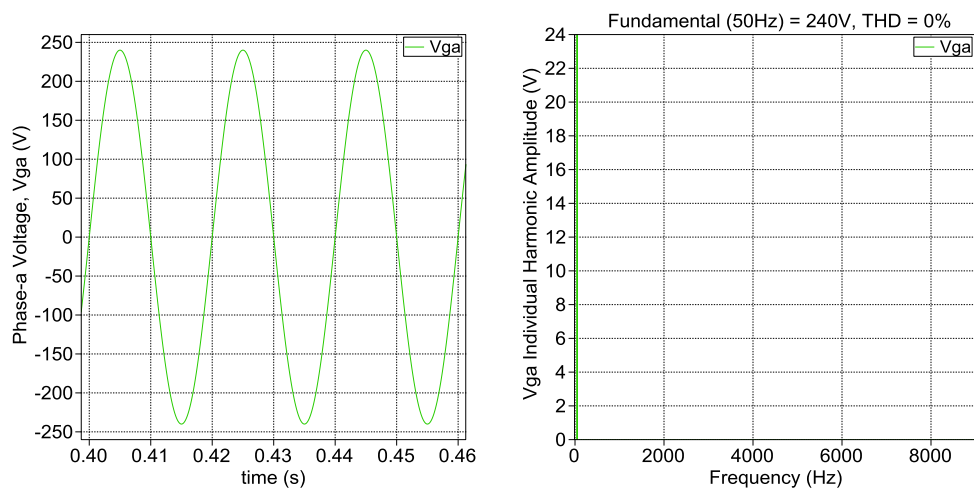


Fig. 4.28: VSC Voltage Waveform (a) and Harmonic Spectrum (b) at 0Z

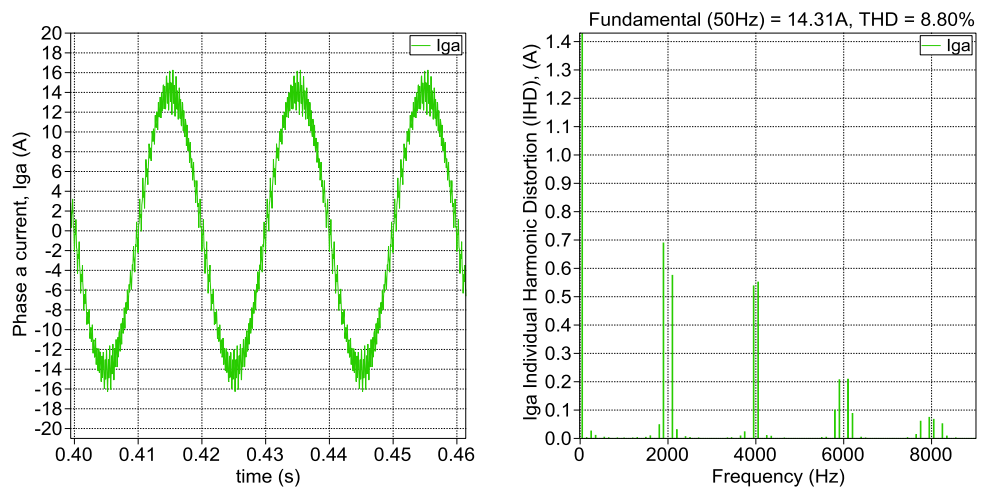


Fig. 4.29: VSC Current Waveform (a) and Harmonic Spectrum (b) at 0.5Z

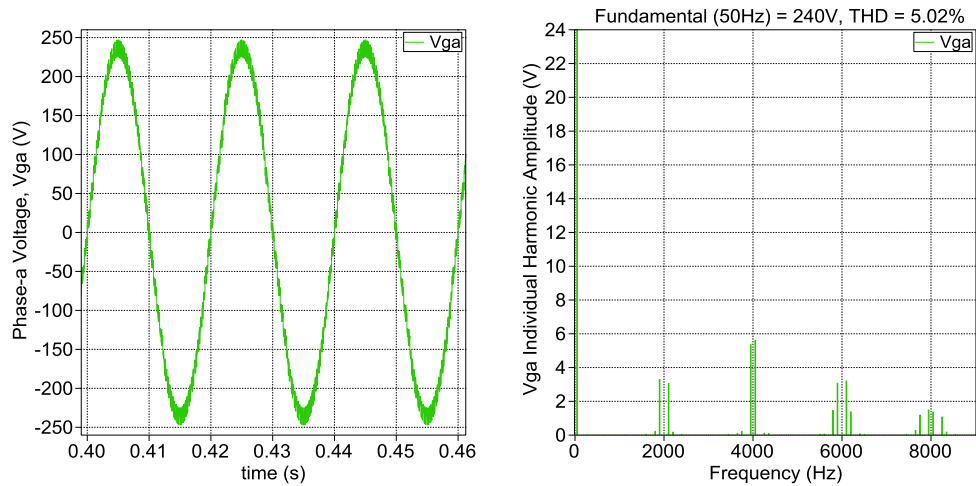


Fig. 4.30: VSC Voltage Waveform (a) and Harmonic Spectrum (b) at 0.5Z

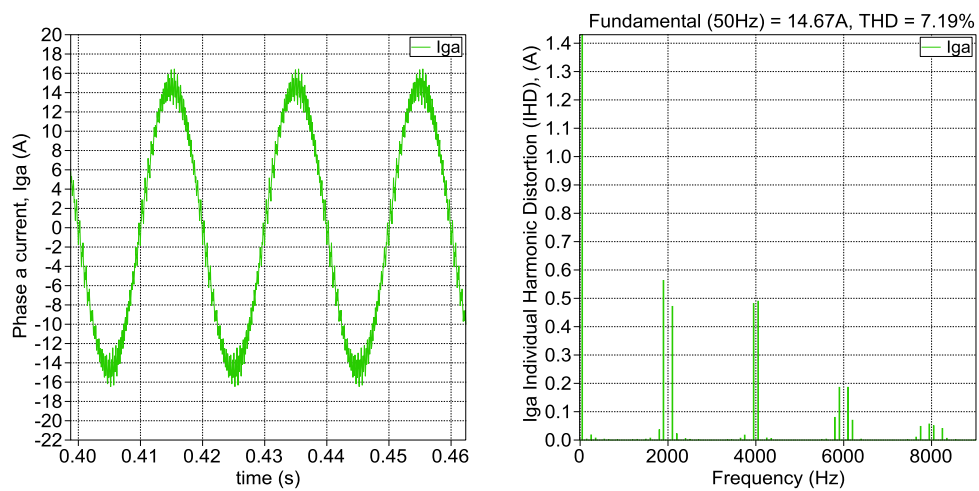


Fig. 4.31: VSC Current Waveform (a) and Harmonic Spectrum (b) at 2Z

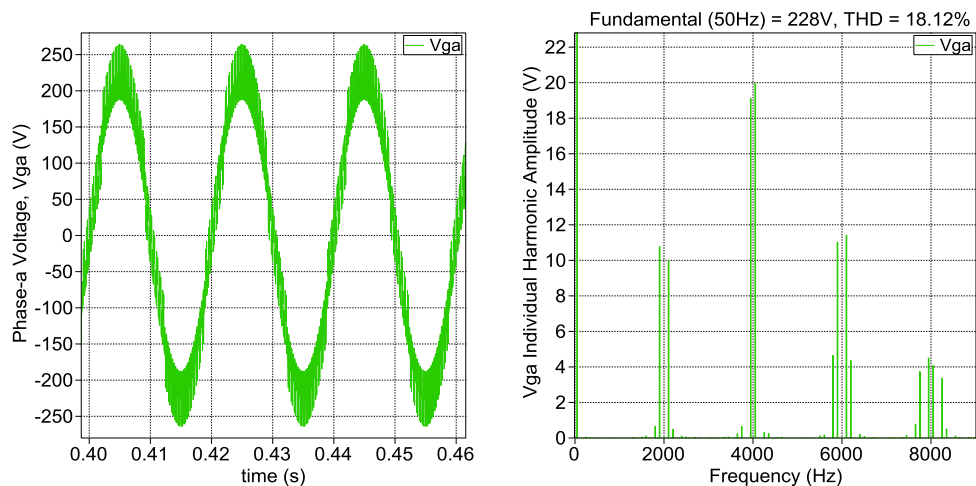


Fig. 4.32: VSC Voltage Waveform (a) and Harmonic Spectrum (b) at 2Z

4.3.3 Inverter Operating Power I

The operating power (P) of the VSC is also important in determining the generated harmonics that would appear at the PCC of the grid. VSC inverters are

usually operated a little below rated power and this might affect the level of harmonics generated by the VSC. The effect of power increased beyond the rated value was also studied to highlight the impact of increased RES penetration at the PCC. However, VSC operation beyond rated is not encouraged.

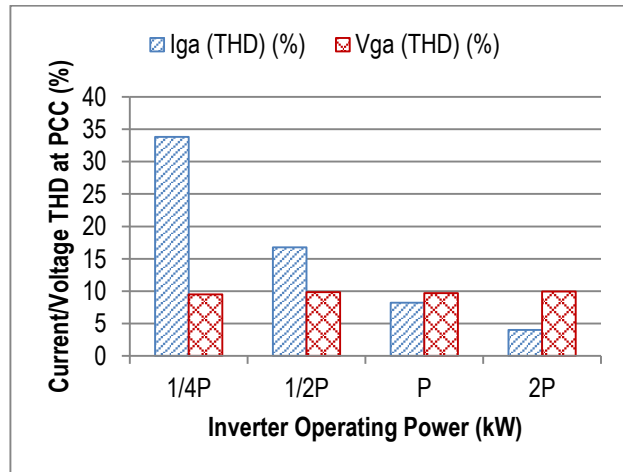


Fig. 4.33: The effect of VSC Operating Power on I_{THD} and V_{THD} at PCC

Fig. 4.33 shows that at lower operating power (<P) the I_{THD} is higher but when the operating power is increased to 2P the I_{THD} reduces below the IEEE 519 harmonic limit. However, it is necessary to state that the individual harmonics do not change but the THD increases for low power and decreases for higher power due to the fundamental current value being small or large for calculating the THD indices. This can be seen in Fig. 4.34 - Fig. 4.39. It could also be observed that the V_{THD} at the PCC is not affected much by the power variation, at all instances the V_{THD} is about 9.5%.

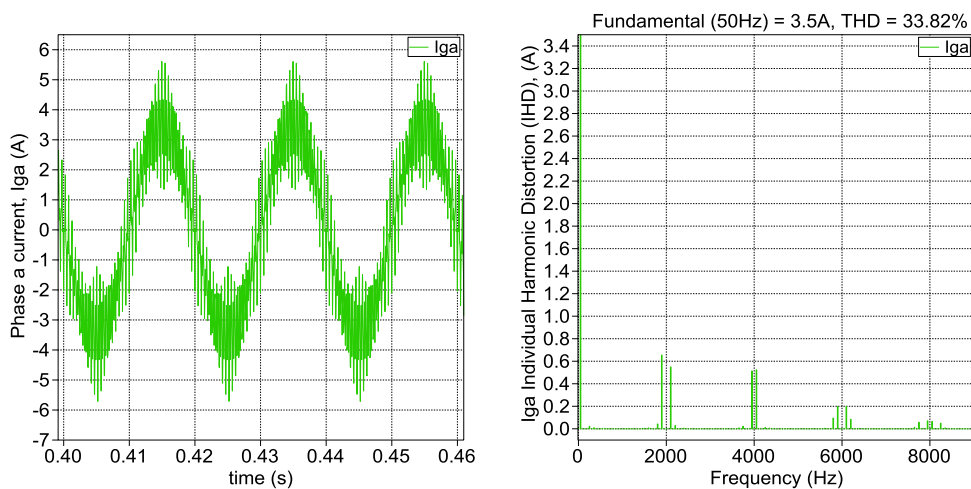


Fig. 4.34: VSC Current Waveform (a) and Harmonic Spectrum (b) at 0.25P

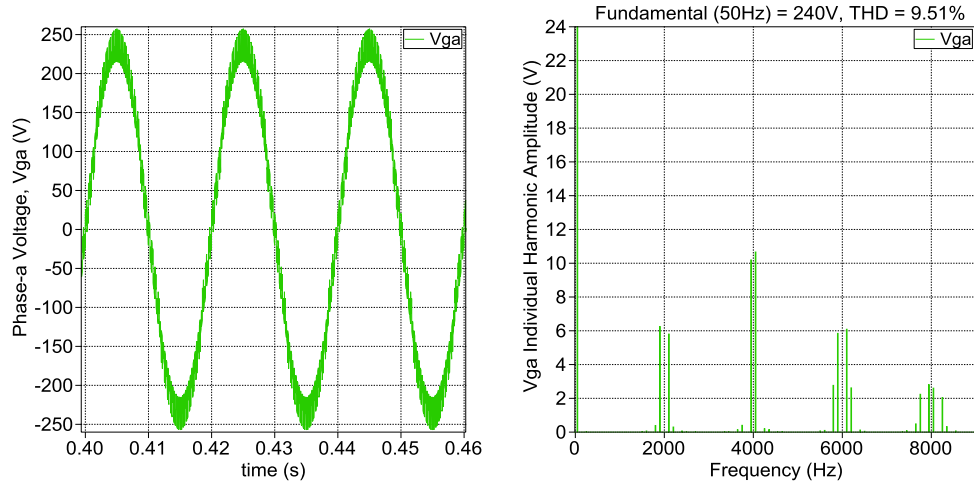


Fig. 4.35: VSC Voltage Waveform (a) and Harmonic Spectrum (b) at 0.25P

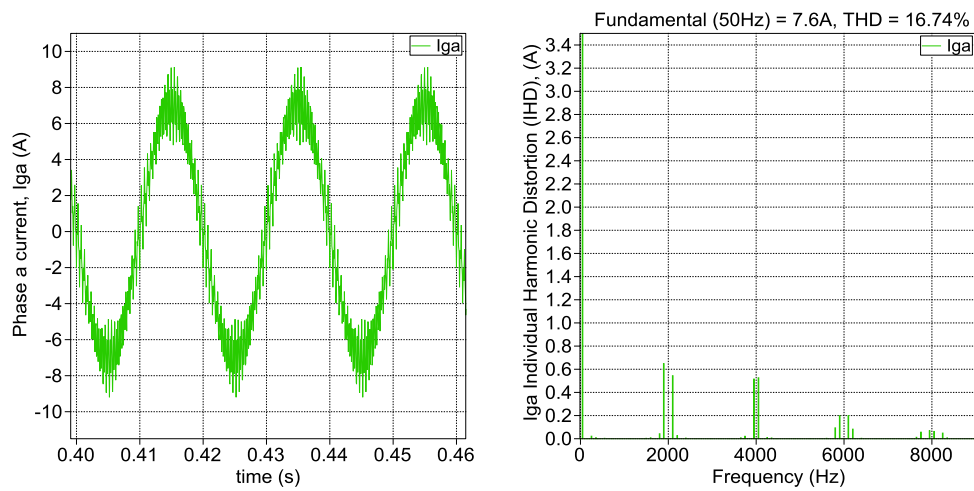


Fig. 4.36: VSC Current Waveform (a) and Harmonic Spectrum (b) at 0.5P

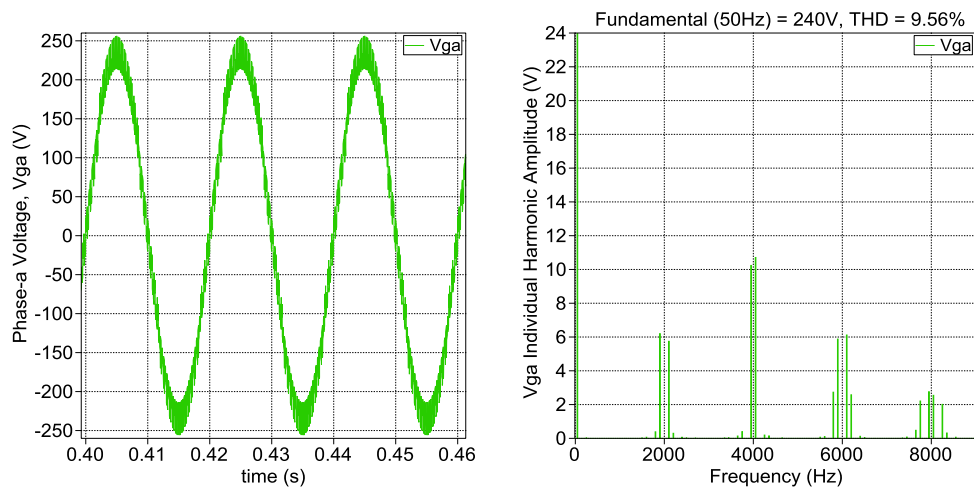


Fig. 4.37: VSC Voltage Waveform (a) and Harmonic Spectrum (b) at 0.5P

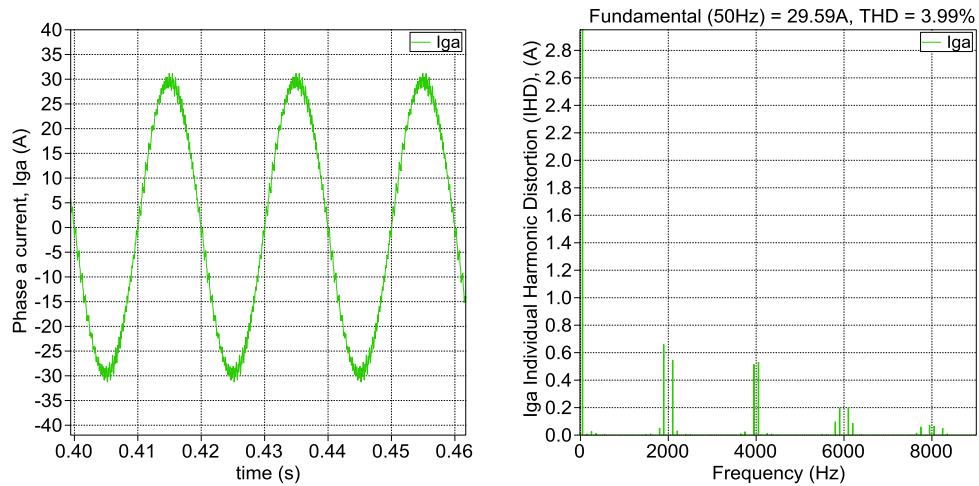


Fig. 4.38: VSC Current Waveform (a) and Harmonic Spectrum (b) at 2P

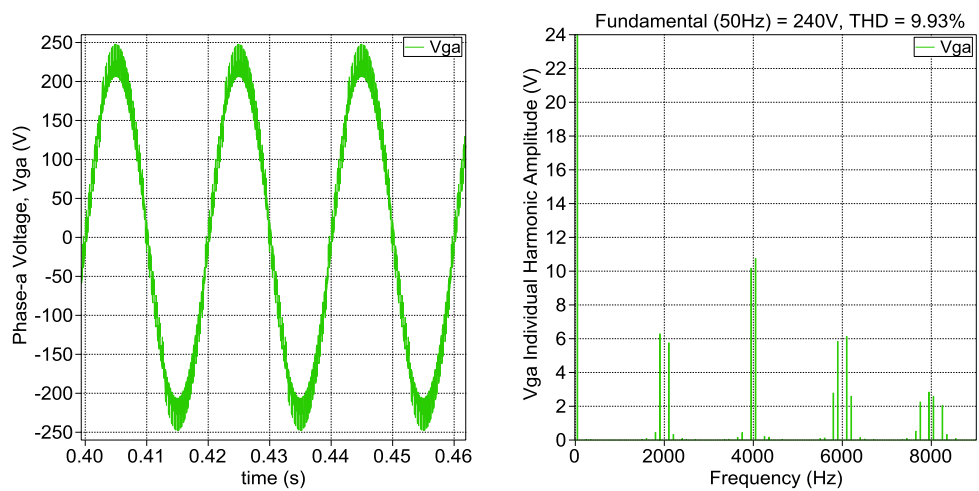


Fig. 4.39: VSC Voltage Waveform (a) and Harmonic Spectrum (b) at 2P

4.4 Attenuation of VSC Harmonics Using Filters

The conventional way of attenuating harmonics to meet the IEEE 519 harmonic standard [31] is by the use of filters. The three most common types of filters used in attenuating VSC harmonics are the L, LC, and LCL filter configuration. These configurations are discussed below.

4.4.1 L Filter

The L -filter could be regarded as the inductor that interfaces the VSC terminals to the grid lines; it is sometimes regarded as the transformer or grid inductance lumped together with the interfacing VSC terminal inductor [4]. This is so because the effective attenuation of harmonics is as a result of the inductances on that line and harmonic levels measured at any point along this line gives the same value unless separated by a capacitor. It is a first order filter and it provides

a simple solution in the attenuation of current harmonics. The L -filter achieves little attenuation of about -20dB/decade over the whole frequency range [66, 67].

In a case where an L -filter is to be connected to the line, the switching frequency of the converter has to be very high for the L -filter to be functional [67, 68]. As the microgrid system becomes larger in terms of kW, the current harmonics becomes larger and the only way for the L -filter to continue eliminating the harmonics is for its rated value to become larger. This is not feasible because the inductor would become bulky, occupy more space and increase cost.

The results given up to this point in the thesis have been achieved by the use of an L -filter.

4.4.2 LC Filter

The LC -filter is commonly used in the attenuation of voltage and current harmonics. It has a higher reactive power consumption and cost. It is a second order filter and achieves an attenuation of -40dB/decade [66]. The shunt component in the form of a capacitor that is introduced provides a low reactance at the switching frequency. Nevertheless, this component will have to present a high magnitude impedance within the control frequency range [66].

The LC -filter is suitable to systems where the impedance of the load across the capacitor is relatively high at and above the converter switching frequency [66, 68]. The LC -filter limitation is that the shunt component is ineffective when connected to a stiff grid system, where the grid impedance is insignificant at the converter switching frequency [66]. The distortion of the current output is the same as the inductor current distortion with an L -filter, where the attenuation depends solely on the filter inductance [66].

4.4.3 LCL Filter

The LCL -filter is proposed in many literatures as a better filter for the attenuation of harmonics generated by the switching of converters [66, 69]. It is a third order filter with an attenuation of -60dB/decade for frequencies in excess of the resonant frequency. It achieves the harmonic attenuation with lower switching frequencies and with less overall energy stored [66, 67]. Notwithstanding, the

LCL-filter has been known to cause lots of instability on the system due to resonance [69]. To overcome this, a damping element in the form of a passive element (such as a resistance) is connected in series or parallel to the filters.

4.5 Filter Design

Given below are some of the design formulas used in calculating the filter parameter values. Some design rules used in [70-72] to calculate passive parameters such as filter inductance and capacitance is based on the active power injected to the grid by the VSC and the equivalent impedance at the fundamental frequency at the PCC to the grid or at the VSC terminal [72]. This can be seen in 4.3 to 4.6 and will be referred to as **Filter Design Method 1**.

$$I_b = \frac{P_b}{V_b} \quad (4.3)$$

$$Z_b = \frac{V_b^2}{P_b} \quad (4.4)$$

$$L_b = \frac{Z_b}{2\pi f_n} \quad (4.5)$$

where P_b is base power, I_b is base current, V_b is base voltage, Z_b is base impedance and f_n is the systems fundamental frequency.

$$C_b = \frac{1}{2\pi f_n Z_b} \quad (4.6)$$

where L_b is the maximum value of inductance on the line and C_b is the maximum value of capacitance that can be on the line.

The filter capacitance can be calculated by using a limiting factor of 0.05 to maintain not more than 5% power factor variation.

$$C_f = 0.05 \times C_b \quad (4.7)$$

The filter inductance one (L_{f1}) would be chosen not to exceed L_b , that is

$$L_{f1} \leq L_b \quad (4.8)$$

It is usually chosen to be 10% of L_b

$$L_{f1} \leq 0.1 \times L_b \quad (4.9)$$

And in the case of an LCL Filter, L_{f2} (filter inductance two) is calculated as,

$$L_{f2} = \alpha L_{f1} \quad (4.10)$$

where α is a factor limiting L_{f2} to be less than L_{f1} .

Filter Design Method 2: In this method, C_f is calculated by limiting the total reactive power required by the capacitor to be within 15% of the total rated active power.

$$C_f = 15\% \times \frac{P_{rated}}{3 \cdot 2\pi f_m \cdot V_{rated}^2} \quad (4.11)$$

However, either of the two formulas (4.7 or 4.11) for calculating C_f gives the same result.

The filter inductance is calculated as a function of the DC capacitor voltage, the VSC switching frequency and the peak ripple of the maximum rated current of the VSC.

$$L_{f1} = \frac{1}{8} \times \frac{V_{dc}}{f_{sw} \cdot \Delta \hat{I}_{Lmax}} \quad (4.12)$$

Where $\Delta \hat{I}_{Lmax}$ is the peak ripple of the maximum rated load current I_{Lmax} .

$$\Delta \hat{I}_{Lmax} = (5 - 20\%) \times I_{rated} \quad (4.13)$$

For an LCL Filter, L_{f2} is calculated as,

$$L_{f2} = \alpha L_{f1} \quad (4.14)$$

Where α is a factor limiting L_{f2} to be less than L_{f1} just as in Design Method 1.

4.5.1 Resonant Frequency and Damping of LC and LCL Filter

It is important to consider resonant frequency of an LC or LCL filter as they usually require a damping element to maintain stability and to ensure optimum operation.

The resonant frequency is usually within $10f_n < f_{res} < \frac{f_{sw}}{2}$

For an LC filter the resonant frequency is calculated from

$$\omega_{res} = \frac{1}{\sqrt{L_{f1}C_f}} \quad (4.15)$$

For an LCL filter it is

$$\omega_{res} = \sqrt{\frac{L_{c1} + L_{c2}}{L_{c1}L_{c2}C_f}} \quad (4.16)$$

The damping resistor is calculated using

$$R_d = \frac{1}{3 \cdot \omega_{res} \cdot C_f} \quad (4.17)$$

Based on the above formula the following values for the filter parameters were designed and listed in Table 4.2 and Fig. 4.40 - Fig. 4.43 show a comparison of the performance between the *L*-filter and the *LCL*-filter for a 2-level VSC as derived through simulation.

Table 4.2: Filter Parameter and Achieved Harmonic Attenuation (THD)

Parameter	L filter	LCL filter
L_{f1}	7.5mH	6.0mH
C_f	–	18.42 μF
L_{f2}	–	1.25mH
R_d	–	4.24Ω
I_{THD}	8.21%	4.38%
V_{THD}	9.68%	2.79%

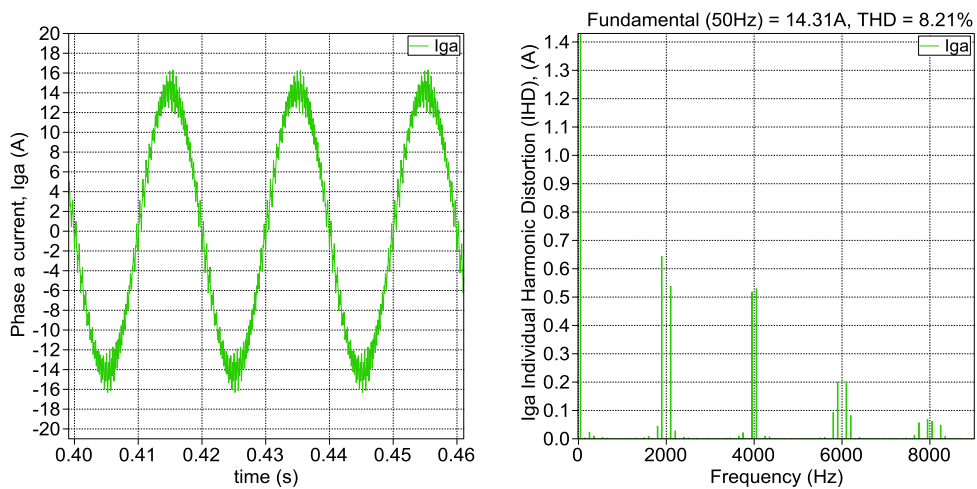


Fig. 4.40: L-filtered VSC Current Waveform (a) and Harmonic Spectrum (b)

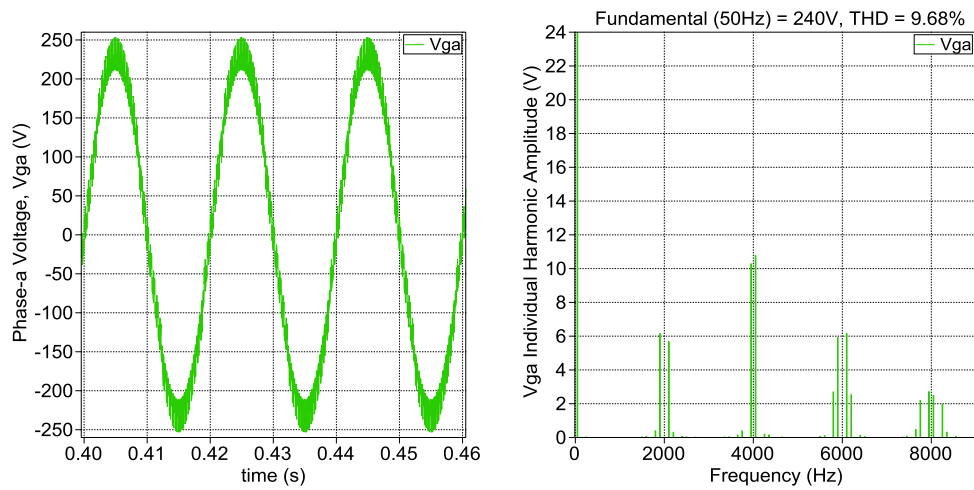


Fig. 4.41: L-filtered VSC Voltage Waveform (a) and Harmonic Spectrum (b)

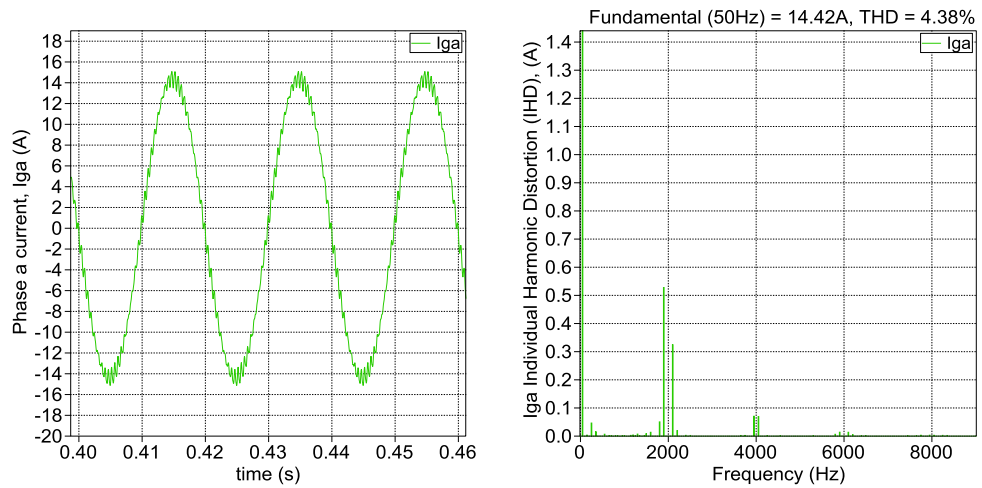


Fig. 4.42: LCL-filtered VSC Current Waveform (a) and Harmonic Spectrum (b)

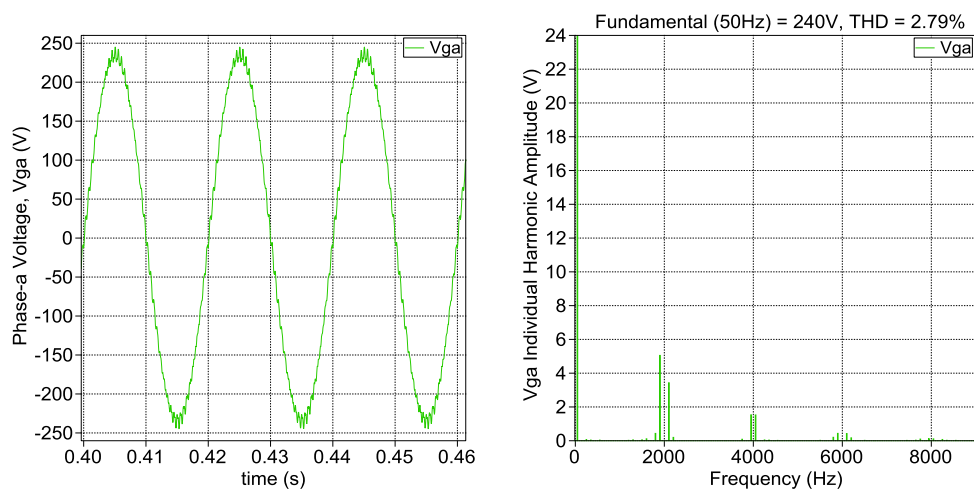


Fig. 4.43: LCL-filtered VSC Voltage Waveform (a) and Harmonic Spectrum (b)

filtered VSC. It also slightly increases the voltage THD [1]. Fig. 4.46 -Fig. 4.49 further clarifies this effect.

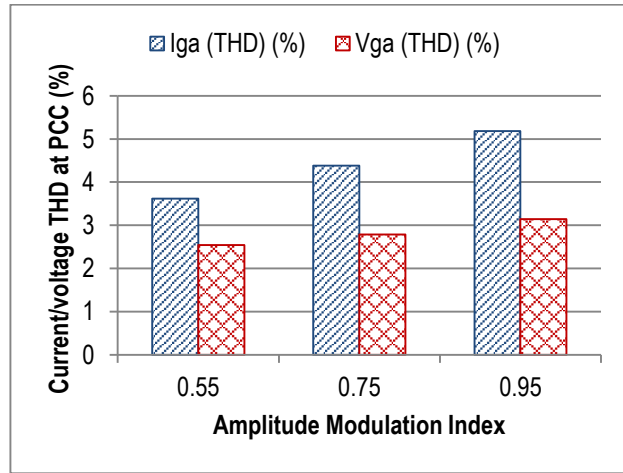


Fig. 4.45: The effect of VSC with LCL Filter m_a on I_{THD} and V_{THD} at PCC

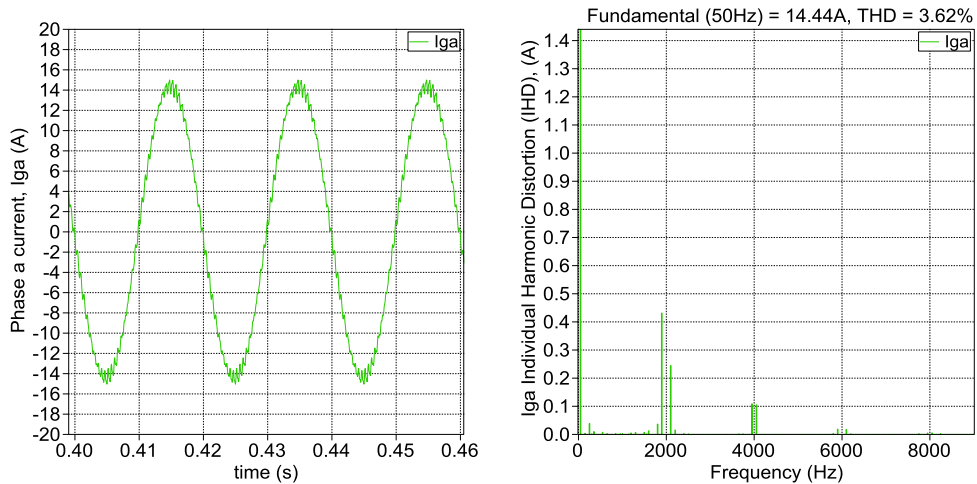


Fig. 4.46: VSC with LCL Filter Current Waveform (a) and Harmonic Spectrum (b) at $m_a = 0.55$

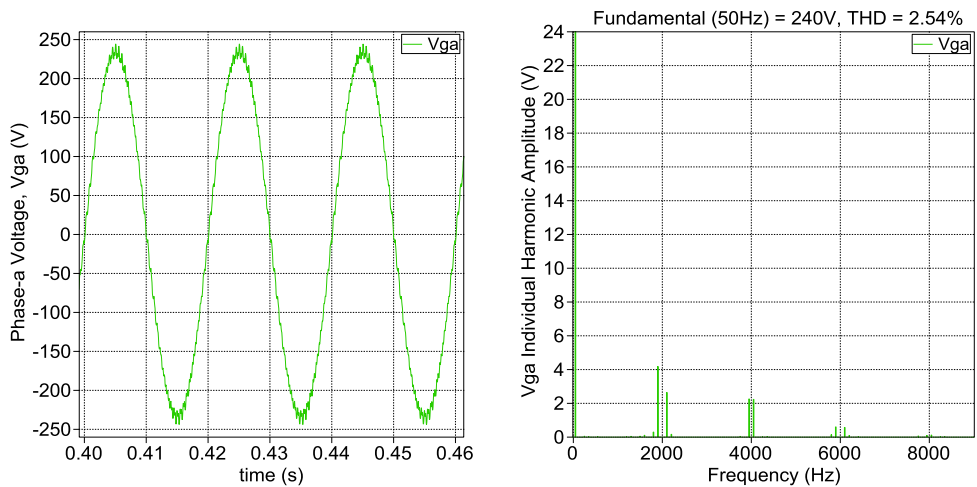


Fig. 4.47: VSC with LCL Filter Voltage Waveform (a) and Harmonic Spectrum (b) at $m_a = 0.55$

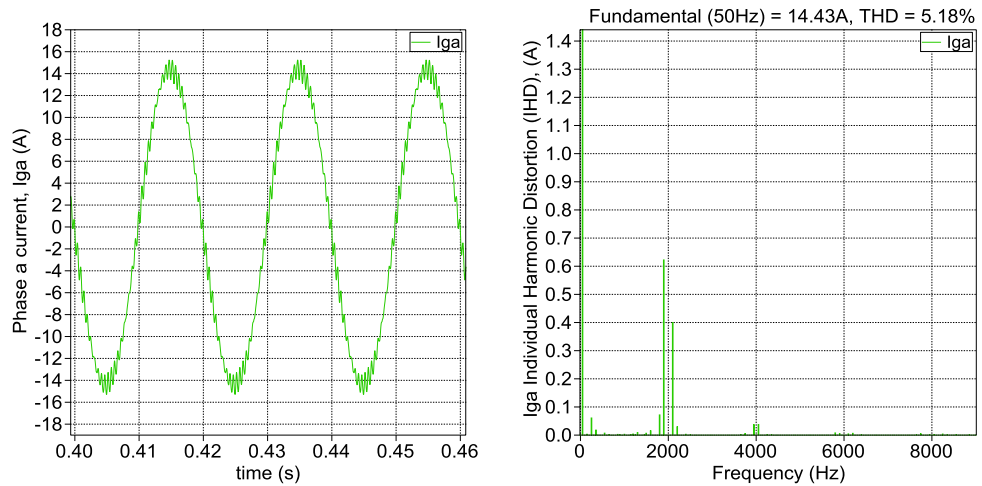


Fig. 4.48: VSC with LCL Filter Current Waveform (a) and Harmonic Spectrum (b) at $m_a = 0.95$

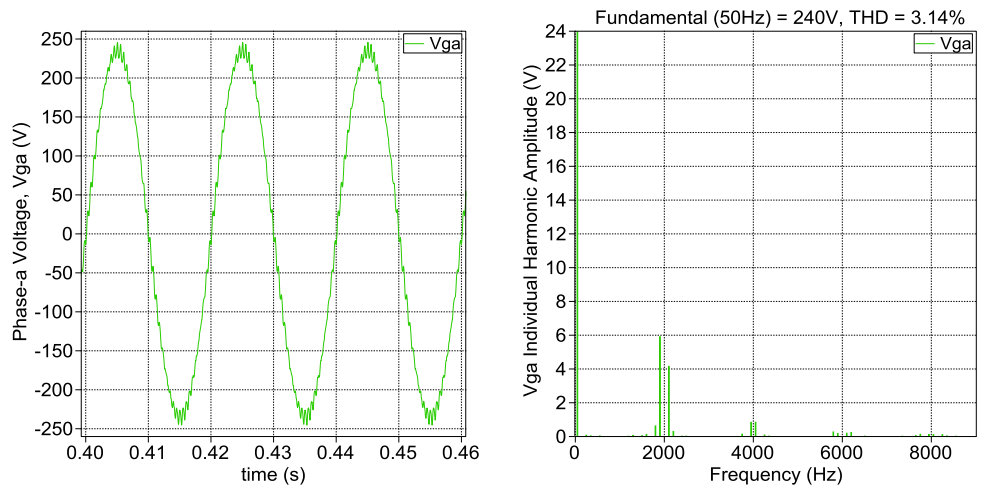


Fig. 4.49: VSC with LCL Filter Voltage Waveform (a) and Harmonic Spectrum (b) at $m_a = 0.95$

4.6.2 Switching Frequency/Frequency Modulation Index II

The generated harmonics are expected to appear at f_{sw} , and its multiples. In an *LCL*-filtered VSC the increase of f_{sw} , reduces both the I_{THD} and V_{THD} (as seen in Fig. 4.50). It can be clearly seen in Fig. 4.51 - Fig. 4.54 that the Individual Harmonic Distortion (IHD) at the f_{sw} and its multiples also reduces with the increase of f_{sw} .

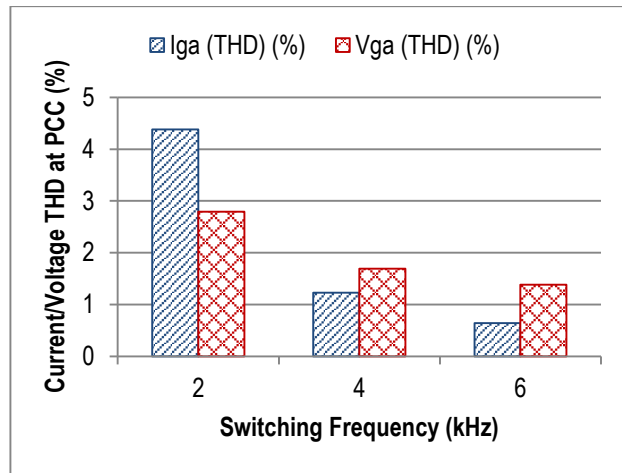


Fig. 4.50: The effect of VSC with LCL Filter f_{sw}/m_f on I_{THD} and V_{THD} at PCC

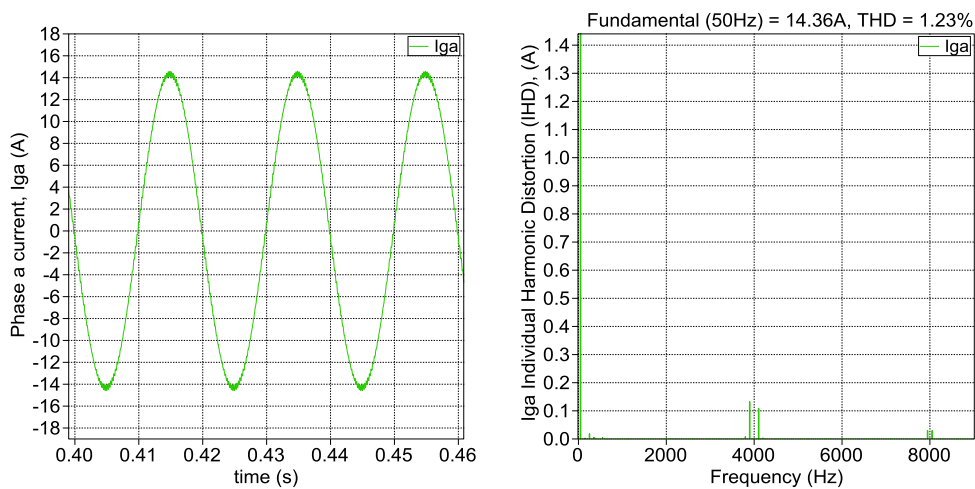


Fig. 4.51: VSC with LCL Filter Current Waveform (a) and Harmonic Spectrum (b) at $f_{sw} = 4\text{kHz}$

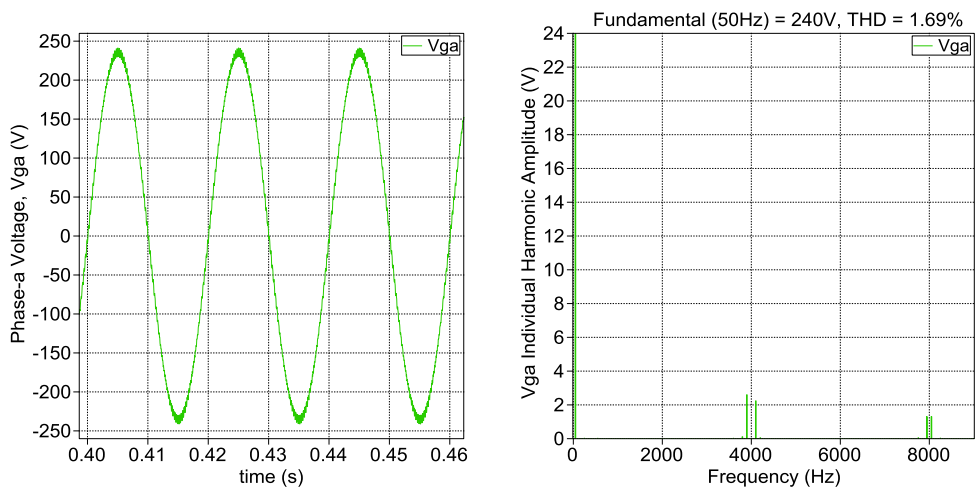


Fig. 4.52: VSC with LCL Filter Voltage Waveform (a) and Harmonic Spectrum (b) at $f_{sw} = 4\text{kHz}$

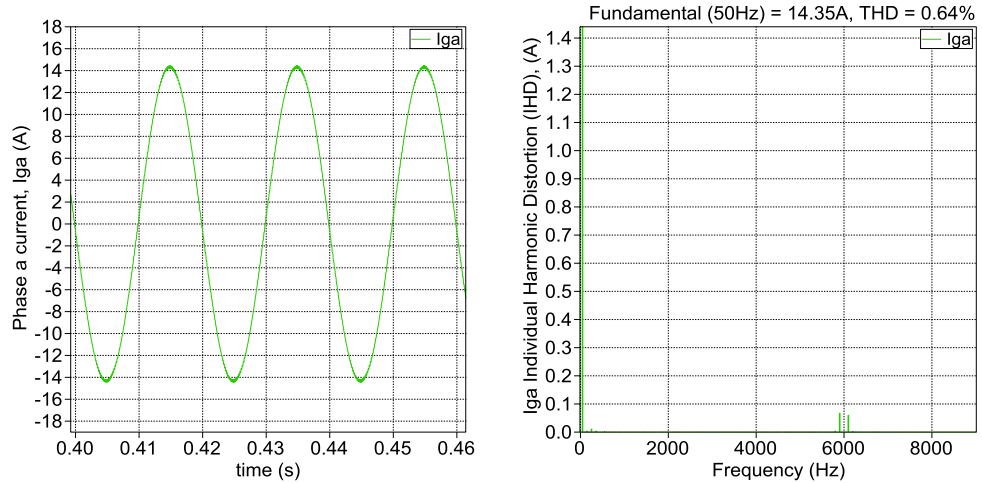


Fig. 4.53: VSC with LCL Filter Current Waveform (a) and Harmonic Spectrum (b) at $f_{sw} = 6\text{kHz}$

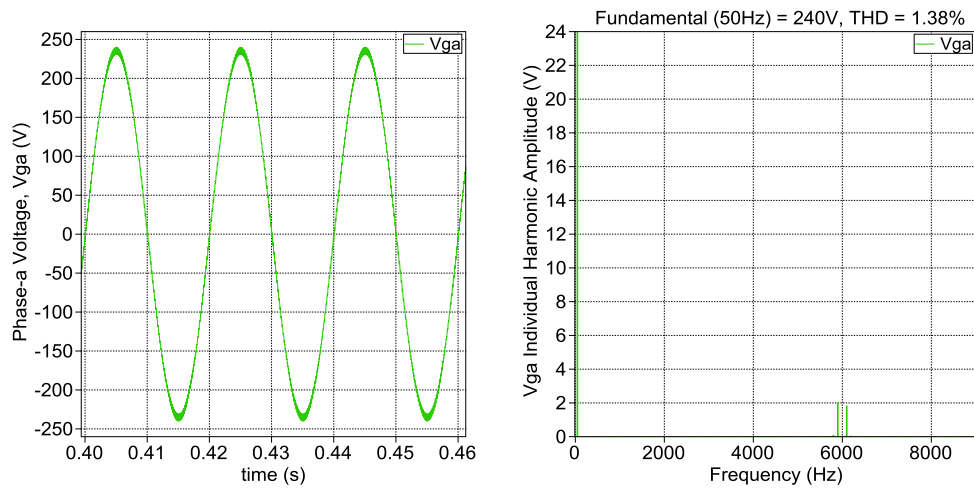


Fig. 4.54: VSC with LCL Filter Voltage Waveform (a) and Harmonic Spectrum (b) at $f_{sw} = 6\text{kHz}$

4.6.3 Converter Topology II

Just as in the case of an L -filtered VSC, the voltage each IGBT is required to switch through reduces with the increase of the VSC topology level [57]. This significantly reduces the current and voltage harmonics generated by the VSC.

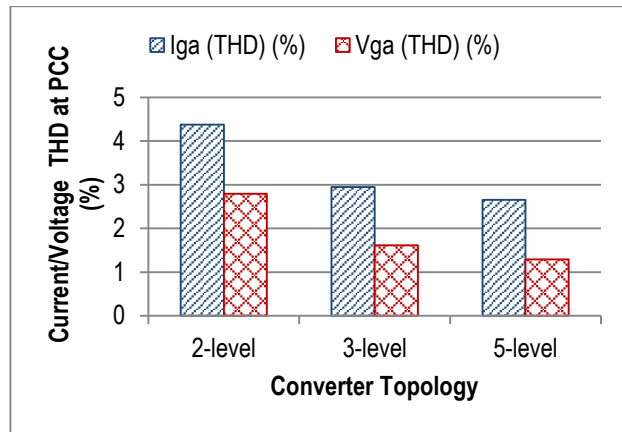


Fig. 4.55: The effect of VSC with LCL Filter Topology on I_{THD} and V_{THD} at PCC

It is clear from Fig. 4.55 that as the VSC topology level increase, the I_{THD} and V_{THD} reduces. The 5-L NPC VSC with *LCL*-filter gives a better harmonic performance compared to the *LCL*-filtered 3-L NPC VSC and the 2-L VSC.

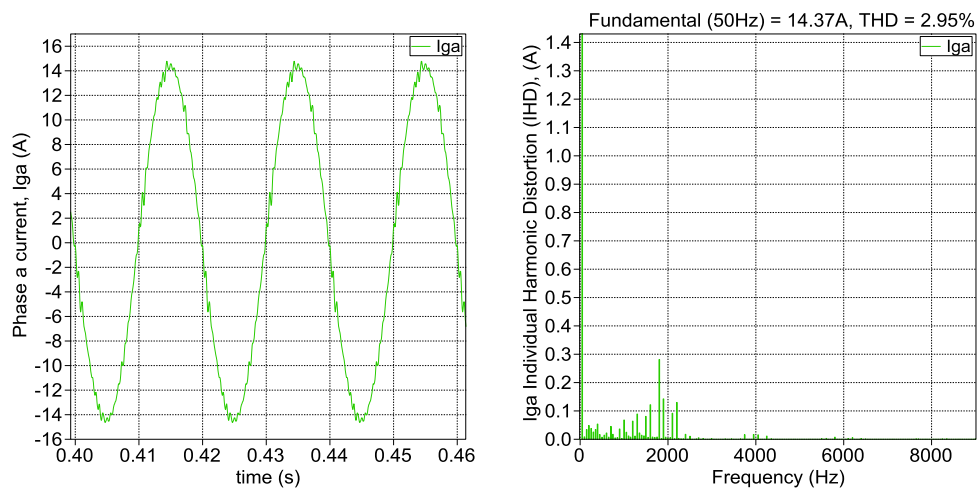


Fig. 4.56: 3-L NPC VSC with LCL Filter Current Waveform (a) and Harmonic Spectrum (b)

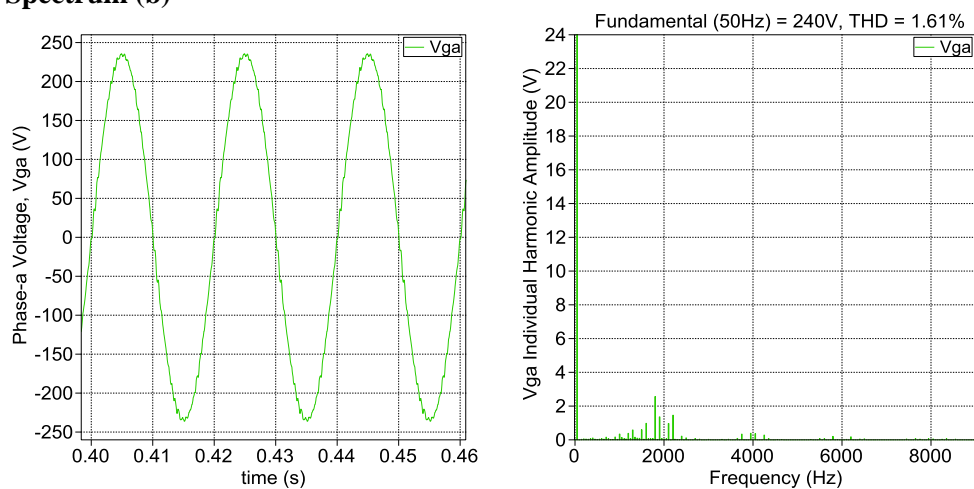


Fig. 4.57: 3-L NPC VSC with LCL Filter Voltage Waveform (a) and Harmonic Spectrum (b)

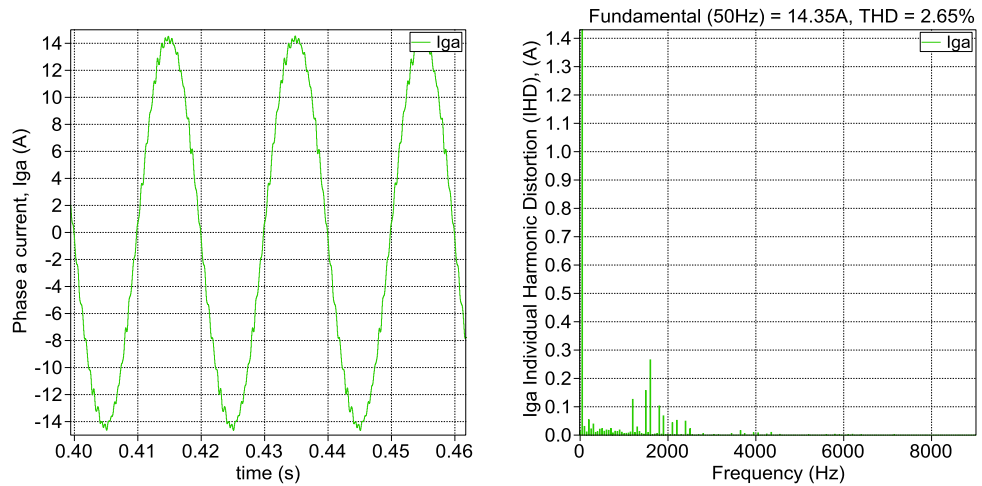


Fig. 4.58: 5-L NPC with LCL Filter VSC Current Waveform (a) and Harmonic Spectrum (b)

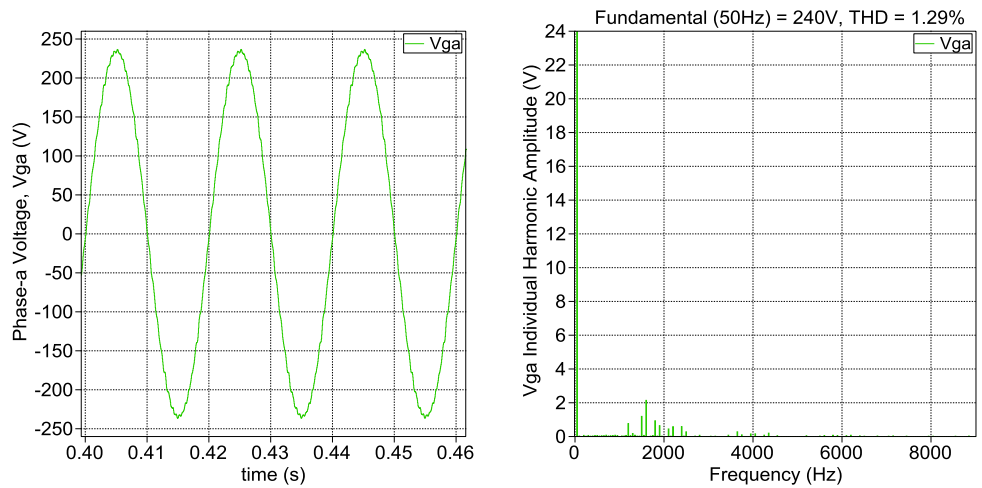


Fig. 4.59: 5-L NPC VSC with LCL Filter Voltage Waveform (a) and Harmonic Spectrum (b)

4.7 Harmonics Generated by an LCL Filtered VSC Based on System/Operation Characteristics

The same investigation carried out in section 4.2 will be performed here for an *LCL*-filtered VSC. The investigation is to analyse the effect of grid system/operation characteristics on the harmonics generated by a VSC converter connected to the grid.

4.7.1 Grid Voltage Waveform II

The effect of grid voltage distortion when varied from 0-5% THD on the VSC harmonics at the PCC is presented in Fig. 4.60. A grid distortion of 5% caused the V_{THD} at the PCC to go above 5%, this is within the IEEE 519 harmonic limit.

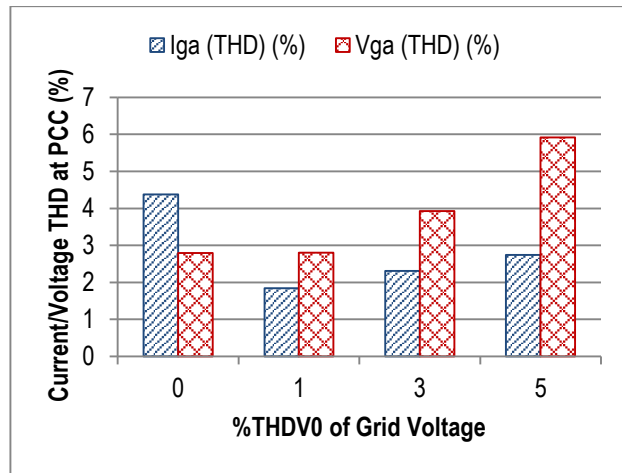


Fig. 4.60: The effect of Grid Voltage Distortion on I_{THD} and V_{THD} at the PCC for an LCL Filtered VSC

Just as in the case of the L -filtered VSC, introducing grid voltage distortion first reduces the I_{THD} but subsequent increase of grid voltage distortion increases the I_{THD} . The introduced grid voltage distortion mainly affects the V_{THD} of the VSC as seen at the PCC to the grid. Fig. 4.61 - Fig. 4.66 clearly shows how this affects the current/voltage waveform and their corresponding individual harmonics distortion.

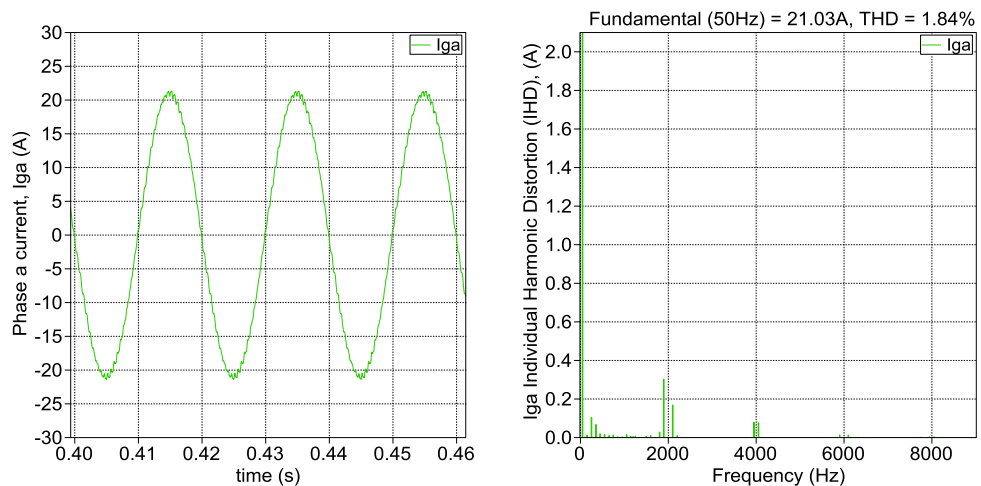


Fig. 4.61: VSC with LCL Filter Current Waveform (a) and Harmonic Spectrum (b) at 1% V_{THD}

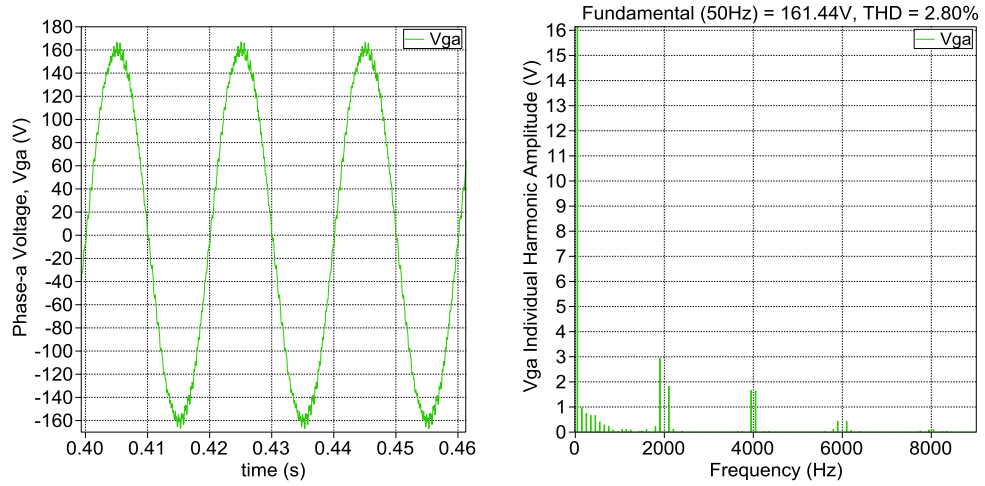


Fig. 4.62: VSC with LCL Filter Voltage Waveform (a) and Harmonic Spectrum (b) at 1% V_{THD}

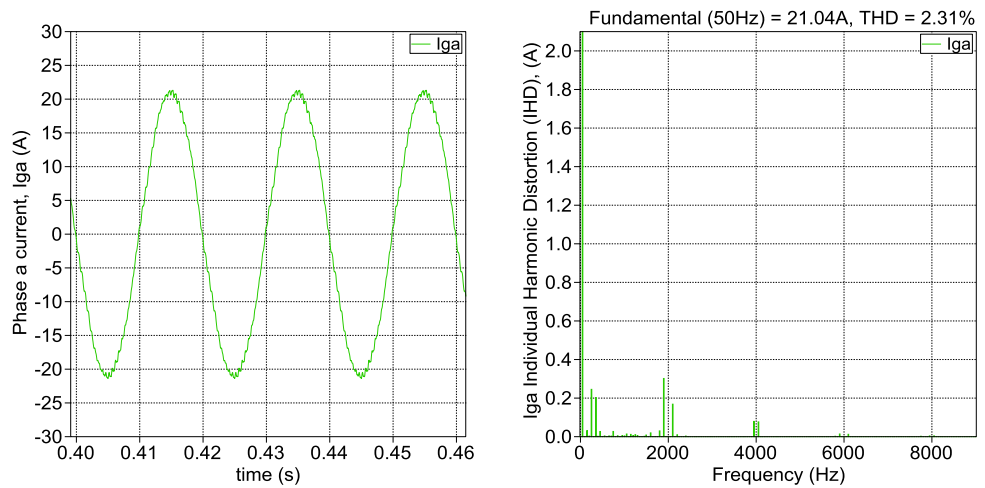


Fig. 4.63: VSC with LCL Filter Current Waveform (a) and Harmonic Spectrum (b) at 3% V_{THD}

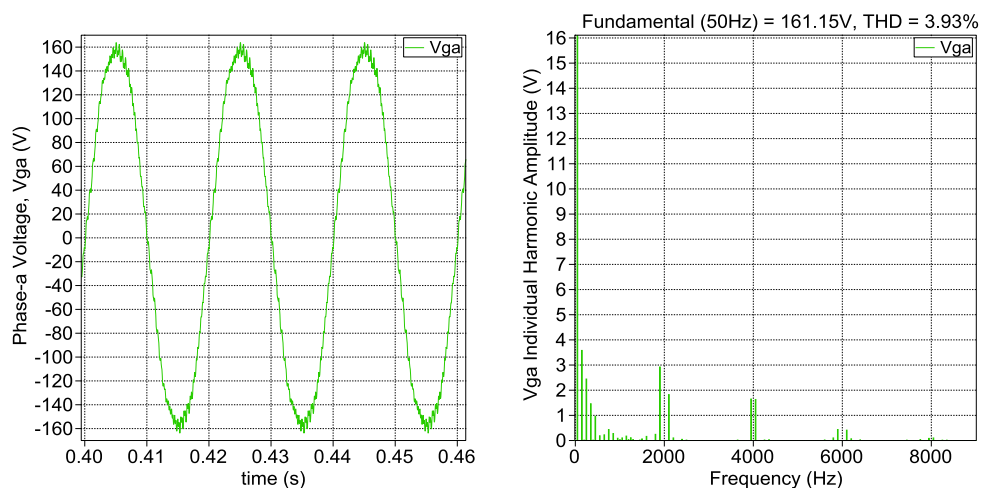


Fig. 4.64: VSC with LCL Filter Voltage Waveform (a) and Harmonic Spectrum (b) at 3% V_{THD}

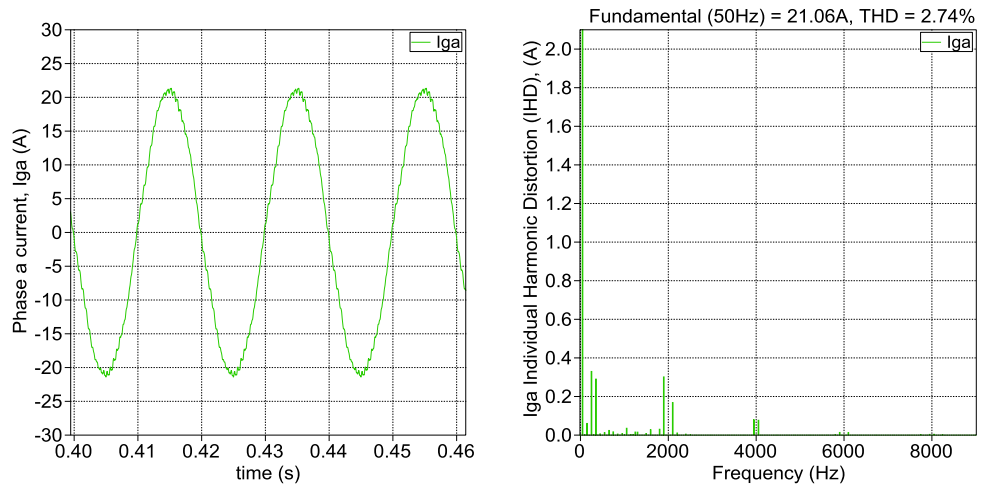


Fig. 4.65: VSC with LCL Filter Current Waveform (a) and Harmonic Spectrum (b) at 5% V_{THD}

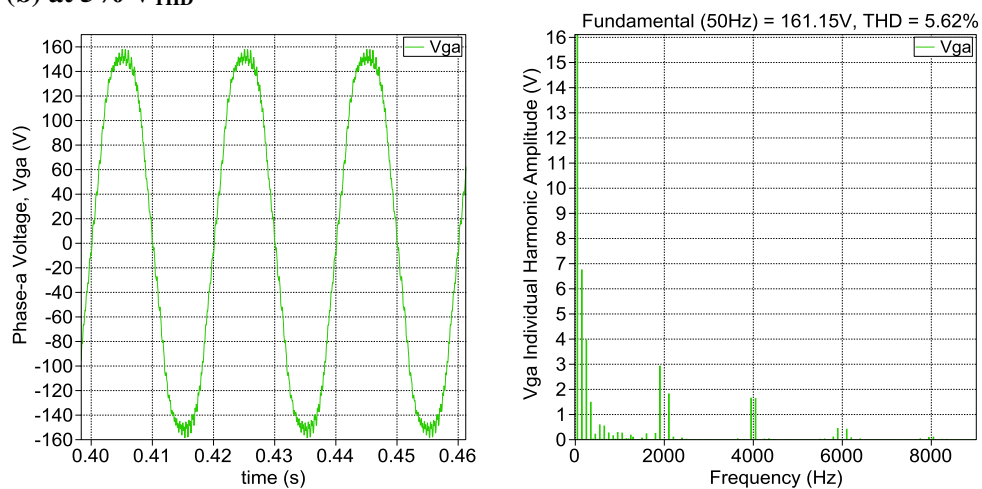


Fig. 4.66: VSC with LCL Filter Voltage Waveform (a) and Harmonic Spectrum (b) at 5% V_{THD}

4.7.2 Grid System Impedance II

The studied system has a typical grid impedance of $(0.4 + j0.25) \Omega$ [62].

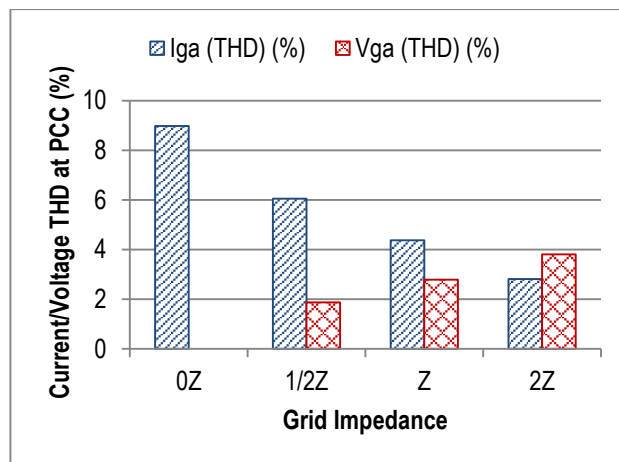


Fig. 4.67: The effect of Grid Impedance Variation on I_{THD} and V_{THD} at PCC for an LCL Filtered VSC

For this case increasing grid impedance reduces the I_{THD} but increases the V_{THD} . In the first case were an assumption of no impedance was simulated the I_{THD} was very high and the voltage harmonics at the PCC was zero.

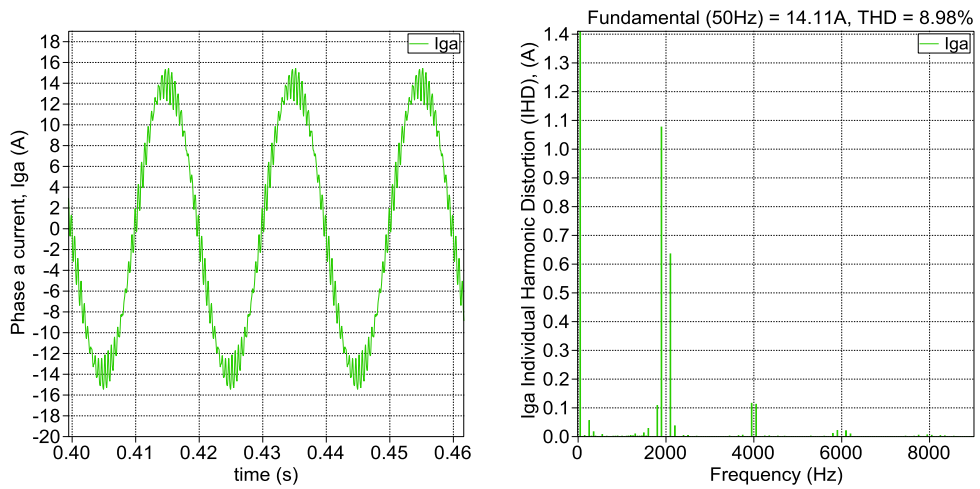


Fig. 4.68: VSC with LCL Filter Current Waveform (a) and Harmonic Spectrum (b) at 0Z

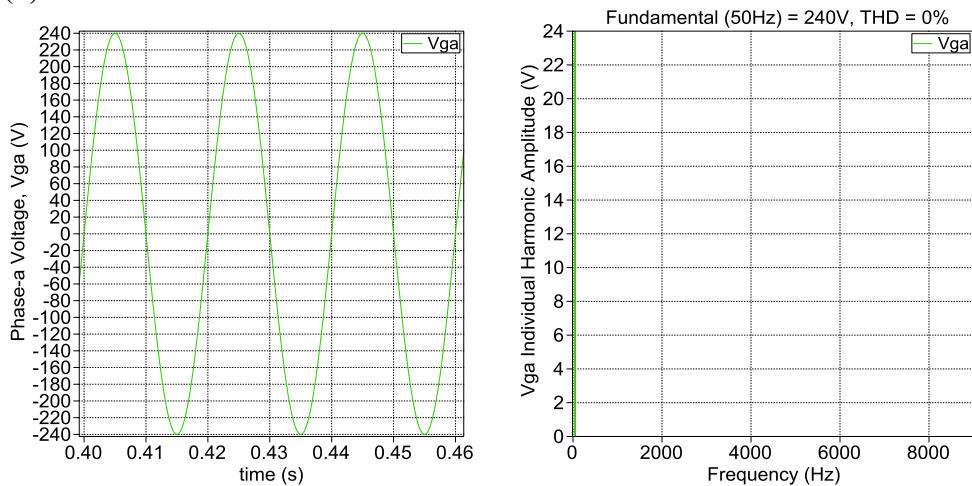


Fig. 4.69: VSC with LCL Filter Voltage Waveform (a) and Harmonic Spectrum (b) at 0Z

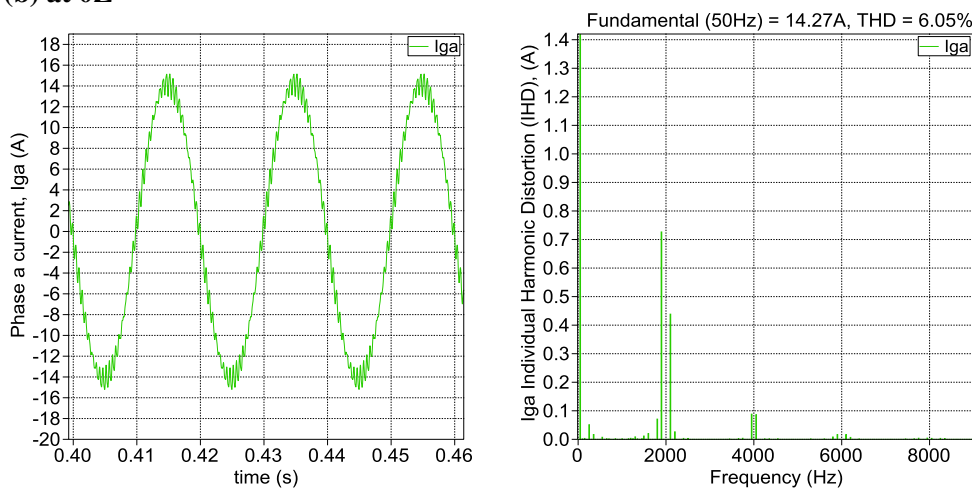


Fig. 4.70: VSC with LCL Filter Current Waveform (a) and Harmonic Spectrum (b) at 0.5Z

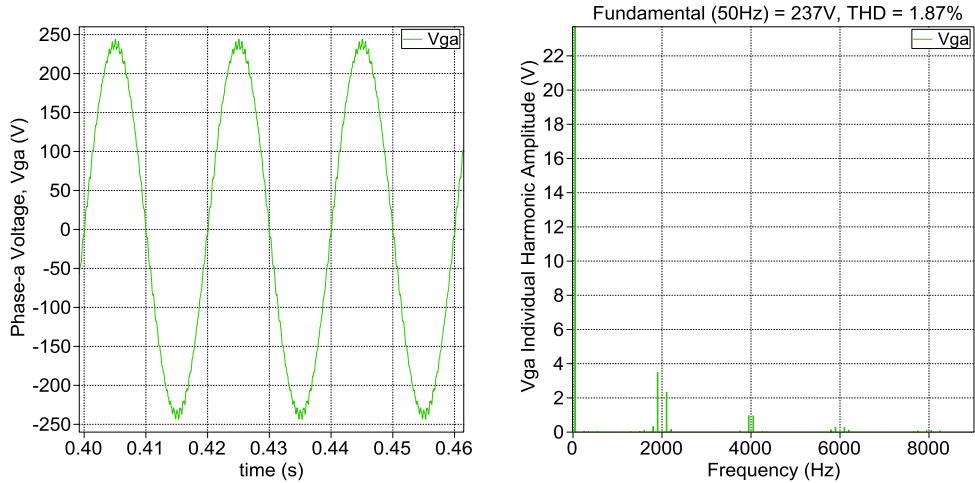


Fig. 4.71: VSC with LCL Filter Voltage Waveform (a) and Harmonic Spectrum (b) at 0.5Z

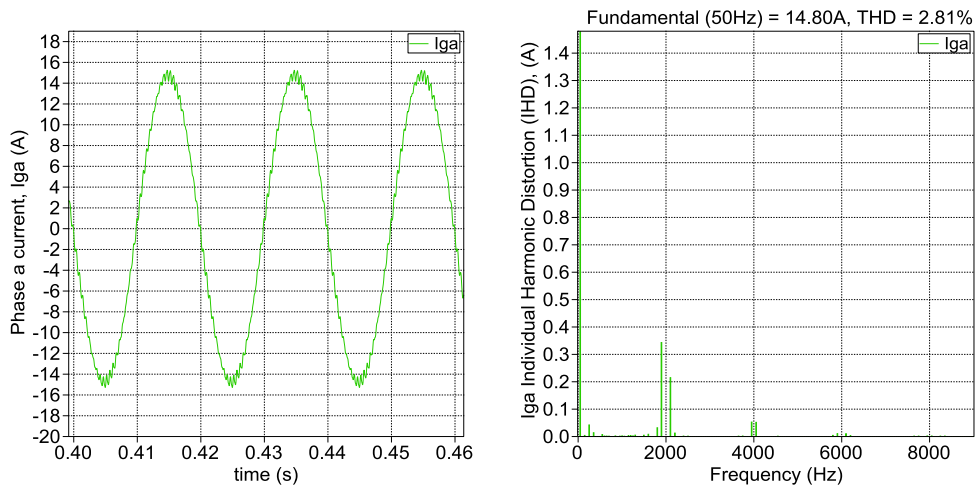


Fig. 4.72: VSC with LCL Filter Current Waveform (a) and Harmonic Spectrum (b) at 2Z

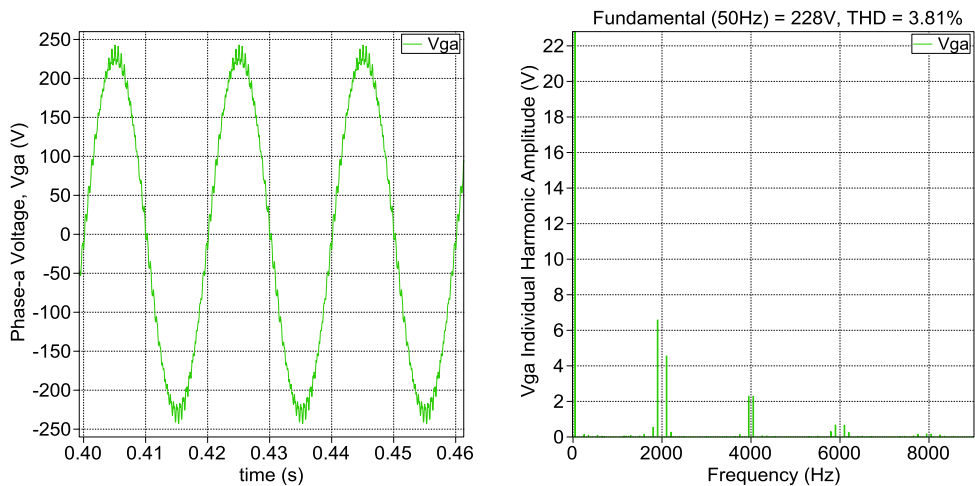


Fig. 4.73: VSC with LCL Filter Voltage Waveform (a) and Harmonic Spectrum (b) at 2Z

4.7.3 Inverter Operating Power II

In this case operating the VSC below its rated power greatly increased the current IHD and THD but an increase in operation power of the VSC reduces both the current and voltage IHD and THD. This is different from what was observed in section 4.2 for an *L*-filtered VSC (see Fig. 4.33), where the increase of operating power only reduced the I_{THD} while the V_{THD} was almost unaffected. Again VSC operation beyond rated is not encouraged but was only investigated to highlight the impact of increased RES penetration at the PCC.

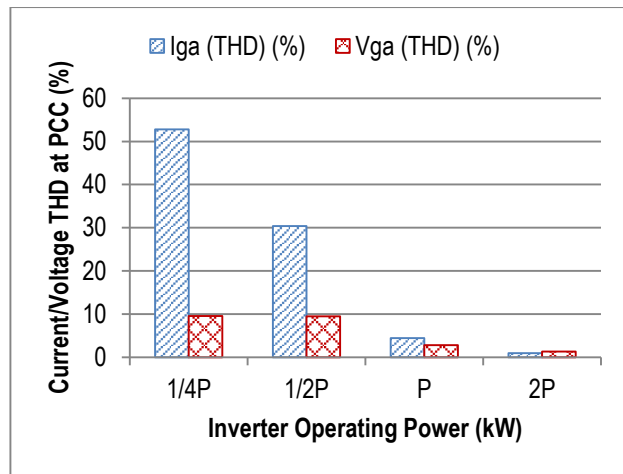


Fig. 4.74: The effect of VSC Operating Power on I_{THD} and V_{THD} at PCC

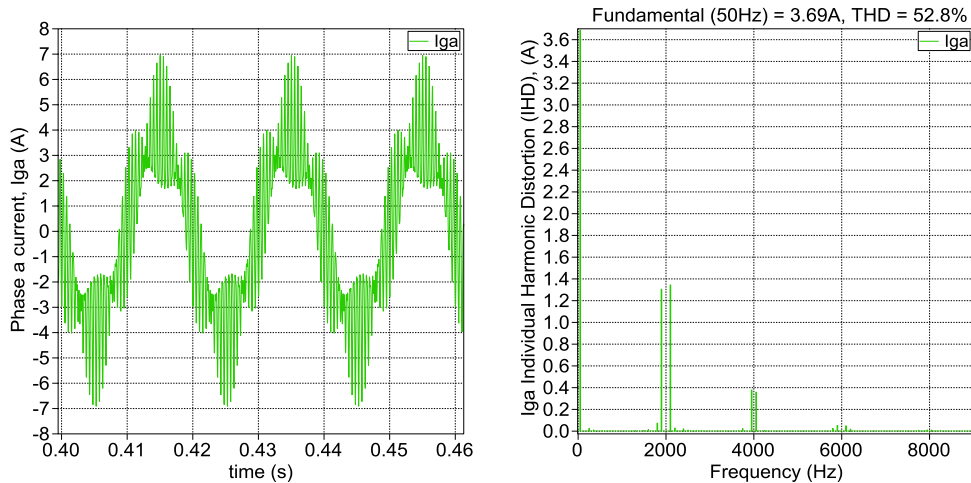


Fig. 4.75: VSC with LCL Filter Current Waveform (a) and Harmonic Spectrum (b) at 0.25P

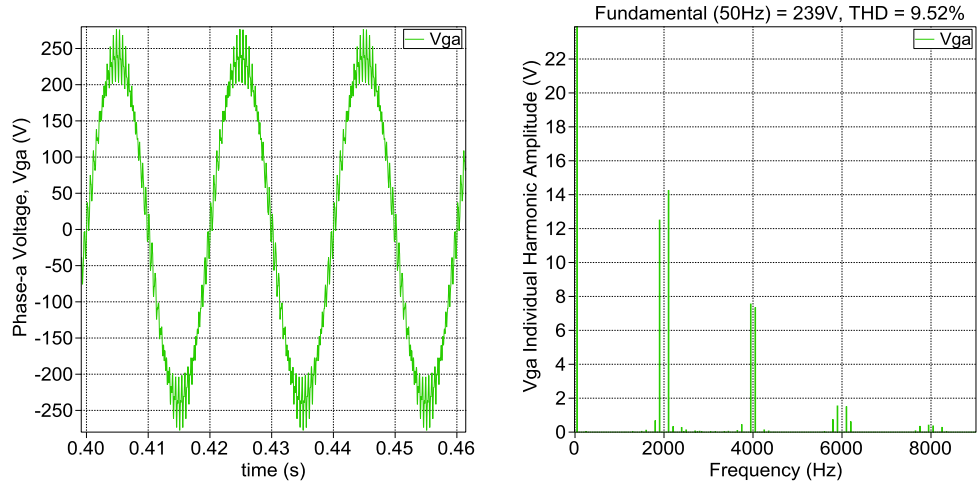


Fig. 4.76: VSC with LCL Filter Voltage Waveform (a) and Harmonic Spectrum (b) at 0.25P

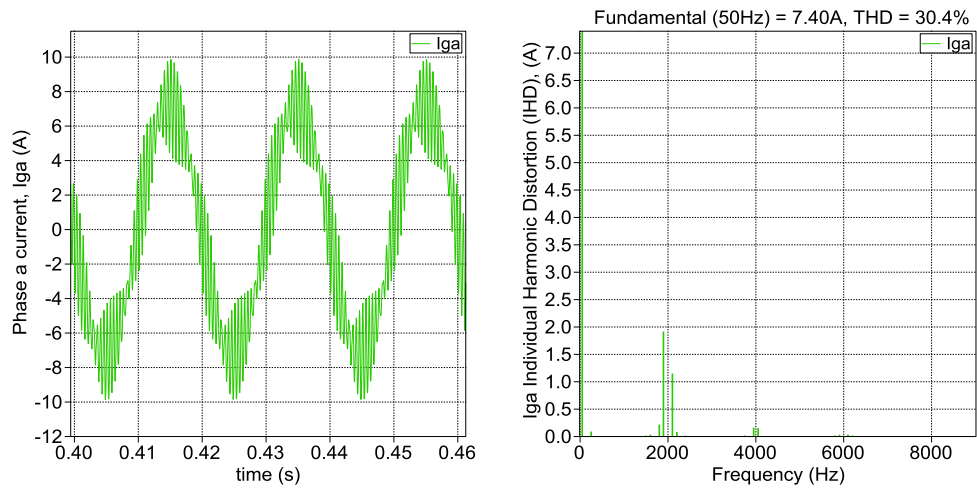


Fig. 4.77: VSC with LCL Filter Current Waveform (a) and Harmonic Spectrum (b) at 0.5P

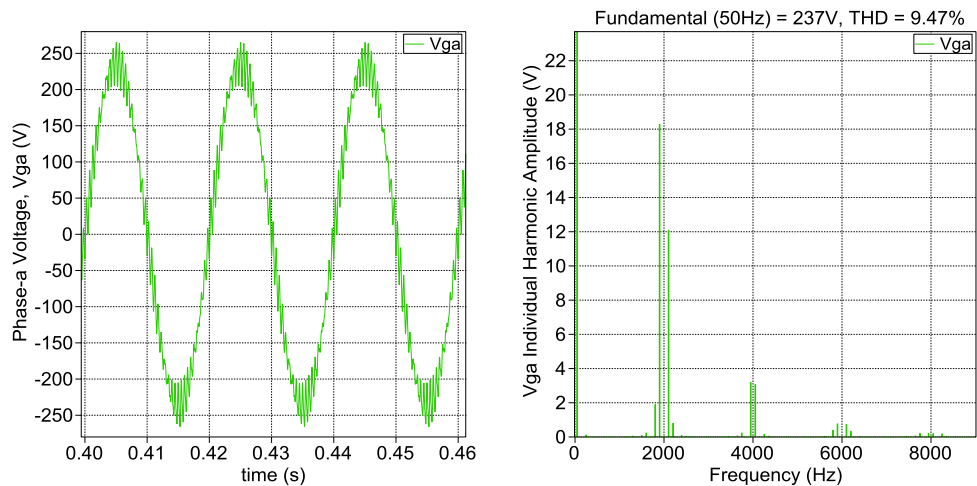


Fig. 4.78: VSC with LCL Filter Voltage Waveform (a) and Harmonic Spectrum (b) at 0.5P

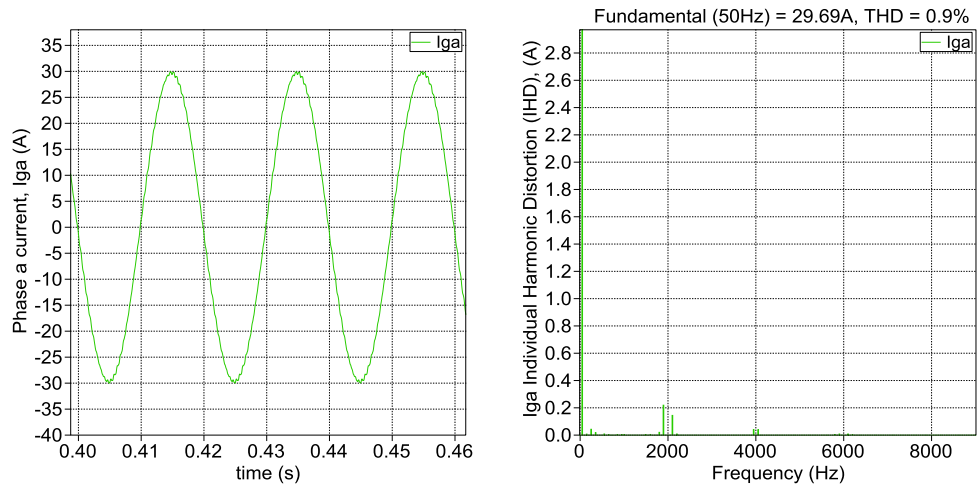


Fig. 4.79: VSC with LCL Filter Current Waveform (a) and Harmonic Spectrum (b) at 2P

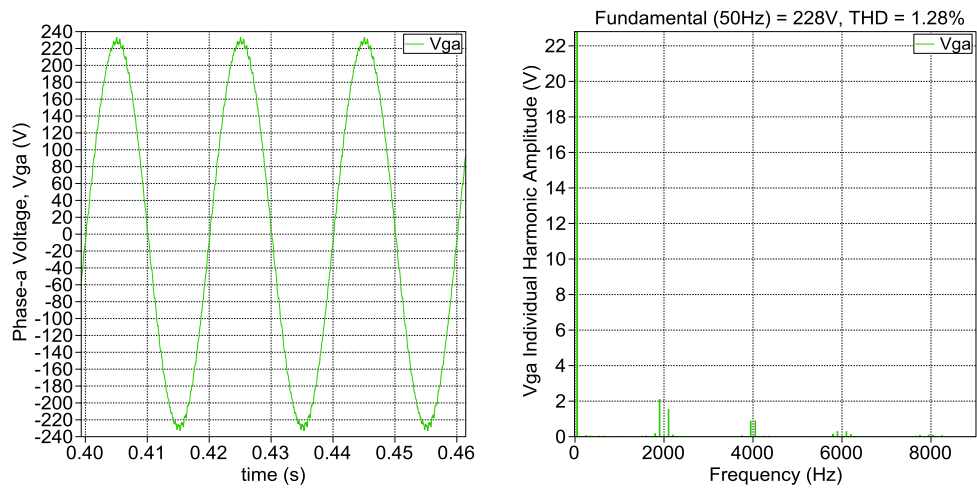


Fig. 4.80: VSC with LCL Filter Voltage Waveform (a) and Harmonic Spectrum (b) at 2P

4.8 Summary

This chapter has discussed the factors that affect the harmonics generated by a 3-phase voltage source converter. It has investigated these factors from two perspectives; firstly, from the point of the VSC design parameters and then from the grid system characteristics. Most of the results obtained are consistent with other studies in [61, 62, 73] however, it was discovered in this study that;

- i) Increasing m_a for an L -filtered VSC system decreases both I_{THD} and V_{THD} while an opposite effect is observed in an LCL -filtered VSC system (increasing m_a causes an increase in I_{THD} and V_{THD}).

- ii) Increasing f_{sw}/m_f for an L -filtered VSC system decreases I_{THD} but has no effect on V_{THD} . For an LCL -filtered system an increase in f_{sw}/m_f causes a decrease in both I_{THD} and V_{THD} .
- iii) A larger percentage reduction (40% - 55%) in I_{THD} and V_{THD} was achieved by using a 3-L NPC VSC instead of a 2-L VSC than between a 3-L NPC VSC and a 5-L NPC VSC. The percentage reduction achieved for using a 5-L NPC VSC instead of a 3-L NPC VSC was between 11% to 40%.
- iv) Increasing output power in an L -filtered VSC system causes a reduction in current THD however, the current IHD remains the same. Also it was discovered that power increase has no effect on V_{THD} and V_{IHD} . However, in an LCL -filtered VSC system increase in output power causes a reduction in both current and voltage THD and IHD.

Notwithstanding this investigation, harmonics do not add up arithmetically and so in a case where the number of VSC increases beyond one, the factors are going to affect the harmonics in a different way.

In the next Chapter, more appropriate methods for analysing the harmonics generated by N number of VSCs will be presented. This method of analysis is usually referred to as “probabilistic harmonic studies” and it involves the use of probabilistic and statistical tools.

Chapter 5

Quantifying/Predicting Harmonics of Multiple Voltage Source Converters

Quantifying current and voltage harmonic is of high important in analysing the power quality of modern day Electric Power Systems (EPS) as they contain lots of harmonic sources and loads. In this chapter, several probabilistic methods used in quantifying/predicting the net harmonics of many connected harmonic sources is reviewed, with their advantages and limitations presented. Definition of mathematical terms used in probabilistic harmonic studies are also given.

5.1 Harmonic Summation for Multiple Sources

In Section 2.2.2, various types and sources of harmonics was presented to give an introduction to harmonics. This section first gives a description of harmonics generation before discussing the summation of harmonics.

Reiterating the points made earlier, when a sinusoidal voltage source is applied to a non-linear load or device, it produces currents that are not ideally sinusoidal. This current further causes a non-sinusoidal voltage drop in the presence of the system impedance thus generating voltage harmonic distortions at the load terminal [74].

Assuming a generator Gen supplies a purely resistive load R_{load} through line impedance ($R_s + jX_s$) and a static converter (see Fig. 5.1). The generator power P_{g1} to the PCC of the load is mostly transferred to P_{load1} while a small amount is transferred to P_{conv1} (which converts the power at different frequency). There is also loss of power (P_{s1}) at the fundamental frequency of the transmission/generation system resistance (R_s) [74].

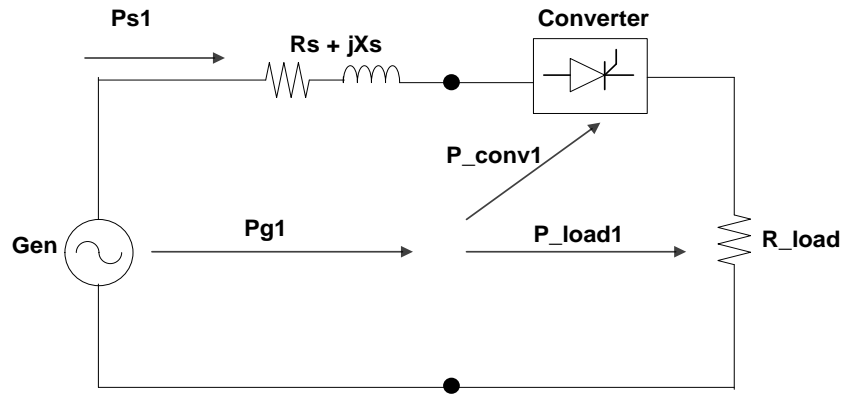


Fig. 5.1: Schematic of Power Flow at Fundamental frequency [74]

The static converter appearing as a current source of non-fundamental frequencies short circuits the generator emf, since the generator only supplies power at fundamental frequency. A small amount of the fundamental converter power (P_{conv1}) is transformed into harmonic power: where some of the power ($P_{sh} + P_{gh}$) is consumed in the system and generator resistances (R_{sh}) and (R_{gh}) while the rest (P_{loadh}) is consumed in the load (see Fig. 5.2). Thus the total power loss is equal to the fundamental frequency power (P_{s1}) + harmonic power losses ($P_{sh} + P_{gh} + P_{loadh}$) [74].

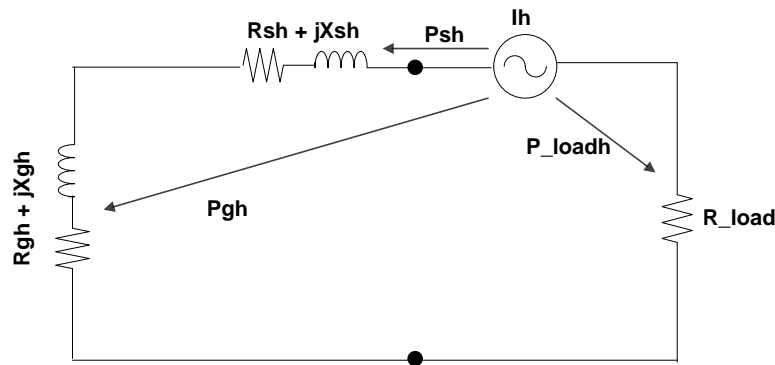


Fig. 5.2: Schematic of Harmonic Power Flow [74]

An equivalent harmonic current in a 3 phase circuit is defined by I_a , I_b , and I_c , where (5.1) is a common approach used by many manufacturers in tabulating data.

$$I_{eq} = \sqrt{(I_a^2 + I_b^2 + I_c^2)} / 3 \tag{5.1}$$

$$3I_{eq}^2 r = (I_a^2 + I_b^2 + I_c^2) r \tag{5.2}$$

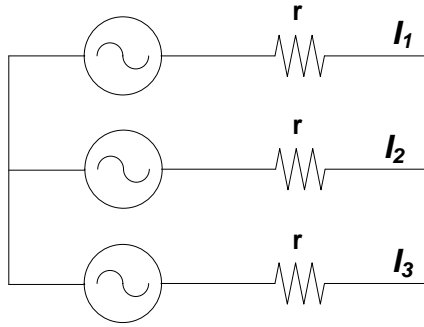


Fig. 5.3: Current flow from 3 phase Harmonic Source

Assuming the 3 voltage sources on each phase of the line in Fig. 5.3 are 3 harmonic sources (converters) and (5.1) can be applied to quantify the level of current IHDs at a common point, then (5.1) will give the algebraic sum average of the current IHDs at the common point to be less than that of the actual measured net current IHD of the harmonic sources at the common point.

Furthermore, harmonics are time variant, varying in a random manner due to continual changes in system configuration and operating conditions which in conjunction with the complexities of each harmonic sources (converter) renders (5.1) inadequate in providing accurate results and necessary information required in quantifying these harmonics. This necessitates the call for statistical techniques to properly record important information required to provide an accurate quantification of harmonic distortion levels of multiple harmonic sources (converters) [75].

5.2 Uncertainty Representation

Various uncertainties may arise in the design/configuration and operation of a RES, microgrid or grid which may affect the overall harmonic distortion level. In an RES dominated power system, there are basically two categories of factors that affect the harmonics generated by power converters (VSCs) as seen at the (PCC) to the grid or microgrid. Excluding the filter system utilized, the harmonics are usually as a result of the RES power converter (VSCs) and its interaction with other grid properties. The categories are [1]:

- The converter design specification
- The system/operation characteristics

Some of these factors investigated in Chapter 4 are linked to the uncertainty that may arise on the grid or at the microgrid containing the VSC, and they include factors such as power variation, grid voltage distortion or grid impedance variation.

An example is in the appropriate design and sizing of a VSC filter. This has a great impact on the system stability and the amount of distortion seen at the grid side. In microgrids operating in the grid connected mode, the main concern is to reduce the harmonic current injected into the grid [66]. Several design methods are typically utilized in designing filters [66, 67, 76], and all give a different filter value when utilized. In the end, the filter value is determined at the discretion of the design engineer considering a trade-off between filter harmonic attenuation and overall cost [72]. The filter parameter values can then be viewed as a stochastic variable such that the optimal size can be determined and it can be represented by a uniform distribution if it has a range with no priority given to a value over another.

Another example is the dependence of the output RES (wind turbines and photovoltaic) on several random factors such as the weather condition. For instance, the output from a wind energy system depends on the prevalent wind speed and the characteristics of the wind turbine used. For the photovoltaic, the solar radiation at a location (which is dependent on the time of the day) alongside factors like cloud index and shading among other things result in the variations of the PV solar system's output. Several models have been proposed in the literature for modelling these uncertainties; wind speed modelled using the Weibull distribution, Rayleigh distribution, normal distribution, etc. [77].

The above discussion has started that a uniform distribution function can be used in modelling the RES power variation, filter inductance variation or system impedance variation. However, this distribution is used for its simplicity, and can easily be extended using other distributions discussed next.

a. Uniform Distribution

A random variable x is said to follow the uniform distribution in the interval (a, b) , $-\infty < a < b < \infty$ if it has a probability density function, $f(x)$ as shown in (5.3);

$$f(x) = \begin{cases} \frac{1}{b-a} & a \leq x \leq b \\ 0 & \text{otherwise} \end{cases} \quad (5.3)$$

The cumulative distribution function $F(x)$ is given by (5.4) in [78];

$$F(x) = \begin{cases} 1 & x \geq b \\ \frac{x-a}{b-a} & a \leq x \leq b \\ 0 & x \leq a \end{cases} \quad (5.4)$$

Other frequently occurring distribution function models that are relevant to this study include;

b. Normal/Gaussian Distribution

A random variable x is normal or Gaussian if its probability density function has the form in (5.5) [78];

$$f(x) = \frac{1}{\sqrt{2\pi\sigma^2}} e^{-(x-\mu)^2/2\sigma^2} \quad (5.5)$$

where μ is the mean and σ^2 is the variance.

The cumulative distribution function of a normally distributed variable is;

$$F(x) = \frac{1}{\sqrt{2\pi\sigma^2}} \int_{-\infty}^{\infty} e^{-(x-\mu)^2/2\sigma^2} dx \quad (5.6)$$

c. Weibull Distribution

A random variable x that is Weibull distributed has a pdf, $f(x)$ and cdf, $F(x)$ as shown in (5.7) and (5.8) respectively [79];

$$f(x) = \frac{\alpha}{\beta} \left(\frac{x-x_o}{\beta} \right)^{\alpha-1} \exp \left[- \left(\frac{x-x_o}{\beta} \right)^\alpha \right] \quad (5.7)$$

$$F(x) = 1 - \exp \left[- \left(\frac{x-x_o}{\beta} \right)^\alpha \right] \quad (5.8)$$

Equation (5.7) is the general representation of a Weibull density function referred to as a 3-parameter Weibull distribution. The 3-parameter Weibull distribution is defined by α , β and x_o , which are respectively the shape, scale and location parameter. However, if x_o is zero, then the distribution can be reduced to a 2-parameter Weibull distribution [79].

The pdf and cdf for a variable x following the 2-parameter Weibull distribution is given in (5.9) and (5.10) respectively [80].

$$f(x) = \frac{\alpha}{\beta} \left(\frac{x}{\beta}\right)^{\alpha-1} \exp\left[-\left(\frac{x}{\beta}\right)^\alpha\right] \quad (5.9)$$

$$F(x) = 1 - \exp\left[-\left(\frac{x}{\beta}\right)^\alpha\right] \quad (5.10)$$

5.3 Mathematical Terminology for Probabilistic Harmonic Studies

This section discusses some fundamental terminologies that are used for the probabilistic harmonic analysis and other parts of the thesis.

5.3.1 Definition

Random Experiment: This counts as any activity or procedure that may give rise to a well-defined set of outcomes [81].

Random Event: The collection of outcomes of a random experiment with a definite probability of occurrence [82, 83].

Stochastic Process: A sequence of states whose evolution is determined by random events [10].

Sample Space: This represents all possible outcomes of an experiment [81, 84].

Random Variable: A random variable is a measurable function from a sample space that can be used to map random events into numerical values [10, 84].

Random Number: A number chosen as if by chance from some specified distribution such that when a large set of these numbers are selected they reproduce the underlying distribution. They are usually required to be independent, to avoid correlations between successive numbers. Pseudorandom numbers refers to computer-generated random numbers [85].

Variate: A generalization of the concept of a random variable that is defined without reference to a particular type of probabilistic experiment. A set of all random variables that obey a given probabilistic law [86].

5.4 Moments of Random Variables

The moments of a random variable or its distribution are the expected values of power or related functions of a random variable. The moments of a random variable or its distribution are a set of descriptive quantities that are useful for measuring its properties and, in some cases, for specifying it. Properties such as location, variation and skew [87]. Moments are not the only set of constants used for this purpose, as cumulants which are seen as superior from a theoretical standpoint are also used to describe the properties of a random variable [87].

The cumulant (K_r) of order r of a variate can be calculated from all its moment not higher than order r and vice versa [88]. There are 2 types of moments; the moment about the origin which is also called the raw moment (μ'_r) and the moment about the mean value of x is called central moment (μ_r) [78].

The raw and central moments for a continuous function $f(x)$, and a discrete distribution with p_k point probabilities are given in (5.11) - (5.14) [78, 88].

$$\mu'_r = \int_{-\infty}^{\infty} x^r f(x) dx \quad (\text{continuous}) \quad (5.11)$$

$$\mu'_r = \sum_{k=0}^n x_k^r p_k \quad (\text{discrete}) \quad (5.12)$$

$$\mu_r = \int_{-\infty}^{\infty} (x - \mu)^r f(x) dx \quad (\text{continuous}) \quad (5.13)$$

$$\mu_r = \sum_{k=0}^n (x_k - \mu)^r p_k \quad (\text{discrete}) \quad (5.14)$$

The first four moments give key information about the random variables distribution as numerical moments higher than the fourth usually give a large margin of error when computed from moderate values, they are also rarely required in practice [87]. The first raw moment also called the mean or expectation ($\bar{\mu}$), is a measure of central tendency. It gives a measure of the “centre” or “location” of a distribution i.e. the measure of tendency of the variables to cluster about the origin [88]. The second central moment is the variance (σ^2) [78]. The variance gives a measure of the spread of the random variable about the mean point [78]. The standard deviation (σ) of the variable is the square root of the variance.

The normalised central third moment is referred to as the skewness (γ_1) of the random variable density function [78] and it gives the measure of deviation of the random variable from the symmetry. The standardised central fourth moment is called the kurtosis (γ_2) and it gives a measure of the ‘peakedness’ of the random variable distribution [78, 87].

$$\gamma_1 = \frac{\mu_3}{\sigma^3}, \gamma_2 = \frac{\mu_4}{\sigma^4} \quad (5.15)$$

5.4.1 Relationship Between Moments and Cumulants

The relationship between moments (μ_r) and cumulants (K_r) is given in (5.16) [88];

$$K_r = m_r - \sum_{j=1}^{r-1} \binom{r-1}{j-1} m_{r-j} K_j \quad m = \mu \text{ or } \mu' \quad (5.16)$$

The cumulant can be easily evaluated given the moment of the distribution. Using (5.16), the first 5 cumulant relative to the central and raw moments are given in (5.17) and (5.18) respectively as:

$$\left. \begin{aligned} K_2 &= \mu_2 \quad (\text{variance}) \\ K_3 &= \mu_3 \\ K_4 &= \mu_4 - 3\mu_2^2 \\ K_5 &= \mu_5 - 10\mu_2\mu_3 \\ K_6 &= \mu_6 - 15\mu_4\mu_2 - 10\mu_3^2 + 30\mu_2^3 \end{aligned} \right\} \quad (5.17)$$

Cumulants relative to the raw moments are

$$\left. \begin{aligned} K_1 &= \mu'_1 \quad (\text{mean}) \\ K_2 &= \mu'_2 - \mu_1'^2 \\ K_3 &= \mu'_3 - 3\mu'_2 \mu'_1 + 2\mu_1'^3 \\ K_4 &= \mu'_4 - 4\mu'_3 \mu'_1 - 3\mu_2'^2 + 12\mu'_2 \mu_1'^2 - 6\mu_1'^4 \\ K_5 &= \mu'_5 - 5\mu'_4 \mu'_1 - 10\mu'_3 \mu_2' + 20\mu'_3 \mu_1'^2 + 30\mu_2'^2 \mu_1' - \dots \\ &60\mu'_2 \mu_1'^3 - 24\mu_1'^5 \end{aligned} \right\} \quad (5.18)$$

5.4.2 Quantiles

The knowledge of the quantiles gives a good idea of the general form of a distribution [87]. For a random variable with ordered set of values, the quantile divides the probability distribution into q equal parts. For a randomly distributed variable x , the k_{th} quantile is the value of x , say x_k , which corresponds to a cumulative frequency of $N.k/q$ [88] (where N is the population size). Depending on the value of q , quantiles can take different names. For 3 variate values that divide the total probability to four equal parts ($q=4$), it is called a quartiles. When the variable is divided into 10 equal parts ($q=10$), it is called deciles. When the variable is divided into 100 equal parts ($q=100$), it is called percentiles. In general, $(n-1)$ variate values that divide the total probability into n equal parts is called the quantiles [87].

The quantile can also be estimated from the cdf of the random variable. The relationship between q -quantile and cdf is given in (5.19) [88];

$$X(q) = F^{-1}(q) \quad (5.19)$$

5.4.3 Cornish Fisher Expansion Method for Distribution Function Reconstruction

The Cornish Fisher series expansion provides a means of reconstructing a variable's cumulative distribution function (cdf) by the use of an approximate method [9]. With the Cornish Fisher method, the normalized quantiles for any distribution $F(x)$ can be approximated by the quantile of the standard normal distribution and the cumulant of the distribution. A comprehensive treatment of the method can be found in [89].

This works by exploiting the inverse relationship between cdf and quantiles; considering that the quantile of a function can be reconstructed using its cumulants and the quantiles of a standard normal distribution [89].

The mathematical expression for approximating the variables cdf is shown in (5.20). Using the first five cumulants has been proven to give a fairly accurate estimate [89].

$$\begin{aligned}
 x(q) \approx & \Phi_z^{-1}(q) + \frac{1}{6}(\Phi_z^{-1}(q)^2 - 1)K_3 + \frac{1}{24}(\Phi_z^{-1}(q)^3 - 3\Phi_z^{-1}(q))K_4 \dots \\
 & - \frac{1}{36}(2\Phi_z^{-1}(q)^3 - 5\Phi_z^{-1}(q))K_3^2 + \frac{1}{120}(\Phi_z^{-1}(q)^4 - 6\Phi_z^{-1}(q)^2 + 3)K_5 \dots \quad (5.20) \\
 & - \frac{1}{24}(\Phi_z^{-1}(q)^4 - 5\Phi_z^{-1}(q)^2 + 2)K_3K_4 + \frac{1}{324}(12\Phi_z^{-1}(q)^4 - 53\Phi_z^{-1}(q)^2 + 7)K_3^3
 \end{aligned}$$

where $x(q)$ is the q -quantile function, $\Phi_z^{-1}(q)$ is the q -quantile of the standard normal distribution and K_r is the r^{th} order cumulant of the distribution function $F(x)$.

Depending on the distribution being reconstructed, the Cornish Fisher method sometimes gives less reliable estimate in the tail region. However, its performance is much better than the Gram Charlier method especially for non-normal distributions [90].

5.5 Schematics of N Number of Harmonic Sources

The schematics of the studied RES based power system shown in Fig. 5.4 comprises multiple number of VSCs connected in parallel and interfaced to the

grid at the PCC via the grid impedance. The system was simulated using PLECSTM [14] and MATLAB SimulinkTM [13] simulation tools.

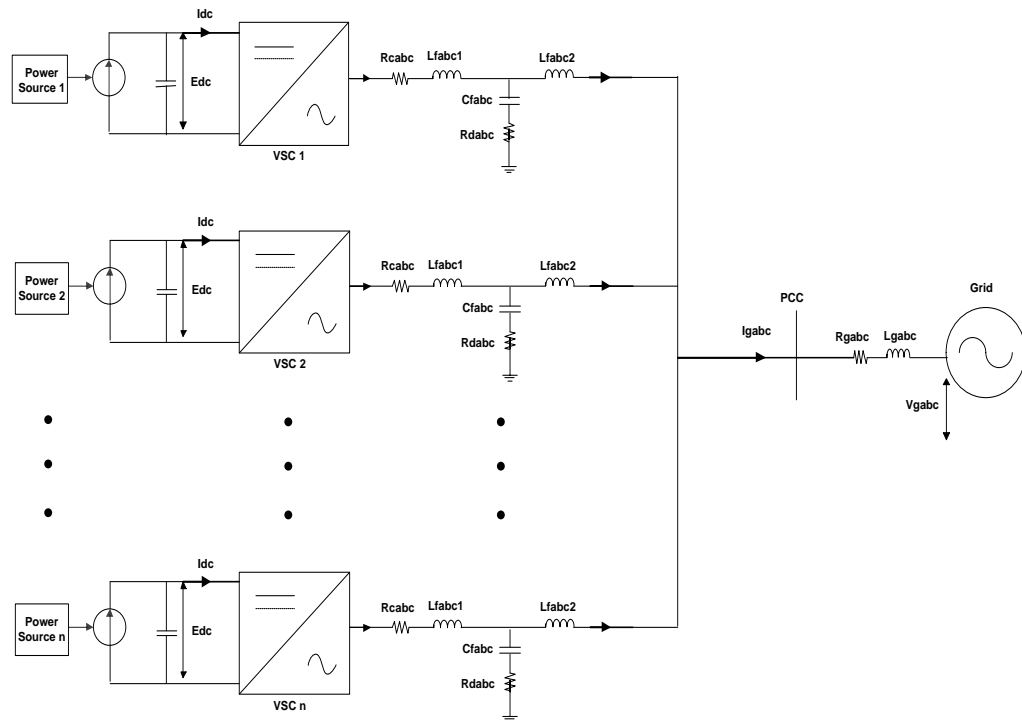


Fig. 5.4: Multiple VSCs connected in Parallel to the PCC

The RES system presented above will definitely produce harmonics from each of the VSC and this will appear as an aggregate sum at the point of common coupling (PCC). This provides the summing of N number of harmonic vectors that will be explained later in this chapter.

5.6 Probabilistic Harmonic Studies

Uncertainties such as the ones discussed in section 5.2 and the corresponding variations in harmonic levels has led the IEEE Probabilistic Aspects Task Force on Harmonics to suggest the use of statistical techniques in quantifying harmonic levels [75]. Hence, probabilistic harmonic studies have been adopted to analyse harmonics due to their stochastic nature and that of uncertainties that might arise during the configuration or operation of an EPS. Probabilistic harmonic studies are usually classed as numerical and analytical methods. The analytical methods entail assumptions to handle complicated mathematical computation and these lead to question its accuracy [91, 92]. While, the numerical approach such as the Monte Carlo Simulation (MCS) and the Unscented Transform (UT) does not

involve assumptions and have better accuracy, however, they require a large number of evaluation and computational time to produce the results.

5.7 Probabilistic Harmonic Summation

Early probabilistic harmonic modelling and analyses involved the application of direct mathematical analysis on instantaneous current values from individual harmonic components [93] as was applied in [94]. The direct mathematical technique described in [94] was applied to sum a large number of similar-order random harmonic with fixed magnitudes. However, in a practical power system harmonic magnitudes and phases are not fixed but vary in a random fashion. It was stated in [93, 95] that N.B. Rowe [96] expanded the work in [94], by considering the sum of random current harmonic vectors with magnitudes varying uniformly between zero and a maximum with random phase angles. The summation of the random harmonic vectors was achieved using phasor notations and some assumptions applied for this technique include: The current phase angle being uniformly distributed between 0 and 2π , the component phasors being statistically independent and the current harmonic magnitude being uniformly distributed between 0 and a peak value [93, 95]. The properties of the summation current were obtained by simplifying the analyses by means of a Rayleigh distribution. This simplification affects the flexibility of modelling other harmonic sources and limits this technique [93].

Notwithstanding in [95], a general expression for summation of current and voltage harmonic vectors whose magnitudes and phase angles are either statistically independent or dependent was presented. The general expression was shown to be more complex than previous techniques and the methods in [94] and [96] were shown as a simplification of this general method. One disadvantage of [95], is that the vectorial sum of the probability density function (pdf) of the harmonic magnitude was given in an integral form which must be solved using numerical methods [97]. Furthermore, the comparative study carried out in [95], still utilized the assumptions in [96] to validate the method presented.

The theories and analysis proposed in [94-96] has formed the basics for the analytical approach of probabilistic harmonic studies. The analysis has been expanded in [97, 98] to involve Bivariate Normal Distributions (BND) and in [99], snapshots of the voltage harmonics obtained from a distribution system was used as field measurements and applied on a 6-pulse converter harmonic generation model. The study first creates a simulated model with some assumptions to mimic the field measurement, then the simulated data was then used to supplement the available field measurement to test the above theory [99].

Before going any further, it will be necessary to explain the analytical framework for the summation of harmonic vectors for probabilistic harmonic studies as seen in a more recent literature [100].

5.7.1 Random Harmonic Phasors

Random harmonic phasor analysis requires injected harmonic currents by harmonic sources to be represented by random vectors. Where the random behaviour of the harmonic currents is related to the parameter of influence stochastic nature such as the harmonic sources operating conditions and the EPS configuration [100].

The injected harmonic current of order h by a harmonic source is represented as a vector \bar{I}_h which can be written in the polar or Cartesian plane as follows [95, 100];

$$\bar{I}_h = I_h \angle \theta_h \quad (5.21)$$

where I_h is the amplitude of \bar{I}_h and θ_h is the phase angle of \bar{I}_h .

$$\bar{I}_h = X_h + jY_h \quad (5.22)$$

where X_h represents the real part and Y_h represents the imaginary part of \bar{I}_h respectively.

Equations (5.21) and (5.22) are related to one another by (5.24) – (5.26).

$$I_h = \sqrt{X_h^2 + jY_h^2} \quad (5.23)$$

$$\theta_h = a \tan\left(\frac{Y_h}{X_h}\right) \quad (5.24)$$

$$X_h = I_h \cos \theta_h \quad (5.25)$$

$$Y_h = I_h \sin \theta_h \quad (5.26)$$

X_h and Y_h are real random variables that are functions of two random variables I_h and θ_h (5.27) and (5.28) [95].

$$X_h = I_h \cos \theta_h = a(I_h, \theta_h) \quad (5.27)$$

$$Y_h = I_h \sin \theta_h = b(I_h, \theta_h) \quad (5.28)$$

In order to statistically characterize \bar{I}_h , the joint statistics of the random variables (X_h, Y_h) or (I_h, θ_h) is required [100].

5.7.2 Important Statistical Functions of X_h and Y_h

- 1) The **joint cumulative probability function** also called the joint cdf $F_{X_h Y_h}(x_h, y_h)$, that is the probability of the event $\{X_h \leq x_h, Y_h \leq y_h\}$ [100].
where $X_h, h = 1, \dots, N$ and $Y_h, h = 1, \dots, N$.
- 2) The joint probability density function (jpdf), which is related to joint cdf and defined by (5.29) [100].

$$f_{X_h Y_h}(x_h, y_h) = \frac{\partial^2 F_{X_h Y_h}(x_h, y_h)}{\partial x_h \partial y_h} \quad (5.29)$$

- 3) The cumulative probability functions, also called the marginal distribution functions, $F_{X_h}(x_h)$ and $F_{Y_h}(y_h)$ [100].
- 4) The marginal probability density functions (pdfs) $f_{X_h}(x_h)$ and $f_{Y_h}(y_h)$ [100].

5.7.3 Summation of N Random Harmonic Vectors

Considering a sum of N random harmonic vectors of the same harmonic order (or frequency) where N represents more than one harmonic source gives (5.30) [95, 100, 101];

$$\bar{I}_h = \sum_{k=1}^N \bar{I}_{h,k} = \sum_{k=1}^N X_{h,k} + j \sum_{k=1}^N Y_{h,k} = S_h + jW_h \quad (5.30)$$

where $I_h = \sqrt{S_h^2 + jW_h^2}$ and $\theta_h = a \tan\left(\frac{W_h}{S_h}\right)$

S_h is the vectorial algebraic sum of X_h components and W_h is the vectorial algebraic sum of Y_h components (i.e. they are the algebraic sums of the N resolved components).

$X_{h,k}$ and $Y_{h,k}$ are respectively, the real and imaginary components of the h -th harmonic current generated by the k -th converter or harmonic source.

The correct theoretical approach to obtain the pdf of the harmonic current I_h , (which is the magnitude of the sum of the real and imaginary resolved components), requires the use of $2N$ -dimensional joint probability density function [100].

$$f_{Z_h}(z_h), \text{ with } Z_h = [X_{h,1}, X_{h,2}, \dots, X_{h,N}, Y_{h,1}, Y_{h,2}, \dots, Y_{h,N}] \quad (5.31)$$

and the distribution of I_h is given by:

$$F_{I_h}(i_h) = \int_{\Gamma} f_{Z_h}(z_h) \prod_{i=1}^{2N} dz_{h,i} \quad (5.32)$$

where Γ is the $2N$ -dimensional region of the hyperspace z where the constraints $I_h(z) \leq i_h$, is verified. It is clear that (5.31) or its integral (5.32) cannot be easily solved as it has no known closed form solution and must be evaluated by numerical or approximation methods [100]. In [102] it was approximated to a generalized gamma distribution where Γ is the gamma function, while in [103] the random variables were assumed to be statistically independent and its pdfs used to solve (5.32).

The vectorial summation of N random harmonic in a defined scenario of space (grid system characteristics, operating conditions) and of time (day, month, year, annual/monthly maximum load days), is in principle very simple if $2N$ -dimensional joint pdf of the $2N$ real random variables representing the N vectors involved is available for the scenario [100].

However, in practice dramatic computational problems are encountered using numerical methods that discretize the hyperspace z and assume M discrete values

for each coordinate in its defined interval [100]. They include; time consuming solution of the integral of (5.32), joint pdf of f_Z given in (5.31) assumes the dimension $D = 2M^{2N}$, and the joint pdf is difficult to obtain by experimental and simulation methods [100]. This leads to two major assumptions made in techniques that utilize this analysis in solving the vectorial sum of N random harmonic vectors. They are;

- The distribution of the harmonic vectors are independent of time.
- The random vectors are statistically independent.

The convolution method discussed in [104] requires the resultant resolved components S_h and W_h to be statistically independent. This method is not discussed in this thesis. Another method for summing N random harmonic vectors is the **Joint Density Method** [100].

The joint density method does not require the statistical independence of S_h and W_h . However, the method requires N to be very high (usually $N > 30$) to make the Central Limit Theorem (CLT) applicable just as in the convolution method [95, 100]. The CLT helps in limiting distribution of the sum of independent variables, and it states that the pdf of the sum of independent variables approaches a normal distribution regardless of the distributions of the individual variables, as long as the number of variables N is sufficiently large and none is dominant.

Applying all of (5.21) – (5.30) and assuming a large number, N , of harmonic sources vectors and applying the CLT, the sum of resolved components becomes a normal distribution function [95]. Since a normal distribution is characterized by its mean and variance it becomes necessary to obtain these parameters for the sum of the X_h and Y_h components.

Let $\mu_{x_{h,k}}$ and $\sigma_{x_{h,k}}^2$ be the mean and variance of each random variable

$$X_{h,k}, k = 1, \dots, N, \text{ for the sum of } X_h \text{ components } S_h = \sum_{k=1}^N X_{h,k}$$

Let $\mu_{y_{h,k}}$ and $\sigma_{y_{h,k}}^2$ be the mean and variance of each random variable

$$Y_{h,k}, k = 1, \dots, N, \text{ for the sum of } Y_h \text{ components } W_h = \sum_{k=1}^N Y_{h,k}$$

The resolved components $X_{h,k}$ and $Y_{h,k}$ can be determined by (5.33) – (5.36) [95].

$$\mu_{x_{h,k}} = \int_{-\infty}^{\infty} \int_{-\infty}^{\infty} a(I_h, \theta_h) f_{I_h \theta_h}(i_h, \phi_h) di_h d\phi_h \quad (5.33)$$

$$\sigma_{x_{h,k}}^2 = \int_{-\infty}^{\infty} \int_{-\infty}^{\infty} (a(I_h, \theta_h) - \mu_{x_h})^2 f_{I_h \theta_h}(i_h, \phi_h) di_h d\phi_h \quad (5.34)$$

$$\mu_{y_{h,k}} = \int_{-\infty}^{\infty} \int_{-\infty}^{\infty} b(I_h, \theta_h) f_{I_h \theta_h}(i_h, \phi_h) di_h d\phi_h \quad (5.35)$$

$$\sigma_{y_{h,k}}^2 = \int_{-\infty}^{\infty} \int_{-\infty}^{\infty} (b(I_h, \theta_h) - \mu_{y_h})^2 f_{I_h \theta_h}(i_h, \phi_h) di_h d\phi_h \quad (5.36)$$

where $f_{I_h \theta_h}(i_h, \phi_h)$ is the joint pdf of the amplitude and angle of the random vector $I_h \angle \theta_h$.

Thus

$$S_h = \sum_{k=1}^N X_{h,k} \text{ has mean } \mu_{x_h} = \sum_{k=1}^N \mu_{x_{h,k}} \text{ and variance } \sigma_{x_h}^2 = \sum_{k=1}^N \sigma_{x_{h,k}}^2$$

$$W_h = \sum_{k=1}^N Y_{h,k} \text{ has mean } \mu_{y_h} = \sum_{k=1}^N \mu_{y_{h,k}} \text{ and variance } \sigma_{y_h}^2 = \sum_{k=1}^N \sigma_{y_{h,k}}^2$$

where S_h and W_h are jointly normally distributed with marginal pdf $f_{S_h}(s_h)$ and $f_{W_h}(w_h)$, respectively [95];

$$f_{S_h}(s_h) = \frac{e^{-\frac{(s_h - \mu_{s_h})^2}{2\sigma_{s_h}^2}}}{\sqrt{2\pi\sigma_{s_h}}} \quad (5.37)$$

$$f_{W_h}(w_h) = \frac{e^{-\frac{(w_h - \mu_{w_h})^2}{2\sigma_{w_h}^2}}}{\sqrt{2\pi\sigma_{w_h}}} \quad (5.38)$$

and a joint probability density function (jpdf) $f_{S_h W_h}(s_h, w_h)$. This time the joint pdf is characterized by mean value μ_{s_h} , μ_{w_h} and the covariance $\sigma_{s_h w_h}^2$ [95]. For statistically independent random vectors, the covariance of the sum of resolved components is equal to the sum of covariances of corresponding components [95]. Therefore,

$$\sigma_{s_h w_h}^2 = \sum_{k=1}^N \sigma_{x_{h,k} y_{h,k}}^2 \quad (5.39)$$

where $\sigma_{s_h w_h}^2$ is the covariance of $X_{h,k}$ and $Y_{h,k}$.

$$\sigma_{x_{h,k} y_{h,k}}^2 = E\{X_{h,k} Y_{h,k}\} - \mu_{x_{h,k}} \mu_{y_{h,k}} \quad (5.40)$$

$$E\{X_{h,k} Y_{h,k}\} = \int_{-\infty}^{\infty} \int_{-\infty}^{\infty} x_{h,k} y_{h,k} f_{X_{h,k} Y_{h,k}}(x_{h,k}, y_{h,k}) dx_{h,k} dy_{h,k} \quad (5.41)$$

where $f_{X_{h,k} Y_{h,k}}(x_{h,k}, y_{h,k})$ is the jpdf of $X_{h,k}$ and $Y_{h,k}$. The jpdf is derived from the probability distribution of I_h and θ_h . Let u be a vector transformation which maps (I_h, θ_h) into a 2-dimensional random harmonic vector $(X_{h,k}, Y_{h,k})$ [95].

$$\begin{bmatrix} X_{h,k} \\ Y_{h,k} \end{bmatrix} = \begin{bmatrix} u_1(I_h, \theta_h) \\ u_2(I_h, \theta_h) \end{bmatrix} = \begin{bmatrix} I_h \cos \theta_h \\ I_h \sin \theta_h \end{bmatrix} \quad (5.42)$$

Let the inverse transform of u be v

$$\begin{bmatrix} I_h \\ \theta_h \end{bmatrix} = \begin{bmatrix} v_1(X_{h,k}, Y_{h,k}) \\ v_2(X_{h,k}, Y_{h,k}) \end{bmatrix} = \begin{bmatrix} \sqrt{X_{h,k}^2 + Y_{h,k}^2} \\ a \tan\left(\frac{Y_{h,k}}{X_{h,k}}\right) \end{bmatrix} \quad (5.43)$$

From [95] $f_{X_{h,k} Y_{h,k}}(x_{h,k}, y_{h,k})$ was shown as

$$f_{X_{h,k} Y_{h,k}}(x_{h,k}, y_{h,k}) = f_{I_h \theta_h}(v(x_{h,k}, y_{h,k})) \left| \frac{\partial(v)}{\partial(x_{h,k}, y_{h,k})} \right| \quad (5.44)$$

where

$$\frac{\partial v}{\partial(x_{h,k}, y_{h,k})} = \begin{pmatrix} \frac{\partial v_1}{\partial x_{h,k}} & \frac{\partial v_1}{\partial y_{h,k}} \\ \frac{\partial v_2}{\partial x_{h,k}} & \frac{\partial v_2}{\partial y_{h,k}} \end{pmatrix} \quad (5.45)$$

S_h and W_h are jointly normal with their joint pdf given in [95, 100] as:

$$f_{s_h w_h}(s_h, w_h) = \frac{e^{-\frac{\eta}{2(1-r^2)}}}{2\pi\sigma_{s_h}\sigma_{w_h}\sqrt{1-r^2}} \quad (5.46)$$

where r is the correlation coefficient [95] given as

$$r = \frac{\sigma_{s_h w_h}^2}{\sigma_{s_h}\sigma_{w_h}} \quad (5.47)$$

and η is given below in (5.48) [95, 100] as

$$\eta = \frac{(s_h - \mu_{s_h})^2}{\sigma_{s_h}^2} - \frac{2r(s_h - \mu_{s_h})(w_h - \mu_{w_h})}{\sigma_{s_h}\sigma_{w_h}} + \frac{(w_h - \mu_{w_h})^2}{\sigma_{w_h}^2} \quad (5.48)$$

From [95] the magnitude of the sum of N random harmonic vectors is given by (5.49):

$$I_h = Z_h = \sqrt{\left(\sum_{k=1}^N X_{h,k}\right)^2 + \left(\sum_{k=1}^N Y_{h,k}\right)^2} = \sqrt{(S_h)^2 + (W_h)^2} = q(S_h, W_h) \quad (5.49)$$

Since S_h and W_h are random variables with jpdf $f_{s_h w_h}(s_h, w_h)$, Z_h is also a random variable described by pdf, $f_{z_h}(z_h)$. The process for deriving the pdf of Z_h is thoroughly explained in [95] and given as

$$f_{z_h}(z_h) = \int_0^{2\pi} f_{s_h w_h}(z_h \cos \theta_h, z_h \sin \theta_h) z_h d\theta_h \quad (5.50)$$

where $s_h = z_h \cos \theta_h$, $w_h = z_h \sin \theta_h$ and $ds_h dw_h = z_h dz_h d\theta_h$

and the pdf of the phase θ is derivable by solving the integral [100]

$$f_{\phi_h}(\phi_h) = \int_0^\infty f_{s_h w_h}(z_h \cos \theta_h, z_h \sin \theta_h) z_h dz_h \quad (5.51)$$

5.8 Probabilistic Harmonic Methods

In some previous studies [97, 99, 101, 105-108], an analytical approach was used to predict the level of harmonics generated by power converters. The studies represented harmonic vectors as phasors having random amplitudes and angles. The probability density functions (pdfs) of the phasors were obtained and represented in the rectangular coordinates for the convenience of adding phasors.

In cases of a large number of harmonic sources/loads the harmonic phasor's pdfs are then vectorially summed as explained in the preceding section. The studies predicted harmonics in terms of low harmonic orders such as the 3rd, 5th, 7th and 11th harmonic orders. This may be due to the type of power converter utilized (6/12 pulse converter) and their associated harmonics generated. In a VSC system, the majority of the harmonics appear at the switching frequency and multiplies of the switching frequency [4, 5], so, a better way to quantify the harmonics to include the harmonics at these frequencies would be to use the Total Harmonic Distortion (THD) [5].

Furthermore, an analytical approach usually entails assumptions to handle the complex interaction of a large number of random harmonic quantities [61, 92] and practical converter systems were usually simplified and represented by mathematical formulas to accommodate the approach as seen in [97, 99, 101, 105-108]. However, other methods which do not require these simplification or assumptions in designing the systems/converters or in generating random occurrences can be deployed. They include the Monte Carlo Simulation (MCS) [109, 110], Unscented Transform (UT) [111, 112], Point Estimate Method (PEM) [113] and Univariate Dimension Reduction (UDR) [88, 114] to name a few. For instance in Probabilistic Load Flow (PLF) studies some of these methods have been utilized [88, 115, 116].

This section discusses two other probabilistic harmonic methods. The Monte Carlo Simulation approach which is commonly used and the Unscented Transform which is an approximate technique for estimating statistical values.

5.8.1 Monte Carlo Simulation Approach

Numerical methods are increasingly becoming the future of statistical engineering and Monte Carlo Simulations (MCS) forms the largest and most important class of numerical methods used for solving probabilistic problems in a wide range of discipline including engineering [117, 118]. The MCS technique is based on sampling variables at random, following the pdf of the stochastic variables and then observing the results. To use the MCS method, the

distribution function of all the uncertain variables within the power system should be known [88].

The MCS attempts to follow the variable dependence of a model for which change, or growth, does not proceed in some rigorously predefined fashion but rather in a stochastic manner which depends on a sequence of random numbers which are generated during simulation. A second, different sequence of random numbers, will not give the simulations identical results but will yield values which agrees with those obtained from the first sequence to within some 'statistical error' [118]. The MCS method is capable of exploring the sensitivity of a complex system by varying parameters within statistical constraints. These systems can include, physical and mathematical models that are simulated in a loop, with statistical uncertainty added between simulations. The results from the simulation are analysed to determine the characteristics of the system [119].

In [10] the MCS was defined as a method that involves the deliberate use of random numbers in a calculation that has a stochastic process. In a computer these random numbers are generated by a deterministic algorithm that generates a sequence of pseudorandom numbers, which mimics the properties of truly random numbers.

The two main features of the MCS are the random number generation (variables/uncertainties) and the random sampling (number of iterations) [91]. The MCS performs uncertainty analysis by building models of possible results by substituting a range of values (variables or pdf) for any factor that has inherent uncertainty. It then calculates the result over and over, each time using a different set of random variables from the pdfs [109]. It usually involves thousands to tens of thousands of iterations before the simulation is complete. The MCS is highly accurate and it also furnishes the researcher not just with what could happen but also the likelihood of each outcome [109].

The advantage of the MCS in predicting harmonics is that it provides the possibility of simulating a wide variety of random system/load characteristics until the resulting statistics agree with the available field measurements. This makes the MCS highly flexible, nevertheless, the direct relationship between the

system/load probability models and the resultant harmonics is not apparent when the MCS is utilized [100]. The major drawback of the MCS is its computational burden in performing tens of thousands iteration and the large amount of time to perform the entire simulation. A large number of samples is needed to increase accuracy of the MCS as this will enable the MCS to converge [88].

Figure 5.5 illustrates the significance of this relationship between sample number and convergence. It presents the results for the mean value (μ) current THD (I_{THD}) and voltage THD (V_{THD}) for a system with 2 VSCs using 10, 100, 1000, 5000 and 10000 simulations using a windows i3 4GB RAM PC.

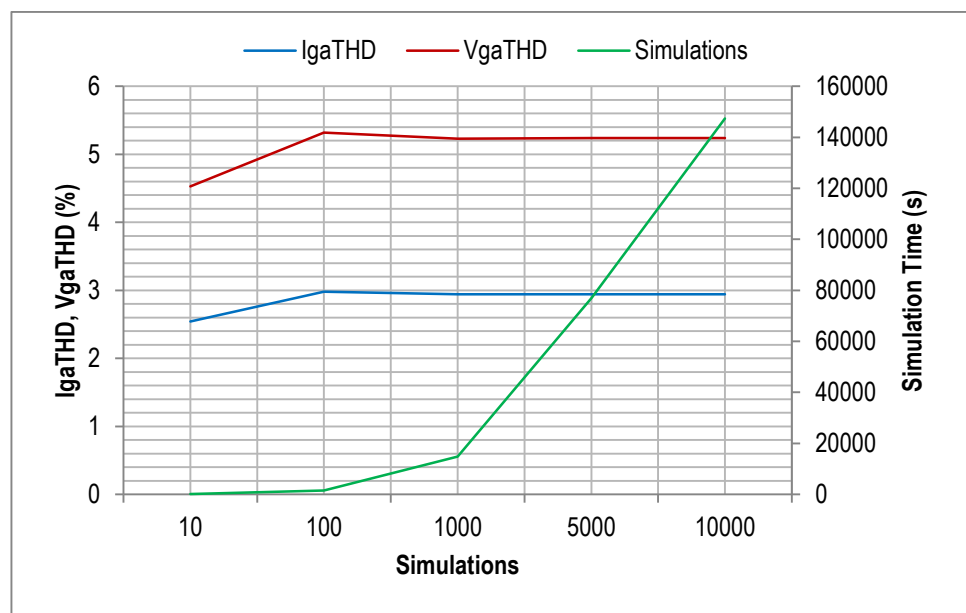


Fig. 5.5: Result of I_{THD} and V_{THD} for 2 VSCs Connected in Parallel for Various Numbers of Simulations

In some probabilistic harmonic studies carried out in [95], [97], [101], [105], [120], the MCS is used to model a stochastic system consisting of 10 AC-DC thyristor based power converters, where their respective firing angles or output power are varied randomly and uniformly. The MCS was used in the studies to either predict the harmonic distortion level or to validate another harmonic prediction method. The MCS also provided the expected mean value, standard deviation and the correlation coefficient of the magnitude associated with the real and imaginary components of the total harmonic currents injected by the converters using the firing angles [120].

Examples to Show the Use of MCS in Predicting Harmonics and Impact of Uncertainty

In this section, the MCS is used to predict the level of harmonic distortion of many connected power converters when certain system and design parameters are only known within certain constraints.

In the considered cases, 1000 simulations were carried out for the MCS to ensure accuracy. This is sufficient as it provides a 95% confidence interval (*CI*) that the errors in the mean THD values are less than 3% as calculated using (5.52) and (5.53). The mean values and std utilized in this calculation were obtained after running the simulations and then used to checked against the 95% *CI*.

$$95\% (CI) = \bar{\mu} \pm Z \frac{\sigma}{\sqrt{n}} \quad (5.52)$$

$$SE = \frac{\sigma}{\sqrt{n}} \quad (5.53)$$

where *CI* implies the confidence interval, *SE* is the standard error of the mean, *n* the number of samples, $\bar{\mu}$ implies the mean value of the samples, σ = standard deviation of the samples and $Z = 1.96$ the constant representing 95% *CI*. Where the *SE* for 2 VSCs at 1000 simulations gives 0.04 using the values for 2 VSCs in Table 5.1.

In this study the filter inductance value and the output power of the VSCs in the microgrid is varied. The filter inductance methods (1 and 2) mentioned in section 4.5 for an *LCL* filter is applied. In filter design methods, the maximum ripple current which is a function of the inductance L_{fabc1} , the switching frequency and the DC link voltage should be less than 20% of the rated current [66]. However, to reduce the ripple current, the inductance is the most flexible factor since changing the switching frequency affects the system efficiency. This variation of the filter inductance is modelled assuming a uniform distribution.

Similarly, there are uncertainties that emanate from various RES due to the dependence of their power output on several random factors such as the weather condition. For simplicity, the power variation is also modelled using the uniform distribution.

5.8.2 Results

To demonstrate the effect of variation in operation power and filter inductor value on the level of total harmonic distortion generated by many connected VSCs at the PCC of a grid, three scenarios were considered. In the first scenario, the effect of filter inductor value L_{fabc1} on the total harmonic distortion in the current and voltage values at the PCC using the MCS approach is examined. For this system, calculating L_{fabc1} using [66], [60] gives a value of 18mH which is very large. However, using [76], [67] gives 5mH which is a typical value for systems of this level. Based on this, and assuming the filter inductor value can be modelled using the uniform distribution, the value was chosen to be between 3mH and 7mH. The range was chosen assuming a $\pm 40\%$ trade-off between effectiveness in filtering harmonics and cost of the filter inductor size. In the study, mean and standard deviation of the THD values when the inductor is designed within this range is presented. The probability of exceeding the limits prescribed in the IEEE 519 standard within the chosen range as the number of VSCs increases is determined.

In the second scenario, the effect of operating power variations on the I_{THD} and V_{THD} as predicted by the MCS is considered. The operating power is assumed to vary randomly within a range following the uniform distribution between 25% and 100% of its rated power, 8 kW. This is assumed to be practical since the output of most RES vary widely.

The third scenario considers varying both the operating power of the VSCs and the filter inductance L_{fabc1} . The variations are within the values used in the first and second study. This is done to investigate the combined effect of filter design choice and operating power variation on I_{THD} and V_{THD} of many connected VSCs. The results obtained for each of the cases are discussed below.

a) *Effect of Filter Variation on Current and Voltage THD*

The MCS approach was able to provide statistical information about the impact of varying the filter inductance on the I_{THD} and V_{THD} . It can be seen from Table 5.1 that I_{THD} progressively reduces as the number of VSC increases, while the V_{THD} increases. This is expected, since the total number of filters in the system increases as the number of VSC increases, thus providing more attenuation of

the current distortion. The increased number of VSCs also provides a higher probability of harmonic cancellation due to current diversity and attenuation factor [62, 66, 121]. The V_{THD} on the other hand follows the opposite trend as increased number of VSCs implies increased voltage harmonics transmitted to the PCC.

Table 5.1: Result of Randomly Varying Filter Inductor Value with Multiple VSCs

TOTAL HARMONIC DISTORTION OF CURRENT AT PCC											
	Index	Number of VSCs									
		1	2	3	4	5	6	7	8	9	10
Current	$\mu(\%)$	3.95	2.94	2.48	2.16	1.9	1.67	1.48	1.54	1.43	1.28
	σ	1.42	0.68	0.50	0.37	0.23	0.20	0.15	0.16	0.15	0.11
Voltage	$\mu(\%)$	1.53	2.30	2.77	3.07	3.32	3.47	3.57	3.74	3.82	3.89
	σ	0.63	0.61	0.55	0.51	0.47	0.43	0.40	0.38	0.36	0.37

To further demonstrate this effect, the cumulative distribution function graph for 1, 5 and 10 VSCs are shown in Figs. 5.6-5.8 for both the I_{THD} and V_{THD} . From Fig. 5.6 for a single VSC, it was observed that there is a 25% probability of the I_{THD} exceeding 5% while the V_{THD} was within the IEEE 519 harmonic limit. It is also noticeable that the plot for a single VSC is skewed to the right unlike other systems with more VSCs. From the cdf curve it can be seen that, the value of the filter inductance must be carefully chosen for lower number of VSC converters, as there is less impact on I_{THD} for higher number of VSCs.

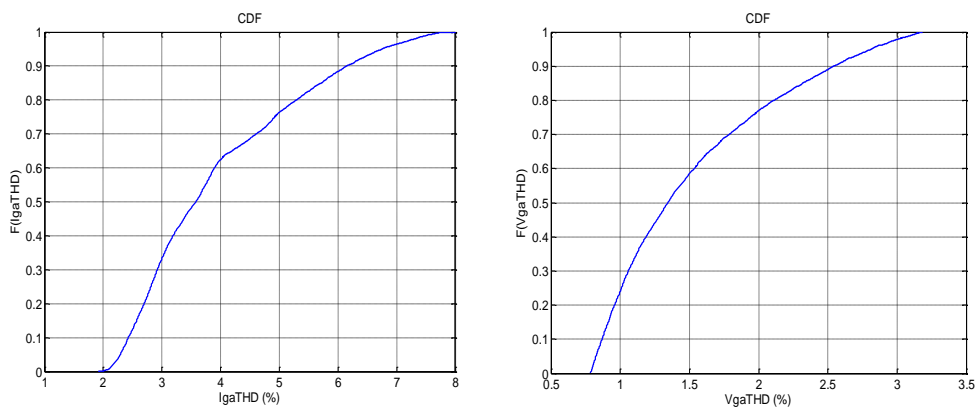


Fig. 5.6 CDF of I_{THD} and V_{THD} of a VSC with Variable Filter Inductance

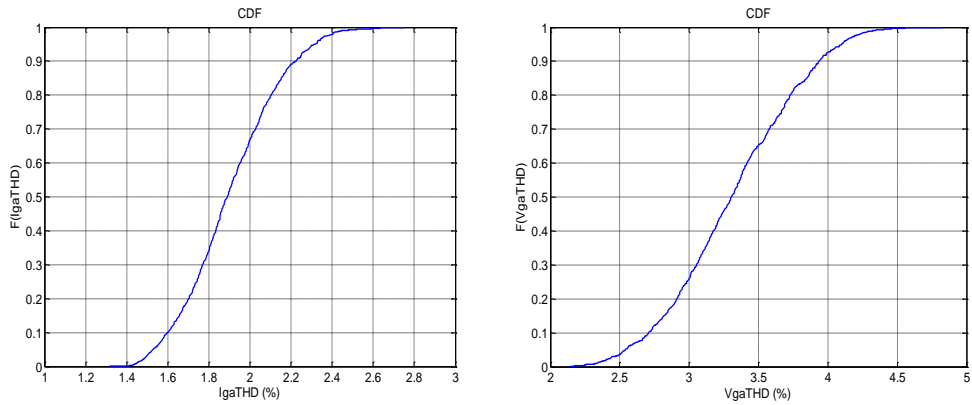


Fig. 5.7: CDF of I_{THD} and V_{THD} of 5 VSCs with Variable Filter Inductance

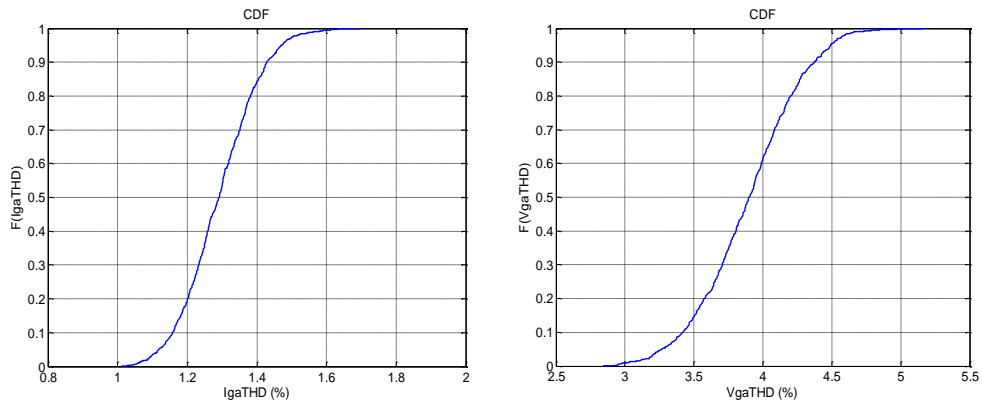


Fig. 5.8: CDF of I_{THD} and V_{THD} of 10 VSCs with Variable Filter Inductance

b) Effect of Operating Power Variation on Current and Voltage THD

Here again the MCS approach was capable of demonstrating the impact of operating power variation on the microgrid and for predicting the I_{THD} and V_{THD} . The mean (μ) and standard deviation (σ) of the I_{THD} and V_{THD} are presented in Table 5.2. From the table, it is seen that the variation of power has little effect on the V_{THD} this is as a result of the robustness of the *LCL*-filter. This is in line with earlier research, which observed that the variation of power has almost no effect on an *LCL* filtered VSC V_{THD} [1]. The increased voltage THD for 10 VSC is only as a result of the increase of the number of VSCs. The effect of power variation is more pronounced on the I_{THD} . However, as with the previous case, the I_{THD} is observed to reduce with the increase of the number of VSCs.

Table 5.2: Result of Randomly Varying Operating Power of Multiple VSCs

TOTAL HARMONIC DISTORTION OF CURRENT AT PCC											
	Index	Number of VSCs									
		1	2	3	4	5	6	7	8	9	10
Current	$\mu(\%)$	6.30	4.37	3.38	2.90	2.54	2.30	2.09	1.93	1.78	1.61
	σ	2.23	1.14	0.72	0.47	0.35	0.27	0.22	0.21	0.24	0.20
Voltage	$\mu(\%)$	1.35	2.01	2.40	2.67	2.86	3.01	3.13	3.22	3.30	3.36
	σ	0.009	0.010	0.011	0.011	0.014	0.015	0.014	0.011	0.011	0.014

The CDF plots using 1, 5 and 10 VSCs are presented in Figs. 5.9 – 5.11. Much larger variation is noticed for systems with a single VSC as compared with others, though the variation in the values generally reduces as the number of VSCs increases. The V_{THDs} were within the IEEE 519 limit however, the I_{THD} for 1 and 2 VSCs had a 60% and 25% probability respectively of exceeding the limit when the power varies between 25%-100% Prated.

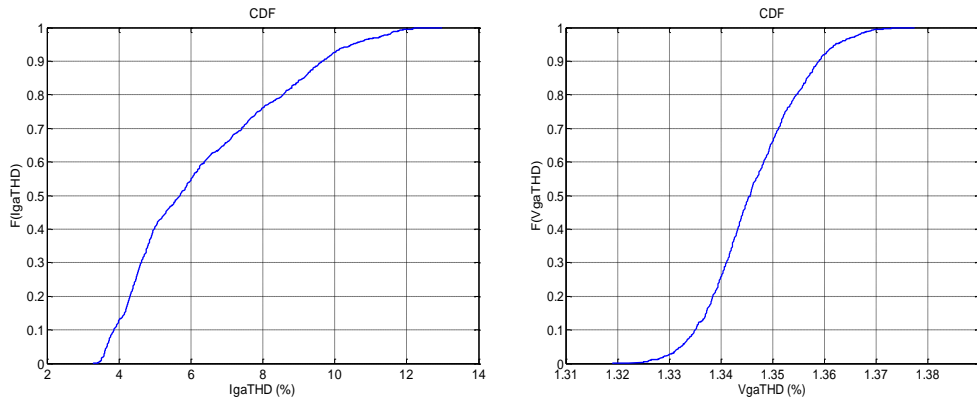


Fig. 5.9: CDF of I_{THD} and V_{THD} of a Single VSC with Variable Power

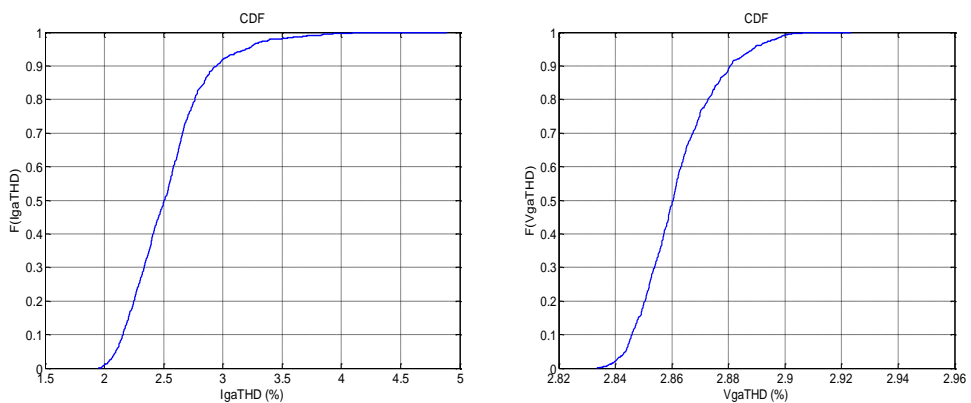


Fig. 5.10: CDF of I_{THD} and V_{THD} of 5 VSCs with Variable Power

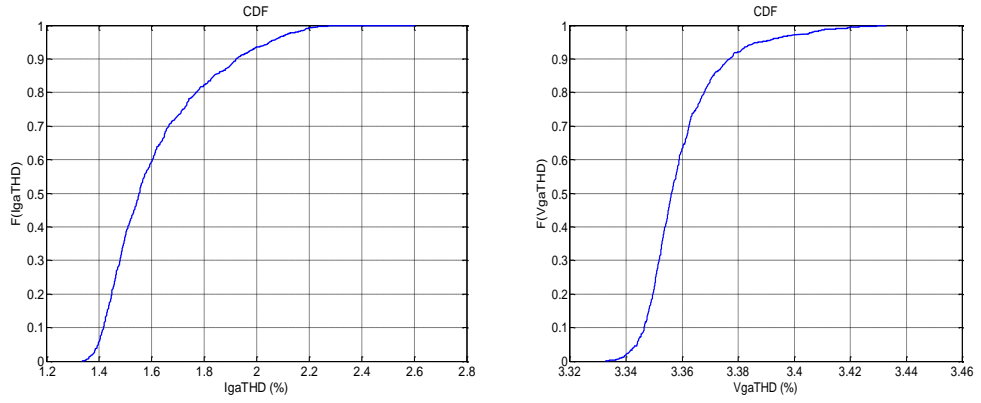


Fig. 5.11: CDF of I_{THD} and V_{THD} of 10 VSCs with Variable Power

c) Effect of Filter and Operating Power Variation on Current and Voltage THD

In this section the operating power and the filter inductance L_{fabc1} are varied simultaneously with the assumption that the VSCs are operating within the constraints applied in the first 2 cases. The mean and standard deviation of the I_{THD} and V_{THD} are presented in Table 5.3.

From the table, it is observed that the simultaneous variation of operating power and L_{fabc1} has severe effect on the I_{THD} and V_{THD} as compared to the other two sections. For a single VSC, the variation of power and choosing a poor filter value could lead to increased harmonic distortions levels. However, the V_{THD} is almost immune to these variations. The cdf plot in Figs. 5.12 – 5.14 gives the probability of the VSCs going beyond the IEEE 519 limit.

Table 5.3: Result of Randomly Varying Filter Inductor Value and Operating Power of Multiple VSCs

TOTAL HARMONIC DISTORTION OF VOLTAGE AT PCC											
	Index	Number of VSCs									
		1	2	3	4	5	6	7	8	9	10
Current	$\mu(\%)$	7.11	4.91	3.83	3.21	2.79	2.51	2.29	2.21	1.95	1.81
	σ	3.76	1.75	1.12	0.75	0.52	0.42	0.33	0.31	0.29	0.26
Voltage	$\mu(\%)$	1.55	2.29	2.73	3.03	3.24	3.42	3.56	3.64	3.74	3.83
	σ	0.63	0.61	0.53	0.50	0.45	0.43	0.41	0.38	0.36	0.35

The cdf plots for 1, 5 and 10 VSCs are presented in Figs. 5.12 – 5.14 respectively. From Fig. 5.12 for a single VSC, it was noticed that there is a 66% probability

of the I_{THD} exceeding 5%. There is also a 5% possibility of the I_{THD} reaching 15% due to the increase of uncertainties in the system. However, the V_{THD} remained below 5% at all combinations.

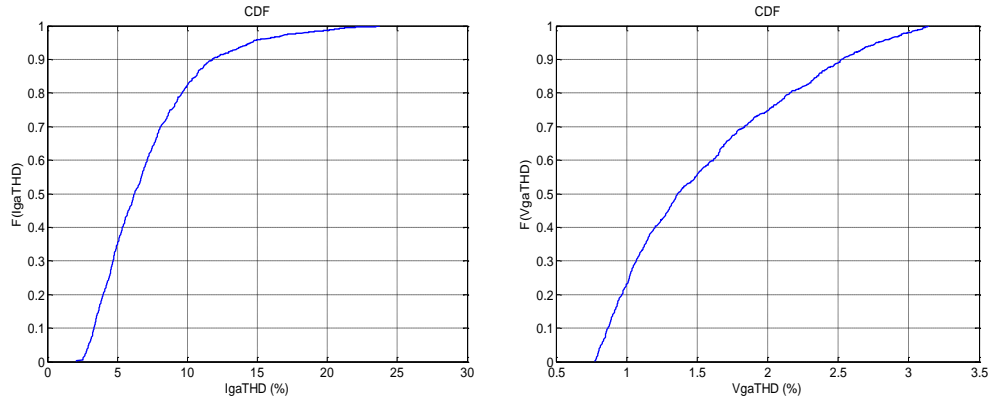


Fig. 5.12: CDF of I_{THD} and V_{THD} of a VSC with Inductor and Power Variation

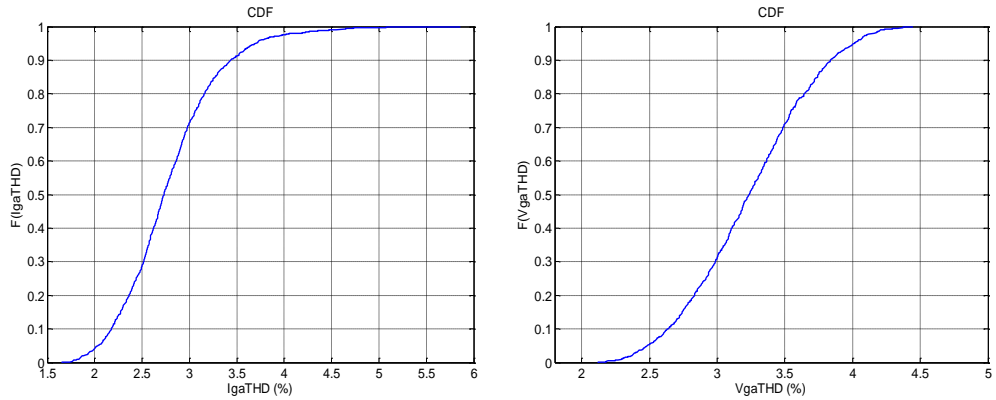


Fig. 5.13: CDF of I_{THD} and V_{THD} of 5 VSCs with Inductor and Power Variation

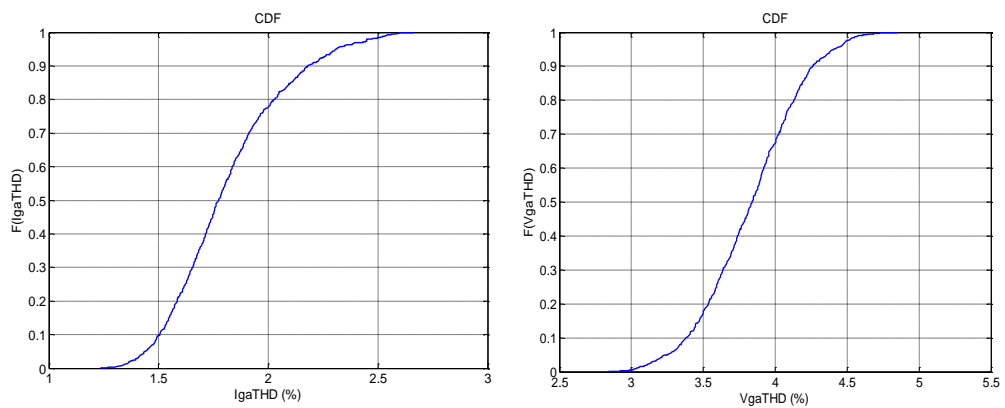


Fig. 5.14: CDF of I_{THD} and V_{THD} of 10 VSCs with Inductor and Power Variation

From the plots, it is clear that variations have greater impact on systems with a smaller number of VSCs and the increase of uncertainty in the RES system caused an increase in the level of distortion.

5.8.3 Unscented Transform Method

The Unscented Transform (UT) earlier mentioned in section 5.8 is a numerical tool that can be used for estimating statistical values within a stochastic process. The UT has been applied in load flow studies [115] and the prediction of electromagnetic statistics [111, 112]. In this section, a step by step procedure of how the UT is implemented in the prediction of harmonic distortion levels of multiple converters is given. The mathematical basis will be presented later in Chapter 6 as part of the introduction to the dimension reduction method.

Step-by-Step Procedure of the UT Technique

A summary of the main steps for implementing the UT technique for predicting harmonic distortion level of VSCs at the Point of Common Coupling (PCC) of the microgrid is highlighted below;

- Step 1) Identify all randomly varying functions within the system (e.g. power, impedance) and obtain their probability distribution functions.
- Step 2) Compute the sigma points and weights using the UT based on Gaussian quadrature.
- Step 3) Input the microgrid system data including the sigma points and weights obtained in 2 into the modelled microgrid.
- Step 4) Run the microgrid simulation while obtaining necessary statistical data for the output variables (current/voltage THD, current/voltage IHD).
- Step 5) Compute the statistical data for the output variables using the measured output data values and weights of the UT (e.g. mean current/ voltage THD/IHD, standard deviation of current/voltage THD/IHD).
- Step 6) Display statistical data of output variables (e.g. mean current/voltage THD/IHD, standard deviation of current/voltage THD/IHD).

Examples to Show the Use of UT in Predicting Harmonics and Impact of Uncertainty

The effectiveness of the UT as an approximate tool for predicting harmonic distortions in the presence of uncertainties is investigated here. Three (3) approximation points were used for the UT method and 1000 MCS simulations which has been shown to be adequate in section 5.8.1 was used as the benchmark. Two scenarios were considered for UT performance evaluation; one showing the impact of power variation on the I_{IHD} and the V_{IHD} at the sidebands of the switching frequency (4 kHz) of the VSCs, and the other investigating the effect of grid system impedance variation.

a) Effect of Variation of Output Power

Fig. 5.15 shows the result for predicting the harmonic distortions at the 78th harmonic order. The results obtained using the UT for the VSCs were in close agreement with the MCS method. In all cases the UT estimated with not more than a difference of 0.02 from the MCS result. The percentage errors were -1.85%, +6.06% and -3.57% for 1, 3 and 5 VSCs respectively.

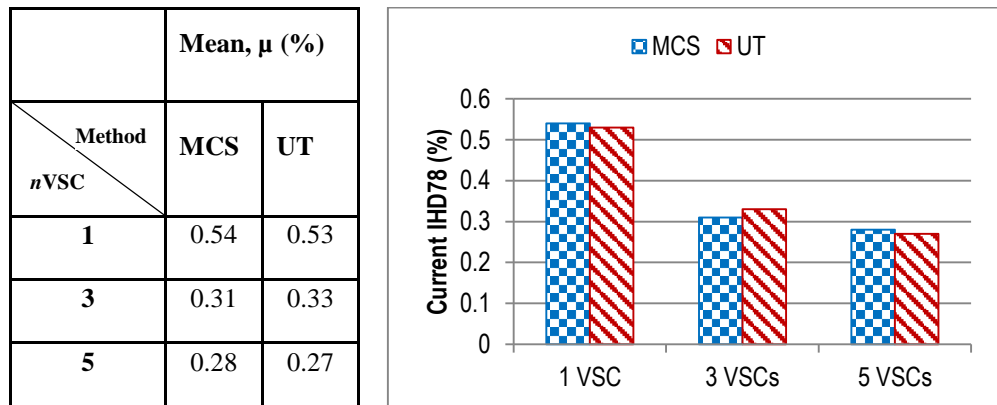


Fig. 5.15: Mean $I_{IHD,78}$ (Power Variation).

Just as in the prediction of harmonic distortions at the 78th order, the predicted harmonic distortion at the 82nd order were well predicted. For 1 VSC the UT predicted the same value with the MCS approach and for 3 VSCs the UT only had a difference of 0.02 (which is +7.7%) from the MCS result. The UT predicted the harmonic distortion for 5 VSCs with an error of +4.55%.

		Mean, μ (%)	
Method n VSC			
	MC S	UT	
1	0.45	0.45	
3	0.26	0.28	
5	0.22	0.23	

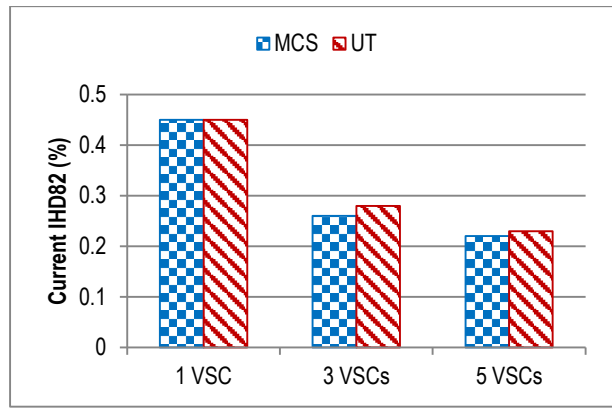


Fig. 5.16: Mean I_{IHD_82} (Power Variation).

b) Grid Impedance Variation

In this case the UT also accurately predicted the harmonic distortions at the 78th and 82nd harmonic orders which are sidebands of the switching frequency. It can be seen in this case of grid impedance variation that the harmonic distortion at the 78th order using the UT was in close agreement with the MCS result. For the case of 1 and 3 VSCs, the UT produced an over estimation of about +4.35% and +4.55% respectively, which a close look at Fig. 5.17 table reveals a difference not more than 0.02 from the MCS. This gives a close agreement with the MCS results. For 5VSCs the UT had an exact prediction with the MCS.

		Mean, μ (%)	
Method n VSC			
	MC S	UT	
1	0.46	0.48	
3	0.44	0.46	
5	0.44	0.44	

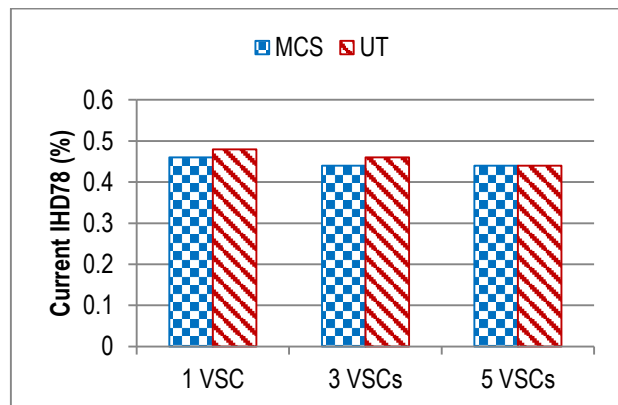


Fig. 5.17: Mean I_{IHD_78} (Grid Impedance Variation).

The predicted harmonic distortion at the 82nd harmonic order using the UT was again in close agreement with the MCS results. Notwithstanding, the UT had a 2.56% and 5.26% overestimation for 1 and 3 VSCs when compared to the MCS result. The UT method predicted the same result as that of the MCS for the case of 5 VSCs.

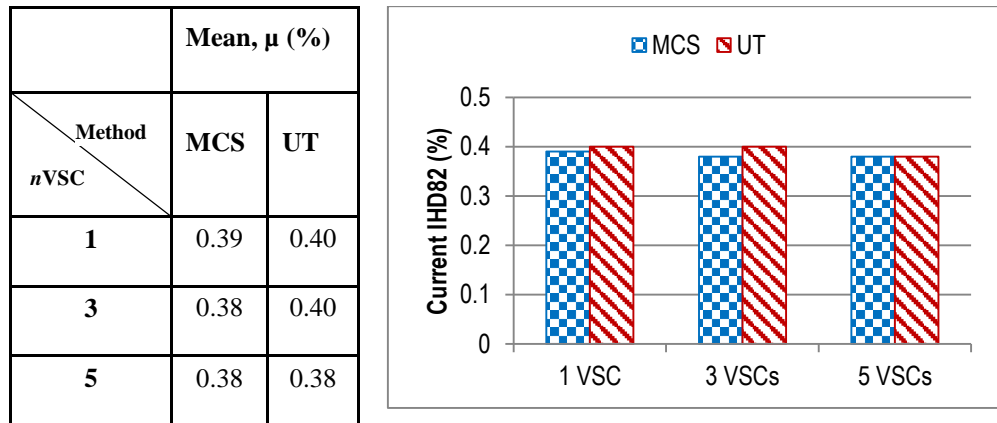


Fig. 5.18: Mean I_{HD_82} (Grid Impedance Variation).

The above examples have highlighted the effectiveness of the UT in predicting harmonic distortions. However, the UT becomes unfeasible for predicting current and voltage harmonics in a system that contains many VSCs as the number of evaluation required for a UT to predict the harmonics increases exponentially with the increase of the number of random variables. For 5 VSCs the number of evaluation was 243 and for 10 VSCs the evaluation number would be 59,049 which is larger than the number of evaluation of the MCS (1000).

5.9 Summary

This chapter discussed the probabilistic analysis of harmonics due to uncertainties present in the power system. The analytical approach for summing random harmonic vectors based on the joint density method was discussed and its drawbacks highlighted. Some statistical terms required for the probabilistic harmonic analysis in this thesis was discussed.

Two numerical approach, the MCS method and the UT method were examined as an alternate to the analytical approach. With the effectiveness of the UT demonstrated and its disadvantages presented, it is clear that a method that will greatly reduce the complexities of the analytical approach and the computational burden of the MCS and UT is required. In the next chapter the UT will be enhanced using dimension reduction techniques to drastically reduce computational time and burden while being able to still produce accurate results.

Chapter 6

Unscented Transform and Dimension Reduction Technique

This chapter discusses the mathematical basics of the Unscented Transform (UT) method based on Gaussian quadrature. It also presents and discusses the mathematical basics of two dimension reduction techniques that can be applied to a UT equation in order to reduce the number of evaluations, computation burden and time for systems containing large number of variables. The effectiveness of the dimension reduction methods in predicting harmonic distortion levels of many VSCs with randomly varying output power in an Electrical Power System (EPS) are then evaluated.

6.1 Unscented Transform based on Gaussian Quadrature

The UT works by approximating a nonlinear mapping by a set of selected points called sigma points. The weighted average of the sigma points produces the expectation of the mapping. The UT uses the moments of a distribution function pdf $w(x)$ to develop the sigma points and corresponding weights [122]. In [115] the UT method was described as an estimator that works by approximating a continuous distribution function with pdf $w(x)$ as a discrete distribution using deterministically chosen points called sigma points (S_i) and weights (w_i) such that the moments of both distributions are equal. A mathematical representation is given in (6.1), while a graphical illustration is presented in Fig. 6.1.

$$E(x^k) = \int x^k w(x) dx = \sum_i w_i S_i^k \quad (6.1)$$

S_i contains the location of the abscissas at which the function $f(x)$ is to be evaluated while w_i are the weighting coefficients which when multiplied by S_i gives an approximation to the integral of $f(x)$. k represents the moments of the expectation (E) where, $k = 1$ implies the mean value and $k = 2$ implies variance.

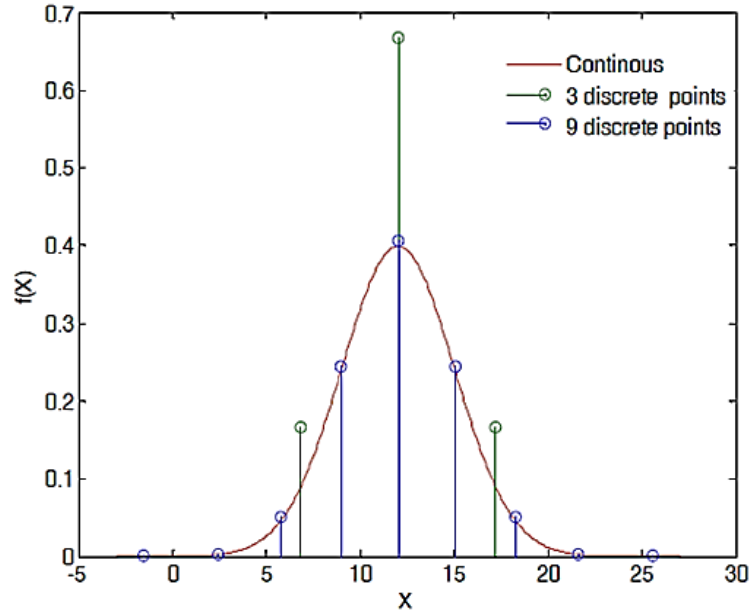


Fig. 6.1: Continuous and Discrete Representation of a function [88]

Although the sigma points and weights may be obtained by solving a Taylor's series expansion [112, 123], its applicability is limited to few orders of approximation and is also inefficient for functions (such as Weibull distribution) with no known classical orthogonal polynomials [88].

The Gaussian quadrature technique solves (6.1) as a quadrature problem such that the integration points for integrating $f(x)$ correspond to the desired sigma points S_i . Hence, for a function $f(x)$ assumed as a polynomial, with pdf (weighting function) $w(x)$, the nonlinear mapping for the expectation is given as;

$$E[f(x)] = \int_{-\infty}^{\infty} f(x)w(x)dx = \sum_i w_i f(S_i) \quad (6.2)$$

The sigma points of the distribution function can be obtained as the roots of its associated orthogonal polynomial when (6.1 or 6.2) is integrating using Gaussian quadrature. This method can be easily applied, as most common distributions have known classical orthogonal polynomials associated with them. The associated orthogonal polynomials for some distribution functions are listed in Table 6.1 and more can be found in [124]. In Table 6.1, it can be seen that a uniform distributed weighting function is orthogonal to the Legendre polynomial.

For a distribution weighting functions $w(x)$ (pdf), with no known classical orthogonal polynomial, the UT method can still be applied if the associated orthogonal polynomial is built from scratch using the Stieltjes procedure (see Appendix B.2). This and the application of the UT method to non-classical polynomials are discussed in [88] while the basic principle of the Gaussian Quadrature is given in the next section.

Table 6.1: Distribution Functions and Associated Orthogonal Polynomials

Distribution	Orthogonal Polynomial	$w(x)$	Support Limit
Normal (Gaussian)	Hermite	e^{-x^2}	$[-\infty, \infty]$
Uniform	Legendre	1	$[-1, 1]$
Exponential	Laguerre	e^{-x}	$[0, \infty]$
Gamma	Generalized Laguerre	$x^\alpha e^{-x}, \alpha > -1$	$[0, \infty]$
Beta	Jacobi	$(1-x)^\alpha (1+x)^\beta, \alpha > -1, \beta > -1$	$[-1, 1]$

6.1.1 Gaussian Quadrature: Basics

The Gaussian Quadrature works by approximately estimating the definite integral of a function $f(x)$ over a given interval. The fundamental theorem of Gaussian quadrature states that “the optimal abscissas of an N -point Gaussian quadrature formula with weighting functions $w(x)$ in the interval (a, b) are precisely the roots of the orthogonal polynomial for the same interval and weighting function” [125]. The Gaussian quadrature approach is optimal because it exactly fits all polynomials up to degree $2N-1$ [115, 125]. This theorem can be applied to the UT equation in (6.1) which is repeated as (6.3)

$$E(x^k) = \int x^k w(x) dx = \sum_i w_i S_i^k \tag{6.3}$$

Following the principle of orthogonality (see Appendix B.1) and assuming $P_m(x)$ is a set of polynomials orthogonal in the interval (a, b) with respect to the weighting function $w(x)$. That is $P_m(x)$ is an m degree polynomial with at least one variable/term not equal to zero then, the integral of (6.3) becomes;

$$\int_a^b x^k w(x) P_m(x) dx = 0 \quad (6.4)$$

From the theorem, the zeros of the polynomial $P_m(x)$ produce m -abscissas x_i (which corresponds to the sigma points S_i). The corresponding m -weights w_i are obtained as [125, 126];

$$w_i = \int_a^b \frac{P_m(x)}{(x - x_i) P_m'(x_i)} dx \quad (6.5)$$

where P_m' is the first differential of P_m .

As earlier stated the above method can be easily applied on weighting functions (pdfs) whose orthogonal polynomials are known by associating the distribution function to its classical orthogonal polynomials. The concept of orthogonal polynomials is explained in Appendix B.1.

6.1.2 Sigma Points and Weights Generation in Multivariate Problems

The generation of sigma points and weights for a single variable involves one dimensional integration and is given in Appendix B.3. While for more than one variable (multivariate problem) with n uncertainties will require n number of integration to be performed.

So modifying (6.3) for a multivariate problem will give (6.6) [88];

$$E(\mathbf{x}^k) = \int \cdots \int \mathbf{x}^k w(\mathbf{x}) d\mathbf{x} \quad (6.6)$$

where vector $\mathbf{x} = \{x_1, x_2, \dots, x_n\}$.

The above process requires large number of integrations; however, the integration can be simplified if it is possible to independently factor out the variables in \mathbf{x} from each other. This will approximate the integration to be the product of the variables one dimensional integration. Using the tensor product will give the above process to be (6.7) [88].

$$E(\mathbf{x}^k) = \int x_1^k w(x_1) dx_1 \cdots \int x_n^k w(x_n) dx_n = \cdots \sum_{i_1} \cdots \sum_{i_n} (w_{i_1} \otimes \cdots \otimes w_{i_n})(S_{i_1}, \dots, S_{i_n}) \quad (6.7)$$

The sigma points for each variable in \mathbf{x} are then generated using the univariate method in Appendix B.3 in conjunction with equation (6.7). The product of the individual weights and sigma points is then used to generate the final sigma points and weights of the multivariate problem [88]. Table 6.2 and 6.3 gives an illustration of the above, involving two random variables with each discretized by 3 points and 5 points respectively [88].

Table 6.2: Generation of Sigma Points (S_{in}) and Weight (W_{in}) for a Multivariate Problem Using 3 points Approximations

Sigma Points Weights	2S_1	2S_2	2S_3
1S_1	${}^1W_1{}^2W_1$	${}^1W_1{}^2W_2$	${}^1W_1{}^2W_3$
1S_2	${}^1W_2{}^2W_1$	${}^1W_2{}^2W_2$	${}^1W_2{}^2W_3$
1S_3	${}^1W_3{}^2W_1$	${}^1W_3{}^2W_2$	${}^1W_3{}^2W_3$

Table 6.3: Generation of Sigma Points and Weight for a Multivariate Problem Using 5 points Approximations

Sigma Points Weights	2S_1	2S_2	2S_3	2S_4	2S_5
1S_1	${}^1W_1{}^2W_1$	${}^1W_1{}^2W_2$	${}^1W_1{}^2W_3$	${}^1W_1{}^2W_4$	${}^1W_1{}^2W_5$
1S_2	${}^1W_2{}^2W_1$	${}^1W_2{}^2W_2$	${}^1W_2{}^2W_3$	${}^1W_2{}^2W_4$	${}^1W_2{}^2W_5$
1S_3	${}^1W_3{}^2W_1$	${}^1W_3{}^2W_2$	${}^1W_3{}^2W_3$	${}^1W_3{}^2W_4$	${}^1W_3{}^2W_5$
1S_4	${}^1W_4{}^2W_1$	${}^1W_4{}^2W_2$	${}^1W_4{}^2W_3$	${}^1W_4{}^2W_4$	${}^1W_4{}^2W_5$
1S_5	${}^1W_5{}^2W_1$	${}^1W_5{}^2W_2$	${}^1W_5{}^2W_3$	${}^1W_5{}^2W_4$	${}^1W_5{}^2W_5$

Applying (6.7) will lead to high number of evaluation (E_v) as shown in Table 6.4 and as indicated in (6.8) when the dimension increases. Equation (6.8) indicates an exponential growth in E_v to be carried out as the dimension increases [88].

$$E_v = NS_i^n \tag{6.8}$$

where NS_i is the number of sigma points used in discretizing each variable for an n dimensional problem (number of random variables) [88]. For example, if $NS_i = 5$, then the number of evaluation (E_v) required for $n = 2, 3, 5$ and 10 would be 25, 125, 3125 and 9765625 respectively. The UT method becomes

computationally burdensome and time consuming, as the number of variables increases. Hence, the UT technique is plagued by the *curse of dimensionality* problem as the number of variables increase.

6.2 Dimension Reduction

Dimension Reduction (DR) of the Gaussian quadrature based Unscented Transform becomes necessary because of the *curse of dimensionality* problem associated with it when dealing with systems with large number of uncertainties or parameter variability.

6.2.1 Basics of Dimension Reduction

Dimension reduction [114, 127-129] is an approximation technique for estimating the statistical moments of an output function. The technique involves an additive decomposition of an N -dimensional function involving n -dimensional integral into a series sum of D -dimensional functions such that $D < N$. It provides a means of efficiently combining the sigma points and weights for a large number of variables such that the number of evaluation points can be minimised [88]. For the case where $D=1$, the technique is referred to as Univariate dimension reduction while it is referred to as Bivariate dimension reduction when $D=2$. A detailed mathematical derivation can be found in [114, 127] while a brief description is given in following sections.

6.2.2 Univariate Dimension Reduction (UDR)

The UDR technique involves decomposing the problem's main function into a summation of n -dimensional functions thus reducing the problem to a one-dimensional integration. The UDR technique can be employed in problems involving a minimum of two random variables. The mathematical basis is presented below as described in [88].

For a function $f(\mathbf{x})$ with N independent variables such that;

$$y = f(\mathbf{x}) \tag{6.9}$$

where $\mathbf{x} = \{x_1, x_2, \dots, x_N\}$

Using (6.6), the mean of (6.9) can be written as;

$$E[f(\mathbf{x})] = \int_a^b \cdots \int_a^b f(\mathbf{x}) d\mathbf{x} \quad (6.10)$$

where the interval $[a, b]$ depends on the distribution type.

Equation (6.10) requires N -dimensional integration.

At the mean points, let;

$$\mathbf{x}_\mu = (\bar{\mathbf{x}}) = \{\bar{x}_1, \bar{x}_2, \dots, \bar{x}_N\}^T \quad (6.11)$$

The Taylor series expansion of $f(x)$ gives;

$$\begin{aligned} y = f(\mathbf{x}) &= f(\bar{\mathbf{x}} + \hat{\mathbf{x}}) = f(\bar{\mathbf{x}}) + \sum_{j=1}^{\infty} \frac{1}{j!} \sum_{i=1}^N \frac{d^j f}{d\hat{x}_i^j}(\bar{\mathbf{x}}) \hat{x}_i^j + \cdots \\ &\sum_{j_2=1}^{\infty} \sum_{j_1=1}^{\infty} \frac{1}{j_1! j_2!} \sum_{i_1 < i_2}^N \frac{d^{j_1+j_2} f}{d\hat{x}_{i_1}^{j_1} d\hat{x}_{i_2}^{j_2}}(\bar{\mathbf{x}}) \hat{x}_{i_1}^{j_1} \hat{x}_{i_2}^{j_2} + \cdots \\ &\sum_{j_3=1}^{\infty} \sum_{j_2=1}^{\infty} \sum_{j_1=1}^{\infty} \frac{1}{j_1! j_2! j_3!} \sum_{i_1 < i_2}^N \frac{d^{j_1+j_2+j_3} f}{d\hat{x}_{i_1}^{j_1} d\hat{x}_{i_2}^{j_2} d\hat{x}_{i_3}^{j_3}}(\bar{\mathbf{x}}) \hat{x}_{i_1}^{j_1} \hat{x}_{i_2}^{j_2} \hat{x}_{i_3}^{j_3} + \cdots \end{aligned} \quad (6.12)$$

Substituting (6.12) into (6.10) gives;

$$\begin{aligned} E[f(\mathbf{x})] &= E[f(\bar{\mathbf{x}})] + \sum_{j=1}^{\infty} \frac{1}{j!} \sum_{i=1}^N \frac{d^j f}{d\hat{x}_i^j}(\bar{\mathbf{x}}) E[\hat{x}_i^j] + \cdots \\ &\sum_{j_2=1}^{\infty} \sum_{j_1=1}^{\infty} \frac{1}{j_1! j_2!} \sum_{i_1 < i_2}^N \frac{d^{j_1+j_2} f}{d\hat{x}_{i_1}^{j_1} d\hat{x}_{i_2}^{j_2}}(\bar{\mathbf{x}}) E[\hat{x}_{i_1}^{j_1} \hat{x}_{i_2}^{j_2}] + \cdots \\ &\sum_{j_3=1}^{\infty} \sum_{j_2=1}^{\infty} \sum_{j_1=1}^{\infty} \frac{1}{j_1! j_2! j_3!} \sum_{i_1 < i_2}^N \frac{d^{j_1+j_2+j_3} f}{d\hat{x}_{i_1}^{j_1} d\hat{x}_{i_2}^{j_2} d\hat{x}_{i_3}^{j_3}}(\bar{\mathbf{x}}) E[\hat{x}_{i_1}^{j_1} \hat{x}_{i_2}^{j_2} \hat{x}_{i_3}^{j_3}] + \cdots \end{aligned} \quad (6.13)$$

Considering a univariate function represented as $f(\bar{x}_1, \dots, x_i, \bar{x}_{i+1}, \dots, \bar{x}_N)$, the

Taylor series expansion is given as (6.14);

$$f(\bar{x}_1, \dots, x_i, \bar{x}_{i+1}, \dots, \bar{x}_N) = f(\bar{\mathbf{x}}) + \sum_{j=1}^{\infty} \frac{1}{j!} \sum_{i=1}^N \frac{d^j f}{d\hat{x}_i^j}(\bar{\mathbf{x}}) \hat{x}_i^j \quad (6.14)$$

Using (6.14), the Taylor series expansion of the first N univariate functions is given as (6.15);

$$\begin{aligned}
f(x_1, \bar{x}_2, \bar{x}_3, \dots, \bar{x}_N) &= f(\bar{\mathbf{x}}) + \sum_{j=1}^{\infty} \frac{1}{j!} \frac{d^j f}{dx_1^j}(\bar{\mathbf{x}}) \hat{x}_1^j \\
f(\bar{x}_1, x_2, \bar{x}_3, \dots, \bar{x}_N) &= f(\bar{\mathbf{x}}) + \sum_{j=1}^{\infty} \frac{1}{j!} \frac{d^j f}{dx_2^j}(\bar{\mathbf{x}}) \hat{x}_2^j \\
&\vdots \\
f(\bar{x}_1, \bar{x}_2, \dots, \bar{x}_{N-1}, x_N) &= f(\bar{\mathbf{x}}) + \sum_{j=1}^{\infty} \frac{1}{j!} \frac{d^j f}{dx_N^j}(\bar{\mathbf{x}}) \hat{x}_N^j
\end{aligned} \tag{6.15}$$

Summing the functions in (6.15) gives

$$\sum_{i=1}^N f(\bar{x}_1, \bar{x}_2, \dots, x_i, \bar{x}_N) = Nf(\bar{\mathbf{x}}) + \sum_{i=1}^N \sum_{j=1}^{\infty} \frac{1}{j!} \frac{d^j f}{dx_i^j}(\bar{\mathbf{x}}) \hat{x}_i^j \tag{6.16}$$

Subtracting (6.14) from (6.16) gives

$$\begin{aligned}
\sum_{i=1}^N f(\bar{x}_1, \bar{x}_2, \dots, x_i, \bar{x}_N) - f(\bar{x}_1, \dots, x_i, \bar{x}_{i+1}, \dots, \bar{x}_N) &= \dots \\
Nf(\bar{\mathbf{x}}) + \sum_{i=1}^N \sum_{j=1}^{\infty} \frac{1}{j!} \frac{d^j f}{dx_i^j}(\bar{\mathbf{x}}) \hat{x}_i^j - f(\bar{\mathbf{x}}) - \sum_{j=1}^{\infty} \frac{1}{j!} \sum_{i=1}^N \frac{d^j f}{dx_i^j}(\bar{\mathbf{x}}) \hat{x}_i^j &
\end{aligned} \tag{6.17a}$$

The summations (second and last terms in the right side of the equation) are equal so they cancel out.

$$\begin{aligned}
\sum_{i=1}^N f(\bar{x}_1, \bar{x}_2, \dots, x_i, \bar{x}_N) - f(\bar{x}_1, \dots, x_i, \bar{x}_{i+1}, \dots, \bar{x}_N) &= Nf(\bar{\mathbf{x}}) - f(\bar{\mathbf{x}}) \\
&= (N-1)f(\bar{\mathbf{x}})
\end{aligned} \tag{6.17b}$$

Rearranging (6.17b) gives;

$$f(\bar{x}_1, \dots, x_i, \bar{x}_{i+1}, \dots, \bar{x}_N) = \sum_{i=1}^N f(\bar{x}_1, \bar{x}_2, \dots, x_i, \bar{x}_N) - (N-1)f(\bar{\mathbf{x}}) \tag{6.17c}$$

Representing $f(\bar{x}_1, \dots, x_i, \bar{x}_{i+1}, \dots, \bar{x}_N)$ as $\hat{f}(\mathbf{x})$, implies $\hat{f}(\mathbf{x})$ is the univariate approximation of $f(\mathbf{x})$ and is given in (6.18) as;

$$\hat{f}(\mathbf{x}) = \sum_{i=1}^N f(\bar{x}_1, \bar{x}_2, \dots, x_i, \bar{x}_N) - (N-1)f(\bar{\mathbf{x}}) \tag{6.18}$$

$\bar{\mathbf{x}}$ are the mean values for the variables in \mathbf{x} which are vector quantities.

The mean of the above univariate approximation (6.18) is given in (6.19);

$$E[\hat{f}(\mathbf{x})] = \sum_{i=1}^N E[f(\bar{x}_1, \bar{x}_2, \dots, x_i, \bar{x}_N)] - (N-1)E[f(\bar{\mathbf{x}})] \tag{6.19}$$

Substituting (6.16) into (6.19) gives;

$$E[\hat{f}(\mathbf{x})] = E[f(\bar{\mathbf{x}})] + \sum_{i=1}^N \sum_{j=1}^{\infty} \frac{1}{j!} \frac{d^j f}{d\hat{x}_i^j}(\bar{\mathbf{x}}) \hat{x}_i^j \quad (6.20)$$

Neglecting the higher order partial derivative terms on the right hand side (R.H.S.), makes $E[\hat{f}(\mathbf{x})]$ approximately equal to $E[f(\mathbf{x})]$ and vice versa. Thus, it can be assumed that the output moments of the function y is $E[\hat{f}(\mathbf{x})]$, where $E[\hat{f}(\mathbf{x})]$ is a summation of one-dimensional functions and involves only one dimensional integration. The difference between (6.13) and (6.20) is referred to as the residual error for the UDR e_{udr} (6.21) [88];

$$\begin{aligned} e_{udr} = E[f(\mathbf{x})] - E[\hat{f}(x)] &= \sum_{j_2=1}^{\infty} \sum_{j_1=1}^{\infty} \frac{1}{j_1! j_2!} \sum_{i_1 < i_2}^N \frac{d^{j_1+j_2} f}{d\hat{x}_{i_1}^{j_1} d\hat{x}_{i_2}^{j_2}}(\bar{\mathbf{x}}) E[\hat{x}_{i_1}^{j_1} \hat{x}_{i_2}^{j_2}] + \dots \\ &\sum_{j_3=1}^{\infty} \sum_{j_2=1}^{\infty} \sum_{j_1=1}^{\infty} \frac{1}{j_1! j_2! j_3!} \sum_{i_1 < i_2 < i_3}^N \frac{d^{j_1+j_2+j_3} f}{d\hat{x}_{i_1}^{j_1} d\hat{x}_{i_2}^{j_2} d\hat{x}_{i_3}^{j_3}}(\bar{\mathbf{x}}) E[\hat{x}_{i_1}^{j_1} \hat{x}_{i_2}^{j_2} \hat{x}_{i_3}^{j_3}] + \dots \end{aligned} \quad (6.21)$$

The error e_{udr} in the univariate function can become significant for systems with large random variation and for higher order moments [88, 127]. Notwithstanding, the residual error in (6.21) can be reduced if the BDR technique is applied. However, this will lead to an increase in number of evaluations and computational time.

6.2.3 Bivariate Dimension Reduction (BDR)

The BDR provides an improvement to the UDR technique as only the third and higher order terms (which are most times trivial) are now contained in its residual error, e_{bdr} . The BDR technique utilizes a combination of one and two-dimensional functions in approximating the output function. The BDR can be applied to problems involving more than two random variables [88].

Considering a bivariate function $f(\bar{x}_1, \dots, x_i, \bar{x}_{i+1}, \dots, x_i, \dots, \bar{x}_N)$, expanded using the Taylor series expansion as shown in (6.22);

$$\begin{aligned}
 f(\bar{x}_1, \dots, x_i, \bar{x}_{i+1}, \dots, x_{i_2}, \dots, \bar{x}_N) &= f(\bar{\mathbf{x}}) + \sum_{j=1}^{\infty} \frac{1}{j!} \sum_{i=1}^N \frac{d^j f}{d\hat{x}_i^j}(\bar{\mathbf{x}}) \hat{x}_i^j + \dots \\
 &\quad \sum_{j=1}^{\infty} \frac{1}{j!} \sum_{i=1}^N \frac{d^j f}{d\hat{x}_{i_2}^j}(\bar{\mathbf{x}}) \hat{x}_{i_2}^j + \dots \\
 &\quad \sum_{j_2=1}^{\infty} \sum_{j_1=1}^{\infty} \frac{1}{j_1! j_2!} \sum_{i_1 < i_2}^N \frac{d^{j_1+j_2} f}{d\hat{x}_{i_1}^{j_1} d\hat{x}_{i_2}^{j_2}}(\bar{\mathbf{x}}) \hat{x}_{i_1}^{j_1} \hat{x}_{i_2}^{j_2}
 \end{aligned} \tag{6.22}$$

From (6.22), the summation of the one and two dimensional functions for a function made up of N variables is given by [128] as;

$$\begin{aligned}
 \sum_{i_1 < i_2}^N f(\bar{x}_1, \dots, x_{i_1}, \bar{x}_{i_1+1}, \dots, x_{i_2}, \dots, \bar{x}_N) &= \frac{N(N-1)}{2} f(\bar{\mathbf{x}}) + \dots \\
 &\quad (N-1) \sum_{j=1}^{\infty} \frac{1}{j!} \sum_{i=1}^N \frac{d^j f}{d\hat{x}_i^j}(\bar{\mathbf{x}}) \hat{x}_i^j + \dots \\
 &\quad \sum_{i_1 < i_2}^N \sum_{j_2=1}^{\infty} \sum_{j_1=1}^{\infty} \frac{1}{j_1! j_2!} \sum_{i_1 < i_2}^N \frac{d^{j_1+j_2} f}{d\hat{x}_{i_1}^{j_1} d\hat{x}_{i_2}^{j_2}}(\bar{\mathbf{x}}) \hat{x}_{i_1}^{j_1} \hat{x}_{i_2}^{j_2}
 \end{aligned} \tag{6.23}$$

The bivariate approximation of The Taylor series expansion of $f(x)$ in (6.12) can be written in terms of $\sum_{i_1 < i_2}^N f(\bar{x}_1, \dots, x_{i_1}, \bar{x}_{i_1+1}, \dots, x_{i_2}, \dots, \bar{x}_N)$ and $\sum_{i=1}^N f(\bar{x}_1, \bar{x}_2, \dots, x_i, \bar{x}_N)$ as (6.24) [88];

$$\begin{aligned}
 \hat{f}(\mathbf{x}) &= \sum_{i_1 < i_2}^N f(\bar{x}_1, \dots, x_{i_1}, \bar{x}_{i_1+1}, \dots, x_{i_2}, \dots, \bar{x}_N) - \dots \\
 &\quad (N-2) \sum_{i=1}^N f(\bar{x}_1, \bar{x}_2, \dots, x_i, \bar{x}_N) + \frac{(N-1)(N-2)}{2} f(\bar{\mathbf{x}})
 \end{aligned} \tag{6.24}$$

The mean of $\hat{f}(\mathbf{x})$ is given as;

$$\begin{aligned}
 E[\hat{f}(\mathbf{x})] &= \sum_{i_1 < i_2}^N E[f(\bar{x}_1, \dots, x_{i_1}, \bar{x}_{i_1+1}, \dots, x_{i_2}, \dots, \bar{x}_N)] - \dots \\
 &\quad (N-2) \sum_{i=1}^N E[f(\bar{x}_1, \bar{x}_2, \dots, x_i, \bar{x}_N)] + \frac{(N-1)(N-2)}{2} E[f(\bar{\mathbf{x}})]
 \end{aligned} \tag{6.25}$$

The difference between (6.13) and (6.25) is referred to as the BDR technique's residual error, e_{bdr} (6.26). The BDR technique gives more accurate results than the UDR method especially for higher order moments. This is as a result of the BDR technique having higher order terms in the approximation.

$$e_{bdr} = \sum_{j_3=1}^{\infty} \sum_{j_2=1}^{\infty} \sum_{j_1=1}^{\infty} \frac{1}{j_1! j_2! j_3!} \sum_{i_1 < i_2}^N \frac{d^{j_1+j_2+j_3}}{d\hat{x}_{i_1}^{j_1} d\hat{x}_{i_2}^{j_2} d\hat{x}_{i_3}^{j_3}} f(\bar{\mathbf{x}}) E \left[\hat{x}_{i_1}^{j_1} \hat{x}_{i_2}^{j_2} \hat{x}_{i_3}^{j_3} \right] + \dots \quad (6.26)$$

6.2.4 Output Moment Estimation

The dimension reduction technique can be used to easily estimate higher order moment of the output function. The k th moment $E[f^k(x)]$ is simply evaluated using a simple assumption [88, 127]. For instance, the n th order of the function $f(x)$ can be represented by $H(x)$ as shown in (6.27) for easy expansion;

$$f^k(x) = H(x) \quad (6.27)$$

For the UDR, the higher moment is given by (6.28);

$$E[f^k(\mathbf{x})] = E[H(\mathbf{x})] \cong E \left[\sum H(\bar{x}_1, \dots, x_i, \bar{x}_{i+1}, \dots, \bar{x}_N) - (N-1)H(\bar{\mathbf{x}}) \right] \quad (6.28)$$

Substituting (6.27) back into the right side of (6.28);

$$E[f^k(\mathbf{x})] = E[H(\mathbf{x})] \cong E \left[\sum f^k(\bar{x}_1, \dots, x_i, \bar{x}_{i+1}, \dots, \bar{x}_N) - (N-1)f^k(\bar{\mathbf{x}}) \right] \quad (6.29)$$

Applying the same principle, the central moment about the mean μ_y , where $\mu_y = E[y] = E[f(x)]$ is given as (6.30);

$$E[f^k(\mathbf{x} - \mu_y)] \cong E \left[\begin{array}{l} \sum (f^k(\bar{x}_1, \dots, x_i, \bar{x}_{i+1}, \dots, \bar{x}_N) - \mu_y) \\ -(N-1)(f^k(\bar{\mathbf{x}}) - \mu_y) \end{array} \right] \quad (6.30)$$

and the raw and central moments of the output function using the BDR technique are given in (6.31) and (6.32) respectively.

$$E[f^k(\mathbf{x})] \cong E \left[\begin{array}{l} \sum_{i_1 < i_2}^N f^k(\bar{x}_1, \dots, x_{i_1}, \bar{x}_{i_1+1}, \dots, x_{i_2}, \dots, \bar{x}_N) \\ -(N-2) \sum_{i=1}^N f^k(\bar{x}_1, \dots, x_i, \bar{x}_{i+1}, \dots, \bar{x}_N) \\ + \frac{(N-1)(N-2)}{2} f^k(\bar{\mathbf{x}}) \end{array} \right] \quad (6.31)$$

$$E[f^k(\mathbf{x} - \mu_y)] \cong E \left[\begin{array}{l} \sum_{i_1 < i_2}^N (f^k(\bar{x}_1, \dots, x_{i_1}, \bar{x}_{i_1+1}, \dots, x_{i_2}, \dots, \bar{x}_N) - \mu_y) \\ -(N-2) \sum_{i=1}^N (f^k(\bar{x}_1, \dots, x_i, \bar{x}_{i+1}, \dots, \bar{x}_N) - \mu_y) \\ + \frac{(N-1)(N-2)}{2} (f^k(\bar{\mathbf{x}}) - \mu_y) \end{array} \right] \quad (6.32)$$

6.3 Dimension Reduction and Unscented Transform

Dimension reduction is applied to the UT method based on the relationship between the moments of a continuous function and its discrete approximation (6.33) [88].

$$E[f(x)] = \sum_{i=1}^N w_i f(S_i) \quad (6.33)$$

where S_i are the sigma points and w_i the weights.

Substituting the values of $f(x)$ into (6.33) gives (6.34) for the UDR techniques.

$$\begin{aligned} E[f(\mathbf{x})] &\cong E[\hat{f}(\mathbf{x})] \cong \sum_{i=1}^N E[f(\bar{x}_1, \bar{x}_2, \dots, x_i, \bar{x}_N)] - (N-1)E[f(\bar{x}_1, \dots, \bar{x}_N)] \\ &\cong \sum_{j=1}^k \sum_{i=1}^N w_i^j f(\bar{x}_1, \bar{x}_2, \dots, S_i^j, \dots, \bar{x}_N) - (N-1)f(\bar{x}_1, \dots, \bar{x}_N) \end{aligned} \quad (6.34)$$

The higher order raw moments of the UDR is obtained by (6.35);

$$E[f^k(\mathbf{x})] \cong \sum_{j=1}^k \sum_{i=1}^N w_i^j f^k(\bar{x}_1, \bar{x}_2, \dots, S_i^j, \bar{x}_{i+1}, \dots, \bar{x}_N) - (N-1)f^k(\bar{x}_1, \dots, \bar{x}_N) \quad (6.35)$$

and the central moment is given as follows;

$$\begin{aligned} E[f^k(\mathbf{x} - \mu_y)] &\cong \sum_{j=1}^k \sum_{i=1}^N w_i^j (f^k(\bar{x}_1, \bar{x}_2, \dots, S_i^j, \bar{x}_{i+1}, \dots, \bar{x}_N) - \mu_y) - \\ &\quad (N-1)(f^k(\bar{x}_1, \dots, \bar{x}_N) - \mu_y) \end{aligned} \quad (6.36)$$

For the BDR, the higher order raw moments is given in (6.37).

$$\begin{aligned} E[f^k(\mathbf{x})] &\cong \sum_{j=1}^k \sum_{i_1 < i_2}^N w_i^j f^k(\bar{x}_1, \dots, S_{i_1}^j, \bar{x}_{i_1+1}, \dots, S_{i_2}^j, \dots, \bar{x}_N) \\ &\quad - (N-2) \sum_{j=1}^k \sum_{i=1}^N w_i^j f^k(\bar{x}_1, \dots, S_i^j, \bar{x}_{i+1}, \dots, \bar{x}_N) \\ &\quad + \frac{(N-1)(N-2)}{2} f^k(\bar{x}_1, \dots, \bar{x}_N) \end{aligned} \quad (6.37)$$

and the central moment is given as (6.38);

$$\begin{aligned}
 E[f^k(\mathbf{x} - \mu_y)] &\cong \sum_{j=1}^k \sum_{i_1 < i_2}^N w_i^j (f^k(\bar{x}_1, \dots, S_{i_1}^j, \bar{x}_{i_1+1}, \dots, S_{i_2}^j, \dots, \bar{x}_N) - \mu_y) \\
 &\quad - (N-2) \sum_{j=1}^n \sum_{i=1}^N w_i^j (f^k(\bar{x}_1, \dots, S_i^j, \bar{x}_{i+1}, \dots, \bar{x}_N) - \mu_y) \\
 &\quad + \frac{(N-1)(N-2)}{2} (f^k(\bar{x}_1, \dots, \bar{x}_N) - \mu_y)
 \end{aligned} \tag{6.38}$$

The number of evaluations (E_v) required for an N -dimensional function using n estimation points (sigma points) is given by (6.39) and (6.40) for the UDR and BDR techniques respectively [129];

$$E_v = (n \times N) + 1 \tag{6.39}$$

$$E_v = \left(\frac{N(N-1)}{2} \times n^2 \right) + ((n \times N) + 1) \tag{6.40}$$

In problems where all random variables are symmetrical and the number of sigma points n is odd, one of the sigma points will always be located on the mean point [88]. Since the last set of estimation using the UDR is done at the mean point (see 6.19), the extra (redundant) point can be removed. For identification, this will be referred to as the reduced UDR and denoted as rUDR. The number of estimation required for the reduced UDR can be estimated using (6.41) [88];

$$E_v = ((n-1) \times N) + 1 \tag{6.41}$$

and for the reduced BDR (rBDR);

$$E_v = \left(\frac{N(N-1)}{2} \times (n-1)^2 \right) + (((n-1) \times N) + 1) \tag{6.42}$$

For random variables, the number of evaluation point required using the conventional UT, the BDR technique, the UDR technique and the rUDR and rBDR are shown in Table 6.4.

Table 6.4: Number of Evaluation Points Required for the Unscented Transform and Dimension Reduction Methods (Using $n = 3$)

Number of Variables (N)	Number of Evaluations (E_v)				
	UT	BDR	rBDR	UDR	rUDR
2	9	16	9	7	5
3	27	37	19	10	7
4	81	67	33	13	9
5	243	106	51	16	11
10	59049	436	201	31	21
20	3.487e+09	1771	801	61	41
50	7.179e+23	11176	5001	151	101
100	5.154e+47	44851	20001	301	201

From Table 6.4, it is clear that the UT method implemented using the full dimensional integration is unfeasible for systems containing a large number of random variables. Assuming an MCS approach utilizes 10,000 evaluation points, the UT method for 10 random variables would have exceeded the evaluation point of the MCS approach more than 5 times. However, the BDR and UDR method uses 436 and 31 number of evaluations for 10 random variables respectively as compared to the MCS approach. In a system with symmetrical random variables the number of evaluation point can be further reduced and more random variables accommodated for. In this case, the UDR can handle 3,333 random variables without exceeding 10,000 evaluation points required for the MCS approach.

6.4 The Use of Dimension Reduction in Predicting Harmonics

The quantification of current and voltage harmonic distortion level is of high important in analysing the power quality of modern day electric power system as they contain lots of harmonic sources and loads. This section illustrates the effectiveness of the UDR and BDR technique in predicting harmonic distortion levels of a number of VSCs in a case where there is large variability in the VSCs output power. The output power is considered to vary uniformly between 25-

100% of rated power. The computational time required to obtain each result will also be presented and compared with the MCS.

6.4.1 Predicting Harmonics of N VSCs Using the UDR

The UDR technique is used in this section to predict the harmonics distortion level of 1-10 VSCs. The UDR is implemented using the 3 point and 5 points approximation. The reduced UDR technique which can be applied to symmetrical random variables with an odd number sigma (approximation) points is also utilized and the results compared to the UDR and the MCS approach. This section is aimed at evaluating the performance of the UDR and the drastic reduction of computation time it achieves while maintaining its accuracy in predicting harmonics as compared to the MCS approach.

Table 6.5: Predicted THD, IHD₃₈ and IHD₄₂ for 1 VSC Using UDR

Current						
		MCS	3pts UDR	3pts rUDR	5pts UDR	5pts rUDR
THD	Mean	6.92	6.68	6.68	6.79	6.79
	Std	3.16	3.02	3.02	3.24	3.24
	Skewness	1.18	0.80	0.80	1.17	1.17
	kurtosis	3.59	1.92	1.92	3.28	3.28
	E_v	1000	3	3	5	5
	Time	17461s	125s	125s	205s	205s
IHD₃₈	Mean	5.14	4.80	4.80	5.08	5.08
	Std	2.30	2.20	2.20	2.32	2.32
	Skewness	1.18	0.78	0.782	1.18	1.18
	kurtosis	3.59	1.92	1.917	3.36	3.36
	Time	17461s	125s	125s	205s	205s
IHD₄₂	Mean	3.33	3.28	3.28	3.28	3.28
	Std	1.50	1.43	1.43	1.49	1.49
	Skewness	1.20	0.80	0.80	1.19	1.19
	kurtosis	3.67	1.91	1.91	3.39	3.39
	Time	17461s	125s	125s	205s	205s
Voltage						
		MCS	3pts UDR	3pts rUDR	5pts UDR	5pts rUDR
THD	Mean	2.27	2.27	2.27	2.27	2.27
	Std	0.021	0.022	0.022	0.023	0.023
	Skewness	0.27	0.68	0.68	0.33	0.33
	kurtosis	2.32	1.89	1.89	1.67	1.67
	Time	17461s	125s	125s	205s	205s
IHD₃₈	Mean	1.69	1.69	1.69	1.69	1.69

	Std	0.024	0.026	0.026	0.021	0.021
	Skewness	-0.015	0.028	0.028	0.11	0.11
	kurtosis	2.20	1.80	1.80	2.20	2.20
IHD₄₂						
	Mean	1.21	1.21	1.21	1.21	1.21
	Std	0.018	0.020	0.020	0.021	0.021
	Skewness	0.55	0.94	0.94	0.61	0.61
	kurtosis	2.50	1.96	1.96	2.12	2.12

Table 6.6: Predicted THD, IHD₃₈ and IHD₄₂ for 2 VSCs Using UDR

Current						
		MCS	3pts UDR	3pts rUDR	5pts UDR	5pts rUDR
THD	Mean	4.96	4.87	4.87	4.94	4.94
	Std	1.41	1.07	1.07	1.12	1.12
	Skewness	1.56	-0.011	-0.011	0.061	0.061
	kurtosis	6.09	1.05	1.05	1.35	1.35
	E_v	1000	7	5	11	9
	Time	21706s	334s	233s	520s	418s
IHD₃₈						
	Mean	3.73	3.70	3.70	3.70	3.70
	Std	1.05	0.88	0.88	0.88	0.88
	Skewness	1.54	0.011	0.011	0.049	0.049
	kurtosis	5.76	1.03	1.03	1.18	1.18
IHD₄₂						
	Mean	2.45	2.42	2.42	2.43	2.43
	Std	0.69	0.57	0.57	0.58	0.58
	Skewness	1.55	0.020	0.020	0.049	0.049
	kurtosis	5.78	1.04	1.04	1.16	1.16
Voltage						
		MCS	3pts UDR	3pts rUDR	5pts UDR	5pts rUDR
THD	Mean	3.32	3.32	3.32	3.33	3.33
	Std	0.029	0.022	0.022	0.031	0.031
	Skewness	0.139	0.012	0.012	-0.036	-0.036
	kurtosis	2.52	0.94	0.94	1.21	1.21
IHD₃₈						
	Mean	2.46	2.46	2.46	2.47	2.47
	Std	0.033	0.024	0.024	0.030	0.030
	Skewness	0.015	0.103	0.103	0.030	0.030
	kurtosis	2.57	1.18	1.18	1.06	1.06
IHD₄₂						
	Mean	1.79	1.78	1.78	1.79	1.79
	Std	0.024	0.022	0.022	0.023	0.023

	Skewness	0.22	0.09	0.09	-0.13	-0.13
	kurtosis	2.59	1.05	1.05	1.45	1.45

Table 6.7: Predicted THD, IHD₃₈ and IHD₄₂ for 3 VSCs Using UDR

Current						
		MCS	3pts UDR	3pts rUDR	5pts UDR	5pts rUDR
THD	Mean	3.67	3.83	3.83	3.73	3.73
	Std	0.69	0.72	0.72	0.69	0.69
	Skewness	1.01	-0.11	-0.11	0.17	0.17
	kurtosis	4.08	0.71	0.71	0.73	0.73
	E_v	1000	10	7	16	13
	Time	24133s	511s	364s	846s	681s
IHD₃₈						
	Mean	2.75	2.87	2.87	2.85	2.85
	Std	0.51	0.49	0.49	0.50	0.50
	Skewness	1.08	-0.24	-0.24	-0.16	-0.16
	kurtosis	4.31	0.70	0.70	0.70	0.70
IHD₄₂						
	Mean	1.83	1.89	1.89	1.89	1.89
	Std	0.33	0.33	0.33	0.33	0.33
	Skewness	1.08	-0.15	-0.15	-0.14	-0.14
	kurtosis	4.32	0.68	0.68	0.69	0.69
Voltage						
		MCS	3pts UDR	3pts rUDR	5pts UDR	5pts rUDR
THD	Mean	3.95	3.94	3.94	3.95	3.95
	Std	0.024	0.017	0.017	0.011	0.021
	Skewness	0.14	2.47	2.47	2.83	2.83
	kurtosis	4.01	13.32	13.32	16.72	16.72
IHD₃₈						
	Mean	2.93	2.92	2.92	2.90	2.90
	Std	0.029	0.028	0.028	0.016	0.016
	Skewness	-0.29	0.17	0.17	1.41	1.41
	kurtosis	3.27	1.04	1.04	9.68	9.68
IHD₄₂						
	Mean	2.15	2.13	2.13	2.14	2.14
	Std	0.025	0.018	0.018	0.019	0.019
	Skewness	-0.033	2.45	2.45	2.69	2.69
	kurtosis	3.33	7.08	7.08	7.69	7.69

Table 6.8: Predicted THD, IHD₃₈ and IHD₄₂ for 4 VSCs Using UDR

Current						
		MCS	3pts UDR	3pts rUDR	5pts UDR	5pts rUDR
THD	Mean	3.31	3.56	3.56	3.35	3.35
	Std	0.55	0.55	0.55	0.54	0.54
	Skewness	1.12	-0.66	-0.66	0.25	0.25
	kurtosis	4.30	0.96	0.96	0.69	0.69
	E_v	1000	13	9	21	17
	Time	25219s	743s	511s	1187s	977s
IHD₃₈	Mean	2.49	2.58	2.58	2.58	2.58
	Std	0.38	0.38	0.38	0.38	0.38
	Skewness	1.00	-0.30	-0.30	-0.33	-0.33
	kurtosis	4.25	0.58	0.58	1.74	1.74
	IHD₄₂	Mean	1.66	1.73	1.73	1.73
	Std	0.25	0.25	0.25	0.25	0.25
	Skewness	0.99	-0.35	-0.35	-0.41	-0.41
	kurtosis	4.21	0.61	0.61	0.69	0.69
Voltage						
		MCS	3pts UDR	3pts rUDR	5pts UDR	5pts rUDR
THD	Mean	4.35	4.33	4.33	4.33	4.33
	Std	0.024	0.020	0.020	0.025	0.025
	Skewness	0.96	0.89	0.89	2.12	2.12
	kurtosis	4.38	1.98	1.98	4.95	4.95
IHD₃₈	Mean	3.22	3.21	3.21	3.22	3.22
	Std	0.029	0.023	0.023	0.027	0.027
	Skewness	0.43	-0.32	-0.32	-0.43	-0.43
	kurtosis	3.65	0.95	0.95	0.76	0.76
IHD₄₂	Mean	2.38	2.38	2.38	2.39	2.39
	Std	0.026	0.023	0.023	0.025	0.025
	Skewness	0.21	0.25	0.25	-0.92	-0.92
	kurtosis	3.49	1.01	1.01	1.18	1.18

Table 6.9: Predicted THD, IHD₃₈ and IHD₄₂ for 5 VSCs Using UDR

Current						
		MCS	3pts UDR	3pts rUDR	5pts UDR	5pts rUDR
THD	Mean	2.93	2.97	2.97	3.01	3.01
	Std	0.34	0.36	0.36	0.34	0.34
	Skewness	0.68	0.13	0.13	-0.18	-0.18
	kurtosis	3.88	0.46	0.46	0.53	0.53

	E_v	1000	16	11	26	21
	Time	28142s	1015s	676s	1592s	1284s
IHD₃₈	Mean	2.18	2.24	2.24	2.25	2.25
	Std	0.27	0.26	0.26	0.27	0.27
	Skewness	0.53	-0.40	-0.40	-0.48	-0.48
	kurtosis	3.18	0.55	0.55	0.61	0.61
IHD₄₂	Mean	1.47	1.51	1.51	1.52	1.52
	Std	0.18	0.17	0.17	0.18	0.18
	Skewness	0.52	-0.41	-0.41	-0.53	-0.53
	kurtosis	3.14	0.58	0.58	0.67	0.67
Voltage						
		MCS	3pts UDR	3pts rUDR	5pts UDR	5pts rUDR
THD	Mean	4.64	4.65	4.65	4.66	4.66
	Std	0.032	0.026	0.026	0.024	0.024
	Skewness	0.53	-0.99	-0.99	-1.62	-1.62
	kurtosis	2.34	1.26	1.26	3.33	3.33
IHD₃₈	Mean	3.44	3.45	3.45	3.45	3.45
	Std	0.037	0.036	0.036	0.034	0.034
	Skewness	0.44	-1.13	-1.13	-1.34	-1.34
	kurtosis	2.29	1.50	1.50	2.37	2.37
IHD₄₂	Mean	2.56	2.56	2.56	2.57	2.57
	Std	0.031	0.028	0.028	0.020	0.020
	Skewness	0.44	-1.11	-1.11	-2.25	-2.25
	kurtosis	2.52	1.56	1.56	5.03	5.03

The results presented in Table 6.5 - Table 6.9 show that the UDR and the rUDR technique predicts the same values for the moments of the VSCs harmonics. This is because the output power has a uniform random variation making it a symmetrical random variable. For this reason, only the rUDR results will be presented in the following analysis as it utilizes a reduced number of evaluation and hence reduced computational time in achieving this.

It is also clear from Table 6.5 - Table 6.9 that the UDR techniques gives a large percentage error in predicting the skewness and kurtosis of the harmonic distortion pdfs hence only the mean and the standard deviation results will be presented in the following analysis.

Table 6.10: Predicted THD, IHD₃₈ and IHD₄₂ for 6 VSCs Using UDR

Current				
		MCS	3pts rUDR	5pts rUDR
THD	Mean	2.60	2.70	2.83
	Std	0.28	0.35	0.31
	E_v	1000	13	25
	Time	34579s	906s	1699s
IHD₃₈				
	Mean	1.91	1.98	1.99
	Std	0.20	0.19	0.19
IHD₄₂				
	Mean	1.29	1.34	1.35
	Std	0.13	0.12	0.12
Voltage				
		MCS	3pts rUDR	5pts rUDR
THD	Mean	4.89	4.88	4.91
	Std	0.030	0.030	0.029
IHD₃₈				
	Mean	3.64	3.64	3.63
	Std	0.036	0.038	0.036
IHD₄₂				
	Mean	2.72	2.71	2.72
	Std	0.031	0.041	0.041

Table 6.11: Predicted THD, IHD₃₈ and IHD₄₂ for 7 VSCs Using UDR

Current				
		MCS	3pts rUDR	5pts rUDR
THD	Mean	2.46	2.63	2.73
	Std	0.27	0.21	0.17
	E_v	1000	22	29
	Time	40280s	1371s	2185s
IHD₃₈				
	Mean	1.81	1.86	1.88
	Std	0.17	0.17	0.17
IHD₄₂				
	Mean	1.23	1.29	1.31
	Std	0.12	0.10	0.09
Voltage				
		MCS	3pts rUDR	5pts rUDR
THD	Mean	5.05	5.05	5.05
	Std	0.023	0.016	0.020

IHD₃₈	Mean	3.77	3.75	3.76
	Std	0.028	0.037	0.030
IHD₄₂	Mean	2.83	2.86	2.88
	Std	0.028	0.022	0.025

Table 6.12: Predicted THD, IHD₃₈ and IHD₄₂ for 8 VSCs Using UDR

Current				
		MCS	3pts rUDR	5pts rUDR
THD	Mean	2.31	2.39	2.39
	Std	0.26	0.19	0.22
	E_v	1000	17	33
	Time	49139s	1541s	3008s
IHD₃₈	Mean	1.70	1.73	1.74
	Std	0.16	0.16	0.15
IHD₄₂	Mean	1.16	1.21	1.22
	Std	0.11	0.093	0.082
Voltage				
		MCS	3pts rUDR	5pts rUDR
THD	Mean	5.19	5.11	5.10
	Std	0.020	0.015	0.015
IHD₃₈	Mean	3.87	3.81	3.79
	Std	0.026	0.020	0.027
IHD₄₂	Mean	2.91	2.91	2.90
	Std	0.027	0.024	0.028

Table 6. 13: Predicted THD, IHD₃₈ and IHD₄₂ for 9 VSCs Using UDR

Current				
		MCS	3pts rUDR	5pts rUDR
THD	Mean	2.14	2.11	2.12
	Std	0.21	0.23	0.23
	E_v	1000	19	37
	Time	61269s	1313s	2497s
IHD₃₈	Mean	1.59	1.62	1.62
	Std	0.14	0.14	0.13
IHD₄₂	Mean	1.09	1.10	1.10

	Std	0.091	0.092	0.094
Voltage				
		MCS	3pts rUDR	5pts rUDR
THD	Mean	5.30	5.33	5.33
	Std	0.027	0.024	0.018
IHD₃₈	Mean	3.96	3.99	3.99
	Std	0.034	0.034	0.025
IHD₄₂	Mean	2.99	2.99	2.98
	Std	0.031	0.029	0.021

Table 6.14: Predicted THD, IHD₃₈ and IHD₄₂ for 10 VSCs Using UDR

Current				
		MCS	3pts rUDR	5pts rUDR
THD	Mean	1.96	2.05	2.06
	Std	0.16	0.19	0.20
	E_v	1000	21	41
	Time	63284s	1651s	3321s
IHD₃₈	Mean	1.46	1.48	1.48
	Std	0.11	0.10	0.098
IHD₄₂	Mean	1.00	1.02	1.01
	Std	0.072	0.070	0.067
Voltage				
		MCS	3pts rUDR	5pts rUDR
THD	Mean	5.41	5.42	5.42
	Std	0.030	0.043	0.047
IHD₃₈	Mean	4.06	4.07	4.08
	Std	0.039	0.043	0.043
IHD₄₂	Mean	3.08	3.08	3.08
	Std	0.035	0.035	0.038

Table 6.5 - Table 6.14 presented the actual values of the current and voltage harmonic distortion level, including the number of evaluations and computational time required for each evaluation. It can be seen from the tables that the UDR predicted harmonic mean and standard deviation values has a close

agreement with the results obtained using the MCS approach. Fig. 6.2-Fig. 6.10 gives a clearer presentation for analysing these results.

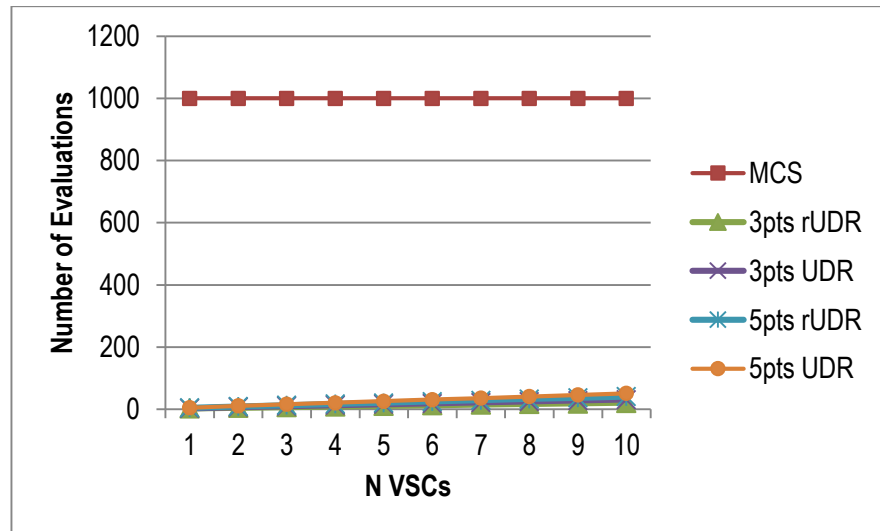


Fig. 6.2: Number of Evaluations Required for the Harmonic Prediction Methods

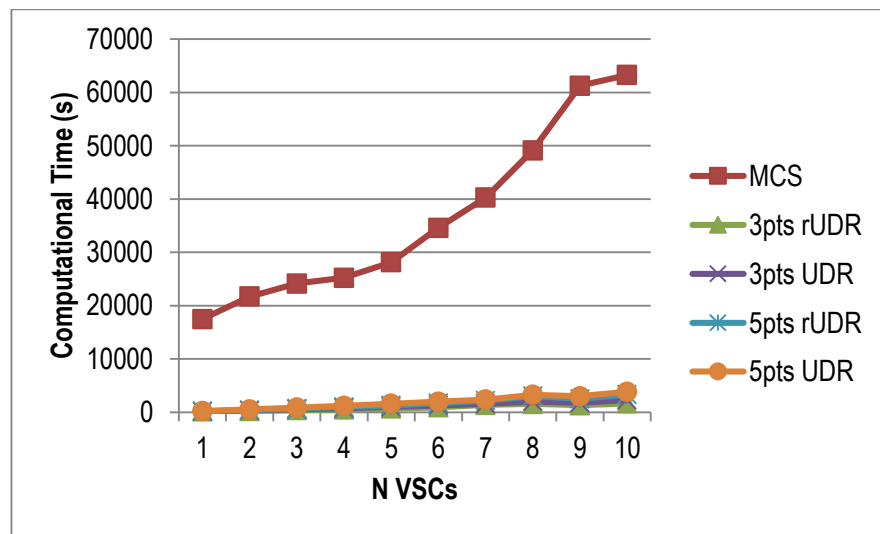


Fig. 6.3: Computation Time Required for the Harmonic Prediction Methods

Table 6.15: Significant Computation Time Saved Using UDR as compared to the MCS Technique for Harmonic Prediction

N VSCs	3pts rUDR (%)	3pts UDR (%)	5pts rUDR (%)	5pts UDR (%)
1	99.28	99.28	98.83	98.83
2	98.93	98.46	98.07	97.60
3	98.49	97.68	97.18	96.49
4	97.97	97.05	96.13	95.29

5	97.60	96.39	95.44	94.34
6	97.38	96.30	95.09	94.26
7	96.60	96.09	94.58	94.17
8	96.86	95.94	93.88	93.34
9	97.86	97.14	95.92	95.11
10	97.39	96.35	94.75	93.94

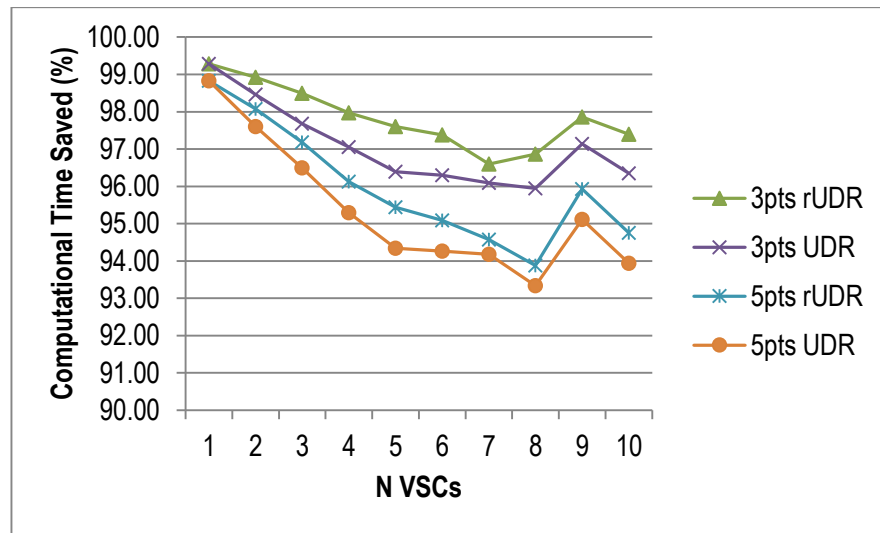


Fig. 6.4: Computation Time Saved Using UDR as compared to the MCS Technique for Harmonic Prediction

It can be deduced from Fig 6.1 that the implementation of the UDR technique requires a few number of evaluation points as compared to the MCS approach. The Ev of the MCS approach remains the same for all numbers of VSCs but the UDR technique increases as the number of variables increase. Notwithstanding, implementing the UDR in predicting the harmonics of 10 VSCs still requires far less amount of Ev (UDR = 51 evaluation points) as compared to the MCS (1000 evaluation points).

Fig 6.3 gives a clear picture of the computation time saved based on the reduced number of evaluation required for implementing the UDR technique. At the case with the highest number of variables (10 VSCs) the UDR technique was still able to save more than 90% computation time when compared to the time required by the MCS approach. The UDR technique drastically reduced the computation time required in predicting the harmonic distortion level of the VSCs and produces results that are in close agreement with the MCS approach.

The performance of the UDR technique in predicting both current and voltage harmonic distortion level is illustrated in Fig. 6.5 - Fig. 6.10.

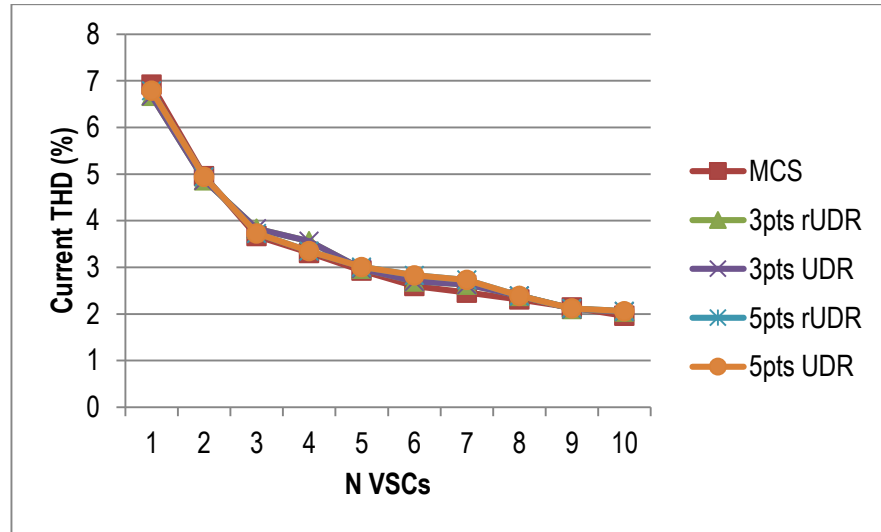


Fig. 6.5: UDR Predicted I_{THD} for 10 VSCs

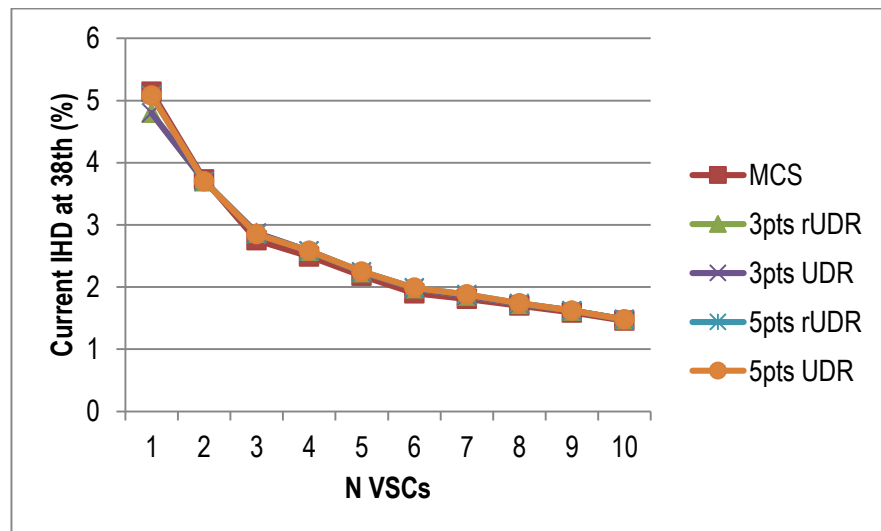


Fig. 6.6: UDR Predicted I_{HD} at the 38th Harmonic Order for 10 VSCs

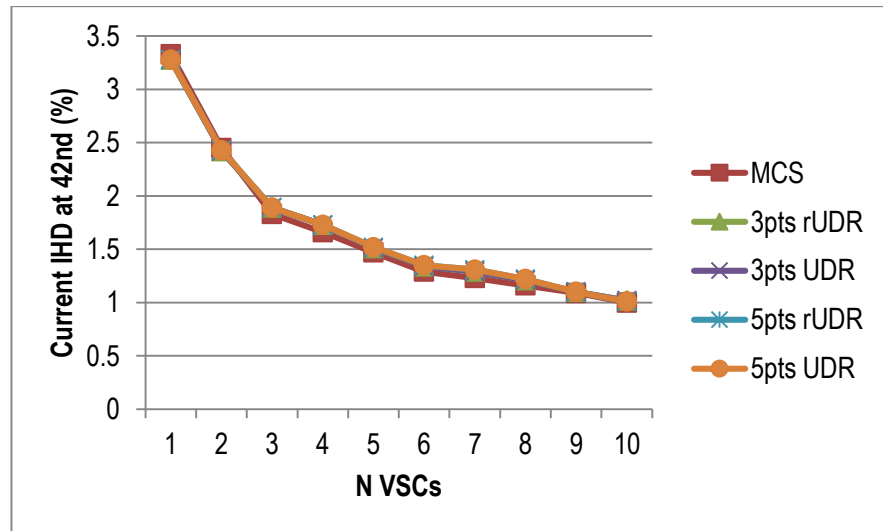


Fig. 6.7: UDR Predicted I_{IHD} at the 42nd Harmonic Order for 10 VSCs

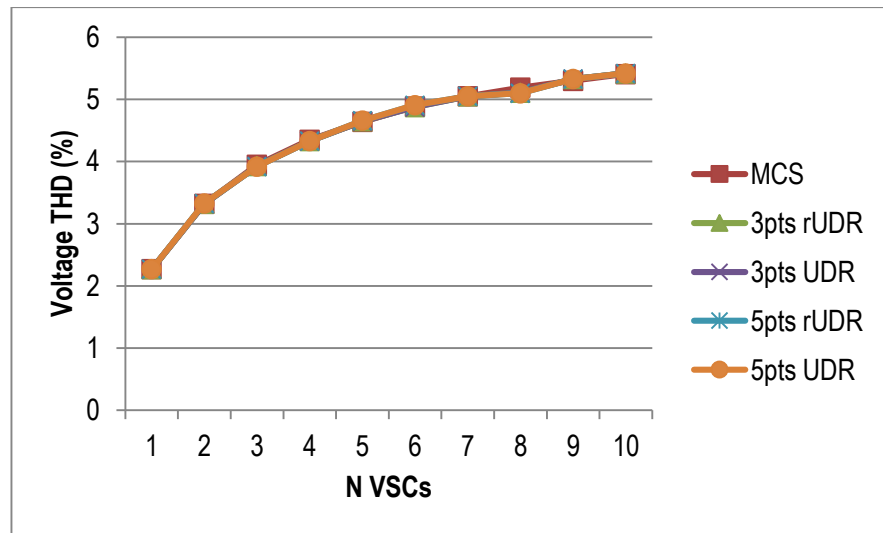


Fig. 6.8: UDR Predicted V_{THD} for 10 VSCs

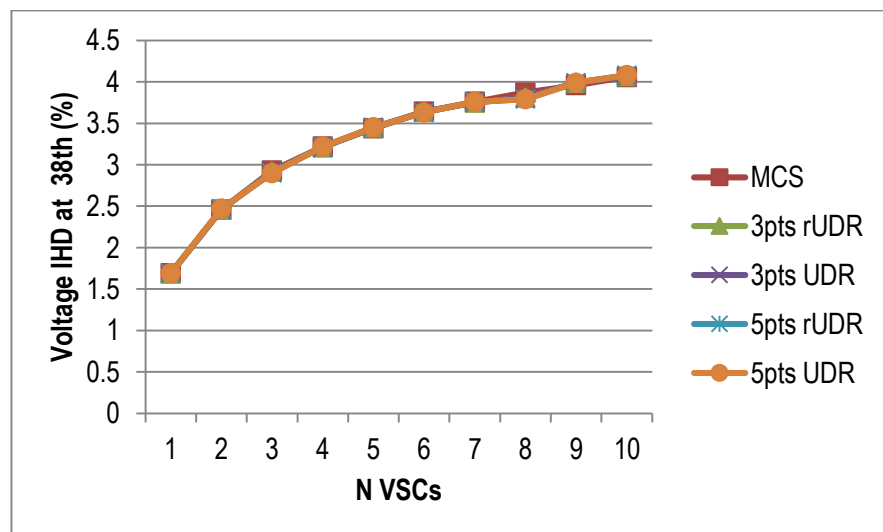


Fig. 6.9: UDR Predicted V_{IHD} at the 38th Harmonic Order for 10 VSCs

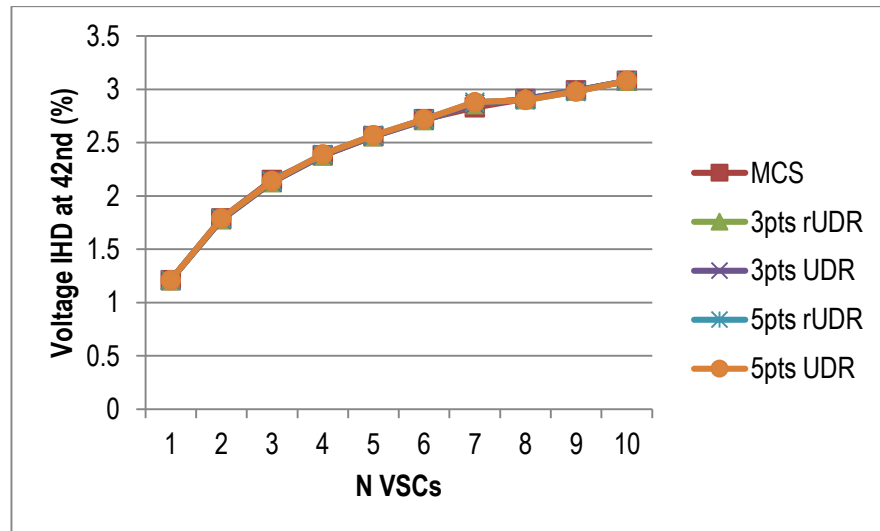


Fig. 6.10: UDR Predicted V_{IHD} at the 42nd Harmonic Order for 10 VSCs

From Fig. 6.5 it is clear that there are slight over prediction and/or under prediction of the I_{THD} however, in all cases the percentage error was not more than 10%. This also applies to the I_{IHD} at the 38th and 42nd harmonic order which are the side bands of the switching frequency. The UDR prediction of the V_{THD} and the V_{IHD} at the 38th and 42nd harmonic order have a closer agreement with MCS approach with a percentage error of less than 2%. The UDR results will be further analysed after the introduction of the BDR (3 and 5 point approximation) predicted harmonic distortion levels.

From the results, it can be seen that the 3pts UDR and 3pts rUDR have the same values of moments in all cases, similarly the 5pts UDR and 5pts rUDR produces the same values. Notwithstanding, the 3pts UDR and rUDR requires less number of evaluation and computation time to achieve these results as compared to the 5pts UDR and rUDR respectively. As the number of approximation points increases from 3pts to 5pts a better accuracy is obtained at the expense of computation time.

6.4.2 Predicting Harmonics of N VSCs Using the BDR

The rBDR was applied in this case as this saves more computation time and produces the same level of accuracy as the BDR for a symmetrical random variable. The rBDR was implemented using the 3 and 5 point approximations and the predicted results were compared with that of the rUDR and the MCS approach.

Table 6.16: Predicted THD, IHD₃₈ and IHD₄₂ for 2VSCs Using BDR

Current						
		MCS	3pts rUDR	3pts rBDR	5pts rUDR	5pts rBDR
THD	Mean	4.96	4.87	4.93	4.94	4.96
	Std	1.41	1.07	1.38	1.12	1.39
	Skewness	1.59	-0.011	1.38	0.061	1.32
	kurtosis	6.09	1.05	4.73	1.35	4.87
	Ev	1000	5	9	9	25
	Time	21706s	233s	473s	418s	1329s
IHD₃₈						
IHD₃₈	Mean	3.73	3.70	3.74	3.70	3.73
	Std	1.05	0.88	1.05	0.88	1.04
	Skewness	1.54	0.011	1.25	0.049	1.33
	kurtosis	5.76	1.03	4.19	1.18	4.90
IHD₄₂						
IHD₄₂	Mean	2.45	2.42	2.45	2.43	2.45
	Std	0.69	0.57	0.67	0.58	0.68
	Skewness	1.55	0.020	1.23	0.049	1.35
	kurtosis	5.78	1.04	4.15	1.16	4.97
Voltage						
		MCS	3pts rUDR	3pts rBDR	5pts rUDR	5pts rBDR
THD	Mean	3.32	3.32	3.32	3.33	3.32
	Std	0.029	0.022	0.024	0.031	0.029
	Skewness	0.14	0.012	0.93	-0.036	0.35
	kurtosis	2.52	0.94	3.28	1.21	2.28
IHD₃₈						
IHD₃₈	Mean	2.46	2.46	2.46	2.47	2.46
	Std	0.033	0.024	0.027	0.030	0.031
	Skewness	0.015	0.103	0.91	0.030	0.31
	kurtosis	2.57	1.18	3.20	1.06	2.68
IHD₄₂						
IHD₄₂	Mean	1.79	1.78	1.78	1.79	1.79
	Std	0.024	0.022	0.024	0.023	0.024
	Skewness	0.22	0.092	0.48	-0.13	0.30
	kurtosis	2.59	1.05	2.84	1.45	2.38

Table 6.17: Predicted THD, IHD₃₈ and IHD₄₂ for 3 VSCs Using BDR

Current						
		MCS	3pts rUDR	3pts rBDR	5pts rUDR	5pts rBDR
THD	Mean	3.67	3.83	3.81	3.73	3.73
	Std	0.69	0.72	0.72	0.69	0.69
	Skewness	1.01	-0.11	0.743	0.17	0.76

	kurtosis	4.08	0.71	2.75	0.73	2.87
	Ev	1000	7	19	13	61
	Time	24133s	364s	1052s	681s	3695s
IHD₃₈						
	Mean	2.75	2.87	2.87	2.85	2.87
	Std	0.51	0.49	0.55	0.50	0.55
	Skewness	1.08	-0.24	0.85	-0.16	0.81
	kurtosis	4.31	0.70	2.73	0.70	2.76
IHD₄₂						
	Mean	1.83	1.89	1.91	1.89	1.90
	Std	0.33	0.33	0.36	0.33	0.36
	Skewness	1.08	-0.15	0.86	-0.14	0.85
	kurtosis	4.32	0.68	2.75	0.69	2.86
Voltage						
		MCS	3pts rUDR	3pts rBDR	5pts rUDR	5pts rBDR
THD	Mean	3.95	3.94	3.95	3.95	3.95
	Std	0.024	0.017	0.029	0.011	0.031
	Skewness	0.141	2.47	-0.47	2.83	-0.36
	kurtosis	4.008	13.32	2.07	16.72	1.86
IHD₃₈						
	Mean	2.93	2.92	2.92	2.90	2.93
	Std	0.029	0.028	0.031	0.016	0.032
	Skewness	-0.29	0.17	-0.59	1.41	-1.21
	kurtosis	3.27	1.04	2.60	9.68	3.77
IHD₄₂						
	Mean	2.15	2.13	2.15	2.14	2.15
	Std	0.025	0.018	0.029	0.019	0.027
	Skewness	-0.033	2.45	-0.39	2.69	-0.52
	kurtosis	3.33	7.08	2.47	7.69	2.16

Table 6.18: Predicted THD, IHD₃₈ and IHD₄₂ for 4 VSCs Using BDR

Current						
		MCS	3pts rUDR	3pts rBDR	5pts rUDR	5pts rBDR
THD	Mean	3.31	3.56	3.40	3.35	3.54
	Std	0.55	0.55	0.62	0.54	0.62
	Skewness	1.12	-0.66	1.14	0.25	0.51
	kurtosis	4.30	0.96	2.82	0.69	1.91
	Ev	1000	9	33	17	113
	Time	24219s	511s	2229s	977s	7584s
IHD₃₈						
	Mean	2.49	2.58	2.58	2.58	2.57
	Std	0.38	0.38	0.42	0.38	0.42
	Skewness	1.00	-0.30	0.789	-0.33	0.83

	kurtosis	4.25	0.58	2.47	1.74	2.48
IHD₄₂	Mean	1.66	1.73	1.72	1.73	1.71
	Std	0.25	0.25	0.28	0.25	0.28
	Skewness	0.99	-0.35	0.75	-0.41	0.89
	kurtosis	4.21	0.61	2.40	0.69	2.65
Voltage						
		MCS	3pts rUDR	3pts rBDR	5pts rUDR	5pts rBDR
THD	Mean	4.35	4.33	4.35	4.33	4.35
	Std	0.024	0.020	0.018	0.025	0.006
	Skewness	0.96	0.89	1.26	2.12	-13.74
	kurtosis	4.38	1.98	2.34	4.95	24.82
IHD₃₈	Mean	3.22	3.21	3.22	3.22	3.21
	Std	0.029	0.023	0.034	0.027	0.025
	Skewness	0.43	-0.32	0.080	-0.43	1.02
	kurtosis	3.65	0.95	1.82	0.76	4.85
IHD₄₂	Mean	2.38	2.38	2.38	2.39	2.36
	Std	0.026	0.023	0.025	0.025	0.017
	Skewness	0.21	0.25	0.036	-0.92	1.58
	kurtosis	3.49	1.00	2.65	1.18	13.26

Table 6.19: Predicted THD, IHD₃₈ and IHD₄₂ for 5 VSCs Using BDR

Current						
		MCS	3pts rUDR	3pts rBDR	5pts rUDR	5pts rBDR
THD	Mean	2.93	2.97	3.03	3.01	2.95
	Std	0.34	0.36	0.31	0.34	0.41
	Skewness	0.68	0.13	1.30	-0.18	0.96
	kurtosis	3.88	0.46	3.36	0.53	2.29
	Ev	1000	11	51	21	181
	Time	28142s	676s	3282s	1284s	11743s
IHD₃₈	Mean	2.18	2.24	2.23	2.25	2.21
	Std	0.27	0.26	0.30	0.27	0.29
	Skewness	0.53	-0.40	0.65	-0.48	0.92
	kurtosis	3.18	0.55	2.17	0.61	2.58
IHD₄₂	Mean	1.47	1.51	1.50	1.52	1.49
	Std	0.178	0.17	0.20	0.18	0.20
	Skewness	0.52	-0.41	0.68	-0.53	0.96
	kurtosis	3.14	0.58	2.16	0.67	2.57

Voltage						
		MCS	3pts rUDR	3pts rBDR	5pts rUDR	5pts rBDR
THD	Mean	4.64	4.65	4.63	4.66	4.62
	Std	0.032	0.026	0.039	0.024	0.032
	Skewness	0.53	-0.99	1.58	-1.62	3.02
	kurtosis	2.34	1.26	3.32	3.33	8.16
IHD₃₈	Mean	3.44	3.45	3.43	3.45	3.42
	Std	0.037	0.036	0.039	0.034	0.035
	Skewness	0.44	-1.13	0.98	-1.34	2.01
	kurtosis	2.29	1.50	3.81	2.37	5.22
IHD₄₂	Mean	2.56	2.56	2.55	2.57	2.56
	Std	0.031	0.028	0.032	0.020	0.037
	Skewness	0.44	-1.11	1.50	-2.25	0.63
	kurtosis	2.52	1.56	3.23	5.03	1.05

Table 6.20: Predicted THD, IHD₃₈ and IHD₄₂ for 6 VSCs Using BDR

Current						
		MCS	3pts rUDR	3pts rBDR	5pts rUDR	5pts rBDR
THD	Mean	2.60	2.70	2.53	2.83	2.66
	Std	0.28	0.35	0.063	0.31	0.21
	Skewness	0.36	-0.072	-100.19	-1.40	-2.30
	kurtosis	3.01	0.48	-116.22	1.92	-3.94
	Ev	1000	13	73	25	265
	Time	34579s	906s	5924	1699s	20803
IHD₃₈	Mean	1.91	1.98	1.90	1.99	1.89
	Std	0.20	0.19	0.21	0.19	0.19
	Skewness	0.65	-0.88	1.17	-1.00	1.65
	kurtosis	3.52	0.96	3.17	1.11	4.65
IHD₄₂	Mean	1.29	1.34	1.29	1.36	1.26
	Std	0.13	0.12	0.14	0.12	0.13
	Skewness	0.67	-0.89	1.03	-1.25	2.02
	kurtosis	3.55	0.99	2.67	1.55	5.35
Voltage						
		MCS	3pts rUDR	3pts rBDR	5pts rUDR	5pts rBDR
THD	Mean	4.89	4.88	4.87	4.91	4.88
	Std	0.030	0.030	0.042	0.029	0.028
	Skewness	-0.68	-0.21	0.35	-2.02	-3.57
	kurtosis	3.09	0.56	1.68	4.05	2.85

IHD₃₈	Mean	3.64	3.64	3.60	3.63	3.64
	Std	0.036	0.038	0.036	0.036	0.059
	Skewness	-0.60	-1.03	0.89	-0.38	-0.62
	kurtosis	2.82	1.29	4.37	0.59	1.21
IHD₄₂	Mean	2.72	2.71	2.71	2.72	2.69
	Std	0.031	0.041	0.025	0.041	0.005
	Skewness	-0.45	0.014	-1.47	-0.60	-0.002
	kurtosis	2.68	0.36	10.08	0.66	21.61

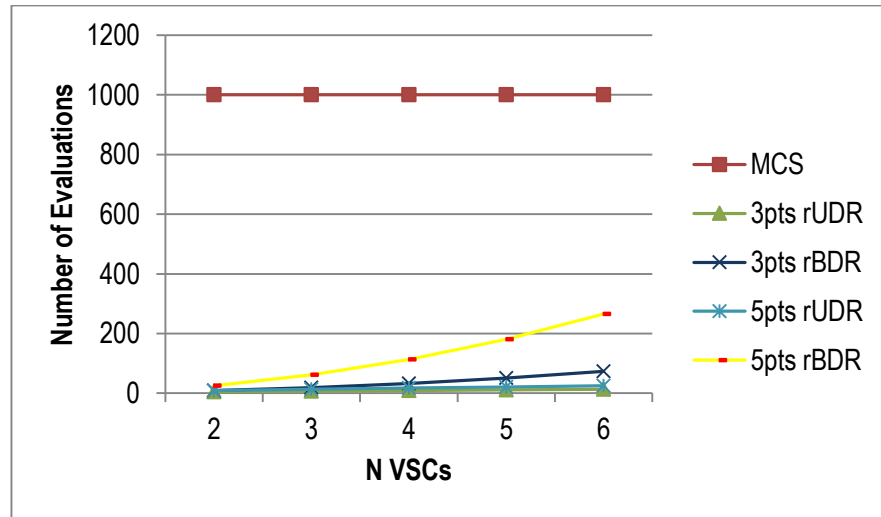


Fig. 6.11: Number of Evaluation Points Required for the Harmonic Prediction Methods

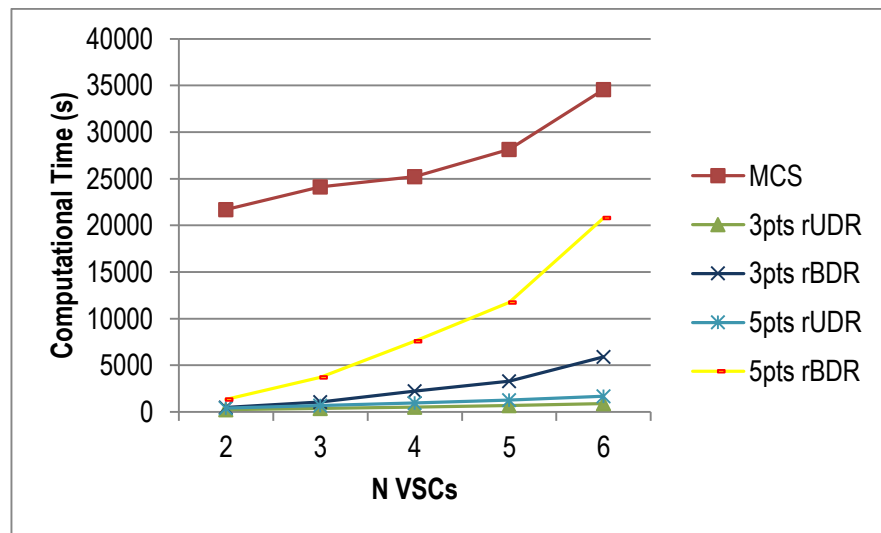


Fig. 6.12: Computation Time Required for the Harmonic Prediction Methods

Table 6.21: Computation Time Saved Using UDR as compared to the MCS Technique for Harmonic Prediction

N VSCs	3pts rUDR (%)	3pts rBDR (%)	5pts rUDR (%)	5pts rBDR (%)
2	98.93	97.82	98.07	93.88
3	98.49	95.64	97.18	84.69
4	97.97	91.16	96.13	69.93
5	97.60	88.34	95.44	58.27
6	97.38	82.87	95.09	39.84

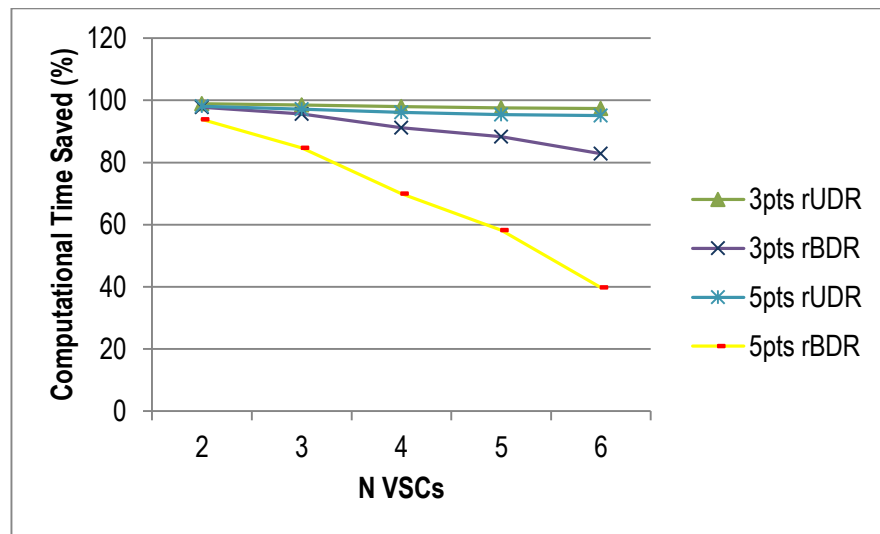
**Fig. 6.13: Computation Time Saved Using DR as compared to the MCS Technique for Harmonic Prediction**

Fig. 6.11 gives a clearer representation of the number of evaluation points required to implement the reduced BDR and reduced UDR 3 points and 5 points approximation as compared to the MCS approach. The Ev for the rBDR and the rUDR technique increases as the number of variables increase. However, the rBDR requires more evaluation points as compared to the rUDR. For a case of 6 VSCs the rBDR (5 points approximation) requires 265 evaluation points while the rUDR requires just 25 points. Since the main advantage of implementing the dimension reduction techniques in predicting harmonics is to save computation time, it was pointless to continue using the rBDR for higher number of VSCs.

As can be seen from Fig. 6.13 the rBDR (5 point approximation) for 6 VSCs was only able to save 40% of computation time with respect to the MCS approach, while the rUDR was able to save 95% of computation time.

The rBDR and rUDR technique reduces the computation time required in predicting the harmonic distortion level of the VSCs and produces results that are in close agreement with the MCS approach. The performance of both techniques in predicting current and voltage harmonic distortion level is presented below in Fig. 6.14 - Fig. 6.19.

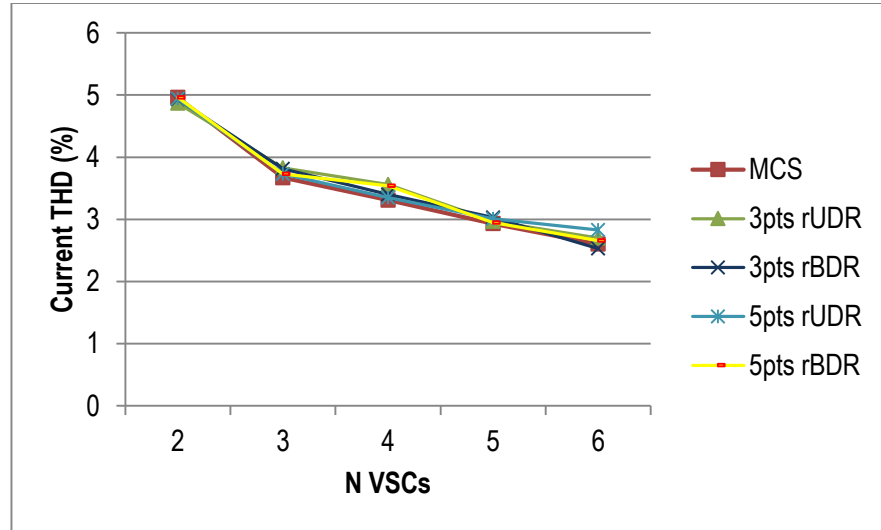


Fig. 6.14: UDR/BDR Predicted I_{THD} for 6 VSCs

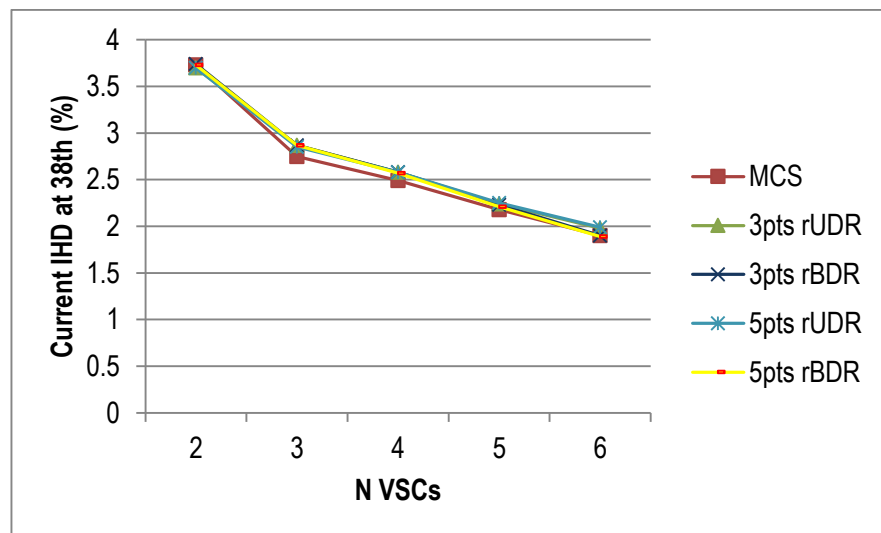


Fig. 6.15: UDR/BDR Predicted I_{IHD_38} for 6 VSCs

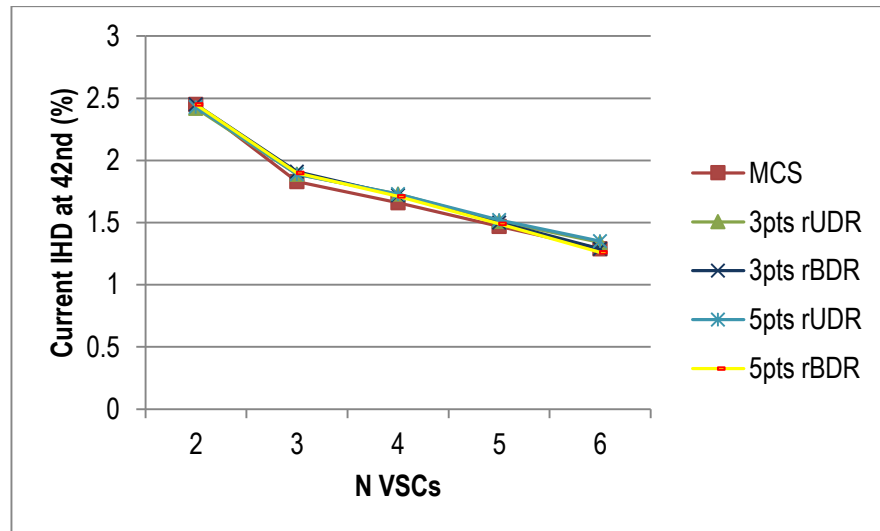


Fig. 6.16: UDR/BDR Predicted I_{IHD_42} for 6 VSCs

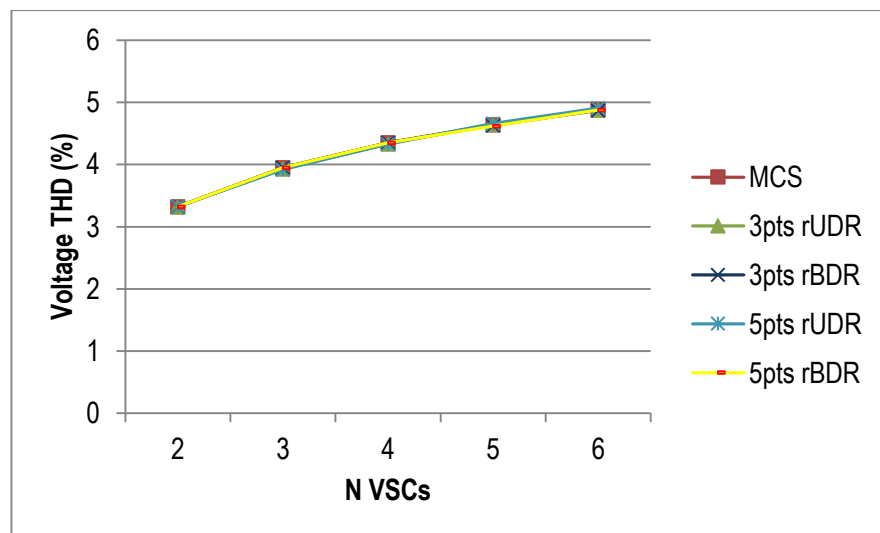


Fig. 6.17: UDR/BDR Predicted V_{THD} for 6 VSCs

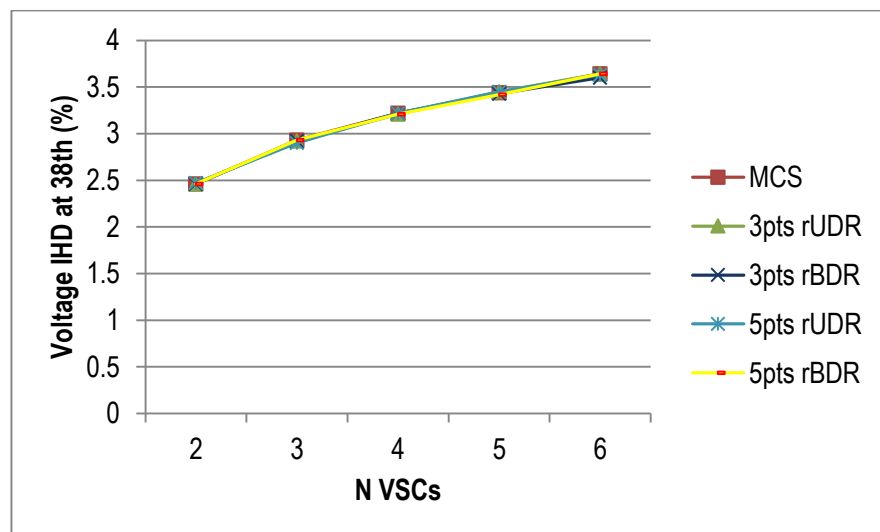


Fig. 6.18: UDR/BDR Predicted V_{IHD_38} for 6 VSCs

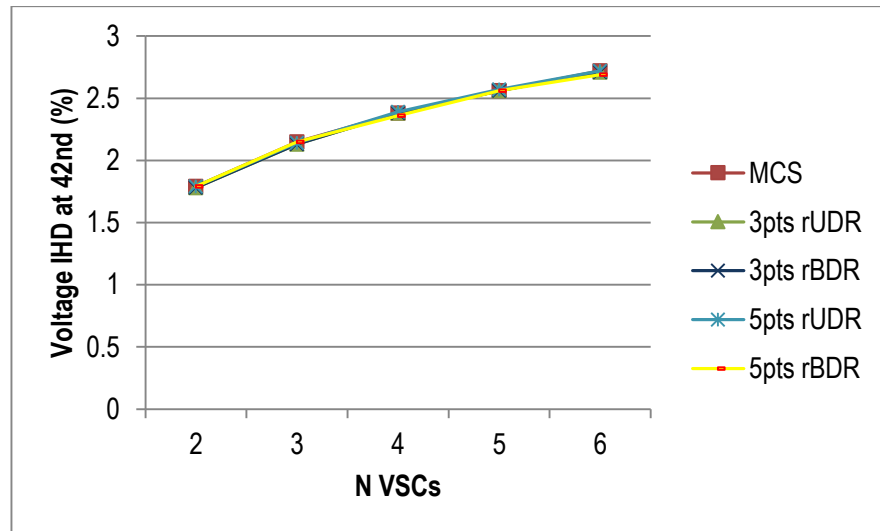


Fig. 6.19: UDR/BDR Predicted $V_{IHD_{42}}$ for 6 VSCs

The chart lines presented in Fig. 6.14 - Fig. 6.16 shows some over prediction and/or under prediction of the I_{THD} and I_{IHD} at the 38th and 42nd harmonic order. The lines do not exactly follow the result of the MCS approach. In general, the rBDR has more accurate predictions of the I_{THD} and I_{IHD} mean values as compared to the rUDR.

Fig. 6.17 - Fig. 6.19 however illustrates that both the rBDR and rUDR techniques gave accurate prediction of the V_{THD} and V_{IHD} at the 38th and 42nd harmonic order. This appears so as most of the chart lines representing each dimension reduction technique used overlaps the MCS approach chart lines.

Fig. 6.20 - Fig. 6.31 gives the skewness and kurtosis of the current and voltage THD/IHD using the UDR and BDR techniques in comparison to the MCS approach. It can be seen that the I_{THD} and I_{IHD} skewness and kurtosis for the 3pts and 5pts BDR gave a better prediction than the 3pts and 5pts UDR. However, the voltage V_{THD} and V_{IHD} skewness and kurtosis appears to be very random predictions for both the UDR and BDR.

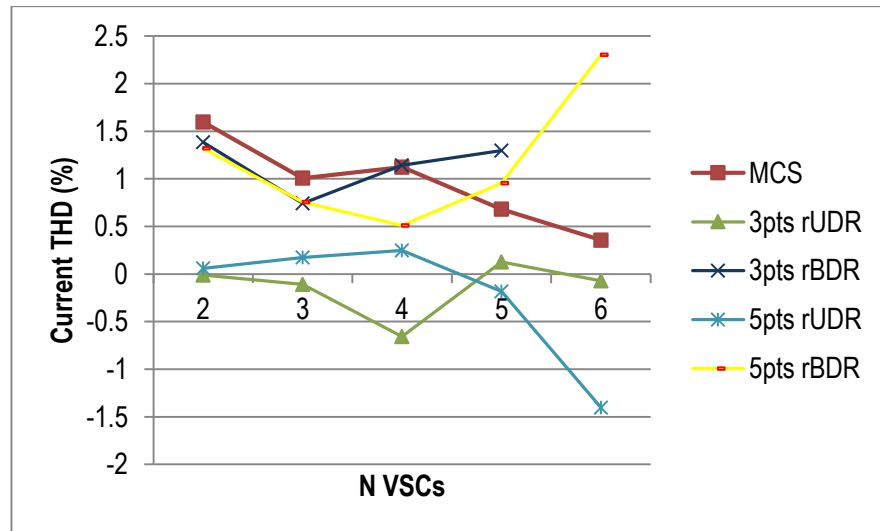


Fig. 6.20 UDR/BDR Predicted Skewness of I_{THD} for 6 VSCs

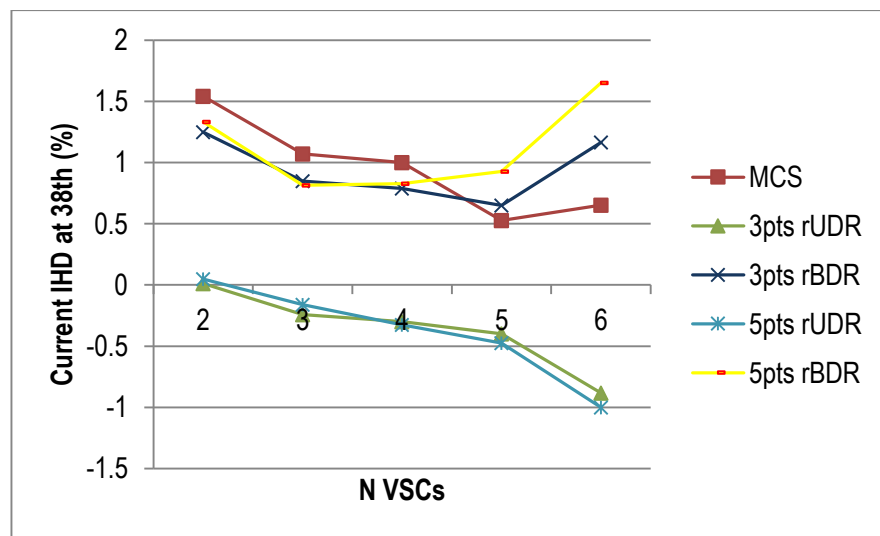


Fig. 6.21 UDR/BDR Predicted Skewness of I_{IHD_38} for 6 VSCs

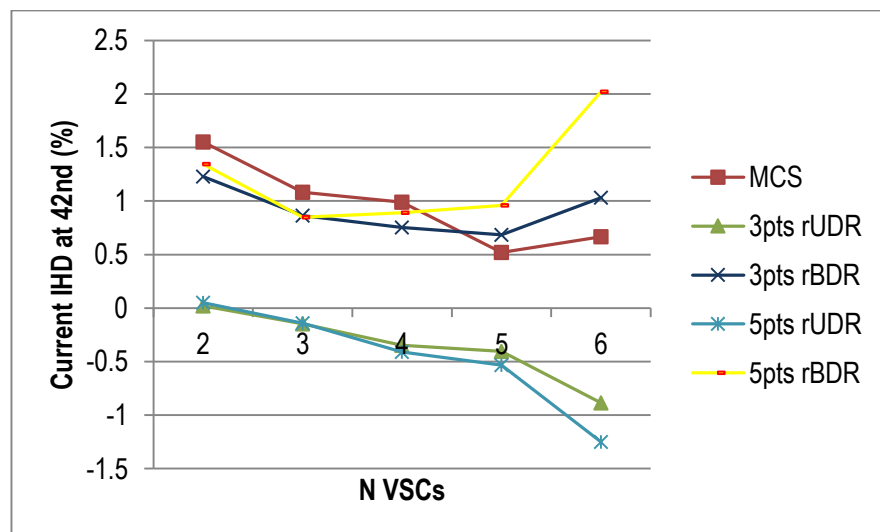


Fig. 6.22 UDR/BDR Predicted Skewness of I_{IHD_42} for 6 VSCs

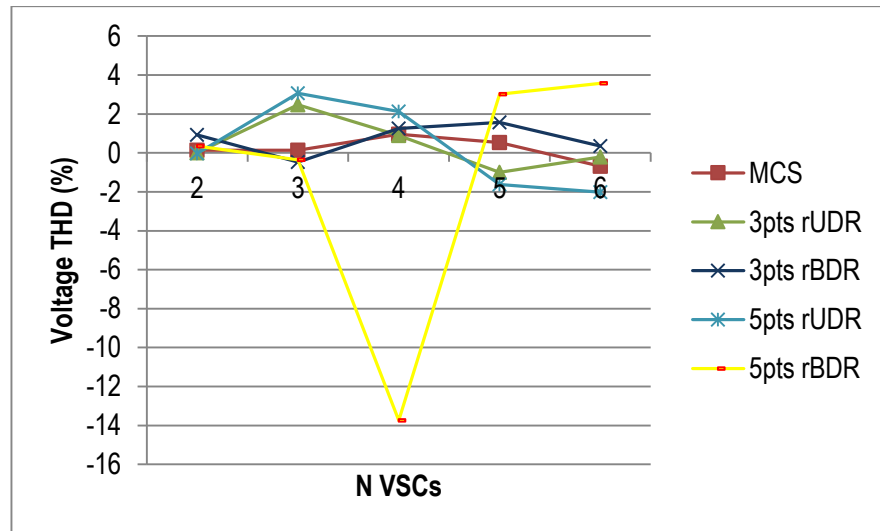


Fig. 6.23 UDR/BDR Predicted Skewness of V_{THD} for 6 VSCs

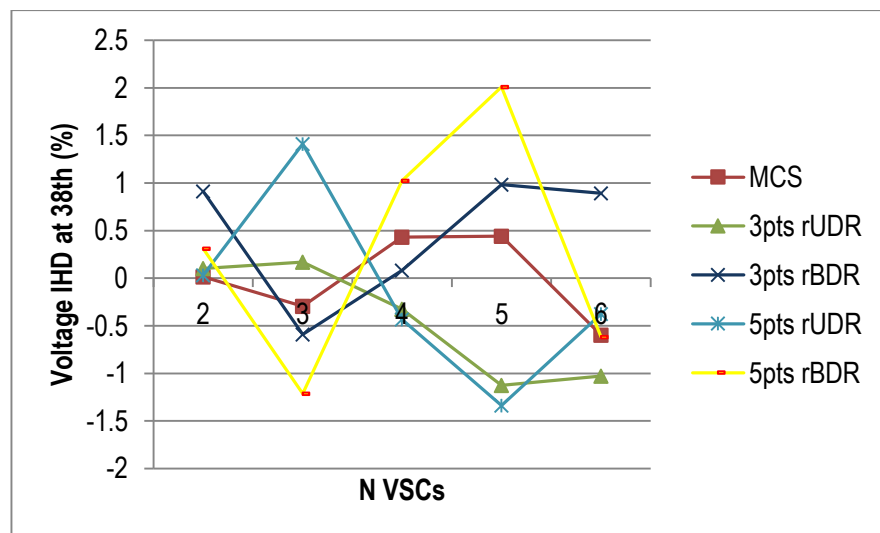


Fig. 6.24 UDR/BDR Predicted Skewness of V_{IHD_38} for 6 VSCs

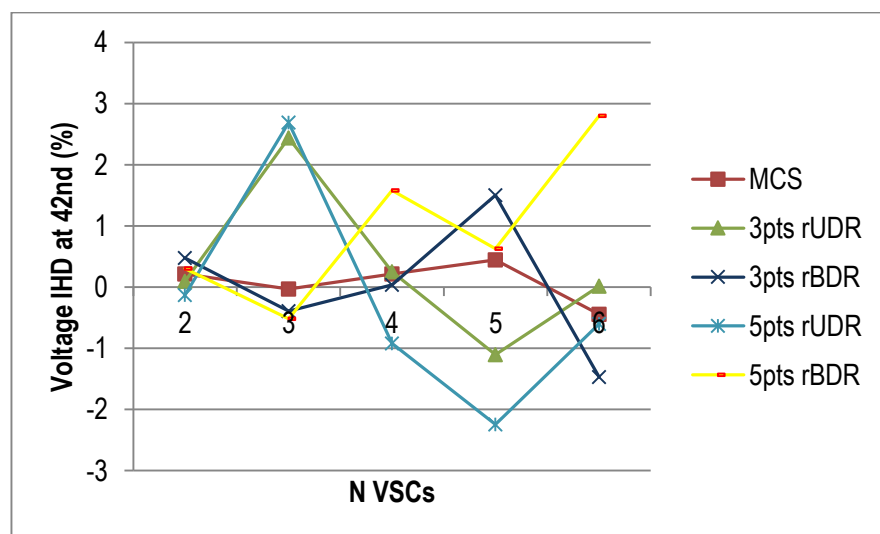


Fig. 6.25 UDR/BDR Predicted Skewness of V_{IHD_42} for 6 VSCs

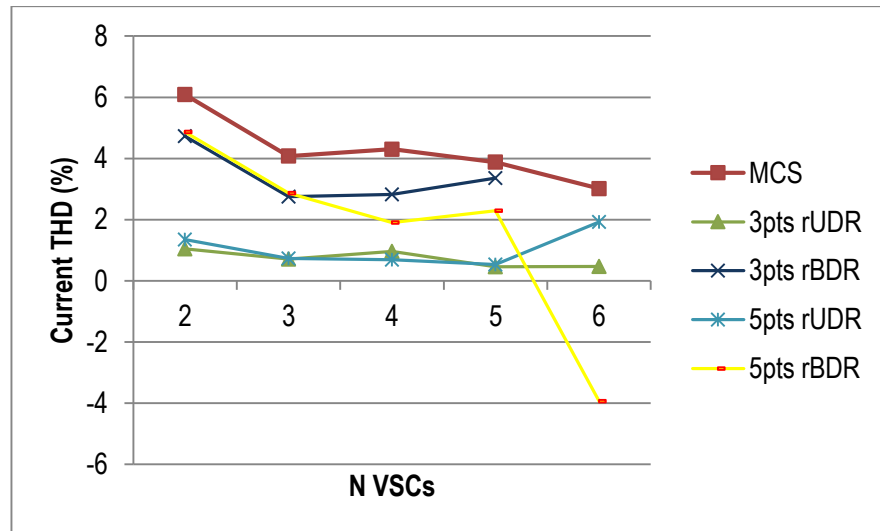


Fig. 6.26 UDR/BDR Predicted Kurtosis of I_{THD} for 6 VSCs

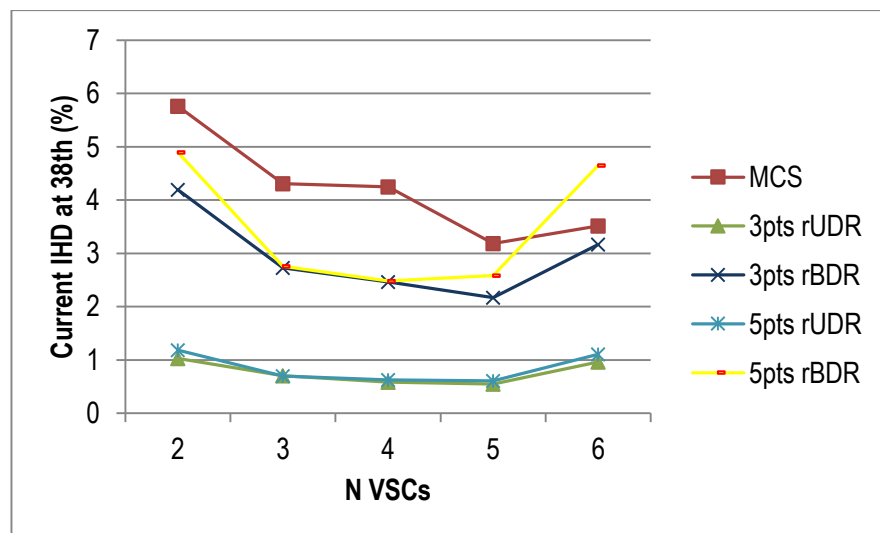


Fig. 6.27 UDR/BDR Predicted Kurtosis of I_{IHD_38} for 6 VSCs

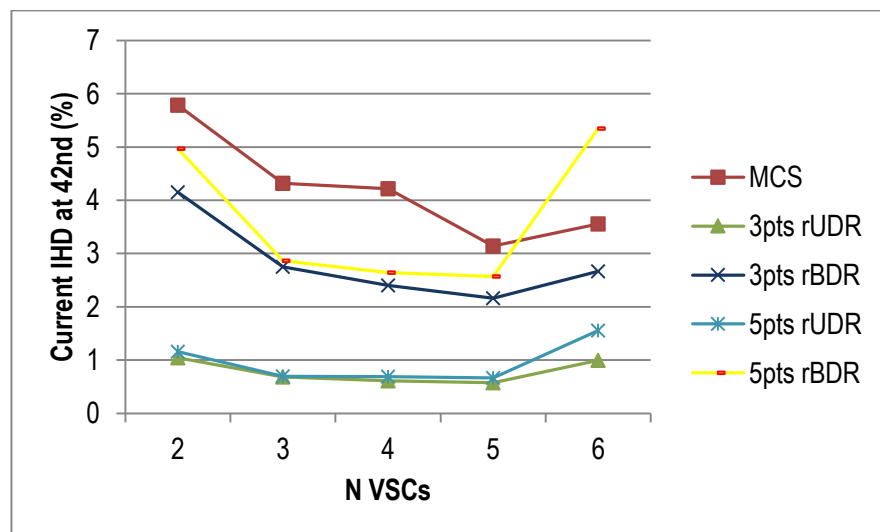


Fig. 6.28 UDR/BDR Predicted Kurtosis of I_{IHD_42} for 6 VSCs

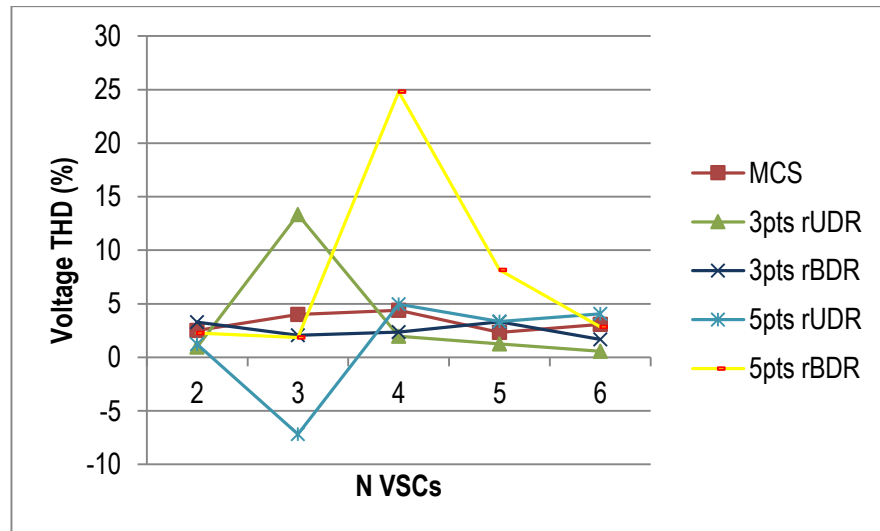


Fig. 6.29 UDR/BDR Predicted Kurtosis of V_{THD} for 6 VSCs

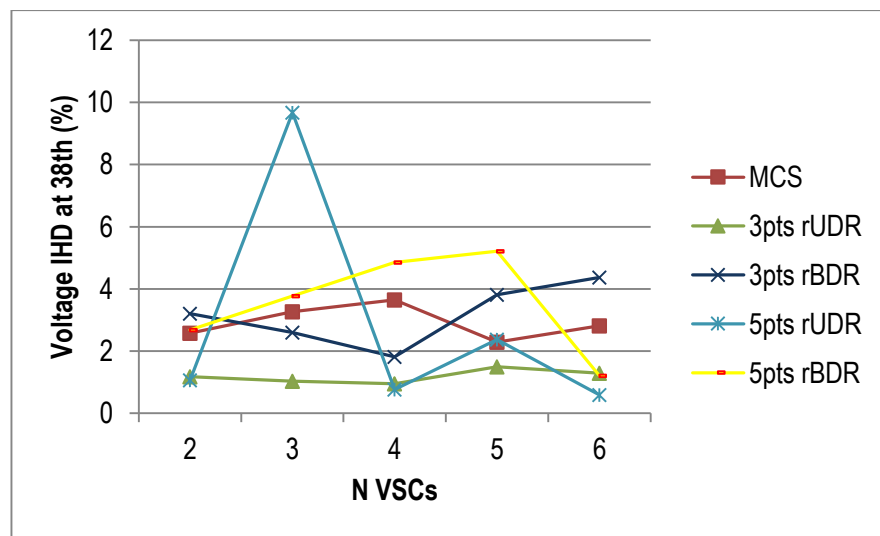


Fig. 6.30: UDR/BDR Predicted Kurtosis of V_{IHD_38} for 6 VSCs

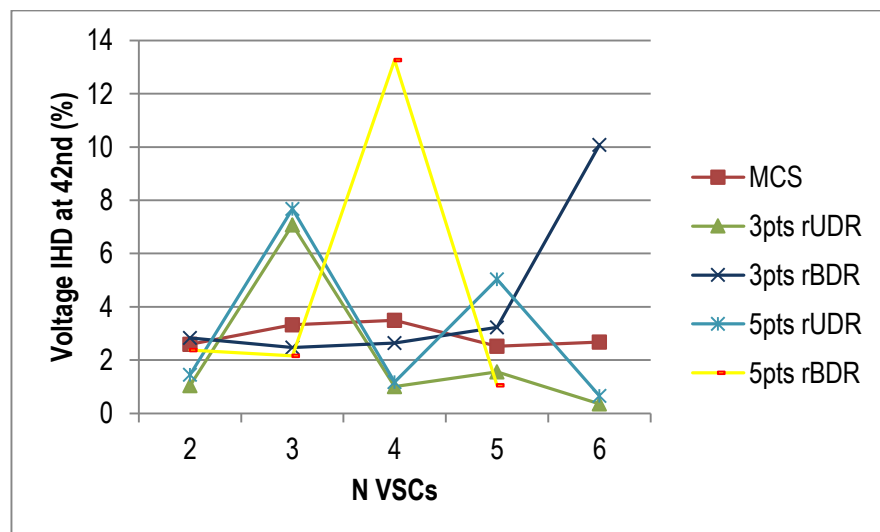


Fig. 6.31: UDR/BDR Predicted Kurtosis of V_{IHD_42} for 6 VSCs

The predicted harmonic distortion levels using the UDR and the BDR have been presented as actual values however, there are minor differences to the reference MCS approach results and the next set of charts will give a clearer depiction of the efficiency of the UDR and BDR techniques in predicting these results by stating the percentage error.

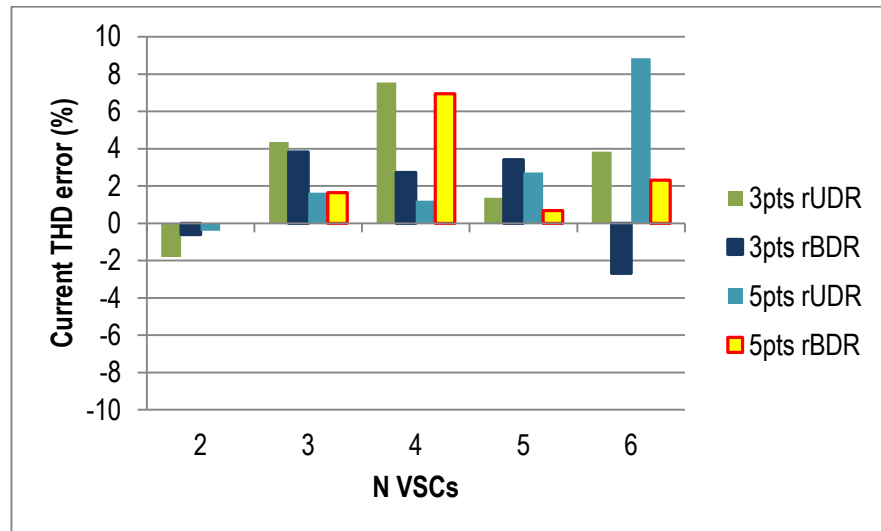


Fig. 6.32: Percentage error of the UDR/BDR Predicted I_{THD}

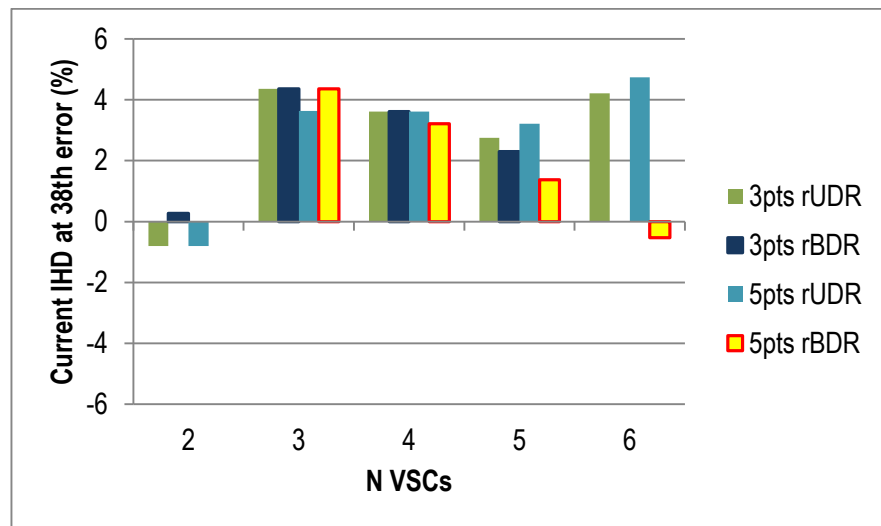


Fig. 6.33: Percentage error of the UDR/BDR Predicted I_{IHD_38}

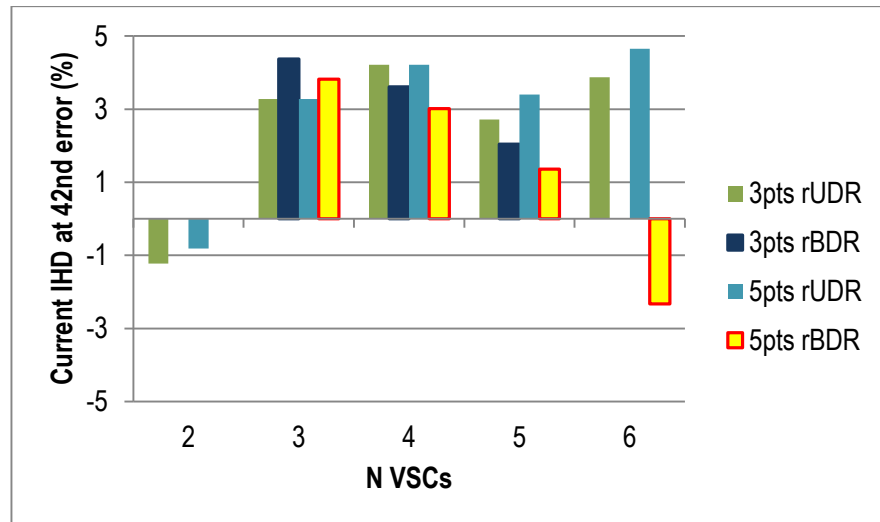


Fig. 6.34: Percentage error of the UDR/BDR Predicted I_{IHD_42}

From Fig. 6.32 - Fig. 6.34 it can be seen that both DR techniques worst prediction was an underestimation of 9% (5 points rUDR) for the I_{THD} of 6VSCs. In some cases the BDR was able to predict the same values as the MCS, hence, 0% error was recorded and no bar appear in that case (see Fig. 6.34 for 2 VSCs).

It can be seen from the percentage errors presented in Fig. 6.35 - Fig. 6.37 that the UDR and BDR techniques were able to give very accurate predictions of the voltage harmonic distortion level. Both dimension reduction techniques were able to predict precisely the same values as the MCS approach in many cases as can be seen in the cases where no bar appears in the chart (see Fig. 6.35 at 6VSCs and Fig. 6.37 at 5VSCs). The worst prediction was an over-estimation of 1.1% for V_{IHD_42} (see Fig. 6.37).

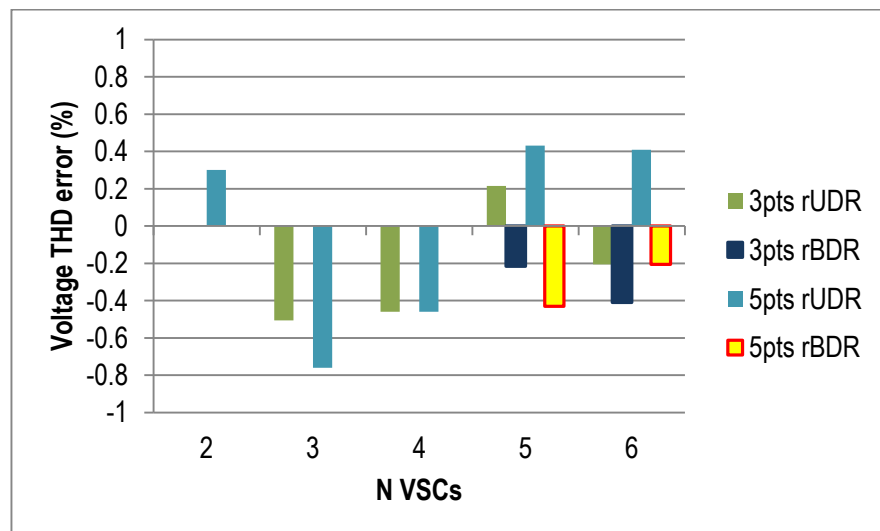


Fig. 6.35: Percentage error of the UDR/BDR Predicted V_{THD}

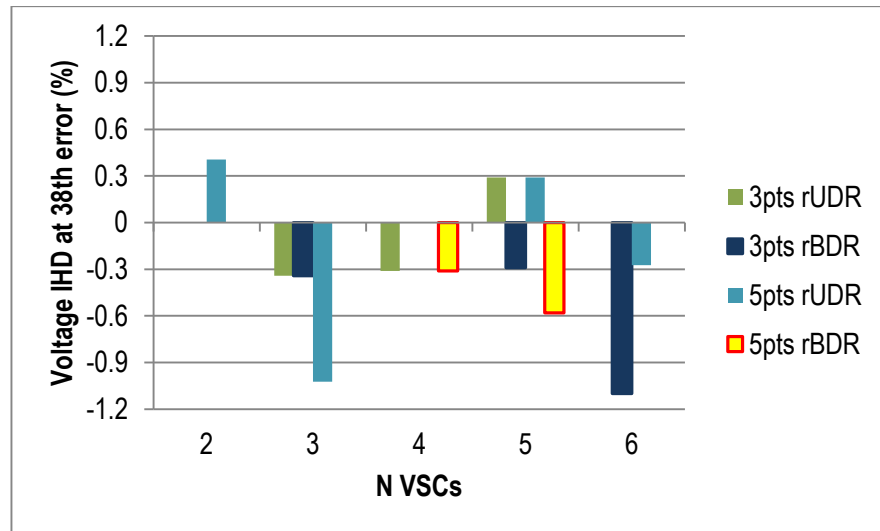


Fig. 6.36: Percentage error of the UDR/BDR Predicted V_{IHD_38}

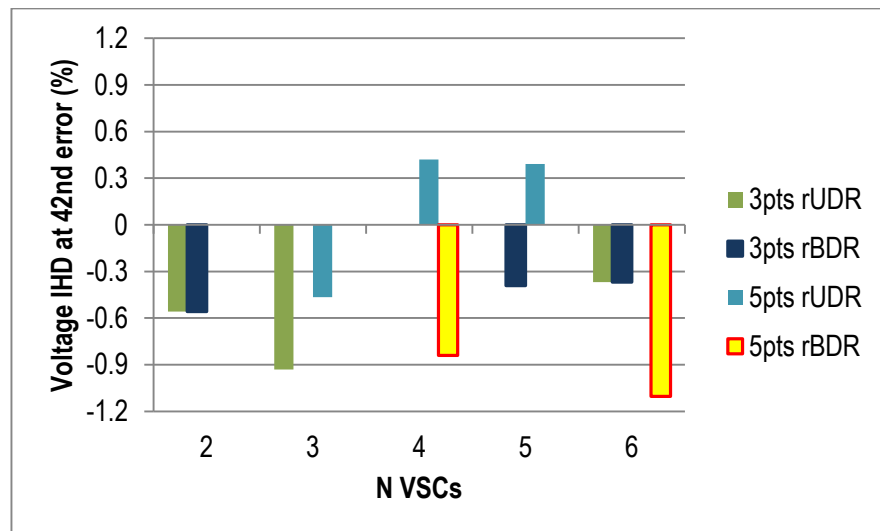


Fig. 6.37: Percentage error of the UDR/BDR Predicted V_{IHD_42}

From the results presented in evaluating the performance of the UDR and BDR technique, it was seen that the BDR gave better predictions of the moments of the harmonic distortion levels (see Table 6.5 - Table 6.20). This was clearer looking at Fig. 6.32 - Fig. 6.37 where the mean values of the current and voltage harmonic distortion levels were predicted. However, the BDR technique required far more computation time as compared to the UDR to produce these results. On the other hand, the UDR predicted mean and standard deviation values of harmonic distortion levels that were in close agreement with the MCS approach. The UDR however, could not produce accurate results for the skewness and kurtosis. The UDR predicted results were achieved in very fast

computation time leading to drastic saving of computation time well above 95% this is with respect to the MCS approach computation time.

Since the mean value and standard deviation of a harmonic distortion is usually enough in estimating if a VSC, an electrical equipment/system or a harmonic source would go beyond the IEEE 519 harmonic limit, then the UDR will be adequate in predicting harmonic distortion level for various operation scenarios.

6.5 Summary

This Chapter has presented the dimension reduction technique by enhancing the Unscented Transform based Gaussian Quadrature. The mathematical basics of the Gaussian Quadrature and the orthogonal polynomial in relation to the Gaussian Quadrature was also presented. The Gaussian Quadrature based UT method becomes unfeasible in a system with a large number of random variables as the “curse of dimensionality” problem limits its application. Hence dimension reduction was applied to the Gaussian Quadrature based UT to reduce the number of evaluation, computation time and burden while still maintaining a high level of accuracy of predicted results.

The UDR and BDR techniques were presented as the two methods deduced from applying the dimension reduction on the Unscented Transform equation and their mathematical basis were also discussed. To evaluate the performance of the UDR and BDR technique in harmonic prediction, the output power of 10 VSCs were first uniformly varied randomly using the MCS approach and then using the UDR and BDR technique. The MCS approach result was then used as a benchmark in evaluating the performance of the UDR and BDR technique in predicting the harmonic distortion level of the VSCs.

The UDR and BDR required less amount of computation time in predicting the harmonic distortion level of the current and voltage of the VSCs. Both the UDR and BDR techniques gives almost the same level of accuracy in predicting the mean and standard deviation values of the current and voltage harmonic distortions level, however, the BDR gives a better prediction for higher order moments like the skewness and kurtosis which are necessary in plotting cdf and pdf curves.

The UDR was able to drastically reduce the computation burden and time required in the prediction of the harmonic distortion level of many VSCs. In most cases the UDR was able to save more than 95% computation time with respect to the MCS approach computation time and effort.

A choice of which dimension reduction technique to use in a particular case depends on a trade-off between speed/accuracy and higher order moments.

Chapter 7

Predicting Harmonics of Multiple VSCs Using the UDR Technique

This chapter focuses on evaluating the performance of the UDR technique under various microgrid operating conditions and configuration. The aim is to highlight the efficiency and accuracy of the UDR technique in predicting harmonics and the impact these harmonics have on the Power Quality (PQ) of a microgrid.

7.1 Application of the UDR Technique

Five case studies will be considered to evaluate the performance of the UDR technique. The first case will look at filter parameter variation, the second will focus on the power variation of a wind turbine system and a photovoltaic which are Weibull distributed and normally distributed respectively. The third case will look at grid line impedance variation which may occur when more loads are added to an existing Electrical Power System (EPS). The fourth case will be on a microgrid containing a larger number of VSCs, and the last case will focus on the UDR technique performance in predicting harmonic distortion levels on a microgrid configuration having non-linear loads. The performance of the UDR technique would be evaluated using the results from the Monte Carlo Simulation (MCS) approach as a benchmark for the predicted mean and standard deviation values. The results presented in most of the case studies are the current and voltage THD and the IHD at the 38th and 42nd order which are the harmonics at the sidebands of the switching frequency (2 kHz) assuming a high fidelity VSC.

7.1.1 Step-by-Step Procedure of the UDR Technique

A summary of the main steps for implementing the UDR technique for predicting harmonic distortion level at the Point of Common Coupling (PCC) of the microgrid is highlighted below;

- Step 1) Identify all randomly varying functions within the system (e.g. power, impedance) and obtain their probability distribution functions.
- Step 2) Compute the sigma points and weights using Univariate Dimension reduced Gaussian quadrature based UT.
- Step 3) Input the microgrid system data including the sigma points and weights obtained in 2.
- Step 4) Run the microgrid simulation while obtaining necessary statistical data for the output variables (current/voltage THD, current/voltage IHD).
- Step 5) Compute the statistical data for the output variables using the measured output data values and weights of the UDR (e.g. mean current/voltage THD/IHD, standard deviation of current/voltage THD/IHD).
- Step 6) Display statistical data of output variables (e.g. mean current/voltage THD/IHD, standard deviation of current/voltage THD/IHD).

7.2 Case Study 1: Microgrid System with Filter Parameter Variation

This study aims to predict the level of harmonic distortion of VSCs in a microgrid using the UDR technique and the impact of filter variation on the harmonic distortion level of the VSCs. Filters are required for attenuating VSC harmonics however, an appropriate design and sizing is necessary to maintain the EPS stability. For microgrids operating in the grid connected mode, the main concern is to reduce the harmonic current injected into the grid [66].

The VSC harmonic filter are designed as in section 4.5, and certain aspects of filter inductance variation stated in section 5.2 reiterated to provide rationale for this case study. In designing VSC harmonic filters, the maximum ripple current (7.2) is usually chosen to be less than 20% of the rated current and the maximum ripple current is a function of the DC link voltage, the VSC switching frequency and the filter inductance L_{fabc} (7.1) [66]. To achieve a decrease of the ripple current the most flexible parameter is the filter inductor since increasing the

switching frequency affects the system efficiency. The value of the inductance can be given by:

$$L_{fabc} = \frac{1}{8} \times \frac{V_{dc}}{f_{sw} \cdot \Delta \hat{I}_{L_{max}}} \quad (7.1)$$

where

$$\Delta \hat{I}_{L_{max}} = 20\% \times I_{rated} \quad (7.2)$$

and f_{sw} is the switching frequency and V_{dc} is the DC voltage.

Another way of deciding the filter parameter value is to choose the value relative to the total system inductance. In [76], [67], it was suggested that the total system inductance should be about 10% of the base inductance value (see section 4.5).

Since no fixed value can be used but that which is determined at the discretion of the designer, the interfacing inductor L_{fabc} can be viewed as a stochastic variable. Considering that the value of the inductance will be in a range with no priority given to a value over another, the uniform distribution can be used in representing the randomness of the choice and the resulting effect on the VSCs generated harmonics can be predicted using the UDR technique. Based on this, the filter inductor value variation range was chosen assuming a $\pm 40\%$ trade-off between harmonic filter effectiveness and cost of inductor.

7.2.1 Predicted Result and Discussion

Table 7.1 shows the predicted level of harmonic distortion at the microgrid PCC to the grid when there are variations in L_{fabc} . It can be observed that the impact of the variation of L_{fabc} on the I_{THD} progressively reduces as the number of VSC increases. This is as expected, since the number of filters in the system increases as the number of VSC increases, thus limiting the current distortion. Also, with increased number of VSCs, there is a higher probability of harmonic cancellation due to current diversity and attenuation factor [62, 66, 121].

Table 7.1: Predicted Current Harmonic Distortion Level Using MCS, 3pts and 5pts UDR under Filter Inductance Variation

I_{THD} Mean	N VSCs	MCS	3pts rUDR	5pts rUDR
	1	4.19	4.26	4.20
	2	3.20	3.11	3.10
	3	2.73	2.79	2.74

	4	2.47	2.53	2.38
	5	2.22	2.32	2.46
	6	2.08	2.14	2.07
	7	1.89	1.83	1.67
	8	1.85	1.90	1.78
	9	1.72	1.48	1.59
	10	1.58	1.21	1.51
I_{IHD_38} Mean	N VSCs	MCS	3pts rUDR	5pts rUDR
	1	3.21	3.21	3.21
	2	2.48	2.47	2.48
	3	2.09	2.06	2.09
	4	1.93	1.96	1.97
	5	1.72	1.71	1.69
	6	1.62	1.66	1.67
	7	1.47	1.48	1.44
	8	1.44	1.46	1.47
	9	1.34	1.34	1.31
	10	1.24	1.24	1.03
I_{IHD_42} Mean	N VSCs	MCS	3pts rUDR	5pts rUDR
	1	2.04	2.04	2.04
	2	1.62	1.60	1.60
	3	1.38	1.37	1.37
	4	1.29	1.31	1.32
	5	1.16	1.15	1.14
	6	1.11	1.13	1.14
	7	1.01	1.02	1.01
	8	1.00	1.01	1.01
	9	0.93	0.94	0.93
	10	0.87	0.86	0.72

Table 7.2: Predicted Voltage Harmonic Distortion Level Using MCS, 3pts and 5pts UDR under Filter Inductance Variation

V_{THD} Mean	N VSCs	MCS	3pts rUDR	5pts rUDR
	1	2.72	2.72	2.72
	2	4.00	3.98	3.99
	3	4.81	4.75	4.77
	4	5.62	5.70	5.66
	5	6.01	5.96	5.97
	6	6.52	6.52	6.53
	7	6.62	6.72	6.70
	8	7.08	7.04	7.00
	9	7.15	7.00	6.91

	10	7.08	7.01	6.36
V_{IHD_38} Mean	N VSCs	MCS	3pts rUDR	5pts rUDR
	1	2.07	2.07	2.07
	2	3.04	3.03	3.05
	3	3.66	3.59	3.64
	4	4.29	4.38	4.36
	5	4.59	4.58	4.57
	6	4.99	5.06	5.05
	7	5.07	5.17	5.08
	8	5.43	5.46	5.44
	9	5.50	5.50	5.39
	10	5.44	5.55	5.00
V_{IHD_42} Mean	N VSCs	MCS	3pts rUDR	5pts rUDR
	1	1.46	1.45	1.46
	2	2.18	2.17	2.18
	3	2.67	2.63	2.64
	4	3.17	3.21	3.22
	5	3.43	3.40	3.42
	6	3.77	3.79	3.83
	7	3.87	3.93	3.99
	8	4.16	4.14	4.15
	9	4.22	4.28	4.25
	10	4.21	4.28	3.90

Fig. 7.2 - Fig. 7.7 show the predicted results of the impact of L_{fabc1} variation on harmonic distortion levels using the MCS and the UDR technique. It is observed that the UDR technique results are in close agreement with that of the MCS. Hence the UDR can be utilized in predicting harmonic distortion levels of VSCs in a microgrid where the filter inductor value is only known within certain constraints. Fig. 7.1 shows the percentage of computation time saved by using the UDR methods.

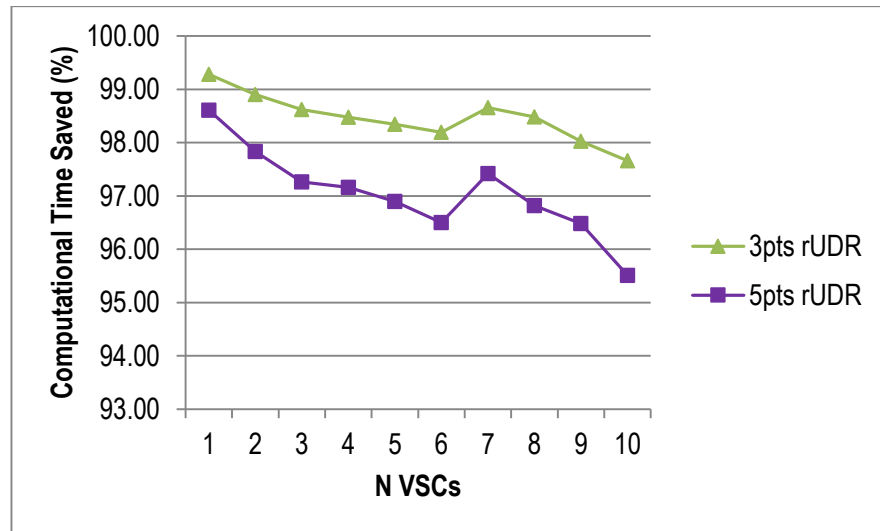


Fig. 7.1: Computation Time Saved by UDR Techniques wrt MCS

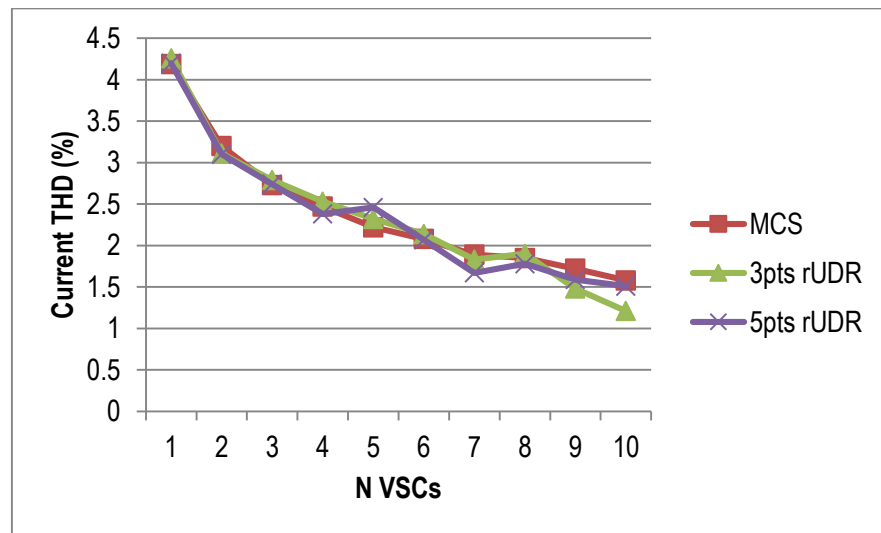


Fig. 7.2: Predicted I_{THD} using MCS, 3pts UDR and 5pts UDR.

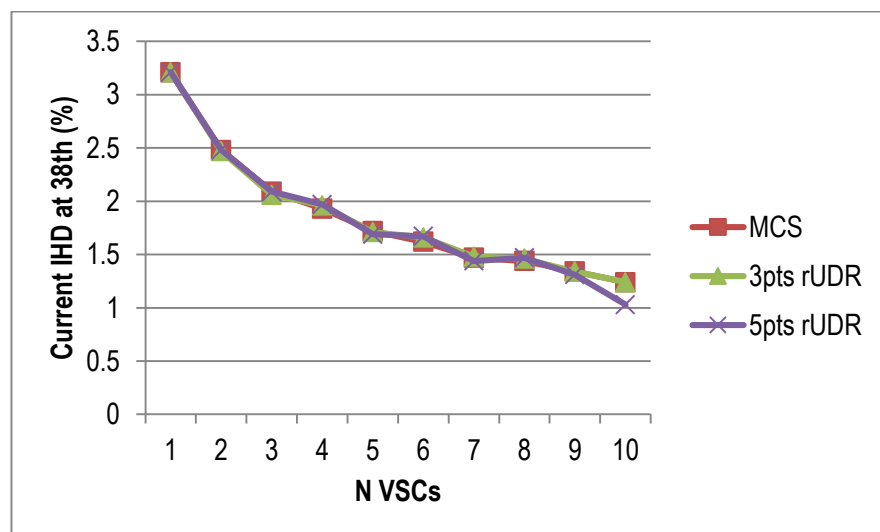


Fig. 7.3: Predicted $I_{HD_{38}}$ using MCS, 3pts UDR and 5pts UDR.

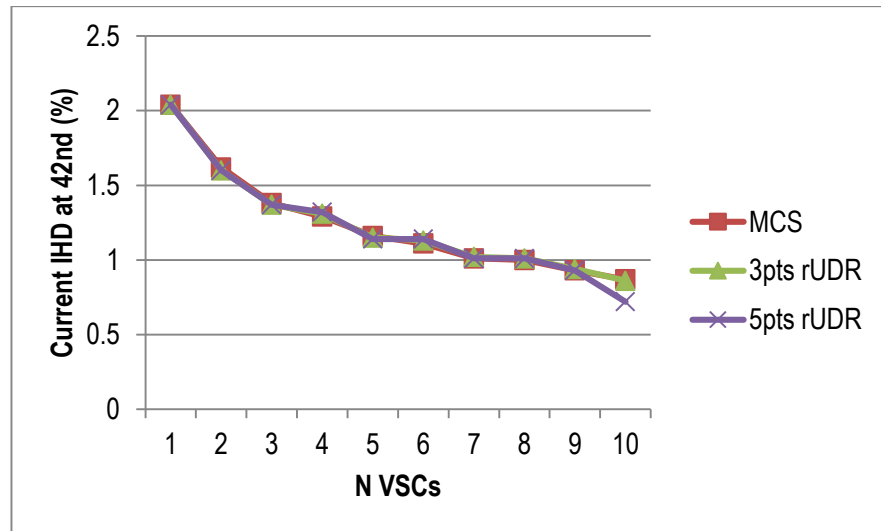


Fig. 7.4: Predicted I_{IHD_42} using MCS, 3pts UDR and 5pts UDR.

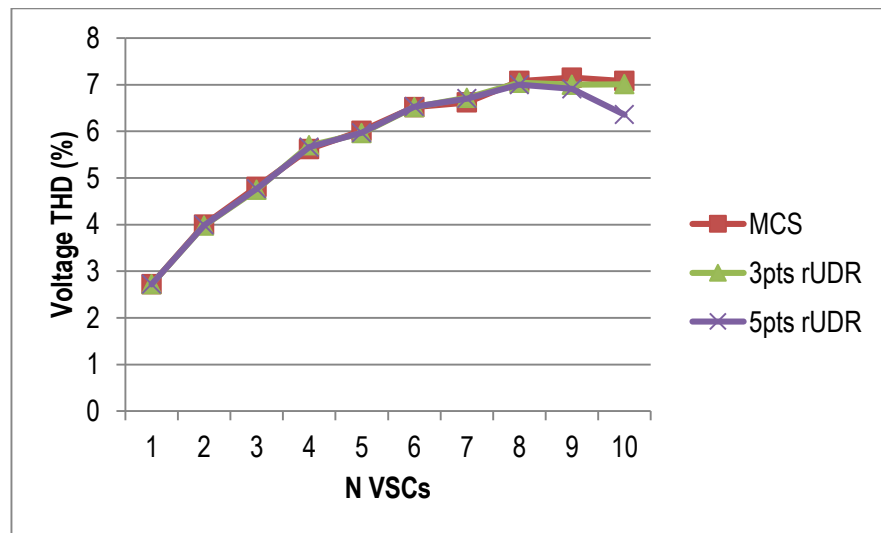


Fig. 7.5: Predicted V_{THD} using MCS, 3pts UDR and 5pts UDR.

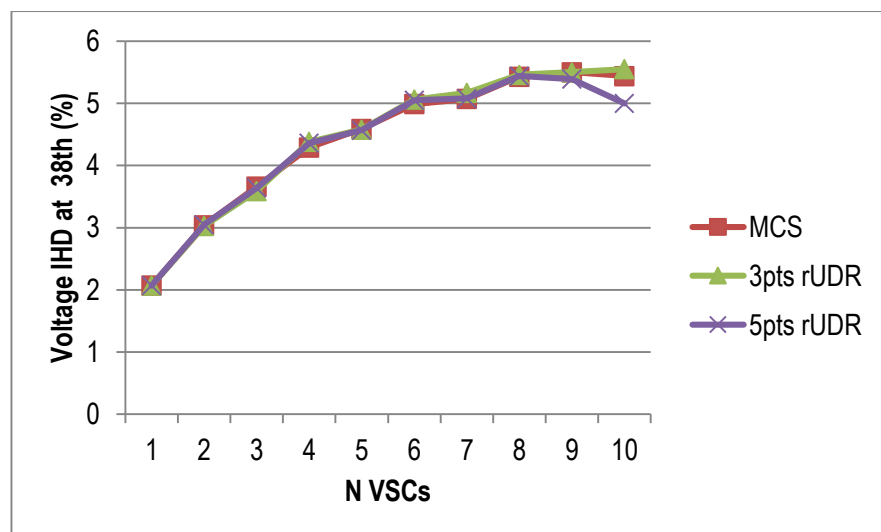


Fig. 7.6: Predicted V_{IHD_38} using MCS, 3pts UDR and 5pts UDR.

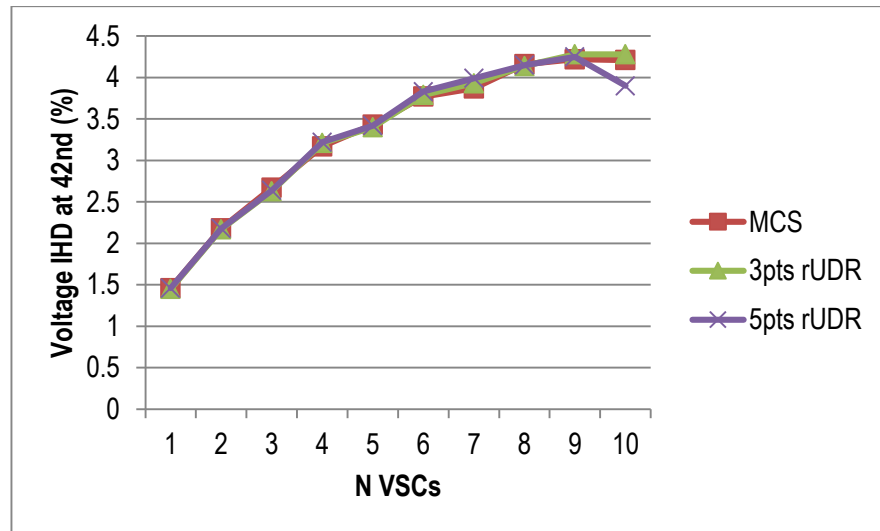


Fig. 7.7: Predicted V_{IHD_42} using MCS, 3pts UDR and 5pts UDR.

As regards the effect of the filter inductance variation on the PQ of the microgrid, Fig. 7.2 - Fig. 7.7 reveal that an increase in the number of VSCs reduces the harmonic distortion of the current but causes a steady increase in the voltage harmonic distortion levels in the microgrid. The effect of filter variation is more prominent at lower numbers of VSCs.

Percentage error of Predicted Results

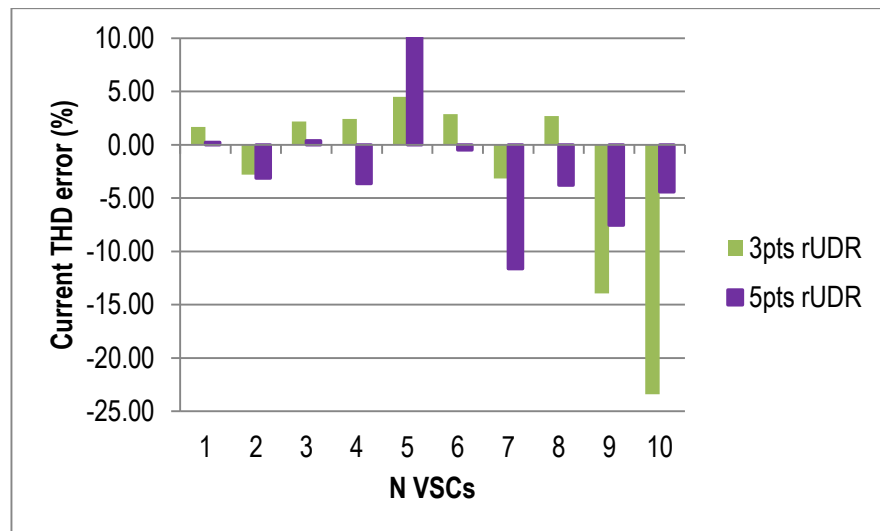


Fig. 7.8: Percentage error in predicted I_{THD} using 3pts and 5pts UDR.

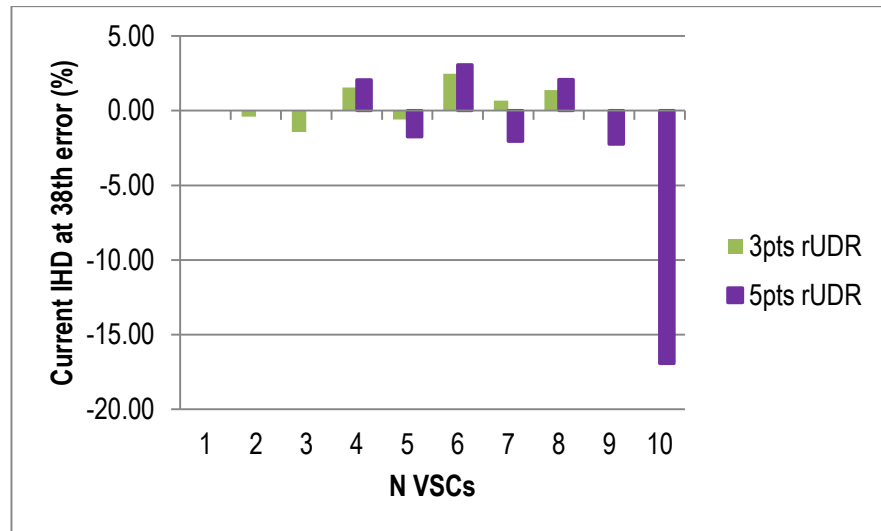


Fig. 7.9: Percentage error in predicted I_{IHD_38} using 3pts and 5pts UDR.

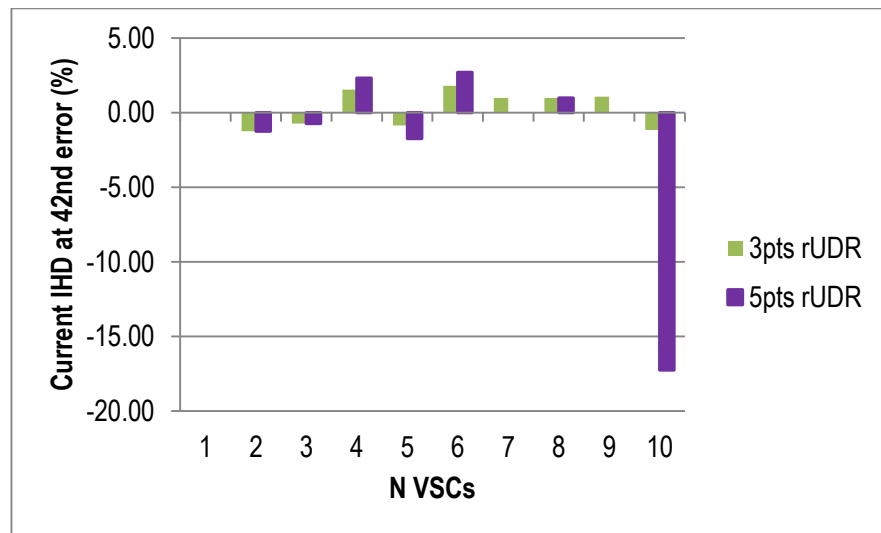


Fig. 7.10: Percentage error in predicted I_{IHD_42} using 3pts and 5pts UDR.

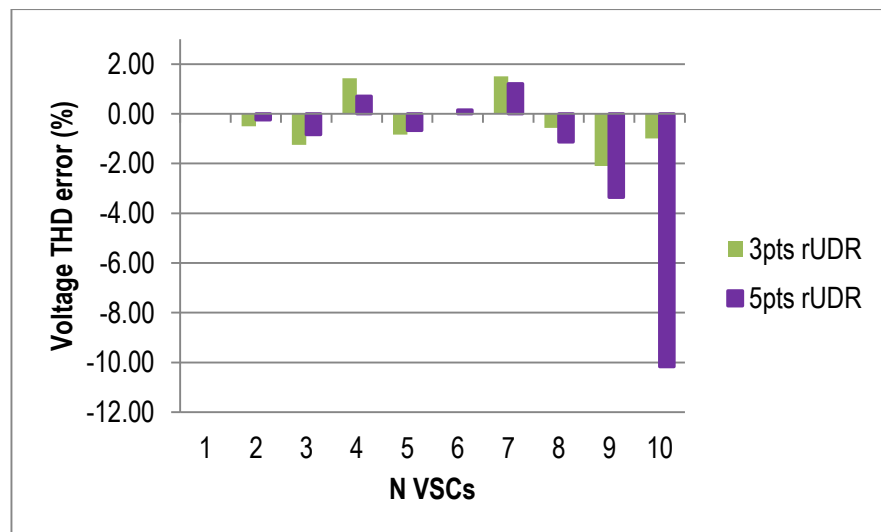


Fig. 7.11 Percentage error in predicted V_{THD} using 3pts and 5pts UDR.

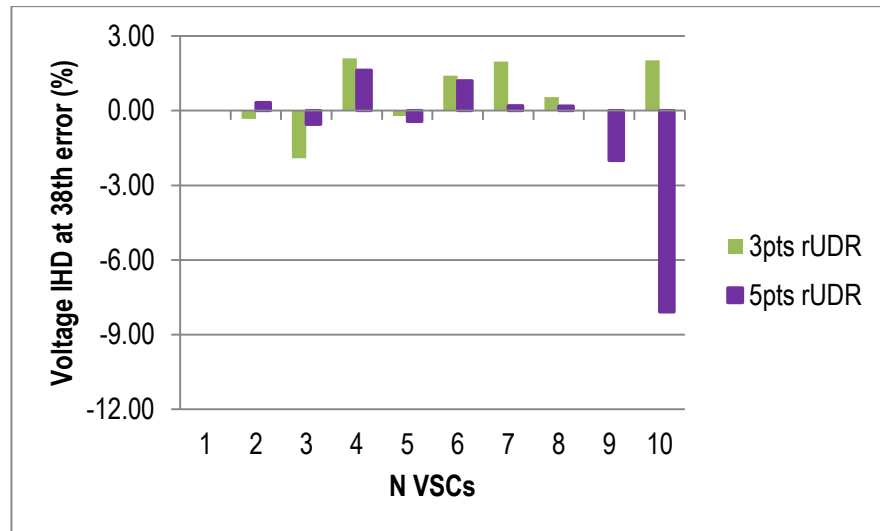


Fig. 7.12 Percentage error in predicted V_{IHD_38} using 3pts and 5pts UDR.

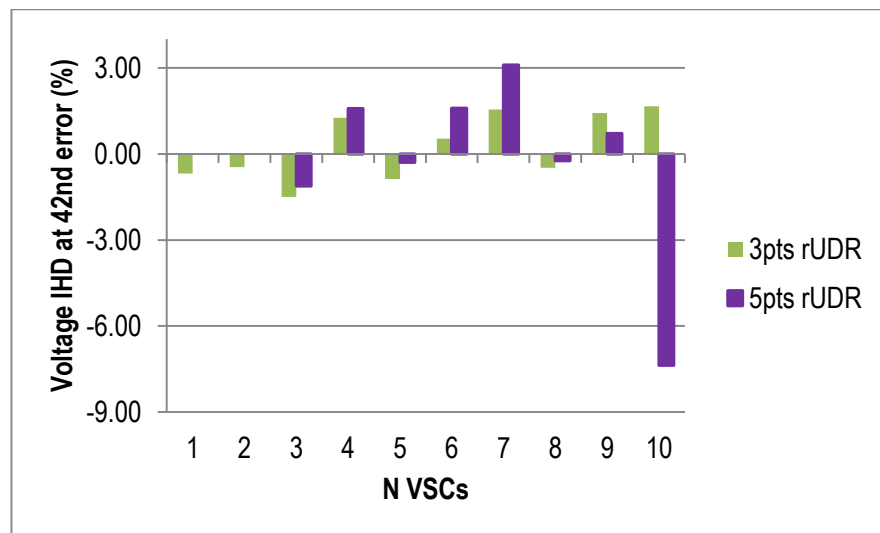


Fig. 7.13: Percentage error in predicted V_{IHD_42} using 3pts and 5pts UDR.

Fig. 7.8 - Fig. 7.10 shows the percentage error of the 3pts and 5pts approximations of the UDR technique with respect to the MCS result. Except for the case of 10 VSCs where an error of about 17% was recorded most of the prediction errors were below 10%. It should however be noted that the difference from the actual values are very small for 10 VSCs IHD at 42nd harmonic order where the MCS was 0.87% while the 5pts UDR was 0.72%. It is also necessary to add that this divergence for 10 VSCs does not in any way affect the 5pts UDR performance when the VSC increases beyond 10VSCs and this will be further investigated in the fourth case study when the number of VSCs is increased to 20. The standard deviation values can be seen in Appendix C.1.

7.3 Case Study 2: Microgrid System with Practical Power Variation

In this study a common uncertainty that emanate from the use of RES such as Wind Turbines (WT) and Photovoltaics (PV) due to the dependence of their power output on several random factors such as the weather is considered. This is necessary as output power variation affects the VSC harmonic distortion levels. The performance of the UDR 5pts approximation in predicting harmonics is evaluated in this case. Statistical distributions which are similar to practical power variations are considered in order to have an accurate estimate of the harmonic distortion at the PCC.

For PVs, the intensity of the sun's light rays (solar irradiance) varies through the day and is different for various locations and hence a variation in the generated power. This variation of power affects the level of harmonics generated by VSCs [1, 64] and solar irradiance/generated power over the day follows a normal (Gaussian) distribution as given in [130]. With this uncertainty/variation of the output power value, the UDR is utilized to predict the level of harmonic distortion of the PV VSCs. Three different output power variations representing locations with low irradiance (Condition 1: 60% coefficient of variation), medium irradiance (Condition 2: 40% coefficient of variation) and high irradiance (Condition 3: 20% coefficient of variation) are considered.

Fig. 7.14 shows the schematics of the studied microgrid containing 2 PV VSCs which are connected to the grid at the PCC.

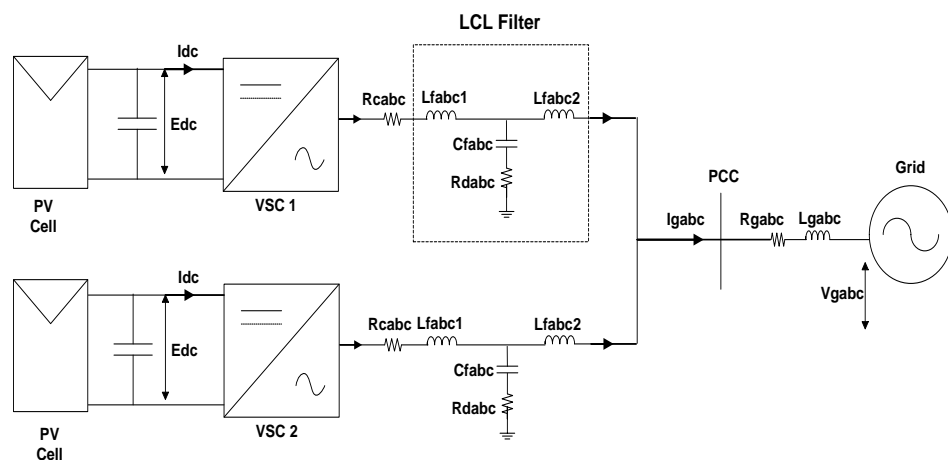


Fig. 7.14: Schematic of 2 PV VSC commonly connected to the grid.

The WTS generates its electrical energy from wind incident upon the blades of the wind turbine. Several models have been proposed in literatures for modelling wind speed and power variations in a WTS and they include; the Weibull distribution, Rayleigh distribution, Gaussian distribution, etc. [77]. However, it is generally accepted that the probability density function (pdf) of the wind speed distribution over time follows a Weibull distribution (see Fig. 7.15). The wind speed varies from days, seasons and location. This wind distribution affects the generated power of the wind turbine which is transmitted to the VSCs.

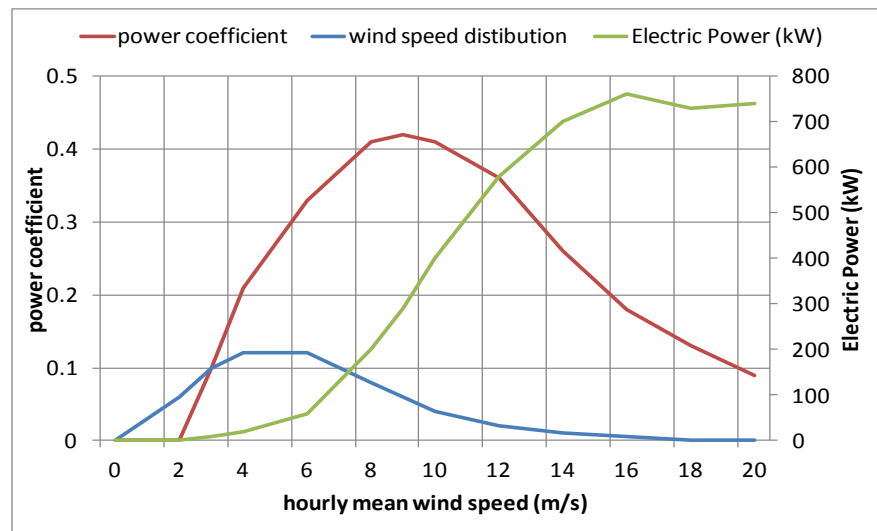


Fig. 7.15: Wind Speed Distribution and Power Curve [131].

For the WTS, three (3) scenarios representing wind speed variations in different locations with a low wind speed profile (Condition 1: $c = 2.16$, $k = 4.95$), medium wind speed profile (Condition 2: $c = 2.58$, $k = 6.13$) and high wind speed profile (Condition 3: $c = 3.97$, $k = 10.7$) is considered. Where, c and k represents the scale and shape factor respectively.

The probability of the harmonic level going beyond the IEEE 519 harmonic limit was defined by the current and voltage harmonic Cumulative Distribution Function (CDF) plots. The CDF curves for the UDR are plotted using the Cornish-Fisher series expansion. As in the previous case study, the MCS approach results were used as a benchmark for the statistical moments and CDF plots obtained using the UDR technique.

7.3.1 Predicted Result and Discussion

The predicted harmonic distortion mean and standard deviation (Std) values of two VSCs connected in parallel and interfaced to the grid are presented in Table 7.3 and Table 7.4. The CDF plot which gives the probability of the VSCs going beyond the IEEE 519 harmonic limit are given in Fig. 7.16 - Fig. 7.21. The CDF plot of the UDR method is plotted using the Cornish-Fisher expansion technique.

Table 7.3 Predicted Current and Voltage THD of the PV VSCs

		I_{THD}		V_{THD}	
		MCS	UDR	MCS	UDR
Condition 1	Mean (%)	5.58	5.66	2.19	2.25
	Std	2.49	2.25	0.14	0.12
Condition 2	Mean (%)	4.67	4.83	1.93	1.93
	Std	1.50	1.90	0.06	0.05
Condition 3	Mean (%)	3.02	2.94	1.95	1.94
	Std	0.79	0.79	0.04	0.03

The predicted mean and Std of the current THD (I_{THD}) and voltage THD (V_{THD}) of the PV VSCs is presented in Table 7.3. It can be seen from Table 7.3 that the UDR accurately predicts the mean and standard deviation of the I_{THD} and V_{THD} . Condition 1 has a higher mean value for the I_{THD} because it has a lower power output. Condition 3 has the lowest mean value for the I_{THD} because the higher irradiance produces a higher power output. Hence, harmonic distortion levels here are lower. Condition 1 also has a 58% probability of exceeding the IEEE 519 harmonic limit as seen in Fig. 7.12. In Condition 2 (Fig. 7.13), output power variations would lead to a 22% probability of I_{THD} exceeding the IEEE 519 harmonic limit. Condition 3 has a higher irradiance value and hence a higher power output, this in turn reduces the I_{THD} of the PV VSCs. In Fig. 7.18 it can be seen that it has only a 4% probability of exceeding the IEEE 519 harmonic limit.

It is important to state that there is little impact on the V_{THD} with output power variations. The V_{THD} was always within the IEEE 519 harmonic limit (that is less than 8%). This is reflected in the low Std in Table 7.3.

Fig. 7.16 - Fig. 7.18 shows the I_{THD} CDF curves plotted using the Cornish Fisher series expansion and the moments and cumulants obtained from the UDR. This was compared against the CDF curves from MCS. It can be seen from the figures

below that the UDR CDF plots are clear approximations of the MCS CDF plots and in all cases the UDR CDF plots can be used to obtain the probability of the harmonic distortion going beyond the IEEE 519 limit. A small inward curve is observed at the bottom of the UDR CF plot in Fig. 7.18 however, this does not affect the accuracy of the overall plot.

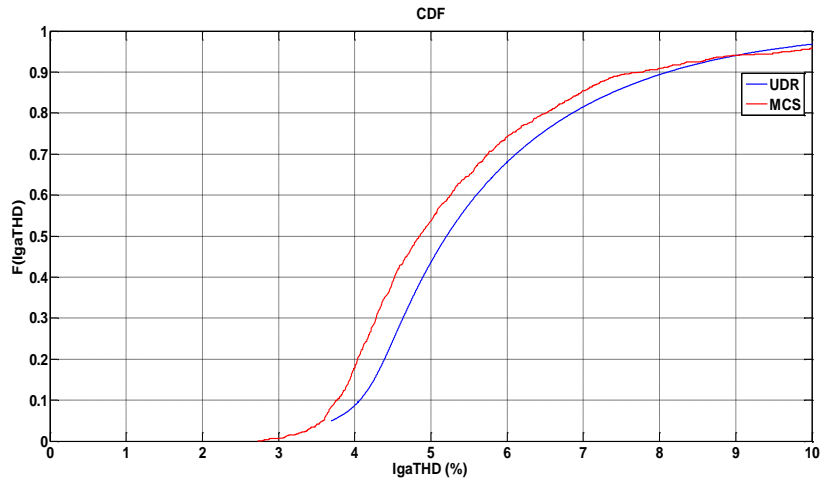


Fig. 7.16: Condition 1 (PV) CDF plot of current THD.

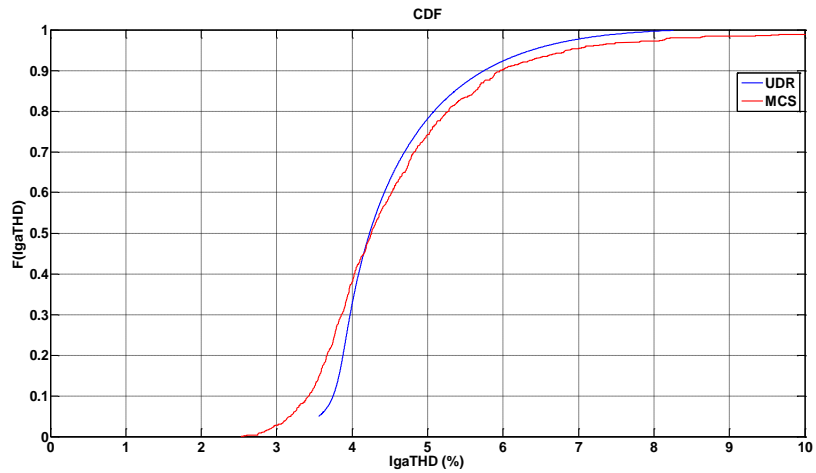


Fig. 7.17: Condition 2 (PV) CDF plot of current THD.

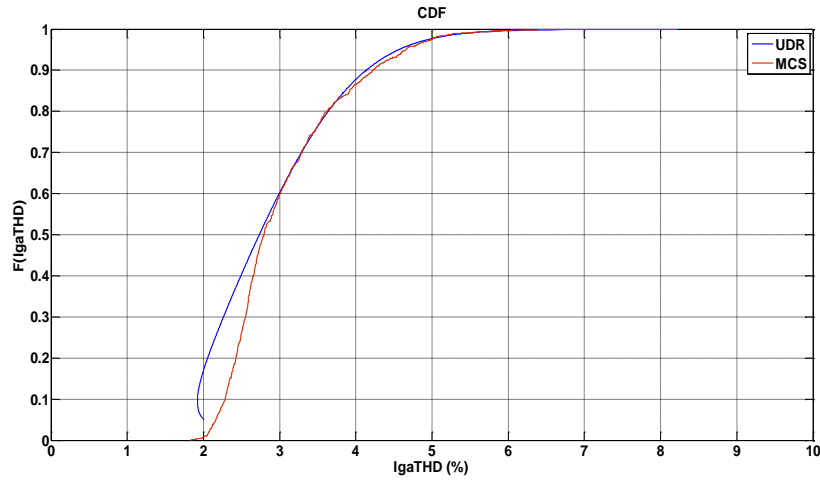


Fig. 7.18: Condition 3 (PV) CDF plot of current THD.

Table 7.4: Predicted Current and Voltage THD of the WT VSCs

		IgaTHD		VgaTHD	
		MCS	UDR	MCS	UDR
Condition 1	Mean (%)	5.39	5.27	1.25	1.23
	Std	2.11	1.79	0.05	0.03
Condition 2	Mean (%)	4.81	4.53	1.25	1.23
	Std	1.36	1.21	0.05	0.04
Condition 3	Mean (%)	4.26	3.88	1.27	1.25
	Std	0.76	0.81	0.05	0.04

The predicted current and voltage THD of the wind turbine VSCs is presented in Table 7.4. It can be observed from Table 7.4 that the UDR gives a close prediction for the mean and Std of I_{THD} and V_{THD} in all cases.

Condition 1 has a high I_{THD} mean value and a high probability (56%) of exceeding the IEEE 519 harmonic limit as seen in Fig. 7.19. Condition 2 results are presented in Fig. 7.20 and it has a 30% probability of exceeding the IEEE 519 harmonic limit. The effect of output power variations in a location with a high wind profile is simulated in Condition 3 and the results presented in Fig. 7.17 gives the probability of the I_{THD} going beyond the IEEE 519 harmonic limit as 12%. The small inward curve at the bottom of the UDR CF plot in Fig. 7.21 does not affect the accuracy of the entire CDF plot.

Table 7.4 shows that the output power variation also has very little impact on the V_{THD} of the WT system VSC. The V_{THD} was always within the IEEE 519 harmonic limit and this is reflected in the low Std in Table 7.4, the low Std value confirms that no real variation is occurring in the V_{THD} values.

It can however be seen that the UDR CDF curves of I_{THD} for the WTS VSCs is more of an approximation compared to the CDF curves from the PV VCS. This is due to the distribution of the harmonics obtained for each system. This is one of the shortfalls of the Cornish Fisher method, notwithstanding, its reproduction is fairly sufficient to serve as a guide. In all cases the UDR CDF plots can be used to obtain the probability of the harmonic distortion going beyond the IEEE 519 limit, thus giving a measure of the impact of these variations on harmonic distortion and the PQ of the microgrid.

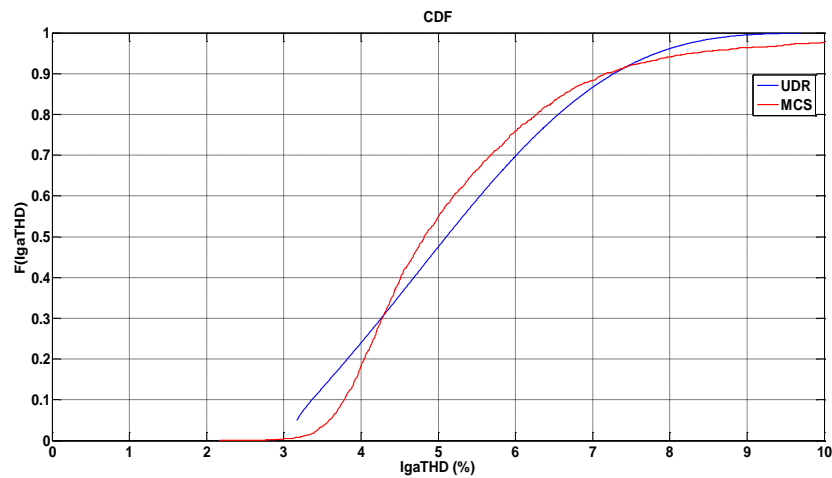


Fig. 7.19: Condition 1 (WT) CDF plot of current THD.

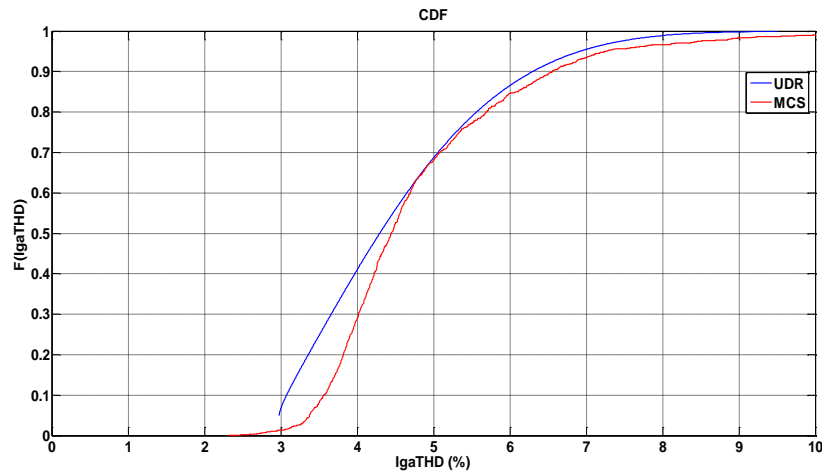


Fig. 7.20: Condition 2 (WT) CDF plot of current THD.

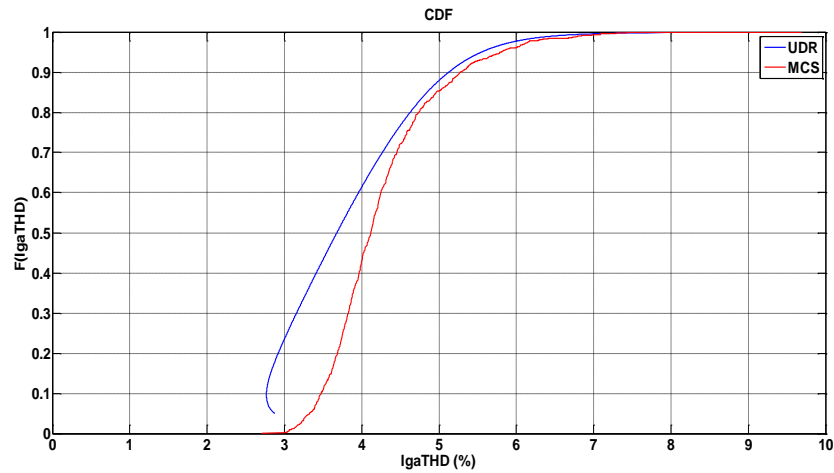


Fig. 7.21: Condition 3 (WT) CDF plot of current THD.

This case study was considered to highlight the compatibility of the UDR with practical RES power variations and distribution such as the Weibull and Gaussian distribution. The UDR technique accurately predicted the mean and standard deviation of the current and voltage THD of the PV and WT VSCs under realistic power variations. However, the percentage error for the case of a Weibull distributed power in a WTS is higher than that of the normal distributed PV system. The Cornish-Fisher (CF) series expansion technique was used to plot the UDR CDF plots and checked against the CDF plots of the MCS technique. The CF technique CDF curves were a clear approximation of the MCS CDF curve. The CDF curves are able to give a measure of the percentage of probability that the VSCs harmonic level will exceed the IEEE 519 harmonic limit and hence the impact of these uncertainties on the PQ of the microgrid. The UDR prediction technique may be used as a guide both during design and operation of microgrid containing RES VSCs.

7.4 Case Study 3: Microgrid System with Grid Impedance Variation

This study considers varying the interfacing grid system impedance values R_{gabc} , L_{gabc} to investigate the overall effect of grid impedance variation on the level of harmonic distortion of many connected RES VSC. The variations are done to reflect a weak and a strong grid as it is not generally known where a designed VSC would be deployed or how the load profile of the microgrid would be at

different times. Small distribution systems like the microgrid sometimes have unbalanced loading which may also affect the grid system impedance at the PCC. The system impedance can be regarded as the transformer impedance and the interconnecting cable impedance measured at the point of use. It can also be said to be the sum of impedance of every component between the grid and the point of use. So an unbalanced loading of a 3 phase system can affect the impedance of the system in a way whereby a high concentration of resistive or inductive load on a particular phase will impact on the cumulative impedance measured on that phase. As unbalanced loading causes unbalanced voltage drop across the systems impedance, and hence, alters the cumulative system impedance measured at the point of use, leading to variability and uncertainty in the microgrid

For this study, Z_{gabc} was obtained from [66] and then assumed to vary randomly following a uniform distribution. The grid impedance variation range was assumed to be between -50% and +150%.

7.4.1 Predicted Result and Discussion

Fig. 7.23 - Fig. 7.28 gives a clear perspective to the predicted current and voltage harmonic distortion levels for nVSCs in a microgrid. Table 7.5 - Table 7.7 and the corresponding figures show that both the 3pts and 5pts UDR have a close agreement with the results of the MCS approach.

Table 7.5: Predicted Total Harmonic Distortion Level Using MCS, 3pts and 5pts UDR under Grid Impedance Variation

I_{THD} Mean	N VSCs	MCS	3pts rUDR	5pts rUDR
	1	3.22	3.14	3.07
	2	2.66	2.83	2.68
	3	2.37	2.23	2.26
	4	2.19	2.11	2.01
	5	2.04	2.02	1.99
	6	2.02	1.86	1.87
	7	2.09	1.99	2.02
	8	2.34	2.22	2.27
	9	2.82	2.80	2.63
	10	3.28	3.09	3.40

V_{THD} Mean	N VSCs	MCS	3pts rUDR	5pts rUDR
	1	2.86	2.88	2.86
	2	3.94	3.99	3.97
	3	4.54	4.61	4.62
	4	4.96	5.03	5.00
	5	5.30	5.36	5.32
	6	5.52	5.56	5.62
	7	5.72	5.71	5.72
	8	5.94	5.96	6.01
	9	6.10	6.14	6.13
	10	6.29	6.34	6.40

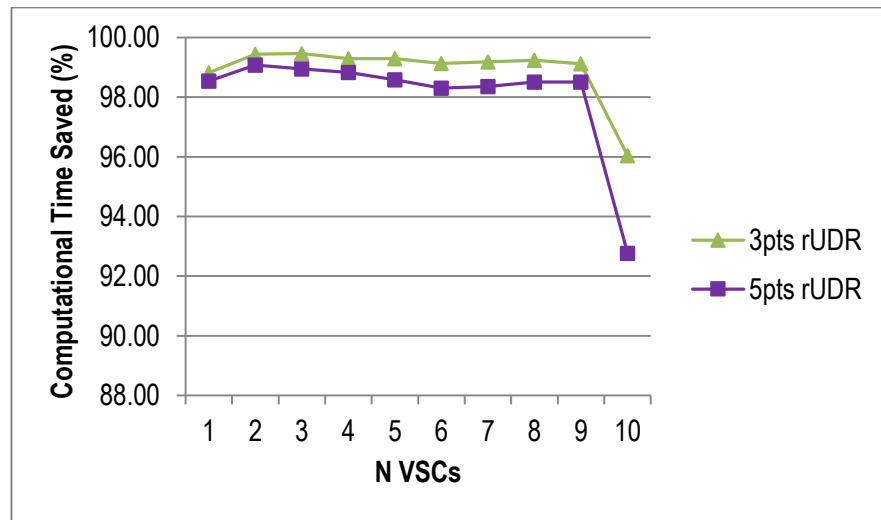


Fig. 7.22: Computation Time Saved using UDR technique wrt MCS

Fig. 7.22 shows the percentage of computation time saved for applying the UDR techniques with respect to the MCS.

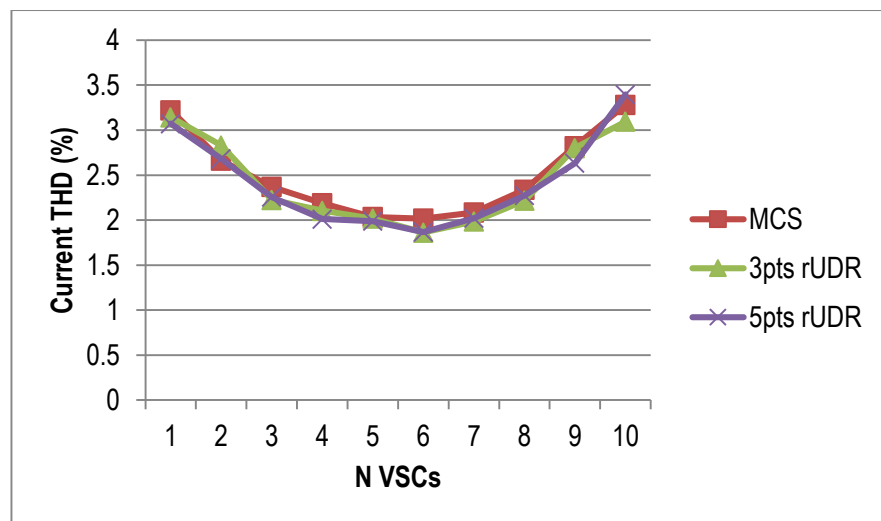


Fig. 7.23: Predicted I_{THD} using MCS, 3pts UDR and 5pts UDR.

From the graph trend in Fig. 7.23, it can be seen that the I_{THD} reduces as the number of VSCs increases from 1 to 6. However, further increase beyond 6 VSCs causes an increase in I_{THD} at the PCC. This may be partly due to increased instability in the system caused by the increase of resonance between the VSC filter and the grid impedance parameters. This effect is not reflected in V_{THD} , where an increase in VSC under these conditions causes an increase in the V_{THD} .

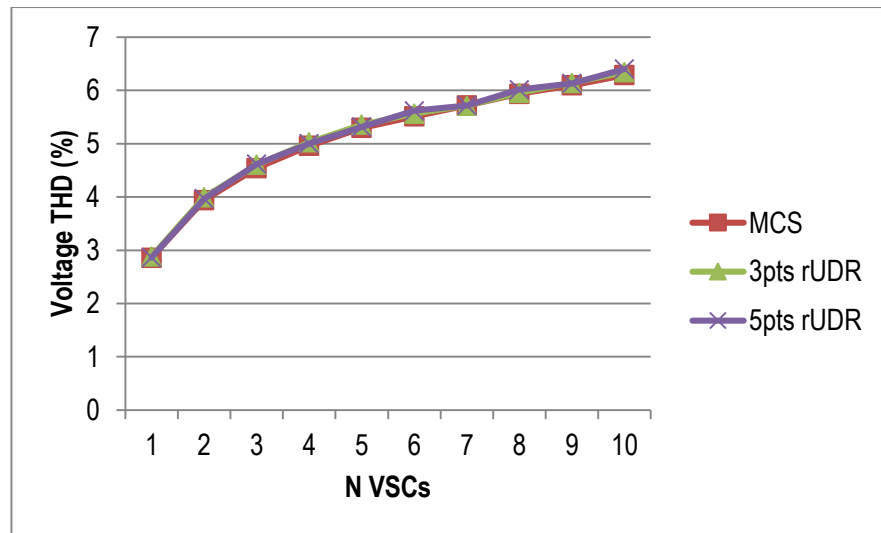


Fig. 7.24: Predicted V_{THD} using MCS, 3pts UDR and 5pts UDR.

The harmonic distortion at the 38th order using the 3pts and 5pts UDR technique was very accurate as can be seen in Table 7.6.

Table 7.6: Predicted 38th order Individual Harmonic Distortion Level Using MCS, 3pts and 5pts UDR under Grid Impedance Variation

I_{IHD} 38 th Mean	N VSCs	MCS	3pts rUDR	5pts rUDR
	1	2.39	2.38	2.34
	2	1.85	1.80	1.79
	3	1.56	1.47	1.46
	4	1.39	1.30	1.32
	5	1.22	1.17	1.16
	6	1.16	1.07	1.08
	7	1.09	1.00	1.00
	8	0.99	0.93	0.93
	9	0.97	0.87	0.86
	10	0.95	0.82	0.84
V_{IHD} 38 th Mean	N VSCs	MCS	3pts rUDR	5pts rUDR
	1	2.14	2.15	2.13

	2	2.93	2.98	2.96
	3	3.38	3.43	3.43
	4	3.71	3.77	3.78
	5	3.97	4.02	3.99
	6	4.13	4.20	4.25
	7	4.28	4.30	4.29
	8	4.40	4.42	4.44
	9	4.42	4.45	4.43
	10	4.44	4.47	4.51

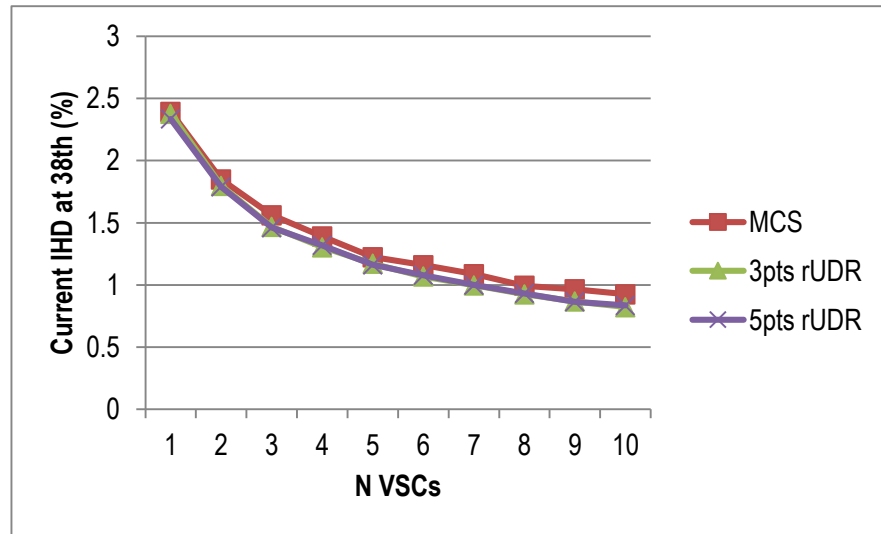


Fig. 7.25: Predicted $I_{\text{IHD}_{38}}$ using MCS, 3pts UDR and 5pts UDR.

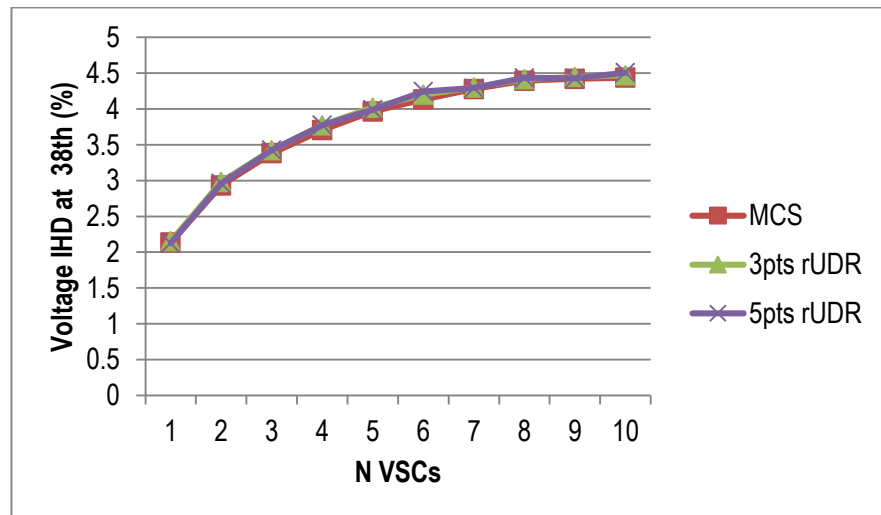


Fig. 7.26: Predicted $V_{\text{IHD}_{38}}$ using MCS, 3pts UDR and 5pts UDR.

The predicted harmonic distortion at the 42nd harmonic order using the 3pts and 5pts UDR were again in close agreement with the MCS approach results (see Fig. 7.27 and Fig. 7.28).

Table 7.7: Predicted 42nd order Individual Harmonic Distortion Level Using MCS, 3pts and 5pts UDR under Grid Impedance Variation

$I_{IHD\ 42^{nd}}\ \text{Mean}$	N VSCs	MCS	3pts rUDR	5pts rUDR
	1	1.57	1.55	1.54
	2	1.23	1.20	1.19
	3	1.05	1.00	1.00
	4	0.95	0.88	0.90
	5	0.84	0.80	0.80
	6	0.80	0.74	0.74
	7	0.76	0.69	0.69
	8	0.70	0.65	0.65
	9	0.68	0.61	0.61
	10	0.65	0.58	0.59
$V_{IHD\ 42^{nd}}\ \text{Mean}$	N VSCs	MCS	3pts rUDR	5pts rUDR
	1	1.55	1.56	1.55
	2	2.17	2.19	2.18
	3	2.53	2.60	2.60
	4	2.80	2.84	2.83
	5	3.02	3.04	3.02
	6	3.17	3.21	3.22
	7	3.29	3.28	3.27
	8	3.40	3.41	3.43
	9	3.44	3.47	3.48
	10	3.47	3.49	3.49

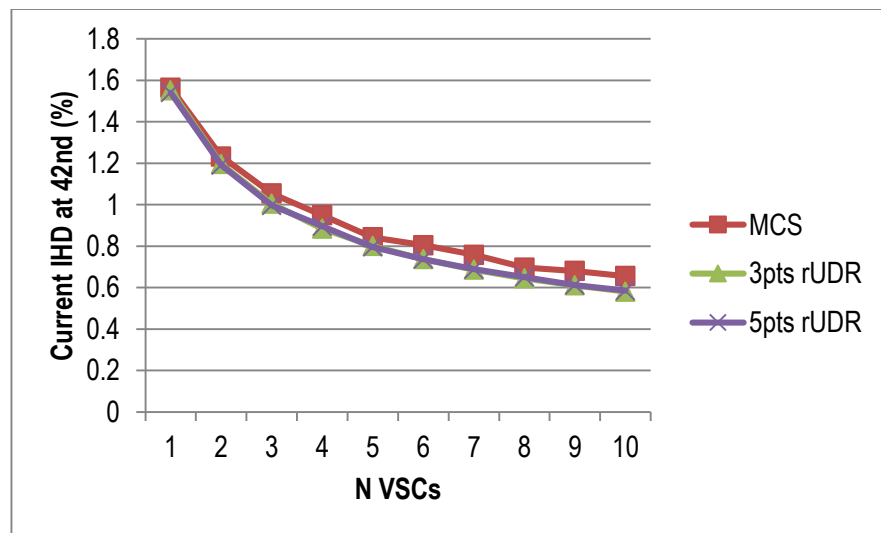


Fig. 7.27: Predicted I_{IHD_42} using MCS, 3pts UDR and 5pts UDR.

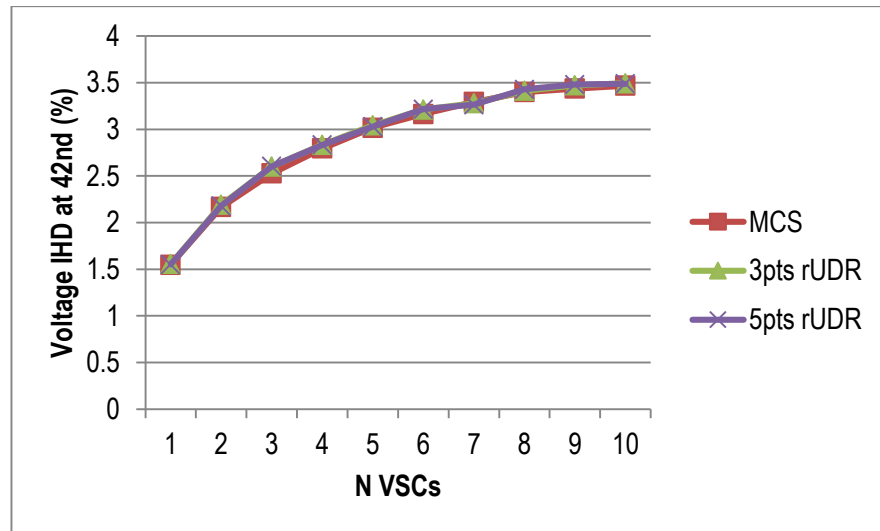


Fig. 7.28: Predicted V_{IHD_42} using MCS, 3pts UDR and 5pts UDR.

Majority of the predicted harmonic distortion results showed that the UDR technique has a good agreement with the MCS approach. Considering the amount of computational time saved by the UDR, the predicted results can be accepted as adequate. In previous case studies the increase of the number of VSCs caused a decrease in the I_{THD} . However, in this case the increase of the number of VSCs does not show a consistent decrease in I_{THD} . The I_{THD} reduces and increases in a non-linear way.

Percentage error of Predicted Results

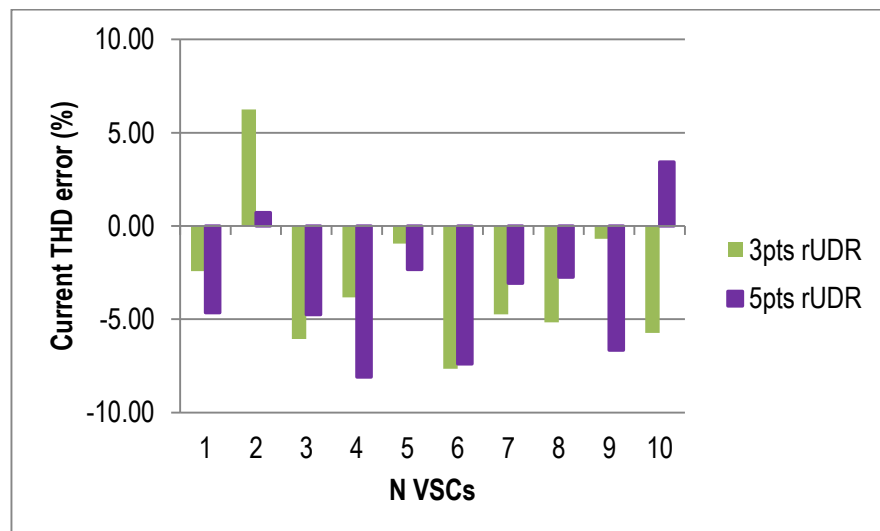


Fig. 7.29: Percentage error in predicted I_{THD} using 3pts UDR and 5pts UDR.

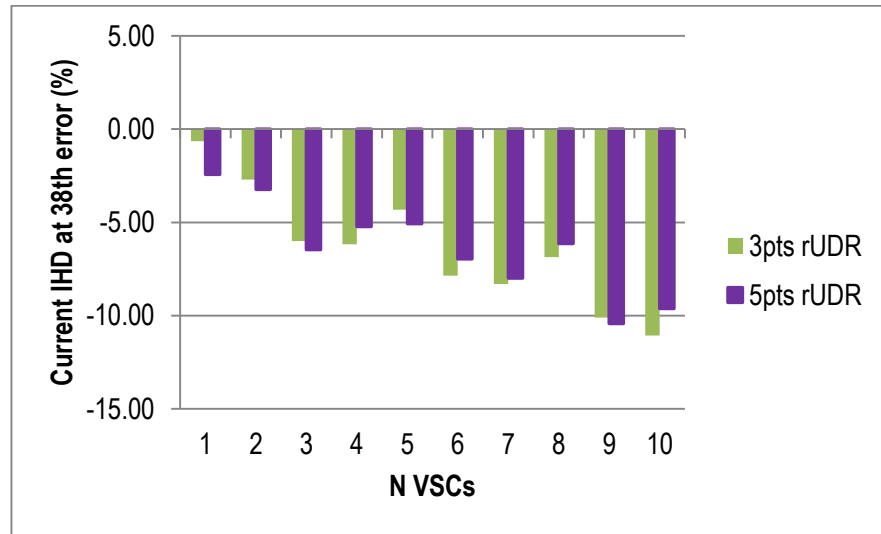


Fig. 7.30: Percentage error in predicted I_{IHD_38} using 3pts and 5pts UDR.

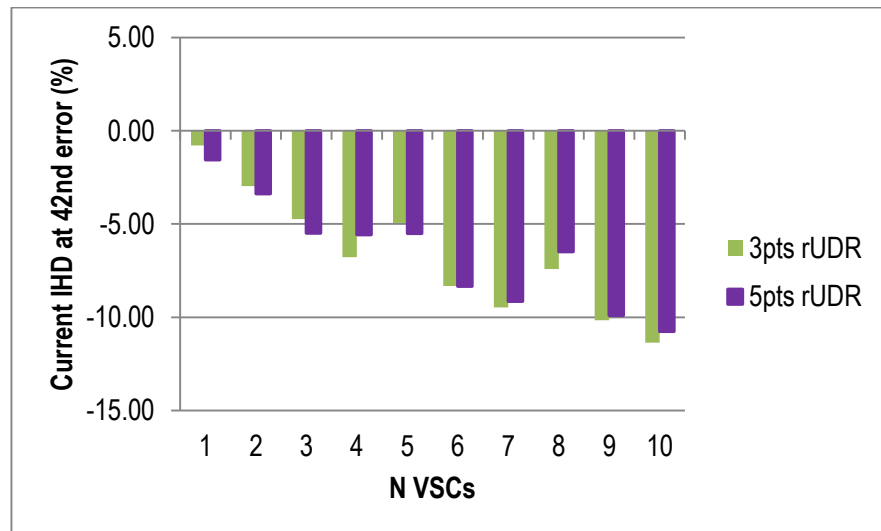


Fig. 7.31: Percentage error in predicted I_{IHD_42} using 3pts and 5pts UDR.

The predicted current harmonic distortion levels errors presented in Fig. 7.29 - Fig. 7.31, shows the maximum percentage error to be an under-prediction of 12%.

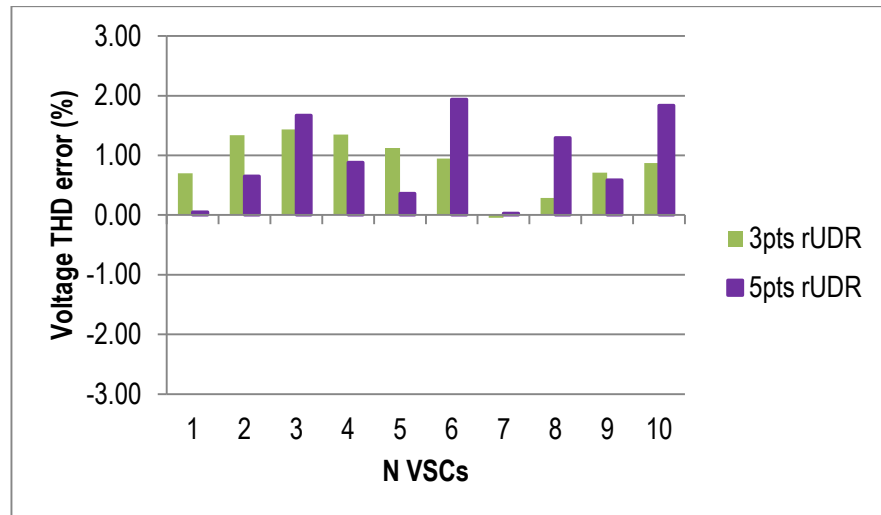


Fig. 7.32: Percentage error in predicted V_{THD} using 3pts and 5pts UDR.

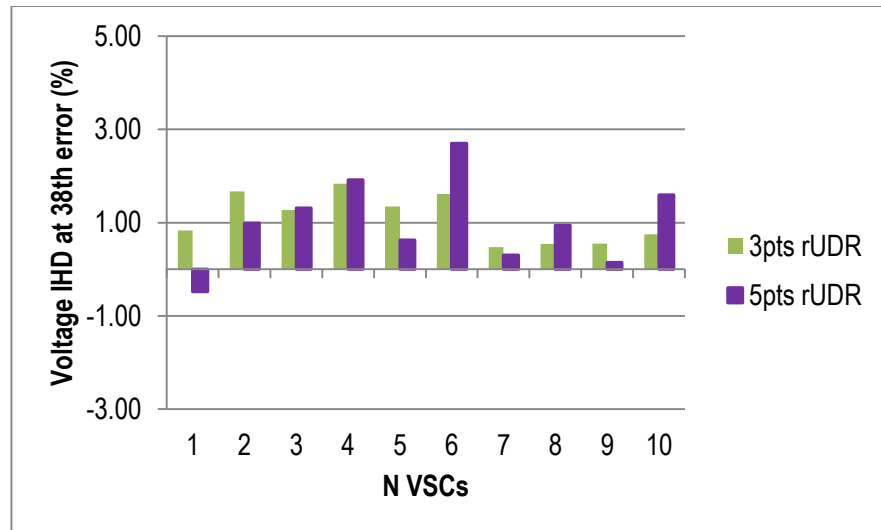


Fig. 7.33: Percentage error in predicted $V_{IHD_{38}}$ using 3pts and 5pts UDR.

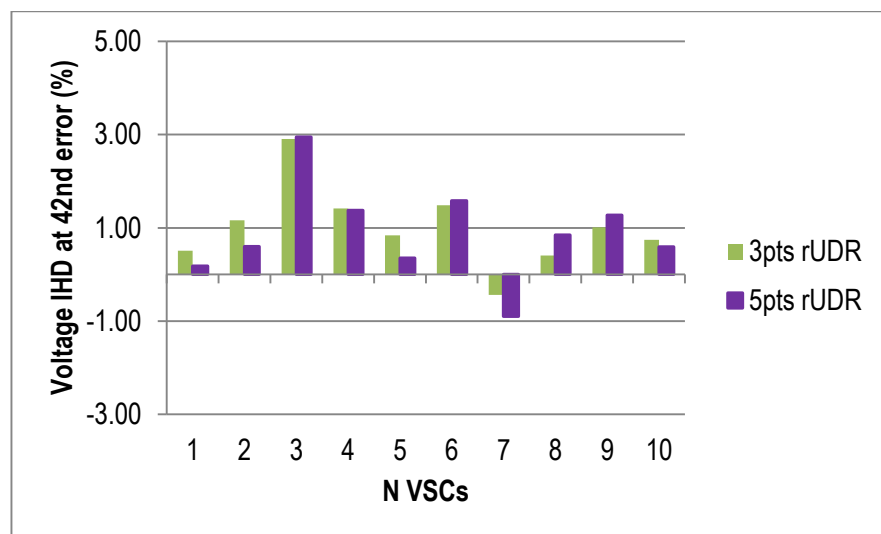


Fig. 7.34: Percentage error in predicted $V_{IHD_{42}}$ using 3pts and 5pts UDR.

Fig. 7.32 - Fig. 7.36 show that the UDR predicted voltage harmonic distortion levels had a maximum error of 3% which was an over-prediction in the V_{IHD} at the 42nd order for 3 VSCs (see Fig. 7.34). The predicted Standard deviation values of the harmonic distortion levels can be seen in Appendix C.2.

7.5 Case Study 4: Microgrid System containing 20 VSCs with Power Variation

This study aims to further emphasize the ability of the UDR technique in handling large number of random variables (in this case; VSCs with variable power output). The previous case studies had a maximum of 10 VSCs utilized in the microgrid model however, in this case study the output power of 20 VSCs will be varied and the harmonic distortion level predicted by the UDR technique. The modelled microgrid VSCs are all realistic switching VSCs models and no assumptions were introduced to modify or simplify the VSC or microgrid structure. For this case the MCS approach was unfeasible as the MCS approach failed because of computational burden. The utilized desktop computer; a windows 7, Intel Core 2 Quad CPU 64-bit operating system with 8GB installed memory RAM was unable to run the simulation because of the magnitude of data to be stored and processed.

7.5.1 Predicted Result and Discussion

Table 7.8: Predicted Current and Voltage Harmonic Distortion Level Using 3pts, 5pts and 7pts UDR for 20 VSCs Variable Power Output

	3pts rUDR	5pts rUDR	7pts rUDR
I_{THD} Mean	1.30	1.10	1.10
I_{IHD} 38th Mean	0.99	1.00	0.99
I_{IHD} 42nd Mean	0.69	0.70	0.69
V_{THD} Mean	6.03	6.02	6.03
V_{IHD} 38th Mean	4.62	4.64	4.65
V_{IHD} 42nd Mean	3.59	3.59	3.58
I_{THD} Std	0.080	0.080	0.070
I_{IHD} 38th Std	0.036	0.040	0.041
I_{IHD} 42nd Std	0.022	0.026	0.021
V_{THD} Std	0.037	0.058	0.056
V_{IHD} 38th Std	0.040	0.023	0.014
V_{IHD} 42nd Std	0.030	0.035	0.043

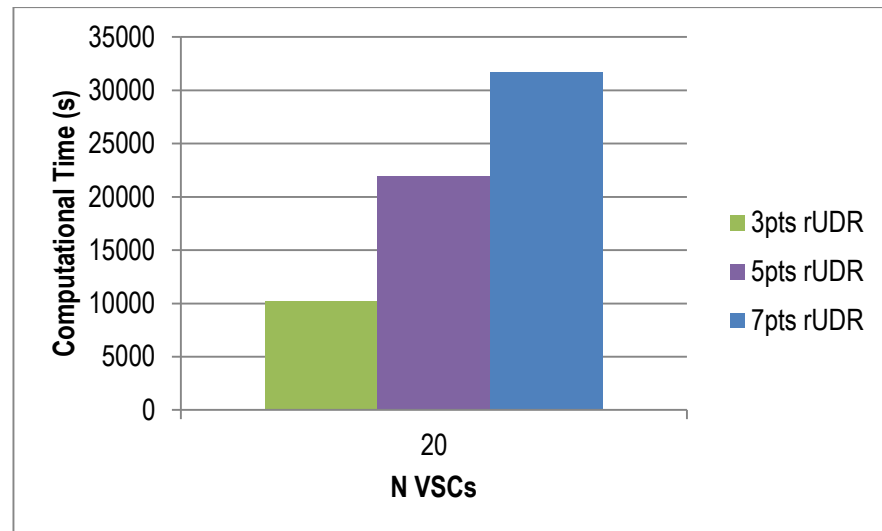


Fig. 7.35: Computation Time for the UDR Technique

Fig. 7.35 shows the computation time utilized by the 3pts, 5pts and 7pts UDR respectively.

Fig. 7.36 and Fig. 7.37 show that the 3pts, 5pts and 7pts approximated UDR technique all have very similar results in the predicted current and voltage THD mean values. However, there were clear differences in the predicted standard deviation values, especially for the voltage and this can be seen in Fig. 7.39.

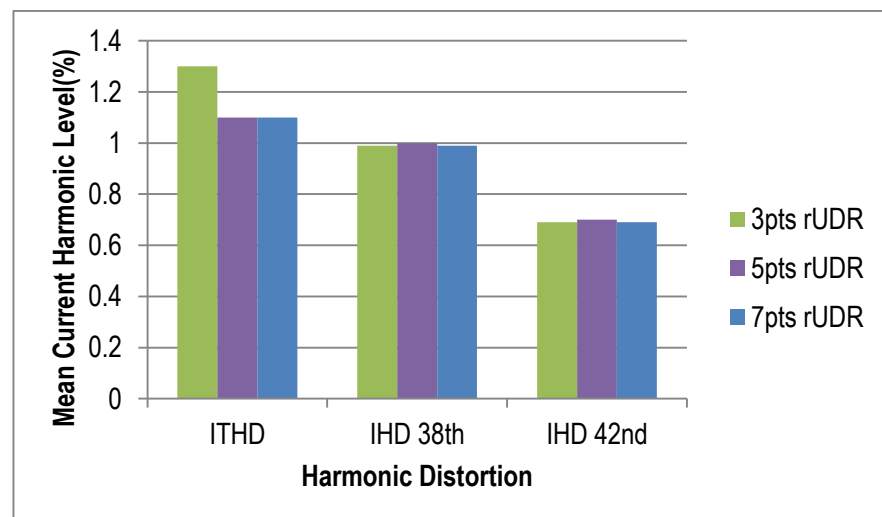


Fig. 7.36: Predicted Mean Current Distortion Level using the 3pts, 5pts and 7pts UDR.

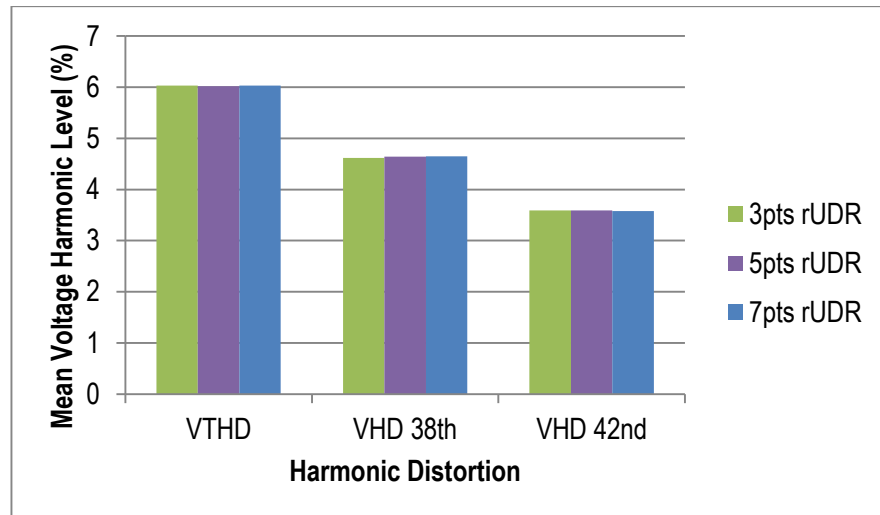


Fig. 7.37: Predicted Mean Voltage Distortion Level using the 3pts, 5pts and 7pts UDR.

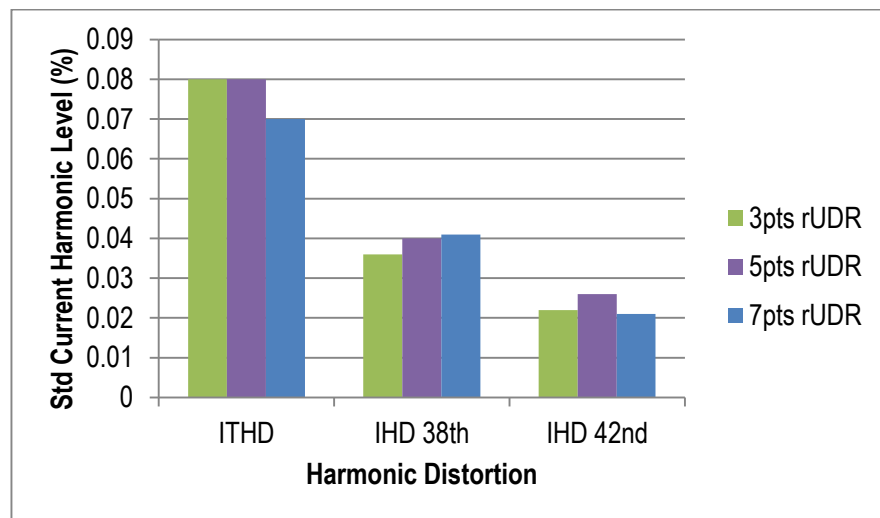


Fig. 7.38: Predicted standard deviation Current distortion levels using the 3pts, 5pts and 7pts UDR.

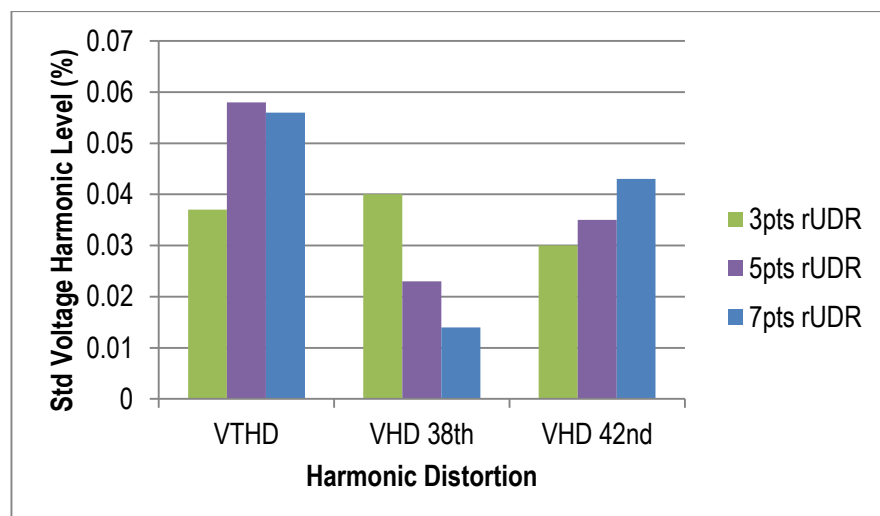


Fig. 7.39: Predicted standard deviation Voltage distortion levels using the 3pts, 5pts and 7pts UDR.

The predicted results of the 3pts, 5pts and 7pts approximations of the UDR technique can be accepted as accurate since earlier studies had shown a good agreement between the UDR results and the MCS results. As earlier stated the MCS cannot be used as a benchmark in this case because of the computational burden associated with the MCS for a microgrid containing large numbers of VSCs. This renders the 20-VSC based microgrid model inoperable by the computer as the computer runs out of memory therefore, the 7pts UDR was introduced to further validate the results obtained by the 3pts and 5pts UDR method.

From the presented results in Fig. 7.36 - Fig. 7.39 and Table 7.8 it is clear that the UDR technique can be used to predict harmonic distortion levels of a large number of VSCs in a microgrid where the MCS is unfeasible.

7.6 Case Study 5: Microgrid System with Other Non-Linear Loads

Non-linear loads such as Adjustable Speed Drives (ASDs), fluorescent light, computers and laptops are commonly used in modern day EPS. Hence a microgrid system containing VSCs as well as other non-linear loads would be modelled and investigated. The UDR technique performance would then be evaluated under this microgrid structure. Fig. 7.40 shows the modelled non-linear load circuit of a diode rectifier used in an adjustable speed drive and Appendix C.3 shows the PLECS circuit diagram of the modelled microgrid structure.

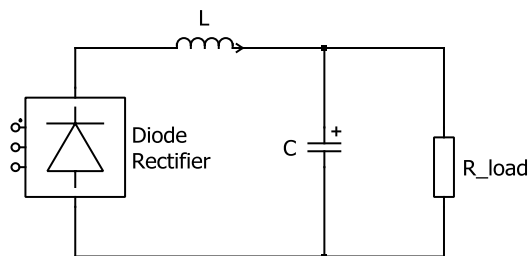


Fig. 7.40: Diode Rectifier Non-Linear Load Model

7.6.1 Predicted Result and Discussion

Table 7.9: Predicted Harmonic Distortion Level Using MCS, 3pts and 5pts UDR for a Microgrid with Non-linear Loads

I_{THD}	N VSCs	MCS	3pts rUDR	5pts rUDR
	Mean	3.54	3.39	3.28
	Std	0.43	0.46	0.33
I_{IHD} 5th	N VSCs	MCS	3pts rUDR	5pts rUDR
	Mean	3.06	3.00	2.97
	Std	0.38	0.45	0.34
I_{IHD} 7th	N VSCs	MCS	3pts rUDR	5pts rUDR
	Mean	1.23	1.17	1.11
	Std	0.15	0.11	0.03
I_{IHD} 11th	N VSCs	MCS	3pts rUDR	5pts rUDR
	Mean	0.72	0.73	0.77
	Std	0.10	0.06	0.04
I_{IHD} 38th	N VSCs	MCS	3pts rUDR	5pts rUDR
	Mean	0.58	0.55	0.54
	Std	0.07	0.07	0.06
I_{IHD} 42nd	N VSCs	MCS	3pts rUDR	5pts rUDR
	Mean	0.37	0.35	0.34
	Std	0.04	0.04	0.03
V_{THD}	N VSCs	MCS	3pts rUDR	5pts rUDR
	Mean	2.91	2.92	2.88
	Std	0.03	0.02	0.02
V_{IHD} 5th	N VSCs	MCS	3pts rUDR	5pts rUDR
	Mean	1.24	1.28	1.29
	Std	0.04	0.04	0.07
V_{IHD} 7th	N VSCs	MCS	3pts rUDR	5pts rUDR
	Mean	0.69	0.67	0.63
	Std	0.04	0.02	0.06
V_{IHD} 11th	N VSCs	MCS	3pts rUDR	5pts rUDR
	Mean	0.64	0.61	0.60
	Std	0.04	0.05	0.05

V_{IHD} 38th	N VSCs	MCS	3pts rUDR	5pts rUDR
	Mean	1.77	1.77	1.77
	Std	0.02	0.02	0.01
<hr/>				
V_{IHD} 42nd	N VSCs	MCS	3pts rUDR	5pts rUDR
	Mean	1.25	1.25	1.25
	Std	0.01	0.01	0.01

Table 7.9 gives the UDR predicted harmonic distortion levels of the microgrid. The predicted results include the 5th, 7th and 11th harmonic orders. It is necessary to include this in the results as non-linear loads are known to generate these harmonic orders. The 3rd, 6th, and 9th harmonic orders were not included as this is a balanced 3 phase system and triplen harmonics are expected to cancel out. It is clear from the results in Table 7.9 that the 3pts and 5pts UDR have a good agreement with the mean and Std values of the MCS approach.

Fig. 7.41 - Fig. 7.48 gives a graphical illustration of the accuracy of the UDR technique in predicting harmonic distortion levels of VSCs in a microgrid.

Table 7.10: Computation Time

	Prediction Methods		
	MCS	3pts rUDR	5pts rUDR
Computation Time (s)	73394	2584	4572
Computation Time Saved (%)	-	96.47	93.77

Table 7.10 shows the computation time saved by the 3pts and 5pts UDR with respect to the MCS approach.

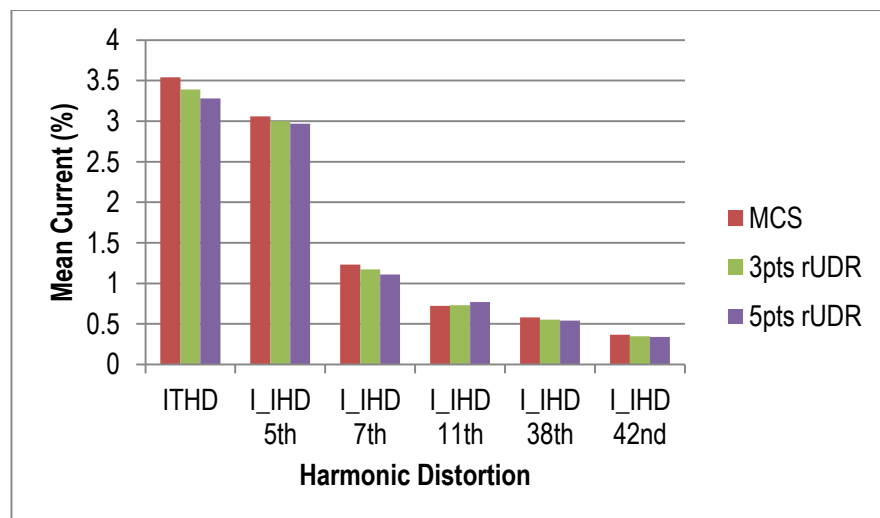


Fig. 7.41: Predicted Mean I_{THD} and I_{IHD_n} using MCS, 3pts and 5pts UDR.

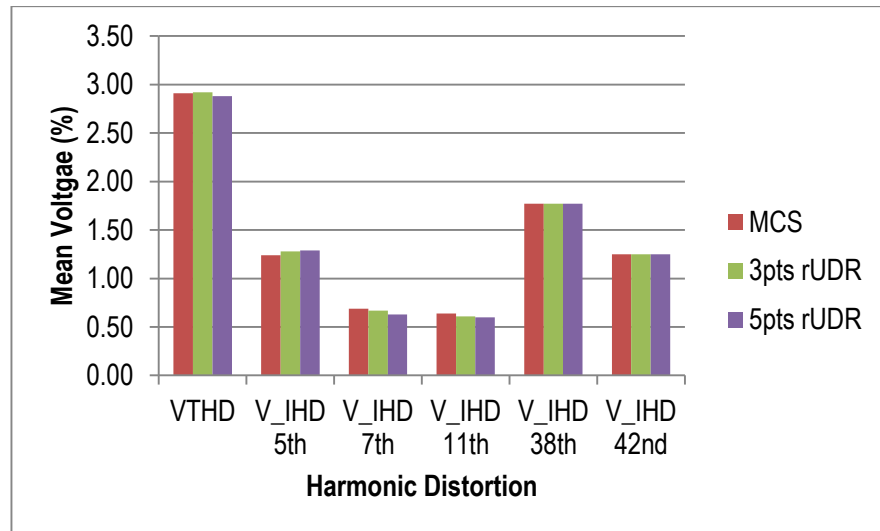


Fig. 7.42: Predicted Mean V_{THD} and V_{IHDn} using MCS, 3pts and 5pts UDR.

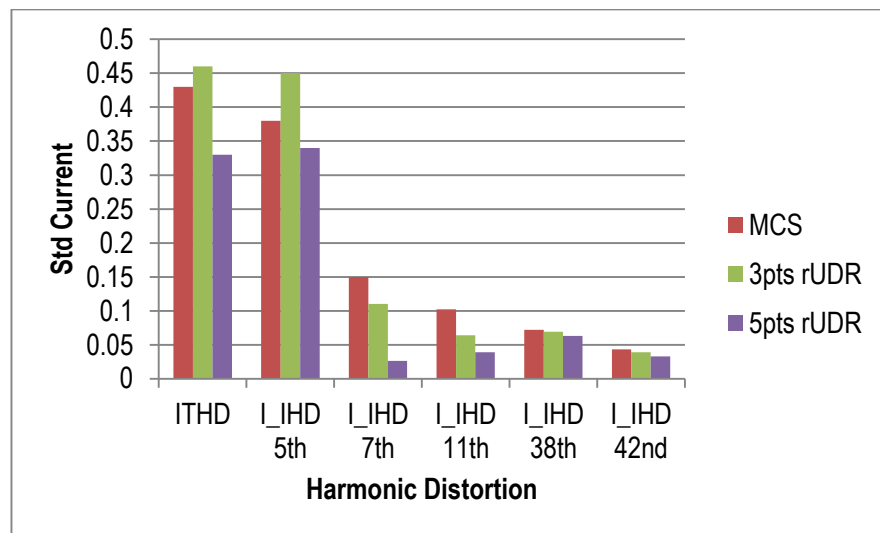


Fig. 7.43: Predicted Std of I_{THD} and I_{IHDn} using MCS, 3pts and 5pts UDR.

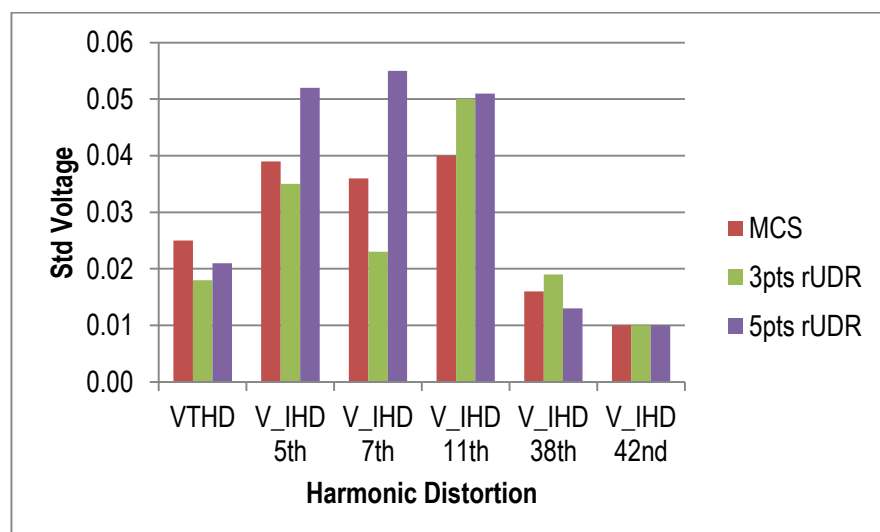


Fig. 7.44: Predicted Std of V_{THD} and V_{IHDn} using MCS, 3pts 5pts UDR.

Percentage error of Predicted Results

Appendix C.4 presents a table that shows the exact percentage error values of the predicted current and voltage harmonic distortion level using 3pts and 5pts UDR for the microgrid with non-linear loads.

The percentage error for the harmonic distortion level mean values are within acceptable error limits as none exceeded $\pm 10\%$ error as compared to the MCS. Higher percentage errors were observed in the predicted standard deviation values however, most of these were within acceptable limits with one exception. The case of Fig. 7.47 I_{IHD} at the 7th harmonic order where the 5pts UDR had an 80% under-estimation of the Std values as compared to the MCS approach.

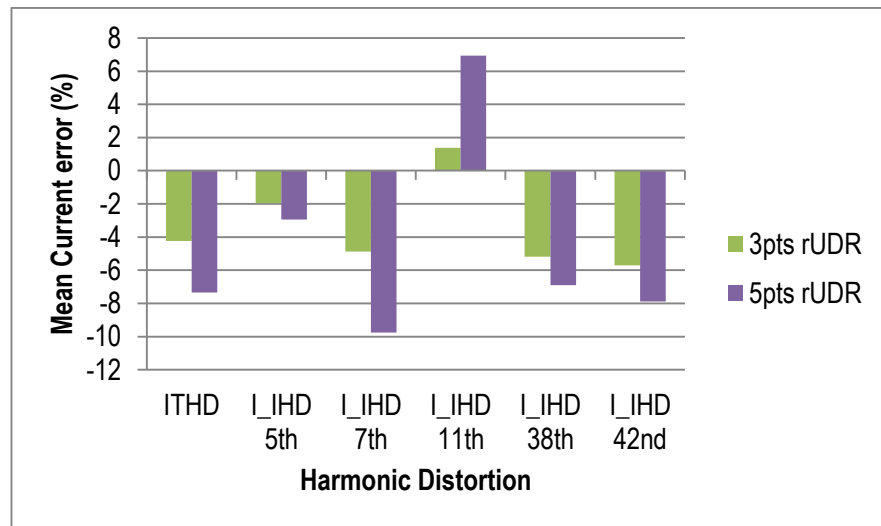


Fig. 7.45: Percentage error in Mean I_{THD} and I_{IHDn} using 3pts and 5pts UDR.

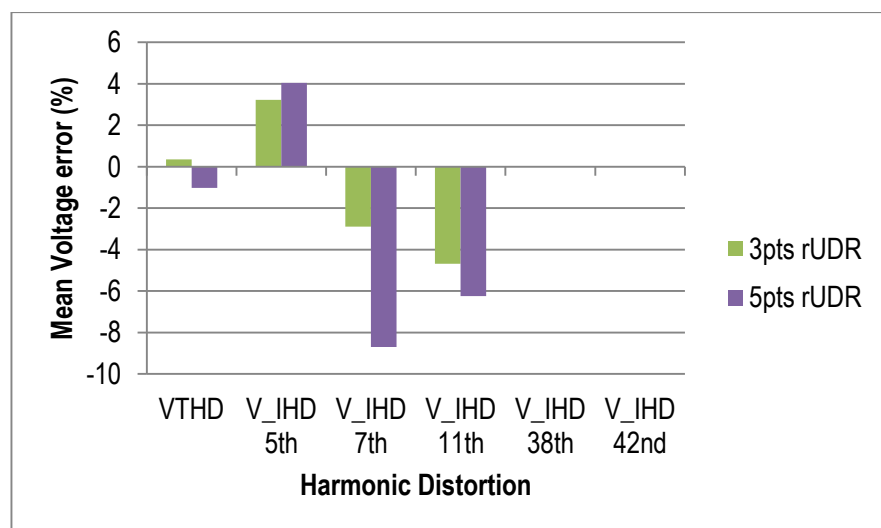


Fig. 7.46: Percentage error in Mean V_{THD} and V_{IHDn} using 3pts and 5pts UDR.

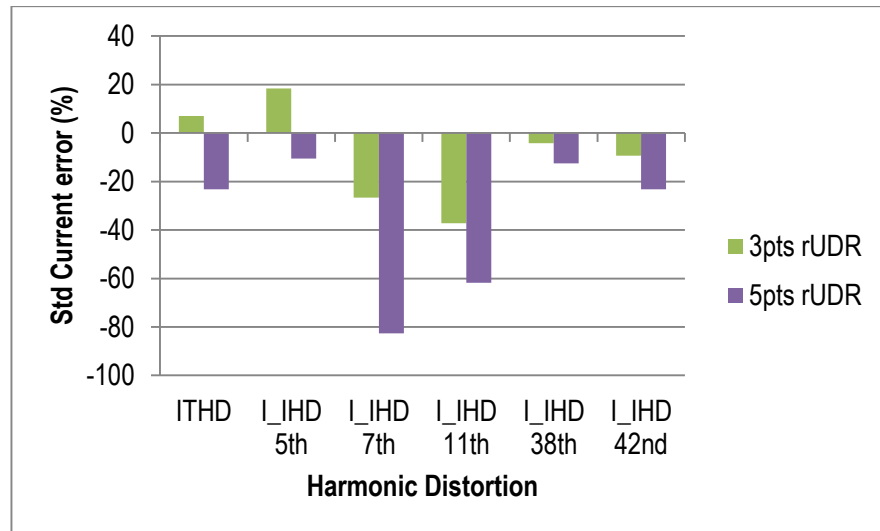


Fig. 7.47: Percentage error in Std of I_{THD} and I_{IHDn} using 3pts and 5pts UDR.

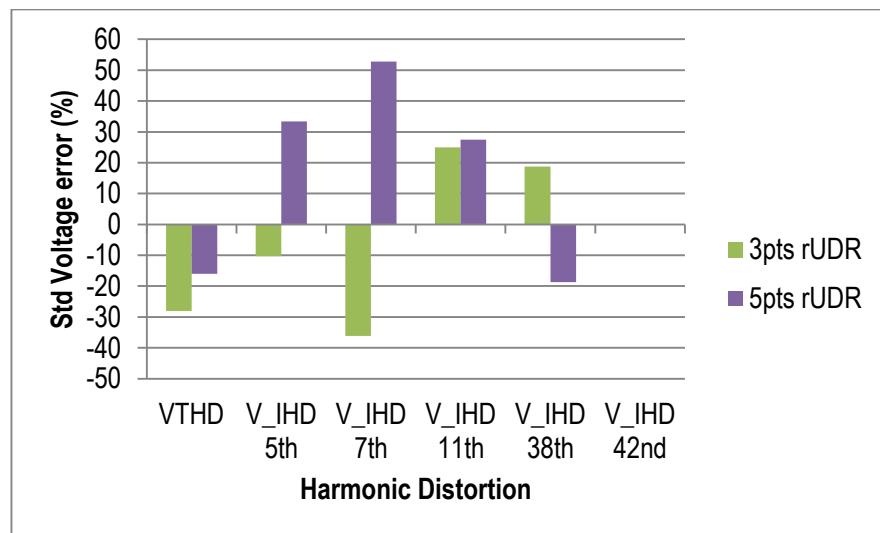


Fig. 7.48: Percentage error in Std of V_{THD} and V_{IHDn} using 3pts and 5pts UDR.

No error was recorded in the mean value of V_{IHD} at the 38th and 42nd order in Fig. 7.46 and the Std values of V_{IHD} at the 42nd order in Fig. 7.48. This confirms that the 3pts and 5pts UDR predicted the same values as the MCS approach.

7.7 Summary

The UDR method was able to accurately predict the mean THD and IHDn using fewer number of evaluations and computational time than the MCS. Majority of the predicted harmonic distortion levels showed that the UDR technique have a good agreement with the MCS approach. Considering the amount of computational time saved by the UDR, it can be used as an alternative to the

MCS in predicting harmonic distortion levels and to evaluate the PQ of a microgrid containing large number of VSCs when there are uncertainties in the EPS or the VSCs.

Despite the effectiveness of the UDR in predicting the mean harmonic distortion values of the VSCs, it sometimes gives less accurate predictions of the standard deviation value. It is important to state that different uncertainties respond differently to the harmonic distortion levels of the VSCs and this affects the prediction ability of the UDR. Some of the important observations in this chapter and the UDR technique as regards the impact of harmonics and uncertainties on the PQ of the microgrid include:

- Under power variations it was observed that the increase of the number of VSCs and the net power at the PCC causes a decrease in the I_{THD} . The I_{THD} reduces and increases in direct relation with the net power at the PCC.
- For the case of the filter variation and system impedance variation, the harmonic distortion does not follow a direct linear relationship on the values of the filter/system parameters. In this case an increase in filter inductor value would generally reduce current harmonic distortion levels but a very large inductor value above the system parameter (power, AC and DC voltage, switching frequency) ratings and this will introduce instability in the EPS and an increase in current harmonics. A similar situation arises with the reduction of the filter inductor value and the case of the system impedance variation.
- For small numbers of VSCs the UDR has a good prediction for such uncertainties (filter/impedance variation) with a non-linear relationship with harmonic distortion levels. However in this type of cases, as the number of VSCs increases the prediction performance of the UDR beyond the mean harmonic values becomes less accurate. Notwithstanding, the UDR always have a close agreement with the MCS result in terms of the mean harmonic distortion values which is necessary in determining harmonic limits.

- The UDR technique accurately predicts harmonic distortion levels of many VSCs in a microgrid system containing linear and non-linear loads.

These studies show that the UDR technique can be applied as an effective tool for predicting harmonic distortions in modern day EPSs. It also presents itself as a method that can be used by utility companies/design engineers in the choice of parameters since the effect of real world uncertainties possible in the microgrid are being taken into account, providing possible outcomes of variation of design parameter/system characteristics on the generated harmonics of a microgrid containing a number of VSCs.

Chapter 8

Experimental Validation of the UDR Technique for Harmonic Prediction

In this chapter, several experiments are conducted to validate the performance of the Univariate Dimension Reduction (UDR) technique in predicting harmonic distortion levels of a number of VSCs in a practical microgrid. Random power values of uniform and Gaussian distributions are generated and fed into the VSCs and the resulting harmonic distortions predicted.

8.1 Objective and Procedure

The aim of this experiment is to validate the efficiency of the UDR technique in predicting the harmonic distortion of VSCs in the presence of uncertainty for a small Electrical Power System (EPS).

The experiment entails randomly varying certain parameters (such as power) within a given constraint. Firstly, pseudorandom power values were generated using a PC, then these values are inputted into the VSCs to emulate the Monte Carlo Simulation (MCS) approach. The corresponding harmonic distortion of the current and voltage are recorded for every power value and the recorded data are analysed to obtain the statistical moments.

The generated power mean value, range and standard deviation of the individual VSCs are then used to generate the sigma points and corresponding weight for the UDR method. The generated sigma points which represent the specific reference power value required for the implementation of the dimension reduction techniques are inputted into the VSCs. The corresponding harmonic distortion of the current and voltage are recorded for each specified power value. The recorded harmonic distortions are scaled using the generated weights and the final results predicted. Lastly, the UDR predicted results are then compared with the MCS approach.

The experiment was conducted using the microgrid set-up at the Flexelec lab, Energy Technology Building, University of Nottingham, UK.

8.2 Structure of Microgrid Lab

Fig. 8.1 shows the schematic of the laboratory setup. The experiment is conducted using 3 VSCs (see Fig. 8.2), a programmable power/voltage supply (Fig. 8.3) as the microgrid source, current and voltage measuring device (see Fig. 8.4) and 3 isolating transformers.

The 3 VSCs are connected in parallel, and supplied from the mains through a 3 phase distribution line and a transformer. The VSCs are isolated by the use of 3 Transformers at the grid side of the VSC and connected to the grid side of the programmable power/voltage supply (Microgrid Source).

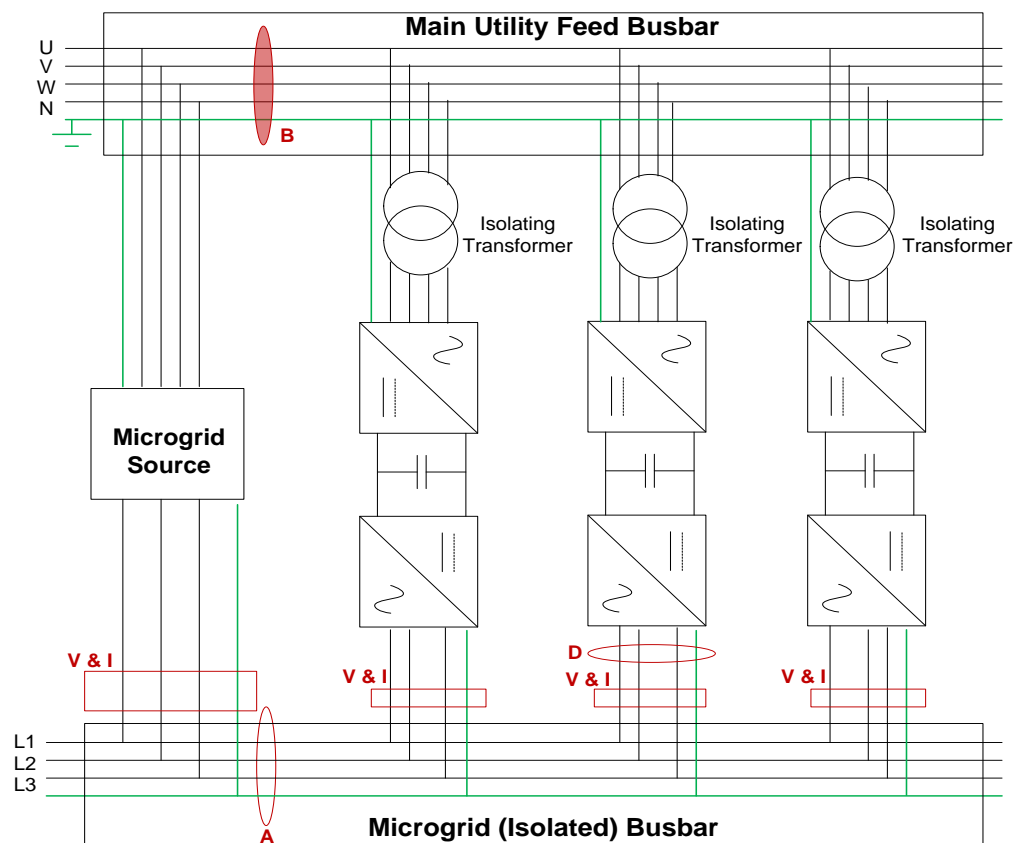


Fig. 8.1: Schematic of the Microgrid Laboratory Set-up

The isolating transformers are necessary to protect the equipment and also to prevent short circuit. The main utility feed represents the grid so the VSCs are operating in the grid tied mode. The voltage and current measurements was done

with Labview on a CompactRIO using NI-9227 and NI-9225 units, the current is passed through 100:5 CT's prior to feeding it into the measuring blocks. The time taken to conduct the practical is presented below (see Table 8.2).

Table 8.1: Microgrid and VSC Laboratory Parameters

VSC Parameter	Rated Power, P	12.5 kW
	Rated line Voltage	415V
	Rated Current	32A
	VSC Topology	3_phase 2 Level VSC
	VSC Filter Configuration	LCL Filter
Microgrid Network	Mains Line Voltage Current	415V Fuse 20A
Microgrid Source (Programmable Power/Voltage Supply)	Rated Power Rated Voltage Rated Current Fuse Rating	90kW 1000V 300A 125A
Statistical Power Variation	Uniform Power Variation	Range = 2.5kW - 10.0kW Mean = 6.25kW
	Normal Power Variation	Mean = 3.44kW Std = 2.02

Table 8.2: Approximate Time Utilized by Microgrid to Conduct Practical

	Case 1			Case 2	
	MCS	UDR 3pts	UDR 5pts	MCS	UDR 5pts
Time (s)	21600	600	2700	24200	2850
Time Saved (%)	-	97	88	-	88



Fig. 8.2: Three VSCs and the Low Voltage Busbar



Fig. 8.3: Triphase Programmable Power/Voltage Supply (Microgrid Source)

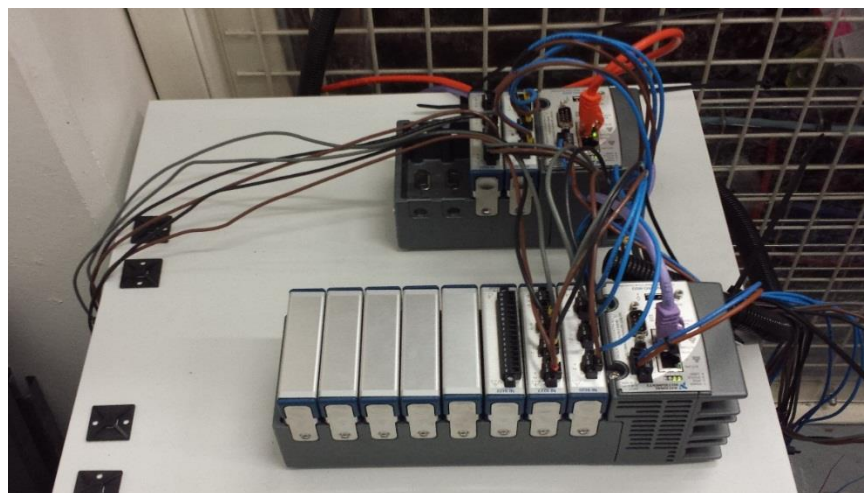


Fig. 8.4: Current and Voltage Measuring Blocks

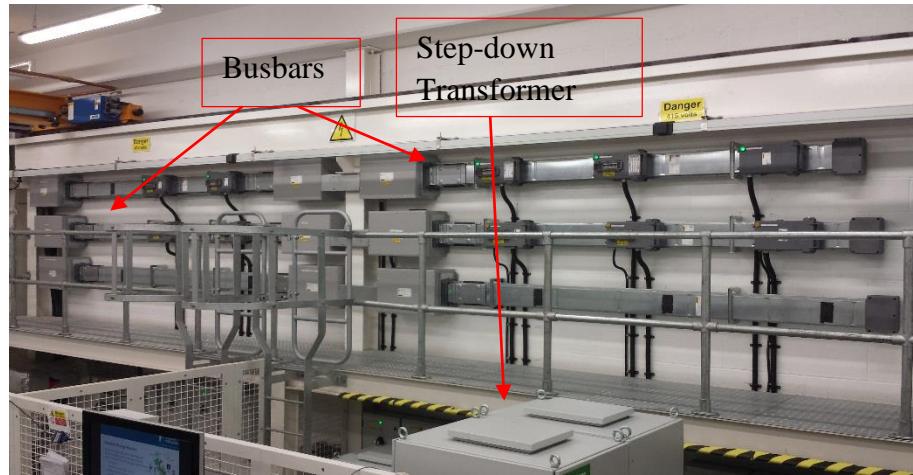


Fig. 8.5: Busbars and Transformer

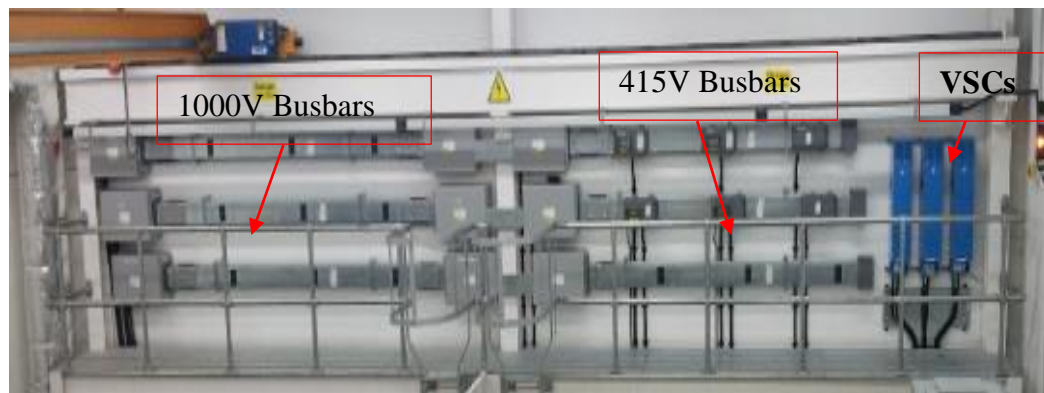


Fig. 8.6: 1000V/415V Busbar and Three VSCs

8.3 Case Study 1 – Prediction of VSCs Harmonics under Uniform Power Variation

The variation of output power have been earlier shown to affect THD. This study aims to predict the net harmonics of 3 VSCs in a case where the output power uniformly varies randomly and independently (range: 2.5kW – 10.0kW).

The VSCs were first varied with thousands of random power input value to imitate the MCS approach. The net harmonics are then measured and recorded. Then using the distribution's statistical information like the range, mean and standard deviation, the UDR is applied to generate the sigma points and weights. The generated sigma points are then fed into the VSCs as the power inputs and the net harmonics measured at point B (in Fig. 8.1). The results of the MCS-type approach and the UDR are then statistically analysed and compared to measure the efficiency of the UDR technique.

Table 8.3 - Table 8.4 and Fig. 8.7 - Fig. 8.10 gives the obtained experiment results.

Table 8.3: Laboratory Results Showing Predicted Moments of I_{THD} and V_{THD} using MCS and 3pts UDR

	I_{THD}		V_{THD}	
	Mean	Std	Mean	Std
MCS	4.46	1.44	1.93	0.52
UDR	4.84	1.11	1.94	0.22
Error (%)	8.52	-22.9	0.52	-57.7
Diff	0.38	-0.33	0.01	-0.30

Table 8.3 show a close agreement between the MCS and the UDR mean value results. The standard deviation values for the V_{THD} was 57% under-predicted as compared to the MCS approach.

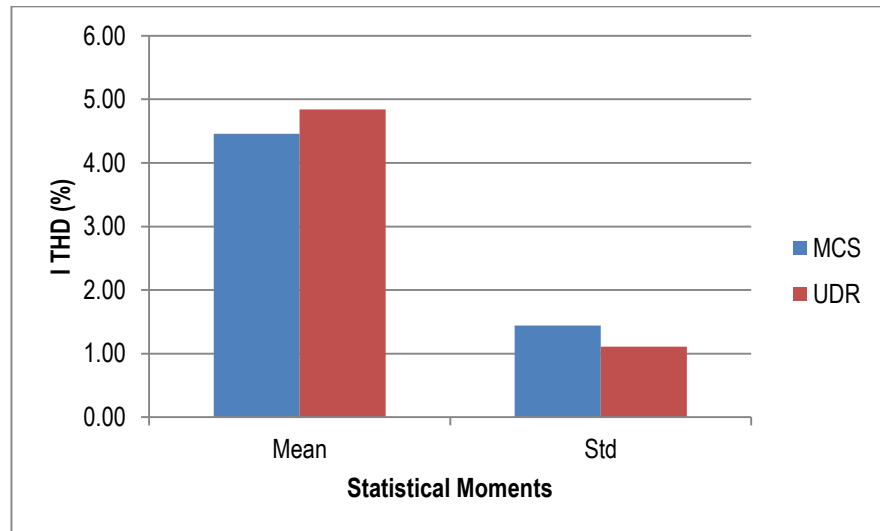


Fig. 8.7: Laboratory Results of I_{THD} Predicted Statistical Moments (3pts UDR).

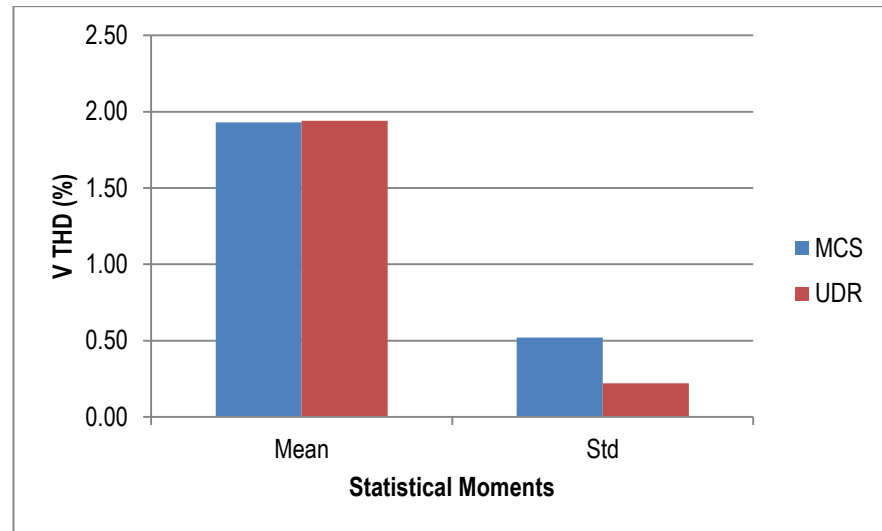


Fig. 8.8: Laboratory Results of V_{THD} Predicted Statistical Moments (3pts UDR).

Fig. 8.7 and Fig. 8.8 shows the obtained statistical moments of the I_{THD} and V_{THD} respectively using 3pts UDR.

Table 8.4: Laboratory Results Showing Predicted Moments of I_{THD} and V_{THD} using MCS and 5pts UDR

	I_{THD}		V_{THD}	
	Mean	Std	Mean	Std
MCS	4.46	1.44	1.93	0.52
UDR	5.07	1.67	2.06	0.60
Error (%)	13.68	15.97	6.74	15.38
Diff	0.61	0.23	0.13	0.08

Table 8.4 shows the laboratory results of the obtained statistical moments of I_{THD} and V_{THD} . It is clear from Table 8.4 that a better prediction of the mean and standard deviation were obtained as it had less percentage errors than the 3pts UDR.

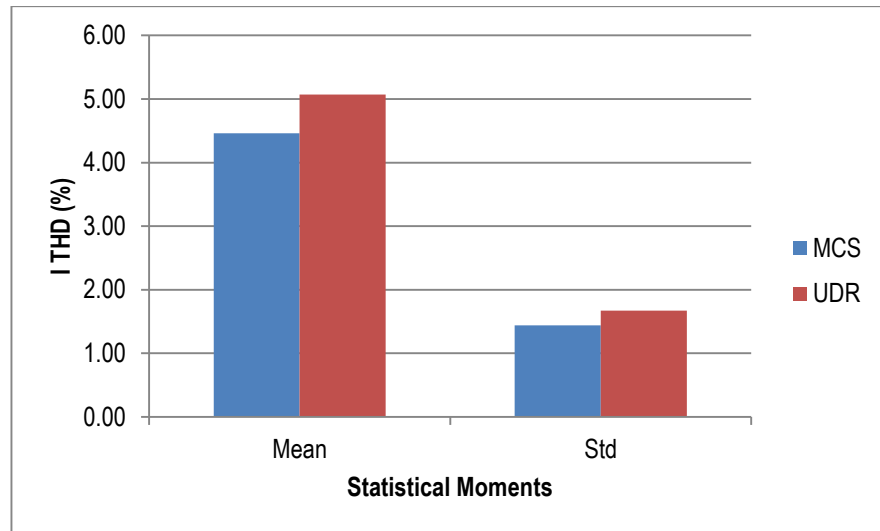


Fig. 8.9: Laboratory Results of I_{THD} Predicted Statistical Moments (5pts UDR).

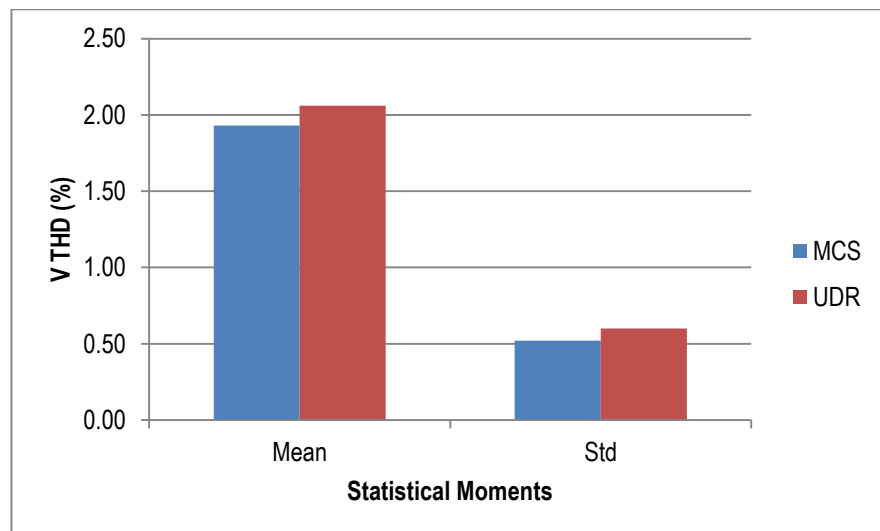


Fig. 8.10: Laboratory Results of V_{THD} Predicted Statistical Moments (5pts UDR).

Fig. 8.9 and Fig. 8.10 shows the obtained mean and standard deviation of I_{THD} and V_{THD} respectively using the 5pts UDR.

8.4 Case Study 2 - Prediction of VSCs Harmonics under Gaussian (Normal) Power Variation

Case study 2 entails predicting the net harmonics of the 3 VSCs in a case where the output power varies randomly following a Gaussian distribution (mean value = 3.44kW and Std = 2.02e+3). Just as in case1 the VSCs power was varied with thousands of random power inputs to mimic the MCS approach. The statistical

formation of the distribution is recorded and the THD measured. Then the 5pts UDR sigma points and weights were generated and inputted to evaluate the performance of the UDR technique using the MCS as a benchmark.

Table 8.5: Laboratory Results Showing Predicted Moments of I_{THD} and V_{THD} using MCS and 5pts UDR Normal Variation

	I_{THD}		V_{THD}	
	Mean	Std	Mean	Std
MCS	4.61	1.62	1.95	0.51
UDR	4.72	1.19	2.25	0.54
Error (%)	2.39	-26.54	15.38	5.88
Diff	0.11	-0.43	0.30	0.03

Table 8.5 show a good match between the UDR and the MCS mean and standard deviation values for I_{THD} and V_{THD} . The UDR under predicted the standard deviation of the I_{THD} by 26%.

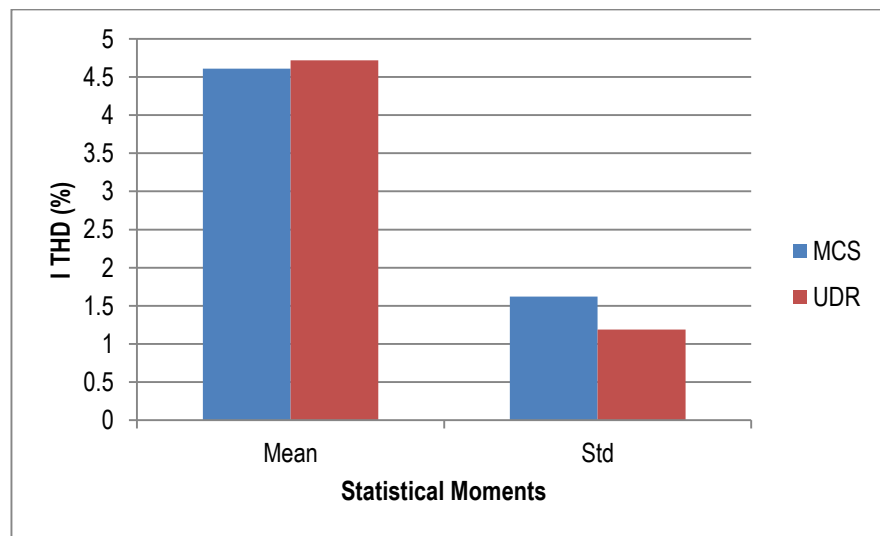


Fig. 8.11: Laboratory Results of I_{THD} Predicted Statistical Moments (5pts UDR Normal).

Fig. 8.11 and Fig. 8.12 shows the obtained statistical moments of the I_{THD} and V_{THD} respectively using 5pts UDR for a Gaussian distributed random variable (power).

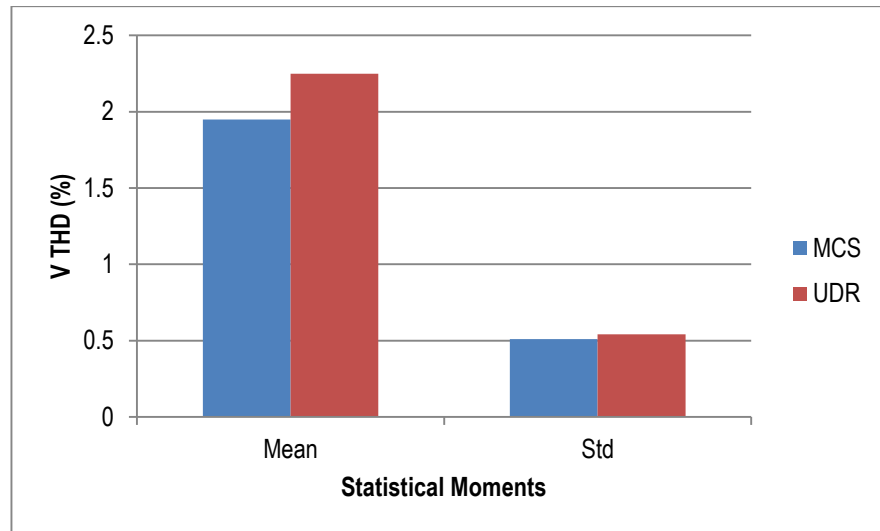


Fig. 8.12: Laboratory Results of V_{THD} Predicted Statistical Moments (5pts UDR Normal).

8.5 Summary

The laboratory results validate the use of the UDR technique in efficiently predicting harmonic distortion in a practical system where the configuration and operation characteristics are only known within certain limits. The UDR practical results gave a good match with the MCS approach results for the mean values and most of the standard deviation values of the I_{THD} and V_{THD} .

This shows that the UDR technique can be used as a predictive tool in analysing practical VSC system's harmonics before commissioning and during operation of an EPS. The UDR gives an accurate statistical measure of the harmonic distortion level in a VSC based RES or microgrid and this is achievable in quick time as compared to other measures. The ability of the UDR in predicting harmonics gives an assessment of the quality of power in the microgrid.

Chapter 9

Conclusion

This chapter summarizes the results and findings of this research. It also examines how the research objectives were achieved. Some of the limitations/challenges faced during the research are discussed and possible areas for further research are also stated.

9.1 Power Quality in a Microgrid

Technological advancements and the increased penetration of renewable energy generation systems in modern day power systems have prompted the research community to develop new concepts like smart grids and microgrids to define such configurations.

Microgrids defined earlier in Chapter 1 optimizes the use of RES such as wind turbines and photovoltaics which are usually interfaced to the electrical network by the use of power electronic converters [3]. In recent times, a class of converters that is commonly used are the Voltage Source Converters (VSCs). Despite their better controllability and fast switching responses, it was discovered that the VSCs produce harmonic voltages and currents which can cause equipment/systems malfunction or damage as seen in Chapter 3.

With more RES VSCs connected to the microgrid, it becomes more significant to analyse the cumulative effect of the VSCs harmonics on the power quality of the microgrid. This analysis however becomes more difficult as the non-linear fashion of harmonics makes simple arithmetic summation give a wrong estimate of the net harmonics at a node, necessitating the need for probabilistic harmonic summation methods.

Probabilistic harmonic methods such as the Monte Carlo Simulation (MCS) approach requires a large amount of computational effort and time in predicting/analysing the VSCs harmonics especially in systems containing a large number of VSCs. While other analytical harmonic summation methods

require complex mathematics and several assumptions (that are not necessarily obtainable) used to simplify the EPS in predicting the net harmonic distortion level. These methods were discussed in Chapter 5.

The drawback of the MCS and the assumptions of the analytical harmonic methods have been driving research aimed at developing alternative fast methods that can accurately predict/quantify harmonic distortion levels of harmonic sources/loads such as VSCs.

An efficient method for predicting harmonics of VSCs in a microgrid should entail;

- Good level of accuracy comparable to the MCS approach
- Significantly reduced computational time and burden than the MCS approach
- Accurate modelling of uncertainties in an EPS (in this case a microgrid)
- Applicability to practical EPS without requiring assumptions to simplify the EPS
- The method should also have the ability to give detailed representation of a realistic EPS.

These led to the following research objectives presented earlier in Chapter 1;

- i. To develop models of typical VSCs applied to various RES and microgrids using Matlab Simulink [13] and PLECS simulation tools [14].
- ii. To simulate and study the effects of VSC harmonics on the PQ of a microgrid.
- iii. To investigate the effects of factors such as switching frequency, converter topology, system impedance and other statistical variations on VSC harmonics in relation to the PQ of the microgrid.
- iv. To propose an efficient and fast harmonic prediction technique for probabilistic harmonic studies on a microgrid, with the aim of quantifying the impact of VSC harmonics on the PQ of the microgrid.
- v. To apply the proposed harmonic prediction technique to a practical microgrid system containing VSCs.

- vi. Propose some design approach to minimise the impact of VSC harmonic distortion on the PQ of the microgrid, by evaluating if the VSC harmonic distortions are within the required harmonic limits as stated by regulatory harmonic standards.

9.2 Factors that Affect Harmonic Distortion Levels of VSCs in a Microgrid

In order to properly understand the statistical nature of harmonics generated by VSCs, an investigation into the factors that affects the VSCs generated harmonics was carried out in Chapter 4. Typical VSCs utilized in integrating RES to the grid were simulated with suitable control and protection techniques incorporated into the VSCs and the microgrid to enable continuity of power supply. The VSCs were then connected to the grid and modelled using MatlabTM Simulink [13] and PLECSTM [14] simulation tools.

It was discovered that the generated harmonics of the VSC in an EPS was affected by design specification factors such as the converter topology, switching frequency and amplitude modulation. The type of filter and filter parameter values utilized in the EPS can also greatly affect the VSC's harmonics as this is the main form of attenuating harmonics generated by harmonic systems including VSCs. In addition to these, the microgrid/EPS characteristics or operating conditions such as the EPS line impedance, the EPS background voltage harmonic distortion or the output power of the VSCs can significantly affect the VSCs harmonics.

Some of these factors especially as regards the VSCs of RES are only known within certain constraints. RES such as wind turbines and photovoltaics are good examples to highlight this variability as their output power is dependent on wind speed profile and solar irradiance respectively. Whereby, uncertainties arise in the EPS as there are no guarantees of the amount of power the RES will generate. In addition, when a large number of RES VSCs are connected together such as in a microgrid, the cumulative harmonics generated by the VSCs becomes difficult to predict as individual VSC harmonics do not add up arithmetically.

This further drives the need for a statistical technique that can easily model these uncertainties while accurately predicting the level of harmonics that such uncertainty will have on the harmonics generated by the VSCs in the microgrid.

9.3 Dimension Reduction Techniques for Predicting Harmonic Distortion Levels of VSCs in a Microgrid

Following the success of the Unscented Transform (UT) method in solving statistical problems in very high frequencies classed as electromagnetic interference, the method was applied in Chapter 5 to predict the harmonic distortions at frequencies below 250 kHz of the VSCs. However, it was discovered that the UT method was disadvantaged in systems containing many random variables (for example; VSCs), as it suffers from the “curse of dimensionality” problem. In a nutshell, the number of evaluation points, computational time and burden greatly increases and exceeds the MCS approach as the number of VSCs increases.

This necessitated the use of dimension reduction techniques in Chapter 6 to drastically reduce the required evaluation points, computation burden and time required in a case containing a large number of VSCs. The dimension reduction technique works by additively decomposing an N -dimensional function involving n -dimensional integrals (which is required for a multivariate problem (many VSCs) using the UT tensor product) into a series sum of D -dimensional functions such that $D < N$. The technique is referred to as the Univariate Dimension Reduction (UDR) when $D = 1$ and Bivariate Dimension Reduction (BDR) when $D = 2$. The UDR and BDR were analysed and employed in predicting the harmonic distortion level of VSCs in a microgrid.

From the simulation results of various uncertainty and EPS configuration it was discovered that the UDR and BDR produced almost the same level of accuracy in predicting the mean and standard deviation values of the harmonic distortion at the Point of Common Coupling (PCC) to the EPS. However, the BDR gave better results for higher order moments.

The UDR was employed for further studies in Chapter 7 because of its significantly reduced computational burden and time as compared to the BDR technique. Another reason for employing the UDR is that, the harmonic mean values of an EPS or the VSCs are usually sufficient in determining if the EPS or VSC meets a harmonic standard limit, as most harmonic standards only specify a single value as the limit. In all cases the UDR technique gave reasonable accuracy in the prediction of harmonic distortion levels comparable to the MCS approach.

The efficiency of the UDR technique in a practical EPS (microgrid) was evaluated using 3 VSCs in Chapter 8. The practical was conducted at the Flexelec lab in the Energy Technology Building, The University of Nottingham. The 3 VSCs were operated with tens of thousands random power values for approximately 6 hours to emulate the MCS approach. The statistical data of the variability and the harmonic distortion results were then obtained and utilized to generate the evaluation points (sigma points) and weights for the UDR technique. The sigma points were applied to the 3 VSCs and the resulting harmonic distortion values were weighted to predict the harmonic distortion level of the 3 VSCs at the PCC to the grid. The 3pts UDR technique required only 11 evaluation points and took 10 minutes to predict the harmonic distortion level mean and standard deviation value which had a very close agreement with the MCS approach. The 5pts UDR was also utilized in the experiments.

The practical results proved that the UDR technique can be applied to realistic microgrids and EPS. It also gives a clear picture of the UDR performance as an efficient harmonic prediction tool that can be employed in probabilistic harmonic studies.

The ability of the UDR technique to effectively predict the level of harmonic distortion of the VSCs in a microgrid gives a means of determining the power quality in a microgrid since microgrids contains VSCs of RES that produce harmonics which affects power quality.

9.4 Research Contributions

The summary of the main contributions of this research work is reiterated as follows;

- vi. The identification of the characteristic responses of various factors that affects the harmonics generated by VSCs in a microgrid/EPS.
- vii. The application of the Unscented Transform method in predicting VSC harmonic distortion level.
- viii. The application of the univariate and bivariate dimensionally reduced Unscented Transform in predicting harmonic distortion levels of many connected VSCs in a microgrid/ EPS.
- ix. The application of a probabilistic harmonic summation method that can accommodate realistic microgrids/EPS without assumptions to simplify the microgrid/EPS. (The studied harmonic sources (VSCs) have full interactions with each other and the EPS, reflective of a realistic EPS.)
- x. The application of a probabilistic harmonic summation method that gives accurate and fast prediction of harmonic distortion levels of VSCs in a microgrid/EPS.

9.5 Possible Areas for Further Research Work

The suggestion of potential areas for further research work is given as follows;

9.5.1 Effect of Different Control Strategy and VSC Switching Pattern on VSCs Harmonic

From the review of literatures in this thesis it was discovered that the control technique and switching pattern employed for any VSC plays a part in the level of harmonic distortion that will be generated by the VSC. Although these factors do not vary during operation of an EPS it would have been relevant to investigate and include these as part of the factors that affects VSC harmonics.

In this research work regular Proportional Integral (PI) controllers were modelled and utilized but other microgrids might contain VSCs with Proportional Integral Differential (PID) controllers or Predictive Dead Beat (PDB) controllers. These controllers may be included to see the general effect of

different control strategy and to represent a more realistic microgrid (EPS). A microgrid with VSCs having different switching patterns was also not modelled and this can be modelled and investigated to represent a more practical microgrid.

9.5.2 Modelling of Microgrid System

The dimension reduction techniques can be applied on a more detailed microgrid model where, the generators and the renewable energy systems such as the wind turbines and photovoltaics, are modelled in detail. A detailed model should include models of the electrical generator for the wind turbine and the Maximum Power Point Tracking (MPPT) of solar panel for the photovoltaic. This research focused only on the converter models of the renewable energy systems.

9.5.3 Predicting other Power Quality Issues using Dimension Reduction Technique

The Dimension Reduction (DR) technique can be further explored to predict other power quality issues stated in [24] such as voltage/current imbalance, voltage sags, swells, interruptions and fluctuations in different EPS configuration, having not just VSCs but also other harmonic sources and loads. This is necessary as the modern day EPS sometimes experience these issues which might be of particular interest to the utility companies, design engineers, researchers or consumers. An assessment of these other PQ issues will give a more comprehensive information about the power quality in an EPS.

9.5.4 Experimental Validation

The experimental validation of the UDR technique principle was achieved using 3 identical VSCs, as at the time of carrying out the practical only 3 VSCs were available. This number can be considered small, as one of the main advantages of the UDR technique is its ability to handle systems containing many random variables (in this case VSCs). Thus, further research can be carried out to test the UDR technique principle on a larger number of VSCs (at least 10 VSCs) including VSCs that have different system rating, topology, and control technique.

References

- [1] P. M. Ivry, M. J. Rawa, D. W. P. Thomas, and M. Sumner, "Power quality of a voltage source converter in a smart grid," in *PowerTech (POWERTECH), 2013 IEEE Grenoble*, 2013, pp. 1-6.
- [2] G. Purevdorj and K. Enkjargal, "Ecological, economic and social aspects from the renewable energy and energy conservation," in *International Forum on Strategic Technology, IFOST*, 2007, pp. 20-23.
- [3] R. H. Lasseter, "MicroGrids," in *IEEE Power Engineering Society Winter Meeting*, 2002, pp. 305-308.
- [4] A. Yazdani and R. Iravani, *Voltage-Source Converters in Power Systems: Modelling, Control and Applications*: John Wiley and Sons, Inc., 2010.
- [5] N. Mohan, T. M. Undeland, and W. P. Robbins, *Power Electronics, Converters, Applications and Design*, Third ed.: John Wiley and Sons, Inc., 2003.
- [6] P. F. Keebler, "Meshing power quality and electromagnetic compatibility for tomorrow's smart grid," *Electromagnetic Compatibility Magazine, IEEE*, vol. 1, pp. 100-103, 2012.
- [7] Siemens. (2013, Harmonics in Power Systems: Causes, effects and control. Available: https://www.industry.usa.siemens.com/drives/us/en/electric-drives/ac-drives/Documents/DRV-WP-drive_harmonics_in_power_systems.pdf
- [8] Roger C. Dugan, M.F. McGranaghan, S. Santoso, and H.W. Beaty, *Electrical Power Systems Quality*, 2nd ed.: Mc-Graw Hill, 2002.
- [9] L. Jiang, G. Ye, Y. Xiang, V. Cuk, and J. F. G. Cobben, "Influence of high frequency current harmonics on (Smart) energy meters," in *Power Engineering Conference (UPEC), 2015 50th International Universities*, 2015, pp. 1-5.
- [10] M. H. Kalos and P. A. Whitlock, *Monte Carlo Methods*, 2nd ed.: Wiley-VCH Verlag GmbH & Co. KGaA, Weinheim, 2008.
- [11] H. Junping, J. Jianguo, H. Jiangjiang, and C. Wei, "Model of EMI coupling paths for an off-line power converter," in *Applied Power*

- Electronics Conference and Exposition, 2004. APEC '04. Nineteenth Annual IEEE*, 2004, pp. 708-713 vol.2.
- [12] M. Ferber, C. Vollaire, L. Krahenbuhl, J. L. Coulomb, and J. A. Vasconcelos, "Conducted EMI of DC-DC Converters With Parametric Uncertainties," *Electromagnetic Compatibility, IEEE Transactions on*, vol. 55, pp. 699-706, 2013.
- [13] "MATLAB 8.1.0.604 (R2013a)," ed: MathWorks, Inc., 2013.
- [14] "PLECS 3.5.1," ed: Plexim GmbH, Zurich, 2014.
- [15] R. H. Lasseter, "Smart Distribution: Coupled Microgrids," *Proceedings of the IEEE*, vol. 99, pp. 1074-1082, 2011.
- [16] P. Piagi and R. H. Lasseter, "Autonomous control of microgrids," in *Power Engineering Society General Meeting, 2006. IEEE*, 2006, p. 8 pp.
- [17] A. J. Roscoe, S. J. Finney, and G. M. Burt, "Tradeoffs Between AC Power Quality and DC Bus Ripple for 3-Phase 3-Wire Inverter-Connected Devices Within Microgrids," *Power Electronics, IEEE Transactions on*, vol. 26, pp. 674-688, 2011.
- [18] H. Jinwei, L. Yun Wei, and M. S. Munir, "A Flexible Harmonic Control Approach Through Voltage-Controlled DG-Grid Interfacing Converters," *Industrial Electronics, IEEE Transactions on*, vol. 59, pp. 444-455, 2012.
- [19] T. Hornik and Z. Qing-Chang, "A Current-Control Strategy for Voltage-Source Inverters in Microgrids Based on H_∞ and Repetitive Control," *IEEE Transaction on Power Electronics*, vol. 26, pp. 943-952, 2011.
- [20] S. Kusagawa, J. Baba, M. Ohshima, and E. Masada, "Supply power quality of a micro grid based on distributed generations in relation with power converter control," in *Power Electronics and Applications, 2005 European Conference on*, 2005, pp. 10 pp.-P.10.
- [21] Ewald F. Fuchs and Mohammad A. S. Masoum, *Power Quality in Power Systems and Electrical Machines*. London, UK: Elsevier Academic Press, 2008.
- [22] C. Sankaran, *Power Quality*: CRC Press LLC, 2001.

- [23] "IEEE Recommended Practice for Powering and Grounding Electronic Equipment," *IEEE Std 1100-2005 (Revision of IEEE Std 1100-1999)*, pp. 1-703, 2006.
- [24] Andreas Sumper and S. Galceran-Arellano, "Monitoring Power Quality," in *Handbook of Power Quality*, A. Baghini, Ed., ed West Sussex: Wiley, 2008, pp. 445-461.
- [25] M. Chindris and A. Sudria-Andreu, "Static Converters and Power Quality," in *Handbook of Power Quality*, A. Baghini, Ed., ed West Sussex: Wiley, 2008, pp. 463-494.
- [26] "IEEE Recommended Practice for Monitoring Electric Power Quality," *IEEE Std 1159-2009 (Revision of IEEE Std 1159-1995)*, pp. c1-81, 2009.
- [27] IEC. (2014, 21 July). *EM disturbance phenomena categories*. Available: www.iec.ch/emc/explained/categories.htm
- [28] K. A. Stroud, *Advanced Engineering Mathematics*. Hampshire, UK: Palgrave Macmillan, 2011.
- [29] A. Baghini and Z. Hanzelka, "Voltage and Current Harmonics," in *Handbook of Power Quality*, A. Baghini, Ed., ed West Sussex, England: John Wiley and Sons Limited, 2008, pp. 187-261.
- [30] A. Croft, R. Davison, and M. Hargreaves, *Engineering Mathematics: A Modern Foundation for Electronics, Electrical and Systems Engineers*. Essex, England: Addison-Wesley Longman Limited, 1996.
- [31] "IEEE Recommended Practices and Requirements for Harmonic Control in Electrical Power Systems," in *IEEE Std 519-1992*, ed, 1993.
- [32] L. Cividino, "Power factor, harmonic distortion; causes, effects and considerations," in *14th International Telecommunications Energy Conference, INTELEC.*, 1992, pp. 506-513.
- [33] Bruce Girdwood and For Energy Mad Ltd. (2007, 05-07-2012). Understanding Power Quality. Available: http://www.esmap.org/esmap/sites/esmap.org/files/51.%20Power_quality_issues_and_CFLs_BG_final_ver.pdf
- [34] "IEEE Recommended Practice and Requirements for Harmonic Control in Electric Power Systems," *IEEE Std 519-2014 (Revision of IEEE Std 519-1992)*, pp. 1-29, 2014.

- [35] S. Qipeng, Y. Zhongdong, X. Jinhui, and Z. Lixia, "Zero-sequence harmonics current minimization using zero-blocking reactor and Zig-Zag transformer," in *Electric Utility Deregulation and Restructuring and Power Technologies, 2008. DRPT 2008. Third International Conference on*, 2008, pp. 1758-1764.
- [36] M. Montoya, R. Sherick, P. Haralson, R. Neal, and R. Yinger, "Islands in the Storm: Integrating Microgrids into the Larger Grid," *Power and Energy Magazine, IEEE*, vol. 11, pp. 33-39, 2013.
- [37] Energy.Gov Office of Electricity Delivery and Energy Reliability. (22 July, 2014). *2012 DOE Microgrid Workshop Summary Report*. Available:
energy.gov/sites/prod/files/2012%20Microgrid%20Workshop%20Report%2009102012.pdf
- [38] M. Smith and D. Ton, "Key Connections: The U.S. Department of Energy's Microgrid Initiative," *Power and Energy Magazine, IEEE*, vol. 11, pp. 22-27, 2013.
- [39] "IEEE Guide for Design, Operation, and Integration of Distributed Resource Island Systems with Electric Power Systems," *IEEE Std 1547.4-2011*, pp. 1-54, 2011.
- [40] T. Basso, J. Hambrick, and D. DeBlasio, "Update and review of IEEE P2030 Smart Grid Interoperability and IEEE 1547 interconnection standards," in *Innovative Smart Grid Technologies (ISGT), 2012 IEEE PES*, 2012, pp. 1-7.
- [41] National Renewable Energy Laboratory (NREL). (22 July, 2014). *Learning About Renewable Energy: Distributed Energy Basics*. Available: http://www.nrel.gov/learning/eds_distributed_energy.html
- [42] Farad Katiraei, "Microgrids are for real," in *QT e-News* vol. 4 Issue 3, ed. Raleigh North Carolina: Quanta Technology Online Newsletter, 2013, pp. 1, 3-5.
- [43] R. Lasseter, A. Akhil, C. Marnay, J. Stephens, J. Dagle, R. Guttromson, A. S. Meliopoulos, R. Yinger, and J. Eto. Integration of distributed energy resources. The CERTS Microgrid Concept [Online]. Available: <http://www.escholarship.org/uc/item/9w88z7z1>

- [44] R. Ahshan, M. T. Iqbal, G. K. I. Mann, and J. E. Quaicoe, "Micro-grid system based on renewable power generation units," in *Electrical and Computer Engineering (CCECE), 2010 23rd Canadian Conference on*, 2010, pp. 1-4.
- [45] M. Barnes, J. Kondoh, H. Asano, J. Oyarzabal, G. Ventakaramanan, R. Lasseter, N. Hatziargyriou, and T. Green, "Real-World MicroGrids-An Overview," in *System of Systems Engineering, 2007. SoSE '07. IEEE International Conference on*, 2007, pp. 1-8.
- [46] M. Barnes, A. Dimeas, A. Engler, C. Fitzer, N. Hatziargyriou, C. Jones, S. Papathanassiou, and M. Vandenberg, "Microgrid laboratory facilities," in *Future Power Systems, 2005 International Conference on*, 2005, pp. 6 pp.-6.
- [47] M. Griffiths and C. Coates, "Behaviour of microgrids in the presence of unbalanced loads," in *Power Engineering Conference, 2007. AUPEC 2007. Australasian Universities*, 2007, pp. 1-5.
- [48] U. Borup, F. Blaabjerg, and P. N. Enjeti, "Sharing of nonlinear load in parallel-connected three-phase converters," *Industry Applications, IEEE Transactions on*, vol. 37, pp. 1817-1823, 2001.
- [49] Hua Bai and Chris Mi, *Transients of Modern Power Electronics*, 1st ed.: John Wiley and Sons Ltd., 2011.
- [50] M. Jamil, B. Hussain, M. Abu-Sara, R. J. Boltryk, and S. M. Sharkh, "Microgrid power electronic converters: State of the art and future challenges," in *Universities Power Engineering Conference (UPEC), 2009 Proceedings of the 44th International*, 2009, pp. 1-5.
- [51] L.Xu and B.R. Anderson, "Grid connection of Large Offshore Windfarms using HVDC," Dec 2005, pp. 371-382.
- [52] P. Boonchiam and N. Mithulanathan, "Diode-Clamped Multilevel Voltage Source Converter Based on Medium Voltage DVR," *International Journal of Electrical Power and Energy Systems Engineering*, vol. 1, pp. 62-67, 2008.
- [53] Bismal K. Bose, *Modern Power Electronics and AC Drives*: Prentice Hall PTR Prentice-Hall, Inc., 2002.

- [54] J. Rodriguez, S. Bernet, W. Bin, J. O. Pontt, and S. Kouro, "Multilevel Voltage-Source-Converter Topologies for Industrial Medium-Voltage Drives," *Industrial Electronics, IEEE Transactions on*, vol. 54, pp. 2930-2945, 2007.
- [55] I. Colak, E. Kabalci, and R. Bayindir, "Review of multilevel voltage source inverter topologies and control schemes," *Energy Conversion and Management*, vol. 52, pp. 1114-1128, 2011.
- [56] Rasoul Shalchi Alishah, Daryoosh Nazarpour, and S. H. Hosseini, "Design of New Multilevel Voltage Source Inverter Structure Using Fundamental Frequency-Switching Strategy," *TSEST Transaction on Electrical and Electronic Circuits and Systems*, vol. 3, pp. 35-41, August 2013.
- [57] Alonso O. Sadaba, Sanchis P. Gurrpide, Lopez J. Taberna, Munoz I. Morales, and Marroyo L. Palomo, "Voltage Harmonics Generated by 3-Level Converters Using PWM Natural Sampling," presented at the IEEE 32nd Annual Power Electronics Specialists Conference, 2001.
- [58] Nanditha Sundaresan, Harisankar M A, Noby George, TVVS Lakshmi, Umashankar S, and K. D. P, "Comparative Evaluation of SPWM Based 3 Level And 5 Level NPC Inverters with Reduced Switching Stress," *International Journal of Electronics Communications and Electrical Engineering*, vol. 3, pp. 48-59, February 2013.
- [59] P. Adhikari and M. Okaro, "Five-level five-phase PWM signal generation using FPGA," in *North American Power Symposium (NAPS)*, 2011, pp. 1-5.
- [60] P. M. Ivry, M. J. Rawa, and D. W. P. Thomas, "Factors Affecting the Harmonics Generated by a Generic Voltage Source Converter Within a Microgrid," in *Saudi Arabia Smart Grid Conference and Exhibition*, Jeddah, 2012, pp. B-65.
- [61] D. G. Infield, P. Onions, A. D. Simmons, and G. A. Smith, "Power quality from multiple grid-connected single-phase inverters," *Power Delivery, IEEE Transactions on*, vol. 19, pp. 1983-1989, 2004.
- [62] A. Mansoor, W. M. Grady, A. H. Chowdhury, and M. J. Samotyi, "An investigation of harmonics attenuation and diversity among distributed

- single-phase power electronic loads," *Power Delivery, IEEE Transactions on*, vol. 10, pp. 467-473, 1995.
- [63] Y. Qingzeng, W. Xiaojie, Y. Xibo, G. Yiwen, and Z. Qi, "Minimization of the DC Component in Transformerless Three-Phase Grid-Connected Photovoltaic Inverters," *Power Electronics, IEEE Transactions on*, vol. 30, pp. 3984-3997, 2015.
- [64] A. D. Simmons and D. G. Infield, "Current waveform quality from grid-connected photovoltaic inverters and its dependence on operating conditions," *Progress in Photovoltaics: Research and Applications*, vol. 8, pp. 411-420, 2000.
- [65] Edward Hughes, John Hiley, Keith Brown, and Ian McKenzie Smith, *Hughes: Electrical and Electronic Technology*, 10th ed. Harlow, England: Pearson Education, 2008.
- [66] K. H. Ahmed, S. J. Finney, and B. W. Williams, "Passive Filter Design for Three-Phase Inverter Interfacing in Distributed Generation," in *Compatibility in Power Electronics. CPE*, 2007, pp. 1-9.
- [67] I. Sefa, N. Altin, and S. Ozdemir, "An implementation of grid interactive inverter with reactive power support capability for renewable energy sources," in *International Conference on Power Engineering, Energy and Electrical Drives (POWERENG)*, 2011, pp. 1-6.
- [68] C. Hanju and T. K. Vu, "Comparative analysis of low-pass output filter for single-phase grid-connected Photovoltaic inverter," in *Applied Power Electronics Conference and Exposition (APEC), 2010 Twenty-Fifth Annual IEEE*, 2010, pp. 1659-1665.
- [69] T. C. Y. Wang, Y. Zhihong, S. Gautam, and Y. Xiaoming, "Output filter design for a grid-interconnected three-phase inverter," in *IEEE 34th Annual Power Electronics Specialist Conference, PESC '03.*, 2003, pp. 779-784.
- [70] R. Teodorescu, M. Liserre, and P. Rodriguez, *Grid Converters for Photovoltaic and Wind Power Systems*: John Wiley and Sons Ltd., 2011.
- [71] A. A. Rockhill, M. Liserre, R. Teodorescu, and P. Rodriguez, "Grid-Filter Design for a Multimegawatt Medium-Voltage Voltage-Source

- Inverter," *IEEE Transaction on Industrial Electronics*, vol. 58, pp. 1205-1217, 2011.
- [72] R. Teodorescu, M. Liserre, and P. Rodríguez, "Grid Filter Design," in *Grid Converters for Photovoltaic and Wind Power Systems*, ed: John Wiley & Sons, Ltd, 2011, pp. 289-312.
- [73] W. Huang, J. Zhang, Q. Xie, and Z. Wu, "The impact on power quality by PWM converter in micro-grid," in *IEEE International Confernce on Sustainable Energy Technologies, ICSET.*, 2008, pp. 239-243.
- [74] J. Arrillaga and N. R. Watson, *Power System Harmonics*, 2nd ed. West Sussex: John Wiley & Sons, 2003.
- [75] Y. Baghzouz, R. F. Burch, A. Capasso, A. Cavallini, A. E. Emanuel, M. Halpin, A. Imece, A. Ludbrook, G. Montanari, K. J. Olejniczak, P. Ribeiro, S. Rios-Marcuello, L. Tang, R. Thaliyam, and P. Verde, "Time-varying harmonics. I. Characterizing measured data," *Power Delivery, IEEE Transactions on*, vol. 13, pp. 938-944, 1998.
- [76] M. Liserre , F. Blaabjerg, and A. Dell'Aquila, "Step-by-step design procedure for a grid-connected three-phase PWM voltage source converter," *International Journal of Electronics*, vol. 91, pp. 445-460, 2004/08/01 2004.
- [77] H. Bayem, M. Peti, P. Dessante, F. Dufourd, and R. Belhomme, "Probabilistic Characterization of Wind Farms for Grid Connection Studies," in *European Wind Energy Conference and Exhibition, Milan, Milan*, 2007.
- [78] P. Z. Peebles, *Probability, Random Variables, and Random Signal Principles*, 2nd ed.: McGraw-Hill, Inc., 1993.
- [79] Z.-j. Li, A.-c. Xue, and T.-s. Bi, "On the characteristics of the predicted wind power based on three-parameter Weibull distribution," in *Control Conference (CCC), 2014 33rd Chinese*, 2014, pp. 7077-7081.
- [80] S.-J. Wu, "Estimation of the Parameters of The Weibull Distribution with Progressively Censored Data," *Journal of the Japan Statistical Society*, vol. 32, pp. 155-163, 2002.
- [81] D. Stirzaker, *Probability and Random Variables: A Beginner's Guide*. Cambridge: Cambridge University Press, 1999.

- [82] Glossary of Statistical Terms. (2002, 09 March). *Random Events*. Available: <http://stats.oecd.org/glossary/detail.asp?ID=3817>
- [83] E. W. Weisstein. (09 March). *Event*. Available: <http://mathworld.wolfram.com/Event.html>
- [84] J. J. Shynk, *Probability, Random Variables, and Random Processes : Theory and Signal Processing Applications*. Somerset, NJ, USA: John Wiley & Sons, 2012.
- [85] E. W. Weisstein. (09 March). *Random Number*. Available: <http://mathworld.wolfram.com/RandomNumber.html>
- [86] E. W. Weisstein. (09 March). *Variate*. Available: <http://mathworld.wolfram.com/Variate.html>
- [87] A. Stuart and K. J. Ord, *Kendall's Advanced Theory of Statistics*, 6th ed. vol. 1. New York: Edward Arnold and Halsted Press, 1994.
- [88] O. A. Oke, "Enhanced Unscented Transform Method for Probabilistic Load Flow Studies," *Electrical and Electronics Engineering*, University of Nottingham, Nottingham, 2013.
- [89] J. Usaola, "Probabilistic load flow in systems with wind generation," *Generation, Transmission & Distribution, IET*, vol. 3, pp. 1031-1041, 2009.
- [90] F. Miao, V. Vittal, G. T. Heydt, and R. Ayyanar, "Probabilistic Power Flow Studies for Transmission Systems With Photovoltaic Generation Using Cumulants," *Power Systems, IEEE Transactions on*, vol. 27, pp. 2251-2261, 2012.
- [91] P. Chen, Z. Chen, and B. Bak-Jensen, "Probabilistic load flow: A review," in *Electric Utility Deregulation and Restructuring and Power Technologies, 2008. DRPT 2008. Third International Conference on*, 2008, pp. 1586-1591.
- [92] H. V. Haghi and M. T. Bina, "A study on probabilistic evaluation of harmonic levels produced by static compensators," in *Power Engineering Conference, 2008. AUPEC '08. Australasian Universities*, 2008, pp. 1-6.
- [93] R. E. Morrison, Y. Baghzouz, P. Ribeiro, and C. A. Duque, "Probabilistic aspects of time-varying harmonics," in *Time-Varying Waveform*

- Distortion in Power Systems*, P. F. Ribeiro, Ed., ed West Sussex: John Wiley & Sons, 2009, pp. 3-18.
- [94] W. G. Sherman, "Summation of harmonics with random phase angles," *Electrical Engineers, Proceedings of the Institution of*, vol. 119, pp. 1643-1648, 1972.
- [95] W. E. Kazibwe, T. H. Ortmeier, and M. S. A. A. Hammam, "Summation of probabilistic harmonic vectors [power systems]," *Power Delivery, IEEE Transactions on*, vol. 4, pp. 621-628, 1989.
- [96] N. B. Rowe, "The summation of randomly varying phasors or vectors with particular reference to harmonic levels," presented at the IEE Conference Publication, 1974.
- [97] Y. J. Wang, L. Pierrat, and L. Wang, "Summation of harmonic currents produced by AC/DC static power converters with randomly fluctuating loads," *Power Delivery, IEEE Transactions on*, vol. 9, pp. 1129-1135, 1994.
- [98] F. S. Prabhakara and W. E. Kazibwe, "Current calculation methodology for manufacturing facilities with intermittent loads," *Industry Applications, IEEE Transactions on*, vol. 28, pp. 324-328, 1992.
- [99] S. R. Kaprielian, A. E. Emanuel, R. V. Dwyer, and H. Mehta, "Predicting voltage distortion in a system with multiple random harmonic sources," *Power Delivery, IEEE Transactions on*, vol. 9, pp. 1632-1638, 1994.
- [100] R. Langella and A. Testa, "Summation of random harmonic currents," in *Time-Varying Waveform Distortion in Power Systems*, P. F. Ribeiro, Ed., ed West Sussex: John Wiley & Sons, 2009, pp. 53-71.
- [101] E. Ngandui, E. J. Mohammed, and A. Cheriti, "Prediction of harmonics produced by multiple variable speed drives with randomly fluctuating loads," in *Electrical and Computer Engineering, 2000 Canadian Conference on*, 2000, pp. 1157-1161 vol.2.
- [102] Y. J. Wang and L. Pierrat, "Vectorial summation of probabilistic current harmonics in power systems: From a bivariate distribution model towards a univariate probability function," *European Transactions on Electrical Power*, vol. 10, pp. 13-18, 2000.

- [103] A. Cavallini, G. C. Montanari, and M. Cacciari, "Stochastic evaluation of harmonics at network buses," *Power Delivery, IEEE Transactions on*, vol. 10, pp. 1606-1613, 1995.
- [104] Y. Baghzouz and O. T. Tan, "Probabilistic Modeling of Power System Harmonics," *Industry Applications, IEEE Transactions on*, vol. IA-23, pp. 173-180, 1987.
- [105] P. T. Staats, W. M. Grady, A. Arapostathis, and R. S. Thallam, "A statistical method for predicting the net harmonic currents generated by a concentration of electric vehicle battery chargers," *Power Delivery, IEEE Transactions on*, vol. 12, pp. 1258-1266, 1997.
- [106] K.-H. Liu, "Analysis of Probabilistic Harmonic Currents and Voltages of Electronic Power Converter Contributed in Distributed Systems," *Research Journal of Applied Sciences, Engineering and Technology*, vol. 5, pp. 1263-1270, 2013.
- [107] Jen-Hao Teng, Rong-Ceng Leou, Chuo-Yean Chang, and S.-Y. Chan. (2013, Harmonic Current Predictors for Wind Turbines. *Energies* 6, 1314-1328.
- [108] Y. G. Hegazy and M. M. A. Salama, "Calculations of diversified harmonic currents in multiple converter systems," in *Power Engineering Society Summer Meeting, 2000. IEEE, 2000*, pp. 727-731 vol. 2.
- [109] Palisade. (2013, 09 June). Monte Carlo Simulation: What Is It and How Does It Work? - Palisade.
- [110] P. Jorgensen, J. S. Christensen, and J. O. Tande, "Probabilistic load flow calculation using Monte Carlo techniques for distribution network with wind turbines," in *Harmonics and Quality of Power Proceedings, 1998. Proceedings. 8th International Conference On*, 1998, pp. 1146-1151 vol.2.
- [111] D. W. P. Thomas, O. A. Oke, L. R. A. X. De Menezes, and C. Christopoulos, "The use of unscented transforms in modeling the statistical response of nonlinear scatterer in a reverberation chamber," in *General Assembly and Scientific Symposium, 2011 XXXth URSI*, 2011, pp. 1-4.

- [112] L. R. A. X. De Menezes, D. W. P. Thomas, C. Christopoulos, A. Ajayi, and P. Sewell, "The use of Unscented Transforms for statistical analysis in EMC," in *Electromagnetic Compatibility - EMC Europe, 2008 International Symposium on*, 2008, pp. 1-5.
- [113] J. M. Morales and J. Perez-Ruiz, "Point Estimate Schemes to Solve the Probabilistic Power Flow," *Power Systems, IEEE Transactions on*, vol. 22, pp. 1594-1601, 2007.
- [114] S. Rahman and H. Xu, "A univariate dimension-reduction method for multi-dimensional integration in stochastic mechanics," *Probabilistic Engineering Mechanics*, vol. 19, pp. 393-408, 2004.
- [115] O. A. Oke, D. W. P. Thomas, and G. M. Asher, "A new probabilistic load flow method for systems with wind penetration," in *PowerTech, 2011 IEEE Trondheim*, 2011, pp. 1-6.
- [116] B. Zou and Q. Xiao, "Probabilistic load flow computation using univariate dimension reduction method," *International Transactions on Electrical Energy Systems*, pp. n/a-n/a, 2013.
- [117] M. E. J. Newman and G. T. Barkema, *Monte Carlo Methods in Statistical Physics*. Oxford: Clarendon Press, 1999.
- [118] D. P. Landau and K. Binder, *A Guide to Monte-Carlo Simulations in Statistical Physics*, 3rd ed. Cambridge: Cambridge University Press, 2009.
- [119] MathWorks. (2015, 09 March). *Monte Carlo Simulation*. Available: <http://uk.mathworks.com/discovery/monte-carlo-simulation.html>
- [120] W. Li and L. Kuo-Hua, "A study on randomly varying harmonic currents and total harmonic distortion of currents in power systems," in *Future Power Systems, 2005 International Conference on*, 2005, pp. 5 pp.-5.
- [121] E. E. Ahmed and W. Xu, "Assessment of harmonic distortion level considering the interaction between distributed three-phase harmonic sources and power grid," *Generation, Transmission & Distribution, IET*, vol. 1, pp. 506-515, 2007.
- [122] L. R. A. X. De Menezes, A. Ajayi, C. Christopoulos, P. Sewell, and G. A. Borges, "Efficient computation of stochastic electromagnetic

- problems using unscented transforms," *Science, Measurement & Technology, IET*, vol. 2, pp. 88-95, 2008.
- [123] A. Ajayi, "Direct Computation of Statistical Variations in Electromagnetic Problems," Electrical and Electronics Engineering, University of Nottingham, Nottingham, 2008.
- [124] Gautschi W., *Orthogonal Polynomials: Computation and Approximation*. New York: Oxford University Press, 2004.
- [125] E. W. Weisstein. (27 March). *Gaussian Quadrature*. Available: <http://mathworld.wolfram.com/GaussianQuadrature.html>
- [126] NIST. (2014, 03 April). *Quadrature: Gauss Quadrature*. Available: <http://dlmf.nist.gov/3.5>
- [127] H. Xu and S. Rahman, "A generalized dimension-reduction method for multidimensional integration in stochastic mechanics," *International Journal for Numerical Methods in Engineering*, vol. 61, pp. 1992-2019, 2004.
- [128] B. Huang and X. Du, "Uncertainty Analysis by Dimension Reduction Integration and Saddlepoint Approximations," *Journal of Mechanical Design*, vol. 128, pp. 26-33, 2005.
- [129] I. Lee, K. K. Choi, L. Du, and D. Gorsich, "Dimension reduction method for reliability-based robust design optimization," *Computers & Structures*, vol. 86, pp. 1550-1562, 2008.
- [130] G. Musser. (2014, May 20). *A solar detective story: Explaining how power output varies hour by hour*. Available: <http://blogs.scientificamerican.com/solar-at-home/2010/07/30/a-solar-detective-story-explaining-how-power-output-varies-hour-by-hour/>
- [131] GreenRhinoEnergy. (2014, 20 May,). *Wind Energy Systems and Wind Farms*. Available: http://www.greenrhinoenergy.com/renewable/wind/wind_systems.php
- [132] W. H. Press, S. A. Teukolsky, W. T. Vetterling, and B. P. Flannery, *Numerical Recipes 3rd Edition: The Art of Scientific Computing*: Cambridge University Press, 2007.
- [133] G. Dahlquist and Å. Björck, *Numerical Methods in Scientific Computing, Volume I*: Society for Industrial and Applied Mathematics, 2008.

Appendix

Appendix A

A.1: Park and Clarke's Transformation Used in Modelling the VSC PI Controller and Transformations

3-Phase Sinusoidal Voltages V_{abc}

$$V_a = V_m \sin(\omega t) \quad (\text{A.1})$$

$$V_b = V_m \sin(\omega t - 2\pi/3) \quad (\text{A.2})$$

$$V_c = V_m \sin(\omega t + 2\pi/3) \quad (\text{A.3})$$

V_{abc} - $V_{\alpha\beta}$

$$\begin{bmatrix} V_\alpha \\ V_\beta \end{bmatrix} = \frac{2}{3} \begin{bmatrix} 1 & -1/2 & -1/2 \\ 0 & \sqrt{3}/2 & -\sqrt{3}/2 \end{bmatrix} \begin{bmatrix} V_a \\ V_b \\ V_c \end{bmatrix} \quad (\text{A.4})$$

$$V_\alpha = \frac{2}{3} V_a - \frac{1}{3} V_b - \frac{1}{3} V_c \quad (\text{A.5})$$

$$V_\beta = \frac{\sqrt{3}}{3} V_b - \frac{\sqrt{3}}{3} V_c = \frac{1}{\sqrt{3}} V_b - \frac{1}{\sqrt{3}} V_c \quad (\text{A.6})$$

$V_{\alpha\beta}$ - V_{dq}

$$\begin{bmatrix} V_d \\ V_q \end{bmatrix} = \begin{bmatrix} \cos(\omega t) & \sin(\omega t) \\ -\sin(\omega t) & \cos(\omega t) \end{bmatrix} \begin{bmatrix} V_\alpha \\ V_\beta \end{bmatrix} \quad (\text{A.7})$$

$$V_d = V_\alpha \cos(\omega t) + V_\beta \sin(\omega t) \quad (\text{A.8})$$

$$V_q = -V_\alpha \sin(\omega t) + V_\beta \cos(\omega t) \quad (\text{A.9})$$

V_{dq} - $V_{\alpha\beta}$

$$\begin{bmatrix} V_\alpha \\ V_\beta \end{bmatrix} = \begin{bmatrix} \cos(\omega t) & -\sin(\omega t) \\ \sin(\omega t) & \cos(\omega t) \end{bmatrix} \begin{bmatrix} V_d \\ V_q \end{bmatrix} \quad (\text{A.10})$$

$$V_\alpha = V_d \cos(\omega t) - V_q \sin(\omega t) \quad (\text{A.11})$$

$$V_\beta = V_d \sin(\omega t) + V_q \cos(\omega t) \quad (\text{A.12})$$

$\mathbf{V}_{\alpha\beta} - \mathbf{V}_{abc}$

$$\begin{bmatrix} V_a \\ V_b \\ V_c \end{bmatrix} = \frac{3}{2} \begin{bmatrix} 1 & 0 \\ -1/2 & \sqrt{3}/2 \\ -1/2 & -\sqrt{3}/2 \end{bmatrix} \begin{bmatrix} V_\alpha \\ V_\beta \end{bmatrix} \quad (\text{A.13})$$

$$V_a = \frac{3}{2} V_\alpha \quad (\text{A.14})$$

$$V_b = \frac{3}{2} \left(-\frac{1}{2} V_\alpha + \frac{\sqrt{3}}{2} V_\beta \right) \quad (\text{A.15})$$

$$V_c = \frac{3}{2} \left(-\frac{1}{2} V_\alpha - \frac{\sqrt{3}}{2} V_\beta \right) \quad (\text{A.16})$$

Direct Transformation from $V_{abc} - V_{dq0}$ $\mathbf{V}_{abc} - \mathbf{V}_{dq0}$

$$V_d = \frac{2}{3} (V_a \cos(\omega t) + V_b \cos(\omega t - 2\pi/3) + V_c \cos(\omega t + 2\pi/3)) \quad (\text{A.17})$$

$$V_q = \frac{2}{3} (V_a \sin(\omega t) + V_b \sin(\omega t - 2\pi/3) + V_c \sin(\omega t + 2\pi/3)) \quad (\text{A.18})$$

$$V_0 = \frac{1}{3} (V_a + V_b + V_c) \quad (\text{A.19})$$

Where ω is the rotation speed (rad/s) of the rotating frame $\mathbf{V}_{dq0} - \mathbf{V}_{abc}$

$$V_a = \frac{3}{2} (V_d \cos(\omega t) + V_q \sin(\omega t) + V_0) \quad (\text{A.20})$$

$$V_b = \frac{3}{2} (V_d \cos(\omega t - 2\pi/3) + V_q \sin(\omega t - 2\pi/3) + V_0) \quad (\text{A.21})$$

$$V_c = \frac{3}{2} (V_d \cos(\omega t + 2\pi/3) + V_q \sin(\omega t + 2\pi/3) + V_0) \quad (\text{A.22})$$

Where ω is the rotation speed (rad/s) of the rotating frame

Appendix B

B.1: Generation of Orthogonal Polynomial

Two functions $f(x)$ and $g(x)$ are said to be orthogonal in an interval $[a, b]$ over a weighting function $w(x)$ if their inner product is zero, while they are orthonormal if the inner product is unity. The inner product refers to the scalar product of $f(x)$ and $g(x)$ which is a number and the relationship between the inner product over $w(x)$ is given as (B.1) in [88].

$$\langle f, g \rangle = \int_a^b w(x) f(x) g(x) dx = \begin{cases} 0 & \text{if } f(x) \neq g(x) \\ 1 & \text{if } f(x) = g(x) \end{cases} \quad (\text{B.1})$$

The inner products shift property (B.2) brings about a 3-term recurrence relation (B.3) for all orthogonal polynomials [124].

$$(xf, g)_{dW} = (f, xg)_{dW} \quad \text{for all } f, g \in \mathbf{P} \quad (\text{B.2})$$

where $dW = w(x)dx$ is the induced positive measure.

The 3-term recurrence relation (B.3) is very important for constructive and computational use of orthogonal polynomials; as knowledge of the coefficients allows for easy computation of the orthogonal polynomial's zeros as the eigenvalues of a symmetrical tridiagonal Jacobian matrix, allows an efficient evaluation of expansion in the orthogonal polynomials [124] in relations to generating orthogonal polynomials.

The 3-term recurrence relation is given as (B.3) in [124, 132];

$$\begin{aligned} P_{m+1}(x) &= (x - a_m)P_m(x) - b_m P_{m-1}(x) \quad m = 0, 1, 2, \dots \\ P_{-1}(x) &= 0 \\ P_0(x) &= 1 \end{aligned} \quad (\text{B.3})$$

where a_m and b_m are the recurrence coefficients given by;

$$a_m = \frac{\langle xP_m, P_m \rangle dW}{\langle P_m, P_m \rangle dW} \quad m = 0, 1, 2, \dots \quad (\text{B.4})$$

$$b_m = \frac{\langle P_m, P_m \rangle dW}{\langle P_{m-1}, P_{m-1} \rangle dW} \quad m = 1, 2, \dots \quad (\text{B.5})$$

$$b_0 = \langle P_0, P_0 \rangle dW \quad m = 0 \quad (\text{B.6})$$

where $P_m(x) = P_m(x; dW)$, $m = 0, 1, 2, \dots$, is a set of monic polynomials with respect to the measure dW .

If a weighting function is non classical and its recurrence coefficients unknown, one way to generate the recurrence coefficients requires a procedure that involves prior knowledge of the first $2N$ moments of the weighting function [132]. This procedure generates a_m and b_m for building the recurrence relation in (B.3) and is given in (B.7) [88, 132].

$$\mu_m = \int_a^b x^m W(x) dx \quad m = 0, 1, \dots, 2N - 1 \quad (\text{B.7})$$

However, the solutions obtained for a_m and b_m using this procedure is extremely ill-conditioned, making the procedure inapplicable [132]. To avoid this limitation, a robust approach is required and this will involve a discretization scheme as applied in [88].

B.2: Stieltjes Procedure

The Stieltjes procedure and the Lanczos-type algorithm are examples of discretization schemes [124]. Discretization schemes use discrete points in computing recurrence coefficients and these discrete points are also used in approximating the weighting function. In a case where discrete points and discrete measures are employed, the technique works perfectly once the discrete measure converges to the continuous one [88, 132]. The Stieltjes procedure was

adopted in [88] as it requires less execution time as compared with the Lanczos type algorithm [124].

The Stieltjes procedure provides a way of computing the recurrence relation of a discrete measure by the use of interpolatory quadrature rule. It involves representing the weighting function dW by an L -point discrete measure dW_L [88]. The interpolatory quadrature helps in approximating the definite integral of a given function f by a weighted sum such that (B.8) [88, 126, 133];

$$\int_{-1}^1 f(x)dx = \sum_{k=-1}^n w_k f(x_k) \quad (\text{B.8})$$

To solve for the recurrence relation terms (B.3) using (B.4) - (B.6), first requires solving for the inner product [88] where the evaluations points are chosen away from the endpoints to avoid singularities [88, 124]. So following the inner product definition in (B.3) and applying (B.8) to (B.3) gives;

$$\int_{-1}^1 w(x)f(x)g(x)dx \cong \sum_{k=-1}^n w_k w(x_k) f(x_k) g(x_k) \quad (\text{B.9})$$

The Fejér's first quadrature rule which is similar to the Clenshaw-Curtis rules is applied as other interpolatory rules such as the Newton Cotes results in large errors [88, 124, 132]. This interpolatory quadrature rule suggests choosing the interpolation points as the zeros of a Chebyshev polynomial of first or second kind such that the nodes and weights are obtained using (B.10, B.11) respectively.

$$x_k = \cos \theta_k, \quad \theta_k = \frac{(2k-1)\pi}{2n}, \quad k = 1:n \quad (\text{B.10})$$

$$w_k = \frac{2}{n} \left(1 - 2 \sum_{j=1}^{\lfloor n/2 \rfloor} \frac{\cos(2j\theta_k)}{(4j^2-1)} \right), \quad k = 1:n \quad (\text{B.11})$$

where $\lfloor n/2 \rfloor$ is the largest integer less than or equal to $n/2$.

With (B.9) defined within the canonical interval $[-1,1]$, a transformation equation (B.12) [124] is required in mapping it to any arbitrary interval $[a,b]$.

$$\int_a^b w(x)f(x)g(x)dx = \int_{-1}^1 w(\phi(\tau))f(\phi(\tau))g(\phi(\tau))\phi'(\tau)d\tau \quad (\text{B.12})$$

The linear transformation for finite $[a,b]$ (B.13) [124] is given below;

$$\phi(\tau) = \begin{cases} \frac{1}{2}(b-a)\tau + \frac{1}{2}(b+a) & \text{if } -\infty < a < b < \infty \\ b - \frac{1-\tau}{1+\tau} & \text{if } -\infty = a < b < \infty \\ a + \frac{1+\tau}{1-\tau} & \text{if } -\infty < a < b = \infty \\ \frac{\tau}{1-\tau} & \text{if } -\infty = a < b = \infty \end{cases} \quad (\text{B.13})$$

The points obtained using Fejér's rule are then used to compute the discrete inner product and hence the discrete recurrence coefficients $a_{m,L}$ and $b_{m,L}$ [88] following this sequence;

$$P_{0,L} \rightarrow a_{0,L}, b_{0,L} \rightarrow P_{1,L} \rightarrow a_{1,L}, b_{1,L} \rightarrow \dots$$

The above sequence is continued until all the coefficients are obtained.

A detailed explanation of the Stieltjes procedure can be found in [124].

B.3: Generation of Sigma Points and Weights for Univariate Problems

As earlier stated, the recurrence relation allows for computation of the polynomial's roots as the eigenvalue of the tridiagonal Jacobi matrix given in (B.14) [124, 132]. The generation of sigma points for a univariate problem is achieved by inputting the recurrence relation coefficient obtained using the Stieltjes procedure into (B.14) [88].

$$J_n = \begin{bmatrix} a_0 & \sqrt{b_1} & 0 & 0 & \cdots & 0 & 0 \\ \sqrt{b_1} & a_1 & \sqrt{b_2} & 0 & \cdots & 0 & 0 \\ 0 & \sqrt{b_2} & a_2 & \sqrt{b_3} & \cdots & 0 & 0 \\ 0 & 0 & \sqrt{b_3} & \ddots & \ddots & 0 & 0 \\ \vdots & \vdots & \vdots & \ddots & \ddots & \sqrt{b_{n-2}} & 0 \\ 0 & 0 & 0 & 0 & \sqrt{b_{n-2}} & a_{n-2} & \sqrt{b_{n-1}} \\ 0 & 0 & 0 & 0 & 0 & \sqrt{b_{n-1}} & a_{n-1} \end{bmatrix} \quad (\text{B.14})$$

The weights are then generated using (B.15) [132]

$$W_m = b_0 v_{m,1}^2 \quad m = 0, 1, 2, \dots \quad (\text{B.15})$$

where $v_{m,1}$ is the first component of the normalized eigenvector corresponding to the m th eigenvalue of J_n [88].

This procedure works efficiently for a single variable problem involving one dimensional integration.

Appendix C

C.1: Standard Deviation of Current and Voltage THD and IHD_n under Filter Inductance Variation

Table C.1: Predicted Standard Deviation of Current and Voltage THD and IHD_n Using MCS, 3pts and 5pts UDR under Filter Inductance Variation

I_{THD} Std	N VSCs	MCS	3pts rUDR	5pts rUDR
	1	1.89	1.83	1.91
	2	0.93	0.88	0.93
	3	0.58	0.41	0.55
	4	0.64	0.50	0.71
	5	0.49	0.32	0.27
	6	0.45	0.29	0.45
	7	0.35	0.40	0.42
	8	0.33	0.07	0.26
	9	0.30	0.31	0.35
	10	0.26	0.10	0.36
I_{IHD 38th} Std	N VSCs	MCS	3pts rUDR	5pts rUDR
	1	1.61	1.59	1.60
	2	0.78	0.72	0.75
	3	0.49	0.44	0.43
	4	0.53	0.39	0.46
	5	0.40	0.27	0.36
	6	0.36	0.29	0.12
	7	0.29	0.01	0.22
	8	0.27	0.16	0.18
	9	0.23	0.06	0.12
	10	0.21	0.15	0.16
I_{IHD 42nd} Std	N VSCs	MCS	3pts rUDR	5pts rUDR
	1	0.96	0.94	0.95
	2	0.48	0.45	0.47
	3	0.31	0.28	0.28
	4	0.36	0.27	0.32
	5	0.28	0.20	0.26
	6	0.27	0.06	0.15
	7	0.21	0.05	0.15
	8	0.20	0.10	0.08
	9	0.17	0.10	0.09
	10	0.16	0.08	0.10

V_{THD} Std	N VSCs	MCS	3pts rUDR	5pts rUDR
	1	1.28	1.25	1.28
	2	1.19	1.11	1.16
	3	1.08	0.96	0.99
	4	1.50	1.16	1.41
	5	1.37	0.97	1.16
	6	1.45	0.74	1.03
	7	1.27	0.41	0.79
	8	1.32	0.64	0.64
	9	1.24	0.79	0.79
	10	1.19	0.46	0.59
V_{IHD} 38th Std	N VSCs	MCS	3pts rUDR	5pts rUDR
	1	1.03	1.01	1.03
	2	0.95	0.88	0.91
	3	0.86	0.77	0.76
	4	1.18	0.87	1.05
	5	1.05	0.69	0.86
	6	1.11	0.37	0.55
	7	0.97	0.24	0.55
	8	1.00	0.55	0.39
	9	0.94	0.54	0.22
	10	0.90	0.77	0.33
V_{IHD} 42nd Std	N VSCs	MCS	3pts rUDR	5pts rUDR
	1	0.68	0.66	0.67
	2	0.65	0.61	0.63
	3	0.60	0.53	0.55
	4	0.87	0.67	0.82
	5	0.83	0.56	0.69
	6	0.89	0.36	0.60
	7	0.79	0.16	0.37
	8	0.83	0.31	0.48
	9	0.78	0.49	0.27
	10	0.76	0.51	0.21

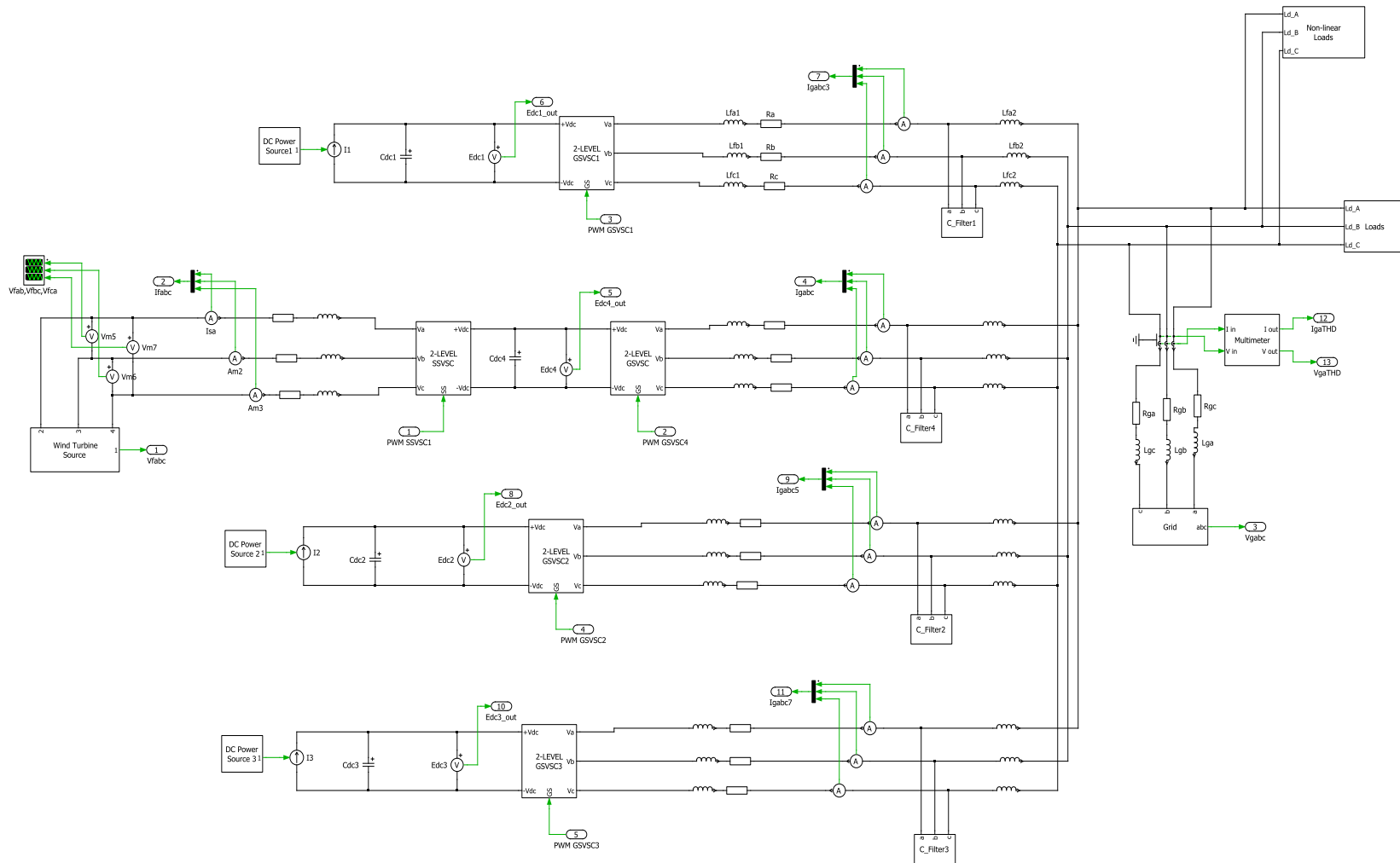
C.2: Standard deviation for Harmonic Distortion Level Using MCS, 3pts and 5pts UDR under Grid Impedance Variation

**Table C.2: Predicted Standard deviation for Harmonic Distortion Level
Using MCS, 3pts and 5pts UDR under Grid Impedance Variation**

I_{THD} Std	N VSCs	MCS	3pts rUDR	5pts rUDR
	1	0.525	0.300	0.343
	2	0.589	0.297	0.331
	3	0.588	0.332	0.276
	4	0.573	0.302	0.358
	5	0.5268	0.2298	0.2239
	6	0.5646	0.3816	0.3583
	7	0.6365	0.225	0.3318
	8	0.8216	0.1036	0.442
	9	1.1249	0.3788	0.4775
	10	1.3025	0.9987	0.1674
I_{IHD} 38th Std	N VSCs	MCS	3pts rUDR	5pts rUDR
	1	0.46	0.32	0.33
	2	0.52	0.31	0.31
	3	0.52	0.29	0.3
	4	0.4991	0.2568	0.2596
	5	0.4494	0.2431	0.2472
	6	0.4669	0.2299	0.2284
	7	0.4503	0.2218	0.2144
	8	0.4114	0.209	0.212
	9	0.4188	0.1987	0.2042
	10	0.4197	0.1864	0.1858
I_{IHD} 42nd Std	N VSCs	MCS	3pts rUDR	5pts rUDR
	1	0.2886	0.2016	0.2045
	2	0.3399	0.2037	0.201
	3	0.3452	0.1798	0.187
	4	0.3393	0.1654	0.175
	5	0.3085	0.1625	0.1658
	6	0.3251	0.1561	0.1541
	7	0.3155	0.1431	0.1463
	8	0.2906	0.1396	0.147
	9	0.2975	0.1294	0.1361
	10	0.3	0.1286	0.1268

V_{THD} Std	N VSCs	MCS	3pts rUDR	5pts rUDR
	1	0.6455	0.445	0.4489
	2	0.688	0.4006	0.3945
	3	0.6317	0.322	0.3324
	4	0.5865	0.2773	0.2615
	5	0.5238	0.2609	0.256
	6	0.5533	0.2413	0.2646
	7	0.5428	0.299	0.2789
	8	0.5345	0.3183	0.3144
	9	0.5843	0.398	0.3907
	10	0.6352	0.4893	0.4554
V_{IHD} 38th Std	N VSCs	MCS	3pts rUDR	5pts rUDR
	1	0.4677	0.322	0.3319
	2	0.4947	0.2954	0.2972
	3	0.4525	0.2385	0.2318
	4	0.4256	0.2099	0.2191
	5	0.3844	0.2328	0.2131
	6	0.4098	0.2088	0.2125
	7	0.40	0.2602	0.24
	8	0.3879	0.2771	0.2723
	9	0.4172	0.2911	0.2763
	10	0.4322	0.3253	0.3301
V_{IHD} 42nd Std	N VSCs	MCS	3pts rUDR	5pts rUDR
	1	0.3518	0.2419	0.2409
	2	0.3754	0.2277	0.2278
	3	0.3469	0.2031	0.2151
	4	0.3241	0.188	0.18
	5	0.2919	0.19	0.1845
	6	0.3075	0.1884	0.1879
	7	0.297	0.2027	0.1771
	8	0.2894	0.2238	0.2323
	9	0.3107	0.2224	0.2456
	10	0.3232	0.2588	0.2641

C.3: Modelled Plects Circuit of Microgrid Structure with Linear and Non-Linear Load



C.4: Percentage Error in Current and Voltage THD and IHD_n for Microgrid with Non-Linear Loads

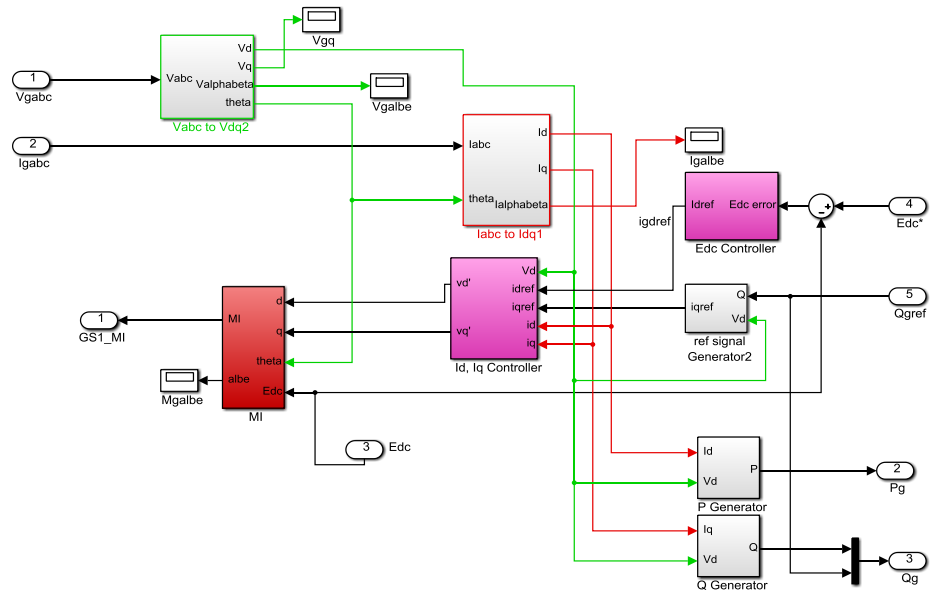
Table C.3: Predicted Current and Voltage Harmonic Distortion Level Percentage Error Using 3pts and 5pts UDR for Microgrid with Non-Linear Loads

I_{THD}	N VSCs	MCS	3pts rUDR	5pts rUDR
	Mean		-4.24	-7.34
	Std		6.98	-23.26
I_{IHD 5th}	N VSCs	MCS	3pts rUDR	5pts rUDR
	Mean		-1.96	-2.94
	Std		18.42	-10.53
I_{IHD 7th}	N VSCs	MCS	3pts rUDR	5pts rUDR
	Mean		-4.88	-9.76
	Std		-26.67	-82.67
I_{IHD 11th}	N VSCs	MCS	3pts rUDR	5pts rUDR
	Mean		1.39	6.94
	Std		-37.25	-61.76
I_{IHD 38th}	N VSCs	MCS	3pts rUDR	5pts rUDR
	Mean		-5.17	-6.90
	Std		-4.17	-12.50
I_{IHD 42nd}	N VSCs	MCS	3pts rUDR	5pts rUDR
	Mean		-5.71	-7.88
	Std		-9.30	-23.26
V_{THD}	N VSCs	MCS	3pts rUDR	5pts rUDR
	Mean		0.34	-1.03
	Std		-28.00	-16.00
V_{IHD 5th}	N VSCs	MCS	3pts rUDR	5pts rUDR
	Mean		3.23	4.03
	Std		-10.26	84.62
V_{IHD 7th}	N VSCs	MCS	3pts rUDR	5pts rUDR
	Mean		-2.90	-8.70
	Std		-36.11	52.78
V_{IHD 11th}	N VSCs	MCS	3pts rUDR	5pts rUDR

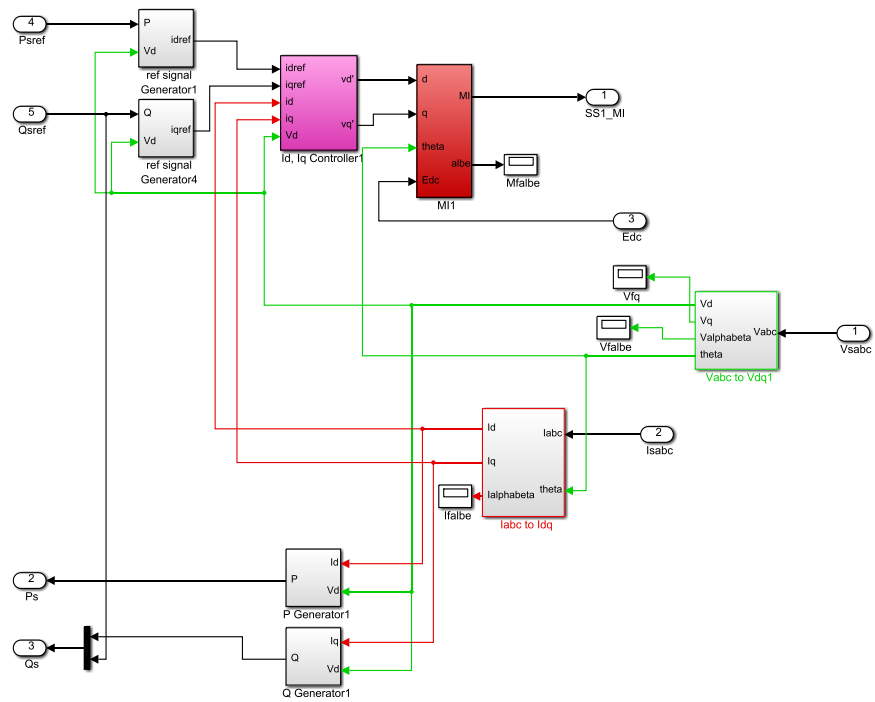
Appendix

	Mean		-4.69	-6.25
	Std		25.00	27.50
V_{IHD} 38th	N VSCs	MCS	3pts rUDR	5pts rUDR
	Mean		0.00	0.00
	Std		18.75	-18.75
V_{IHD} 42nd	N VSCs	MCS	3pts rUDR	5pts rUDR
	Mean		0.00	0.00
	Std		0.00	0.00

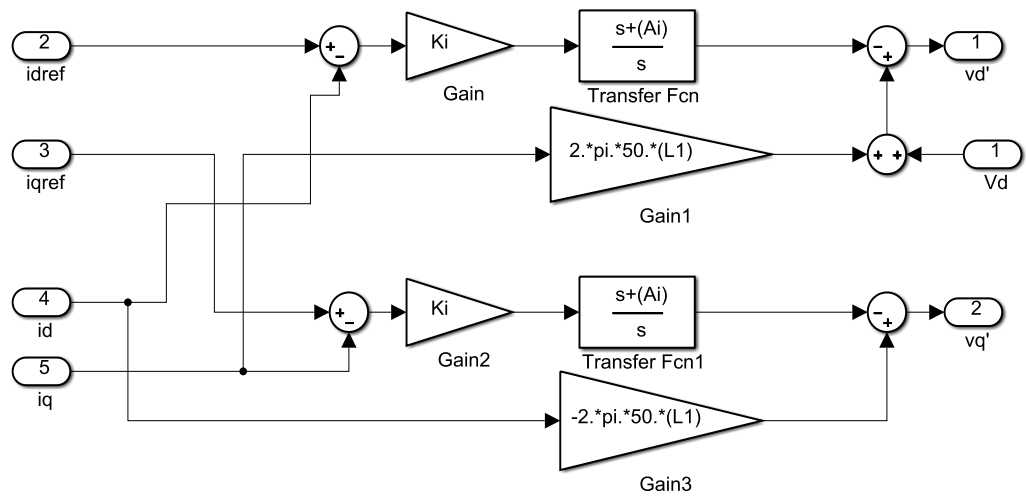
D.2: Control and Transformation Blocks



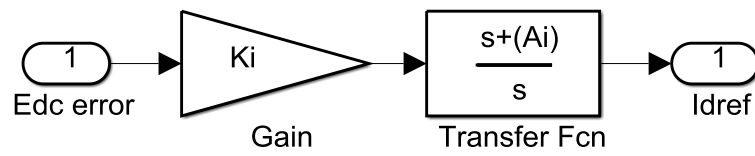
Grid Side Control Structure and Transformation



Source Side Control Structure and Transformation



Active and Reactive Current Component Control



DC Capacitor Voltage Control